OPTIMIZATION OF COMPOSITE LAMINATE UNDER MECHANICAL AND THERMAL LOADING USING FINITE ELEMENT METHOD AND MACHINE LEARNING TECHNIQUES

BY

OMAR SHABBIR AHMED

INTERNATIONAL ISLAMIC UNIVERSITY MALAYSIA

2024

OPTIMIZATION OF COMPOSITE LAMINATE UNDER MECHANICAL AND THERMAL LOADING USING FINITE ELEMENT METHOD AND MACHINE LEARNING TECHNIQUES

BY

OMAR SHABBIR AHMED

A thesis submitted in fulfilment of the requirement for the degree of Master of Science in Engineering

Kulliyyah of Engineering
International Islamic University Malaysia

March 2024

ABSTRACT

Thin-walled composite structures have gained significant traction for diverse engineering uses due to their laminated composition, featuring layers of composite materials with unique properties shaped by fiber orientation. Stress analysis of such thin-walled composite sections under mechanical and thermal loads is complex, often requiring optimization to achieve optimal designs. However, the reduced thickness of these structures makes them susceptible to buckling. Incorporating lightning holes reduces weight but compromises stiffness and buckling strength. This study focuses on assessing the buckling strength of thin-walled composites with various hole shapes under mechanical and thermal loads. A parametric investigation aims to identify the best material and structural parameters for resilience against both mechanical and thermal stress. Initially, a finite element-based numerical approach was used to model the c-section thin-walled composite structure. Structural and material parameters like spacing ratio, opening ratio, hole shape, fiber orientation, and laminate sequence are systematically varied under mechanical and thermal loads. The resulting data drives the identification of optimal parameter combinations through machine learning algorithms. Multiple techniques are compared to finite element results for accuracy. The simulation model effectively captures changes in critical buckling load under distinct mechanical and thermal conditions due to alterations in structural and material features. The machine learning approach accurately predicts optimal critical buckling load under both scenarios. Furthermore, the study's findings indicate that the optimal critical buckling values for the current problem are achieved with specific parameter combinations. For mechanical loading conditions, the best configuration involves a quasi-isotropic structure with a circular hole, an opening ratio of 1.4, and a spacing ratio of 1.6, resulting in a critical buckling load of 8804 N. In the case of thermal loading, an angle-ply structure with a circular hole, an opening ratio of 1.4, and a spacing ratio of 1.7 leads to a critical buckling load of 308.2 (T-critical). In summary, this thesis comprehensively explores the stability of c-section thin-walled composite structures with holes under mechanical and thermal loads, utilizing finite element analysis and machine learning.

خلاصة البحث

اكتسبت الهياكل المركبة الرقيقة طلبا كبيرا نحو الاستخدامات الهندسية المتنوعة بسبب تركيبتها ذات الطبقات، حيث تتميز بطبقات من المواد المركبة ذات الخصائص الفريدة التي تتشكل حسب اتجاهات الألياف، كما يعد تحليل الاجهاد للهياكل المركبة الرقيقة تحت التحميل الميكانيكي والحراري أمرا معقدا، حيث يتطلب في كثير من الأحيان تحسينه لتحقيق أفضل التصاميم. ومع ذلك، كلما قلت سماكة الهياكل كلما كانت عرضة للانبعاج، أضف إلى ذلك أن إضافة فتحات يخفف الوزن ولكن يضر بالصلابة وقوة الالتواء. تركز هذه الدراسة على تقييم قوة الالتواء للهياكل المركبة الرقيقة ذات الفتحات المختلفة تحت التحميل الميكانيكي والحراري، تهدف التحقيقات الحدودية إلى تحديد أفضل المواد والهياكل والتي تتحمل التوترات الناتجة عن التحميل الميكانيكي والحراري. في البداية، تم استخدام نهج عددي قائم على العناصر المحدودة لنمذجة الهيكل المركب الرقيق على شكل "C"، كما تتنوع المعلمات الهيكلية مثل نسبة التباعد، ونسبة الفتح، وشكل الثقب، واتجاه الألياف، وتسلسل الصفائح بشكل منهجي تحت الأحمال الميكانيكية والحرارية. حيث تقود النتائج إلى تحديد تركيبات المعلمات المثلى من خلال خوارزميات التعلم الآلي. كما يتم مقارنة تقنيات متعددة مع نتائج العناصر المحدودة للتأكد من دقة النتائج. كما يلتقط نموذج المحاكاة بشكل فعال التغييرات الحرجة للالتواء تحت ظروف ميكانيكية وحرارية متميزة بسبب التغييرات في ملامح الهياكل والمواد. علاوة على ذلك، يتنبأ نهج التعلم الآلي بدقة بحمل الالتواء الحرج الأمثل في كلا الطريقتين. لذلك تشير نتائج الدراسة إلى أن قيمة الالتواء الحرجة المثلى للمشكلة الحالية يمكن تحقيقها باستخدام مجموعات محددة من المعلمات، حيث أن النتيجة المثلى في ظروف التحميل الميكانيكي للقالب ذات الثقب الدائري ونسبة الافتتاح تبلغ 1.4، مع نسبة تباعد تبلغ 1.6، حيث تبلغ قيمة الالتواء الحرجة 8804 نيوتن. أما في حالة التحميل الحراري، فيتم استخدام القالب بزاوية مع ثقب دائري ونسبة افتتاح تبلغ 1.4، مع نسبة تباعد تبلغ 1.7، مما يبلغ قيمة الالتواء الحرجة 308.2 (تي). في النهاية تسلط هذه الرسالة الضوء باختصار بشكل شامل استقرار الهياكل المركبة ذات الجدران الرقيقة والتي تتشكل على شكل "سي" تحت التحميل الميكانيكي والحراري، باستخدام تحليل العناصر المحدودة والتعلم الآلي.

APPROVAL PAGE

I certify that I have supervised and read this study and that in my opinion it conforms to acceptable standards of scholarly presentation and is fully adequate, in scope and quality, as a thesis for the degree of Master of Science in Engineering.

…………………………………..
Jaffar Syed Mohamed Ali
Supervisor

…………………………………..
Meftah Hrairi
Co-Supervisor

…………………………………..
Norfazrina Mohd Yatim
Co-Supervisor

…………………………………..
Abdul Aabid
Field-Supervisor

I certify that I have read this study and that in my opinion it conforms to acceptable standards of scholarly presentation and is fully adequate, in scope and quality, as a thesis for the degree of Master of Science in Engineering.

…………………………………..
Mohamed Thariq Bin Hameed Sultan
Internal Examiner

…………………………………..
Mohd Sultan Ibrahim
External Examiner

This thesis was submitted to the Department of Mechanical and Aerospace Engineering and is accepted as a fulfilment of the requirement for the degree of Master of Science in Engineering.

…………………………………..
Hanan Bt. Mokhtar
Head, Department of Mechanical and Aerospace Engineering

This thesis was submitted to the Kulliyyah of Engineering and is accepted as fulfilment of the requirement for the degree of Master of Science in Engineering.

...……………………………….
Khairul Azami Sidek
Covering Dean, Kulliyyah of Engineering

DECLARATION

I hereby declare that this thesis is the result of my own investigations, except where otherwise stated. I also declare that it has not been previously or concurrently submitted for any other degrees at IIUM or other institutions.

Omar Shabbir Ahmed

Signature: Omar Shabbir Date: 06 – 03 – 2024

COPYRIGHT PAGE
INTERNATIONAL ISLAMIC UNIVERSITY MALAYSIA

DECLARATION OF COPYRIGHT AND AFFIRMATION OF FAIR USE OF UNPUBLISHED RESEARCH

OPTIMIZATION OF COMPOSITE LAMINATE UNDER MECHANICAL AND THERMAL LOADING USING FINITE ELEMENT METHOD AND MACHINE LEARNING TECHNIQUES

I declare that the copyright holders of this thesis are jointly owned by the student and IIUM.

No part of this unpublished research may be reproduced, stored in a retrieval system, or transmitted, in any form or by any means, electronic, mechanical, photocopying, recording or otherwise without prior written permission of the copyright holder except as provided below.

1. Any material contained in or derived from this unpublished research may be used by others in their writing with due acknowledgement.

2. IIUM or its library will have the right to make and transmit copies (print or electronic) for institutional and academic purposes.

3. The IIUM library will have the right to make, store in a retrieved system and supply copies of this unpublished research if requested by other universities and research libraries.

By signing this form, I acknowledged that I have read and understand the IIUM Intellectual Property Right and Commercialization policy.

Affirmed by Omar Shabbir Ahmed

Omar Shabbir — 06 – 03 – 2024

Signature — Date

AKNOWLEDGEMENTS

In the Name of Allah, the Most Compassionate, the Most Merciful

Allah - beginning with the name of - the Most Gracious, the Most Merciful Most Auspicious is he in whose control is the entire kingship; and he can do all things [67:1]. All Praise to Allah, the Lord of the creation, and countless blessings and peace upon our Master Mohammed, the leader of the Prophets.

I express my sincere gratitude to Associate Professor Ir. Dr. Jaffar Syed Mohamed Ali for his unwavering support, encouragement, and exemplary leadership throughout this research journey. His guidance and prompt assistance in resolving any research-related challenges were invaluable, and I am deeply grateful for his mentorship. I extend my heartfelt thanks to my co-supervisors, Professor Dr. Meftah Hrairi and Dr. Norfazrina Mohd Yatim, whose cheerful guidance and support greatly contributed to the success of my research work. Special mention goes to my field supervisor, Dr. Abdul Aabid from Prince Sultan University, Saudi Arabia, for his continuous support and motivation during my thesis work, which proved instrumental in my postgraduate studies.

I would like to dedicate this work to my dear parents and family members for their unwavering belief in my abilities and their unending support and patience. Your encouragement has been a driving force behind my accomplishments, and I am forever grateful. A heartfelt thank you goes to my life partner, whose involvement, sacrifices, patience, and understanding played a vital role in making this thesis possible.

I would like to express my gratitude to all those who dedicated their time, energy, and assistance to this project. I extend my heartfelt thanks to my thesis committee members for their unwavering support. I am profoundly thankful to everyone who contributed, and I hope that your efforts are rewarded.

TABLE OF CONTENTS

LIST OF TABLES

LIST OF FIGURES

LIST OF ABBREVIATIONS

2D	Two-dimensional
3D	Three-dimensional
ASTM	American Society for Testing and Materials
Coef	Coefficient
FE	Finite Element
FEA	Finite Element Analysis
FEM	Finite Element Method
LEFM	Linear Elastic Factor Mechanics
ML	Machine Learning
NE	Number of Elements
NN	Number of Nodes

LIST OF SYMBOLS

σ *or* σ_0	Applied Tensile Load/Stress
E	Young's Modulus
ν	Poison's ratio
G	Shear Modulus
S	Stiffness Ratio

CHAPTER ONE

INTRODUCTION

1.1 OVERVIEW

This introductory chapter lays down a foundation and discusses the background of this thesis, describes broadly the problem statement which this thesis will deal and from that identify objectives to be solved detailed methodology is discussed at the end of this chapter. Additionally, illustrated the flow chart of the thesis chapter that has been provided the chapters content.

1.2 BACKGROUND OF THE STUDY

A composite material is a multiphase substance composed of two or more components with distinct compositions or forms that retain their individual characteristics when bonded together. This unique composition results in the newly formed material surpassing the performance of its separate components. Due to their versatility and ease of integration with other materials, composites have become widely used in various applications. In civil engineering, composites have demonstrated a fascinating evolution, finding application in material shaping and foundation for construction projects.

Over time, civil engineers have become increasingly aware of the advantages offered by composite materials in construction. As a result, the use of composites in the building and construction industry has increased significantly. With growing demands for strength, safety, and reliability, composite engineering has become indispensable in numerous industries. Although composites may be more expensive than traditional construction materials, their benefits, such as being lightweight, corrosion-resistant, and stronger, outweigh the costs. The incorporation of fiber reinforcements in composites also provides excellent damping properties and remarkable fatigue resistance.

For engineers to make appropriate material choices and ensure safety during planning and execution, it is essential to have a thorough understanding of the chemical, physical, and mechanical properties of different polymers and how they can affect the structure. This knowledge enables engineers to utilize composite materials effectively in constructing reinforced structures capable of withstanding natural disasters like earthquakes and hurricanes. Presently, composites are being employed worldwide to enhance the earthquake resistance of concrete constructions.

A specific type of composite, known as Fiber Reinforced Polymer (FRP) composite, consists of a thermoset or thermoplastic polymer matrix reinforced with fibers or other materials possessing sufficient aspect ratios for reinforcing functions. It is important to distinguish FRP composites from traditional construction materials like steel or aluminum because of their distinctive properties and applications. As we move forward, the role of composite engineering is predicted to expand further within civil engineering, playing a crucial and increasingly important role in shaping the future of construction and infrastructure development.

1.3 PROBLEM STATEMENT

Structures such as beams, plates and shells or other types of structures are mostly assemblies of laminated composite structures, these structures are exposed to environmental factors such as high stress and temperature, which can have a negative impact on their strength and stiffness.

The challenges in designing and analyzing laminated composite structures exposed to mechanical and thermal loads include complex material behavior, numerous design parameters, thermal effects, computational complexity, and the need for efficient optimization methods, with the potential for improvement through modern machine learning approaches. Environmental factors, such as high stress and temperature, can weaken laminated composite structures by degrading material properties, inducing thermal expansion, increasing moisture absorption, creating residual stresses, causing creep, thermal buckling, and thermal fatigue, ultimately reducing their strength and stiffness. Design and analysis of composite laminate such as civil application under mechanical and thermal loads is tedious because of the numerous parameters involved and further optimization is required to achieve an optimal composite civil structure. Most of the optimization work that has been carried out is just based on genetic algorithms in an existing work for such applications whereas the optimization based on the present modern machine learning approach was not found in the literature. In this work, we attempt to optimize the performance of composite laminates under mechanical and thermal loading conditions using machine learning algorithms. We perform optimization study to achieve the buckling strength and deformation stresses, by optimizing parameters such as the stacking sequence, ply orientation angle, spacing ratio, opening ratio and shape of the hole.

1.4 RESEARCH OBJECTIVE

This study aims to investigate and explore the composition of composite laminate material. The objectives of the study are.

1- To simulate a laminated composite thin-walled structures with holes under mechanical and thermal loading using the finite element method to evaluate the buckling strength.

2- To conduct an in-depth parametric study utilizing a finite element model, aimed at understanding the influence of parameters including spacing ratio, opening ratio, laminate sequence, lamina orientation, and hole shape on buckling strength.

3- To determine the optimum parameters combinations of laminated composite structures with holes under mechanical and thermal loads via machine learning algorithms and comparison of algorithms to fit the best possible solution.

1.5 RESEARCH METHODOLOGY

The overall aim of this research is to propose an analytical/numerical model that will relate the strength and stiffness of the laminated composite. Therefore, the following plan is stated to achieve the objectives of this study (Figure 1.1):

- Literature review: The first step that is going to be taken is a review of the current state-of-the-art technologies on the potential application of composite materials FRP for civil structural engineering. This will give an overview and review of the research that has been carried out in this area.
- A finite element model will be used to investigate the effects of parameters and analysis on the laminated composite shell structure under mechanical and thermal loading conditions. For this, ANSYS software will be used to do the simulation. Initially, a finite element model will be validated with existing benchmark results.
- The FE modeling will be conducted in ANSYS software, utilizing SHELL181, ideal for analyzing thin to moderately thick shell structures. SHELL181 is a four-node element with six degrees of freedom per node, encompassing

translations in x, y, z, and rotations about x, y, and z-axes. For membrane applications, it offers translational degrees of freedom exclusively. This element excels in linear, large rotation, and large strain nonlinear scenarios, accounting for varying shell thickness in nonlinear analyses. It supports both full and reduced integration schemes. Additionally, it accommodates follower effects from distributed pressures and handles layered applications, especially for composite shells, adhering to the first-order shear deformation theory. It employs logarithmic strain and true stress measures, permitting finite membrane strains with small, assumed curvature changes within time increments.

- FE models will be created first for new composite structures and then for laminate structures to determine delamination. The simulation results will be compared with the existing optimization work. After the developed FE model is validated, a numerical simulation will be performed with each parameter and dimension to produce a database. The machine learning algorithm will then be trained and tested using a random input vector from the data set to ensure good aggregation capabilities. Finally, the machine learning algorithm error location prediction model will be tested with numerical data. Some validation of FE results with existing data and then further parametric study was performed for the machine learning algorithm.
- Based on several simulations of composite parameters, established guidelines have been envisaged by supervised or unsupervised machine learning techniques. This standard array stipulates the way of performing the minimum number of simulations which could provide the full knowledge of all the factors that affect the output parameter.

In general, it is important to note with machine learning algorithms that it is random because of the arbitrary weight generated in the hidden layer. This can produce different accuracy depending on the random weights. Simple sequential heuristic search techniques are used to achieve the best accuracy. It is important to note that in LM the number of neurons in the hidden layer is randomly selected. In other words, there are no clear mathematics rules for deducing the right numbers of neurons to train. Huang et al., (2006) have shown that with the differentiable activation functions, the number of neurons required in the hidden layer is smaller than the data size. In this application, some neurons select sigmoid as their activation function based on previous studies (S. Park et al., 2006). It is used in hidden layers because the selection is based entirely on greedy testing.

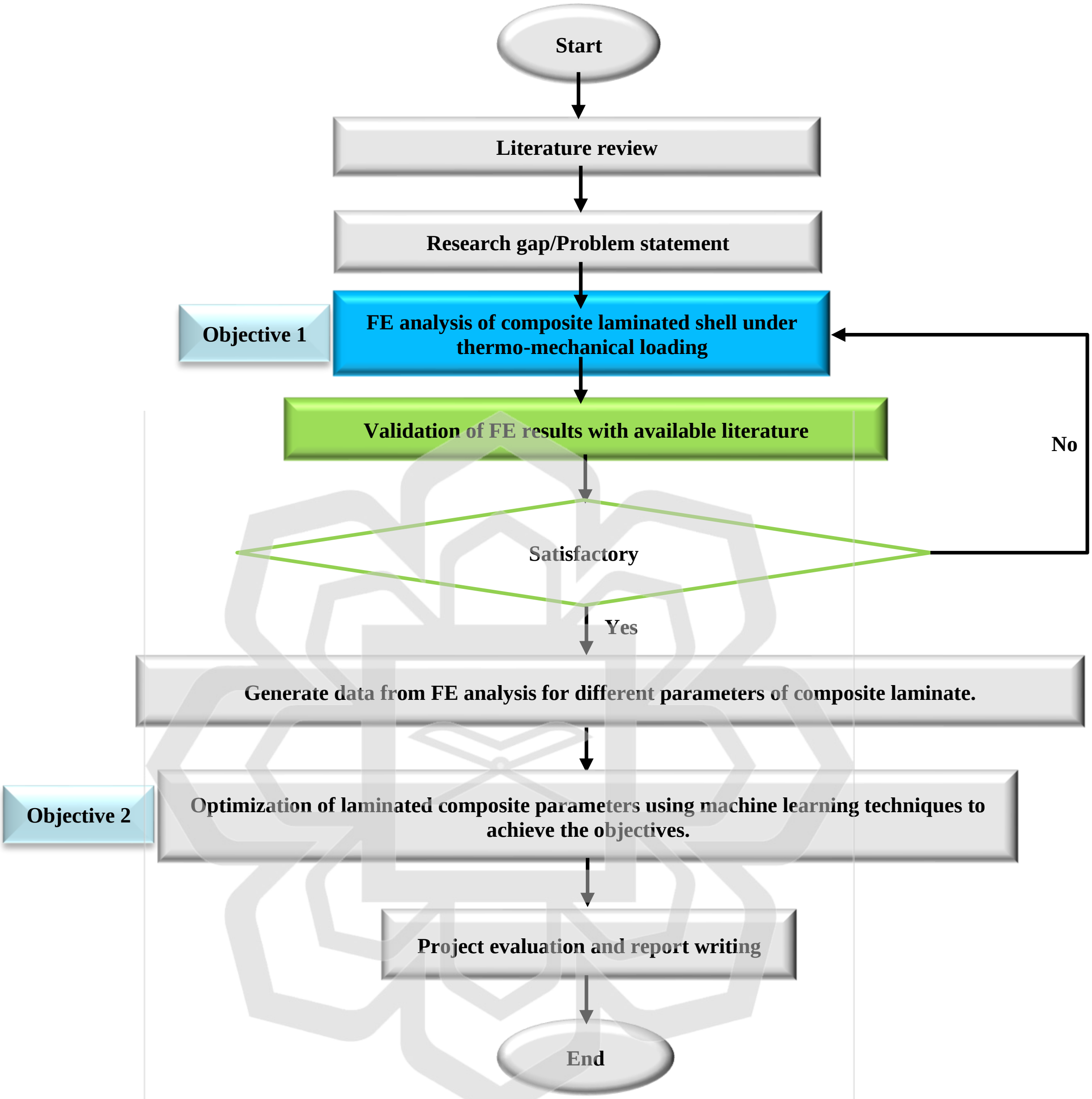

Figure 1.1. Research methodology flow chart

1.6 RESEARCH SCOPE

This research aims to analyze the structures using the finite element method and machine learning techniques for the optimum solution. The scope of this research is,

- Different laminated composite parameters were analyzed in this study to investigate the quality of the structures.

- Data optimization with machine learning algorithms is proposed to determine the effective parameters of the laminated composite structure.

1.7 THESIS OUTLINE

This thesis is structured into five chapters, as outlined below:

- **Chapter One:** Background of the thesis study, problem statement, research objective, research scope and methodology are briefly explained and also thesis organization is discussed in this chapter.
- **Chapter Two:** Previous studies in the structure and various forms of structural parameters in beams and columns and other types of composite structures are overviewed and summarized. Some key factors were chosen to summarize the existing work such as the problem defined, the methodology adopted and the applications. A data optimization technique to define the composite parameters for structural analysis was explored and criticized. Furthermore, the other common types of optimization methods for different structures have been summarized. Finally, based on the existing work and methodology and a research gap was proposed for the current work.
- **Chapter Three:** The detailed methodology of the research is discussed in chapter three which includes finite element modelling and analysis of different types of structures and variation in the properties that will used for machine learning algorithms to optimize the best possible solution of the structural component. Additionally, discussed in detail machine learning algorithms and error rate performance compared to the structural model.
- **Chapter Four:** The simulation results are discussed in this chapter. The performance of all parameters and machine learning performance. The

performance for different conditions of the structures and materials under mechanical and thermal load.

- **Chapter Five:** The thesis is concluded in chapter five and future recommendation of this research is also discussed briefly. The organization of chapters is shown in Figure 1.6.

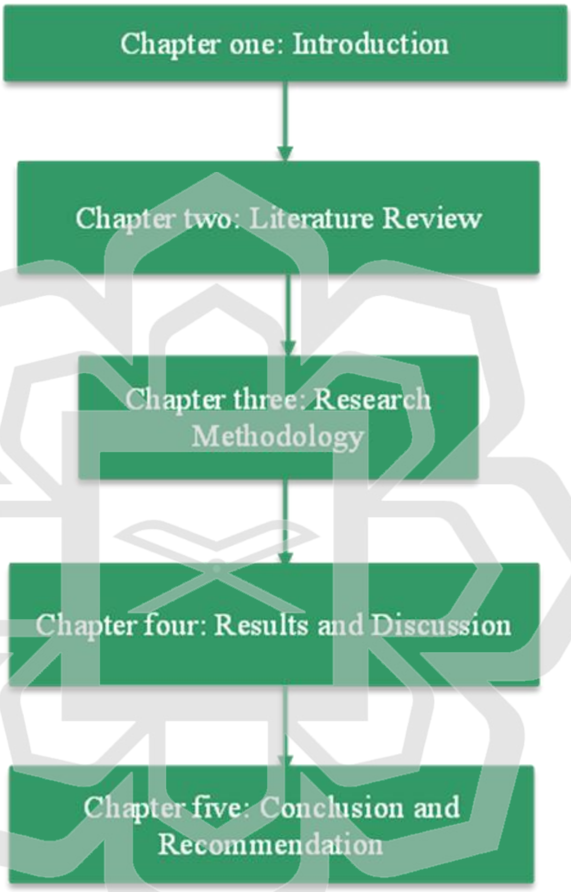

Figure 1.2. Overview of research methodology flow-chart

CHAPTER TWO

LITERATURE REVIEW

2.1 OVERVIEW

In this chapter a previous study in the structure and various forms of structural parameters in beams and columns and other types of composite structures are overviewed and summarized. Some key factors were chosen to summarize the existing work such as the problem defined, the methodology adopted and the applications. A data optimization technique to define the composite parameters for structural analysis was explored and criticized. Furthermore, the other common types of optimization methods for different structures have been summarized. Finally, based on the existing work and methodology and a research gap was proposed for the current work.

2.2 THIN-WALLED STRUCTURES

Thin-walled members offer advantages in terms of preventing global buckling due to their high slenderness ratio, which makes them more resistant to buckling under axial compression or bending loads. This is particularly beneficial in applications where lightweight and efficient structural elements are required. However, thin-walled structures can be prone to local buckling, especially in the constituent plates. Local buckling occurs when individual plates within the thin-walled member buckle independently due to high stresses or geometric imperfections. This can reduce the overall load-carrying capacity and structural integrity. Thin-walled truss members may experience local buckling under high compression, which can affect structural integrity. Design adjustments and analysis are needed to prevent this issue. The behavior of a typical thin-walled composite structure is characterized by three main states: elastic, post-buckling, and failure. The critical load is significant as it marks the transition from the elastic state to the post-buckling state, indicating the point at which structural stability is compromised, and deformation accelerates towards failure, influencing design and safety considerations (Kamarudin et al., 2022).

The thin-walled member is considered one of the most efficient systems for preventing buckling due to its effective use of materials. By utilizing multiple thin-walled parts, this type of member allows for the creation of various shapes with a high shape factor, minimizing the amount of material required. However, despite these advantages, the thin-walled member does have some drawbacks, particularly in relation to local buckling caused by constituent plates. In compressive loading scenarios, the component plates of a thin-walled column often buckle before experiencing complete collapse (Lee et al., 2009).

A thin-walled structure is widely recognized as a type of structure where the thickness is significantly smaller than the height and width dimensions. It plays a crucial role as a load-bearing profile and finds extensive applications in modern technology, such as automotive, construction industries, and aerospace. This is primarily because its exceptional characteristics, including high strength and stiffness coupled with a lightweight design (Różyło, 2017). The example of thin-walled structure can be illustrated in Figure 2.1.

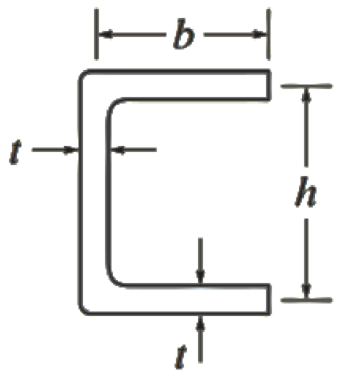

Figure 2.1. Thin-walled structures dimensions

Thin-walled structures are employed in a diverse range of shapes to cater to specific applications within industries. For instance, in a study by (Biagi et al., 2020), T-shaped thin-walled structures with varying geometries were examined for their use as ribs in aircraft. Additionally, Rozylo and Debski, (2020) conducted an experiment on Z-shaped composite thin-walled structures. One intriguing aspect of thin-walled structures is their capacity for self-improvement as well as enhancement of other members. A more detailed on this topic will be presented in the following section of this chapter.

Optimization plays a vital role in improving the buckling performance of thin-walled structures by fine-tuning critical parameters like cutout diameter and hole spacing. Precise optimization helps in finding the optimal combination of these factors to enhance structural stability while minimizing weight and cost. Varying fiber orientation, composite type, and thickness in thin-walled composites significantly impact buckling performance. The text underscores the need for optimization by highlighting the complex interplay of these variables and their influence on structural behavior. Proper optimization, guided by modern techniques like machine learning, enables designers to achieve superior buckling resistance and efficiency in thin-walled composite structures.

2.2.1 Thin-walled composite structures

Thin-walled members are highly efficient in resisting buckling because they can be easily formed into a variety of shapes with a high shape factor and less material. However, they are also susceptible to local buckling, which can occur when the component plates of the member buckle before the member collapses (Lee et al., 2009). Thin-walled structures are load-bearing profiles that are characterized by a small thickness relative to their height and width. They have unique properties, including significant strength and stiffness with low weight, which make them suitable for a lot of applications in current technology, like aerospace, automotive, and construction industries (Różyło, 2017). Different forms of thin-walled structures are used depending on the application in the industries. For example, Biagi et al., (2020) studies T-shaped thin-walled with various geometry that is used in aircraft as ribs. Next, Rozylo and Debski, (2020) On composite thin-walled Z-shape structures, an experiment is conducted. Thin-walled structures are intriguing since they can be improved for both them and other members.

Fiber-reinforced composite materials like glass fiber-reinforced polymer (GFRP) and carbon fiber-reinforced polymer (CFRP) are gaining increasing traction in various fields due to their numerous benefits, including low weight, high strength, and versatile manufacturing capabilities. These materials have witnessed a surge in popularity in recent years and are now widely utilized in diverse industrial sectors such as aviation, manufacturing, and structural engineering, as noted by Doan and Thai, (2020). To meet the growing demand for lightweight and efficient structures, engineers and scientists have incorporated composite materials into various applications, leveraging their unique strengths and thermomechanical properties beyond the reach of conventional materials, as highlighted by Sudhirsastry et al., (2015). It's worth noting that the alignment of fibers significantly impacts the physical properties of composites, thereby influencing shell stiffness and its impact on critical buckling load, as discussed by Lvov et al., (2015).

2.2.1.1 Composite laminates

The loss of stiffness in laminated composites is a significant physical and mechanical response that occurs during damage and failure. This can happen under a variety of conditions, such as continuous or cyclic loads. To accurately study the mechanical properties of composite laminates, it is important to replicate the initiation and subsequent development of this type of damage phenomenon (Liu and Zheng, 2010). In this regard, a proposed approach based on energy-based stiffness degradation Liu and Zheng, (2008), rooted in the CDM theory, The goal is to predict how Al-carbon fiber/epoxy composite laminates will fail over time. This method provides insight into the evolution process of damage within the material.

Delamination and matrix microcracking are frequent first steps in the failure of laminated resin matrix composite materials. Interlaminar stresses are the driving force behind these three-dimensional damage mechanisms. An analytical strategy that offers accurate stress estimations in crucial areas is a crucial component to comprehending and, eventually, predicting breakdowns in composite materials. Traditional laminate theories, which are predicated on global displacement assumptions, are insufficient for this task. Furthermore, in the original formulations, the interlaminar stresses are frequently overlooked. Solutions based on these theories are therefore unable to produce realistic stress distributions. A recent theoretical study demonstrates that bending-related behavior is influenced by several nonclassical factors. Included in them are transverse normal strain and section warping, as well as their related nonclassical surface-parallel stress contributions. When these nonclassical factors are considered, the stress prediction ability of a bending theory is greatly enhanced (Tsukrov et al., 2014). Figure 3 shows microcracking in a woven composite.

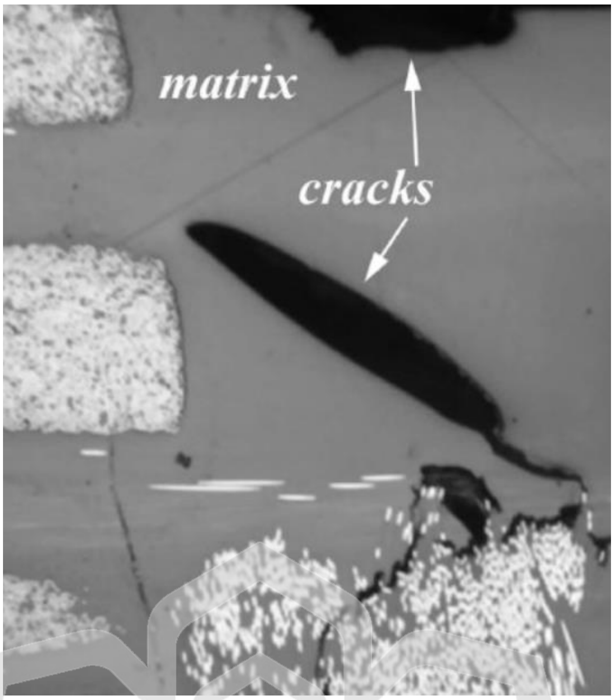

Figure 2.2. Microcracks in a composite (Tsukrov et al., 2014)

In the research by Özaslan et al., (2019), both experimental and numerical approaches were employed to conduct stress analysis and predict the strength of carbon/epoxy laminates containing holes in specific orientations. Their investigation delved into the interplay among these holes, considering their positions and the direction of applied loads. The study aimed to pinpoint the maximum stress within the laminate around the hole peripheries across various hole orientations. By considering the location of maximum tension at the hole edges, they identified the critical zone. Bogetti and Gillespie, (2016) focused on thermosetting composite laminates and analyzed the stress and deformation induced during the manufacturing process. They developed a methodology to anticipate the formation of residual stress as the material cured. Furthermore, Li et al., (2017), expanded on this theme by creating two transient models, the viscoelastic and linear elastic models, to explore the curing deformation of thermosetting resin composites. These models, simulated using COMSOL Multiphysics, encompassed the intricate interplay between physical and chemical changes during the composite's curing process, accounting for the time-dependent nature of material performance factors.

Dai et al., (2019) proposed a numerical model that couples multiple physics aspects of the curing process in thermosetting resin composites. They used the modified "cure hardening instantaneously linear elastic (CHILE)" model and the viscoelastic model to predict residual stress and deformation during curing. They also used ultrasonic-guided waves to detect and monitor delamination in composite double cantilever beams (DCBs) subjected to low-velocity impact (Ouyang et al., 2021). They set up an experimental system to detect damage in composite materials using ultrasonic guided waves and piezoelectric sensors. They processed the response signals using the Hilbert transform (HT), Fourier transform (FFT), and wavelet transform (CWT) techniques. (Zhao et al., 2019).

To accurately evaluate composite structures under dynamic conditions or simulate high-strain-rate manufacturing processes, a constitutive model that accounts for these effects is essential. Eskandari et al., (2019) proposed a phenomenological approach, considering continuum damage and visco-plastic behavior in composites subjected to high strain rates. They studied how composite structures deform under dynamic loading conditions. Additionally, Kharghani and Guedes, (2018) studied the deflection and maximum tensile strain in composite laminates under bending conditions. They used different equivalent single-layer and layer-wise theories with polynomial form functions. They used the Rayleigh-Ritz approximation and the conception of minimum energy to determine the unknown coefficients of the displacement field. They compared their results to experimental studies and three-dimensional finite element FE analysis. They also emphasized the importance of accurately capturing the rate-dependency of composite materials when modeling design-critical impact loading events on laminated composite structures. In this context, a study examined the rate dependence of the strain-energy release rate for high-rate loading conditions and the failure of fibers in tension (Hoffmann et al., 2018).

2.2.1.2 Fiber orientation of composites

Understanding the impact of fiber orientation on critical buckling is crucial. Erkliğ and Yeter, (2012) study revealed that varying fiber orientations result in different critical buckling loads. This investigation employed theoretical calculations and finite element analysis, utilizing the mechanical properties of laminated glass-polyester composite plates. Eight-ply laminates, each with eight different stacking sequences, were formed from the composite plies. These laminates incorporated fiber orientations at 0, 15, 30, and 45 degrees within the six-ply layers. The study's findings indicated that the buckling load is at its lowest when the fiber angle is 45 degrees, progressively increasing with higher orientation angles.

According to a study conducted by (Lvov et al., 2015), the critical buckling stress tended to increase when the fiber orientation changed. Additionally, this research version demonstrates no differences regarding the influence of thickness, with the same pattern being shown in the results as they repeat the process for thicker models. After all, it is important to recognize that each research uniquely uses materials. (Erkliğ & Yeter, 2012) used laminated glass-polyester composite plate material in their experiments meanwhile (Lvov et al., 2015) used fiber-reinforced polymer (FRP). From these two publications, we may therefore conclude that various composite materials also influence the critical buckling stress on thin-walled parts.

Due to the popularity of structures, numerous types of research have been done to examine the gaps that are present and so enhance the use of columns, beams, shells, and laminate structures in various sectors. Generally, the maximum load that a thin-walled structure can withstand before it buckles member is then estimated using linear analysis, and after buckling, the researcher examines the column's behavior in nonlinear stages to determine the ultimate load. Additionally, once the experiment or simulation is completed for a specific thin-walled member, multiple types of failure might be seen. Using Euler's equation, we may anticipate the mode of buckling. The supporting option employed to support the column is another aspect that adds attention to this subject. As we comprehend Euler's classic, different supports result in various responses. This is because different buckling coefficients will be used based on the kind and dimensions of the supports. According to reviews of prior literature, the performance of perforated thin walls tends to decline as the size of the holes rises. To determine the acceptability of the cutout diameter for a specific thin-walled structure, optimization is therefore required. Additionally, since a smaller distance between the holes reduces the critical stress for buckling, it is also required to optimize this value. Finally, a variety of factors, including fiber orientation, composite type, and thickness, influence the buckling performance of thin-walled composite structures.

Fiber orientation in composite materials is significant because it determines their mechanical properties. The direction of fibers affects a composite's stiffness, strength, and critical buckling load. Properly aligned fibers can enhance a composite's resistance to buckling, while misaligned fibers can lead to premature buckling failure due to reduced stiffness and load-bearing capacity. Therefore, precise control of fiber orientation is crucial in optimizing composite structures for buckling resistance and overall performance. Based on the results obtained from Erkliğ and Yeter, (2012) it has been found that the increasing the fiber orientation angle leads to a reduction in the buckling loads of plates. The most critical buckling load occurs when the fiber angle is set at 45 degrees. Beyond this angle, the critical buckling load starts to rise. In the range of 0 to 45 degrees of fiber orientation angle, plates with elliptical cutouts exhibit the highest buckling loads. However, after 45 degrees, plates with circular cutouts show the highest buckling loads. An increase in the cutout aspect ratio (COA) has only a minimal impact on reducing plate buckling loads, making it less effective in this regard.

2.3 STRUCTURAL ANALYSIS UNDER MECHANICAL LOAD

The properties of laminated composite materials can vary greatly depending on the orientation of the layers, the properties of the materials used (fibers and matrix), and the number of layers. There are different analysis methods the structures in particular finite element method found more successful method to analyzing the structures in different modes (Kosanke, 2019; Sanghi et al., 2016). Additionally, specific analysis of modes is available to define the stresses and strains via buckling analysis, failure mode, etc.

Researchers evaluate the behavior of thin-walled structures under mechanical loads through a combination of experimental testing and numerical simulations. They use specialized testing equipment to subject physical prototypes to mechanical loads while measuring factors such as deflection, stress, and strain. Additionally, FE analysis is employed to create numerical models that consider the orientation of layers, material properties, and the number of layers. These simulations help predict structural behavior, assess performance, and optimize design parameters. The modes of analysis depend upon the type of structures such beam, truss and columns and based on the loading conditions where the critical buckling load will impact rate high (Z. Li et al., 2023; Rio Prabowo et al., 2021).

2.3.1 Buckling analysis

Local buckling in thin-walled elements involves the collapse of individual wall elements or plates under compressive loads, often due to geometric imperfections or high stress concentrations. Distortional buckling, on the other hand, arises from overall twisting or warping of the cross-section, affecting the entire element. In columns, local buckling can lead to localized failures, reducing load-carrying capacity, while distortional buckling affects overall stability, leading to global structural failure. Both models are crucial considerations in column design to ensure structural safety and load-carrying capacity (Ye et al., 2019).

Buckling is a flaw mostly brought on by a member's lateral deflection when an axial force is applied. This makes the column bend due to its frailty. Buckling is a sudden and rapid failure that can be dangerous. The length, strength, and other properties of a column determine whether it will buckle. Long columns may experience elastic buckling in relation to their thickness (Paul, 2014).

In an ideal model, a typical thin-walled composite structure can be characterized by three main states of work: pre-buckling, critical-buckling, and post-buckling. In this state, there is little deflection and only slight compression of the structures. The maximum axial load that the structure can support before buckling is known as the critical load. The system reaches equilibrium at critical load, which also serves as the bifurcation point between the two states of pre-buckling and post-buckling. The linearity of a structure terminates at this point, and non-linearity should be considered after the applied load exceeds the bifurcation point. Finally, a post-buckling condition is one in which bending-related deformation increases. In a post-critical state with severe overloading present, structural integrity is lost, leading to damage. The first stage of moving the structure into a post-critical condition of operation is reaching the bifurcation point. Post-critical behavior notably influences axial compression in structures, primarily governed by buckling and load-carrying capacity. As compressive loads increase, wall deflection rises consistently in post-critical equilibrium. This allows the structure to remain operational even after buckling occurs.

In general, linear-buckling analysis and nonlinear-buckling analysis are the two types of analysis that are frequently employed to analyze the buckling on thin-walled structures. The critical buckling load for the plate is determined by using Eigenvalue buckling analysis, also referred to as the linear analysis or Euler's buckling analysis. A load factor or load multiplier will be generated by ABAQUS when a system is subjected to an arbitrary load to reach the bifurcation point. ABAQUS will apply the critical buckling load by multiplying the input load, regardless of whether the load that applied is smaller or greater than the critical buckling load. Linear buckling analysis is a method for predicting the potential buckling capacity of an ideal linear elastic system. It is also known as eigenvalue buckling analysis. The classical Euler method calculates column buckling through linear analysis. For more precise buckling load predictions, non-linear analysis is superior. It involves a non-linear static analysis, pinpointing the instability point as loads increase, as discussed by Sudhirsastry et al., (2015). In summary, linear analysis is simpler, while non-linear analysis provides a more robust solution.

2.3.2 Effect of Cutout

To save weight and to allow for assessment and construction services, thin-walled parts are frequently sliced open. Due to the transfer of stresses caused by this perforation, the structural member's ultimate strength and elastic stiffness may alter. Typically, as a section of the structure is lost, the critical load of a thin-walled member with cutouts should drop. However, due to its size, this type of structure is vulnerable to buckling, which is made worse by the existence of gaps. The buckling behavior of structural members with perforations is directly affected by the type, size, location, and number of perforations (Khazaal et al., 2021). Thin-walled perforated channel beams under compression loads were the subject of the study. To examine their effect on the beam's buckling strength, three parameters—the geometry of the apertures, the opening ratios, and the spacing proportion—were chosen. Using the Taguchi technique and ANOVA, the authors aimed to find the ideal combination of the aforementioned factors in a perforated thin-walled construction for aluminum 6061-T6. According to their findings, a hexagonal form with an opening ratio of 1.7 and a spacing ratio of 1.3 provides the best buckling strength. Cutouts can significantly affect the buckling behavior of thin-walled structural members by reducing their load-carrying capacity. Factors like cutout size, shape, location, and aspect ratio influence this impact on buckling behavior.

To determine their impact on buckling, research was done on the thin-walled members with I-section cross-member changeable hole length and diameter. They claimed that the length has no discernible influence on buckling (Różyło & Wrzesińska, 2016). However, the dimension of the holes does alter the member's capacity to support greater loads. The size of the critical load that a member may apply increases with diameter, it has been determined. In contrast to previous research by (Khazaal et al., 2021), this report does not specify a maximum hole width or number of holes. In addition towards his study of the relationship between slenderness ratio and stability, (Guo, 2020) the impact of perforations on thin-walled members has been researched. It was determined that for a single hole during the structure, the buckling overall stability coefficient decreased as hole size increased. In contrast, for thin-walled members with numerous circular holes, stability rises as hole spacing increases. The size of the entrance, however, affects this. According to his research, adding additional holes has no discernible impact on stability when smaller holes are present. This was made evident by including the subject's dimensions, as may be seen below.

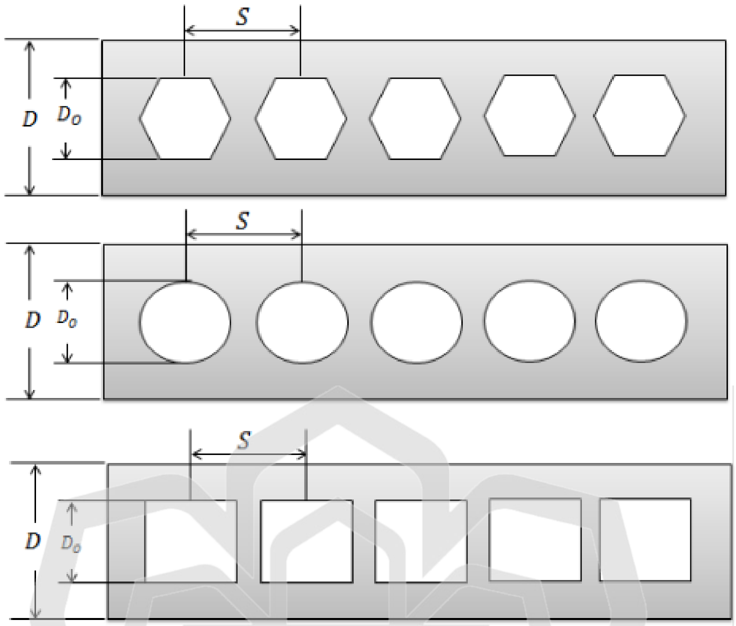

Figure 2.3. Perforated thin-walled (Khazaal et al., 2021)

Composite plates often incorporate cutouts of various sizes and shapes. These serve multiple purposes, such as access ports for mechanical or electrical systems, damage assessment, or even functioning as doors and windows. Additionally, they contribute to reducing the overall structure's weight, as highlighted by Erkliğ and Yeter, (2012). Figure 4 from their research reveals that elliptical cutouts exhibit the highest critical buckling load up to a 45° orientation, while circular cutouts surpass others beyond this angle. Furthermore, the study indicates that as the cutout area increases, the critical buckling load decreases (Erkliğ & Yeter, 2012).

2.4 BUCKLING ANALYSIS UNDER THERMAL LOAD

Buckling, also known as a loss of stability, is typically a bad thing. It has been demonstrated that a structure can continue to support a compressive force even after buckling while functioning steadily. However, buckling analysis of various structures is still important to ensure the structural integrity completely and to perform the design optimization.

2.4.1 Thermal buckling in thin-walled sections

Thin-walled members are highly efficient in utilizing materials to resist buckling. They can be easily shaped into various forms with a high shape factor, requiring minimal material due to their composition of multiple thin-walled parts. However, like formed plates, thin-walled members are prone to experiencing issues such as local buckling. Figure 2.7 illustrates some of the most used thin-walled sections.

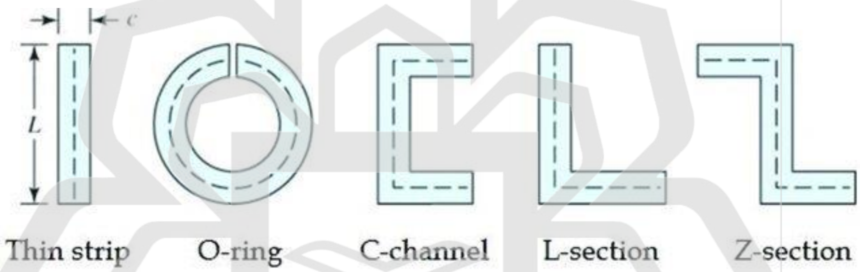

Figure 2.4. Thin walled sections (Hwong, 2019)

In most cases, when a thin-walled column is subjected to a compressive force, the individual plates that make up the member buckle before the column collapses (Lee et al., 2009). As everyone is aware, a thin-walled structure is one whose thickness is significantly less than its height and width. Due to its unique properties, including having significant strength and stiffness with low weight, It is a load-bearing profile that is widely used in current technology, including the aerospace, automotive, and construction industries (Różyło, 2017). Different forms of thin-walled structures are used depending on the application in the industries. For instance, Biagi et al., (2020) investigated T-shaped thin-walled structures with diverse geometries, commonly employed as ribs in aircraft. Similarly, Rozylo and Debski, (2020) conducted experiments on composite thin-walled Z-shaped structures. Thin-walled structures hold particular interest due to their potential enhancements, benefiting not only themselves but also other structural components.

Various industries, including aviation, manufacturing, and structural engineering, widely employ these materials (Doan and Thai, 2020). In response to the growing demand for lightweight and efficient structures, engineers and scientists have embraced composite materials in diverse applications. Composite material design, with its unique strengths and thermomechanical characteristics, seeks to achieve superior performance not achievable with conventional materials (Sudhirsastry et al., 2015). The physical characteristics of composite materials are greatly influenced by the orientation of the fibers. Due to these characteristics, the shell stiffness affects the critical buckling load (Lvov et al., 2015). The buckling attitude of axially loaded columns with thin-walled open sections and non-uniform cross-sectional properties has been studied analytically in (Cheng et al., 2015). The results demonstrate that nonuniform temperature distribution can result in nonuniform mechanical property distribution. The pre-buckling stress in axially laden columns can be affected by the nonuniformity of both the temperature and mechanical characteristics. Angles and channels with thin walls and open monosymmetric sections are prone to buckling in both flexural and flexural-torsional modes. The importance of either mode depends on the cross-section's dimensions and shape. As a result, flexural-torsional buckling must be considered when designing these members. This is typically done by using the same column strength curve as for flexural buckling and the same slenderness ratio calculation.

Thin-walled composite structures, often featuring central cutouts, possess substantial load-carrying capacity potential under axial compression. However, comprehending factors that may induce permanent structural deterioration, such as damage initiation, delamination, and material cracking, is vital. This knowledge is pivotal for developing more accurate predictive models for these structures' limit states. In an exhaustive investigation by Rozylo and Falkowicz, (2021), thin-walled composite structure failure phenomena were explored via a multi-pronged approach. This encompassed employing a universal testing machine, the acoustic emission method, and optical deformation measurement using the ARAMIS system. Additionally, finite element simulations incorporated three distinct models: progressive failure analysis (PFA), cohesive zone model (CZM), and a model centered on material crack initiation and propagation (xFEM). This comprehensive strategy enabled a meticulous assessment of structural failure behavior. Test results facilitated the establishment of damage initiation criteria, facilitating both experimental and numerical assessment through post-critical equilibrium paths and acoustic emission signals. In another innovative contribution by Barut and Madenci, (2010) a novel analytical/numerical method was devised to analyze the buckling behavior of symmetric laminates featuring circular or elliptical cutouts. This method amalgamates variational formulation with complex potential theory, automatically upholding equilibrium equations in the pre-buckling phase. Consequently, it formulates total potential energy in a streamlined manner dependent solely on boundary integrals. The pre-buckling analysis's in-plane response serves as the baseline state for the subsequent buckling investigation.

2.4.2 Thermal Buckling in Column

In civil, mechanical, and aeronautical engineering, structural components such as columns and plates find common use. In aircraft structures, like landing gears, vented inter-stages, stub adaptors, inter-tank structures, and mounting legs, slender and short columns play vital roles. In these weight-sensitive, highly optimized structures, precise evaluation of buckling and post-buckling stresses is paramount (Gupta et al., 2010). Researchers have extensively employed analytical or approximative continuum (energy) approaches and finite element (FE) methods to analyze post-buckling problems related to thermal or mechanical aspects in structural members such as columns and plates.

Figure 2.5. Buckled steel column.

To study the thermal or mechanical post buckling of columns and plates, approximate continuum (energy) approaches like Rayleigh-Ritz and finite element ways are used. It is necessary to assume that the field variables considered in the problem have sufficient approximative admissible displacement functions to accurately estimate buckling and post-buckling loads using an energy approach, such as the Rayleigh-Ritz method. The correctness of the R-R method-obtained solution depends on the exactness of the selected approximative acceptable displacement field variation (Gupta et al., 2009).

In contrast to the post buckling behavior of mechanically compressed columns, the column demonstrates remarkable resilience in the presence of thermal loading, meaning that temperature can rise over the buckling value before the collapse. Material constants can always be expressed as polynomials since they are continuous functions of temperature, as has been demonstrated. Columns behave very differently in a fire or at elevated temperatures than they do at room temperature. In addition to altering the material characteristics of steel, elevated temperatures also cause more compressive stress because of the thermal constraint. Steel constructions are often more prone to fire than reinforced concrete structures because the temperature in steel can rise very quickly. In recent years, the issue of steel constructions exposed to fire conditions has drawn more and more attention (Birman, 2022).

2.4.3 Thermal buckling in plates

Aerodynamic heating may be the cause of plate elements in supersonic aircraft deflecting off the plate's plane. If the plate is unrestrained and the temperature that distribution is linear throughout the plate's volume, deflections may happen without thermal strains manifesting. Thermal stresses are nevertheless induced if the plate is constrained or if the temperature distribution is nonlinear. If the temperature changes across the thickness of a plate, deflections of a plate happen as the heating process begins, but if the temperature is constant, they don't happen until a critical temperature is achieved. This final type of distortion is an illustration of middle-surface stresses that vary across the plate buckling a flat plate.

Laminated composite is often used in place of conventional metal for the skin panels of aircraft wings and fuselage to lighten the weight of flight apparatus. One of the most important factors to consider when designing composite skins for aircraft wings is panel buckling. The structural panels of high-speed aircraft are susceptible to both aerodynamic heating and aerodynamic loading. The increase in temperature could cause the plate to buckle and run out of load-bearing capacity (Shiau et al., 2010). In their initial effort to comprehend thermal buckling in plates, Gossard et al., (1952) used The Rayleigh-Ritz procedure to analyze a simply supported rectangular homogeneous isotropic plate that was exposed to a tent-like temperature distribution.

Exploring the buckling and post-buckling characteristics of thin plates, especially advanced composites with cutouts, is a crucial research field. Composite plates with cutouts are increasingly used in aeronautical structures due to their impressive stiffness-to-weight and strength-to-weight ratios, offering substantial weight reduction opportunities (Nemeth, 1995). Figure 2.6 depicts a composite plate featuring a circular cutout.

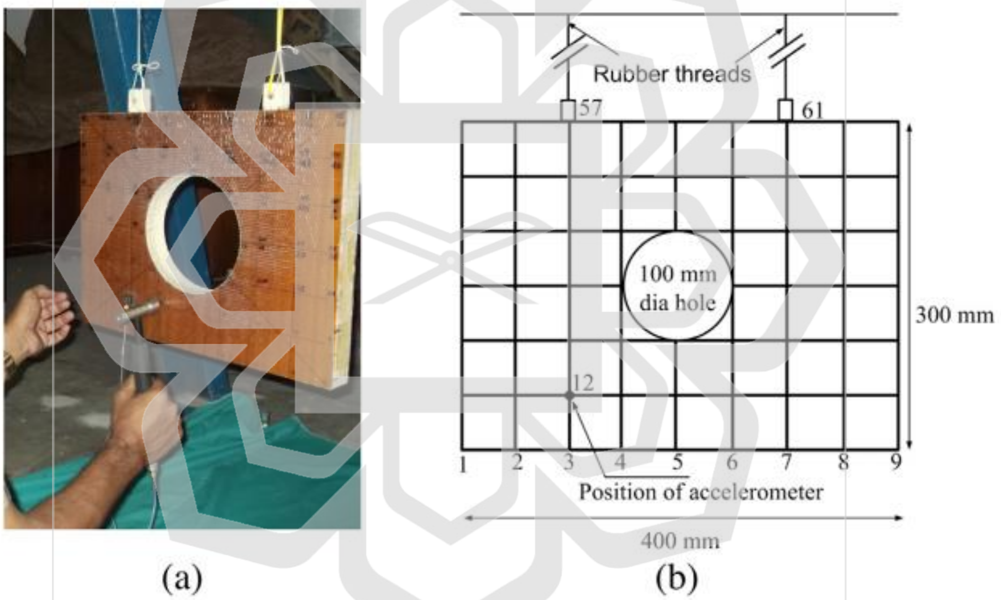

Figure 2.6. Composite plate with cut out (a) Model testing and (b) schematic diagram (Mondal et al., 2015)

Considerable research efforts are focused on buckling in composites, as evident from various studies. For instance, Emam and Nayfeh, (2009) explored the post-buckling behavior of composite beams employing linked displacement criteria. They employed the equilibrium equation to ascertain axial displacement. Chen et al., (1991) investigated thermal buckling in laminates under uniform or non-uniform temperature fields via finite element analysis (FEM), also considering the influence of cutting using

FEM. Shaterzadeh et al., (2014) conducted research on the thermal buckling of composite plates featuring cutouts. The researchers developed a first-order shear deformation theory, which is a mathematical model that accounts for the shear deformation of plates, and used isoperimetric elements, which are a type of finite element that is well-suited for modeling plates with cutouts. They investigated the influence of various factors on critical thermal buckling temperature and found that anti-symmetric composite plates had higher critical thermal buckling temperatures than symmetric plates.

Cutouts are frequently integrated into structural elements to enhance efficiency and reduce weight. They are crucial in the design of wing spars and cover panels for both military and commercial transport wings, enabling access to hydraulic and electrical lines, as well as facilitating damage inspection. Nevertheless, the thermal buckling behavior of rectangular composite plates featuring square/rectangular and elliptical/circular cutouts has received less attention compared to other buckling types. Such plates with cutouts commonly experience membrane stresses from thermal or mechanical loads, making buckling a primary mode of failure (Lakshmi Narayana et al., 2018). Analyzing the thermal buckling behavior of plates with cutouts is crucial for efficient structural design. Unlike plates under uniform compression with analytical buckling solutions, plates with cutouts require the development of numerical techniques because the non-uniform stress field is caused by the presence of the cutout.

Analytical techniques for assessing plate buckling with cutouts entail two consecutive phases: (1) evaluating the pre-buckling condition to ascertain in-plane stress distribution prior to buckling, and (2) assessing the buckling state, which arises from in-plane stresses linked to the pre-buckling state. A plethora of both numerical and analytical investigations have been undertaken to comprehend plate responses to thermal and mechanical loads (Shaterzadeh et al., 2014).

In thermal buckling analysis, columns behave differently when subjected to thermal loading compared to mechanical loading. Mechanical loads apply uniform stresses across the column's length, while thermal loads cause temperature gradients that result in uneven thermal expansion. This differential expansion can induce lateral displacement, leading to thermal buckling. In fire conditions, elevated temperatures reduce the steel's yield strength, further compromising structural integrity. The combination of reduced material strength and uneven thermal expansion can accelerate thermal buckling, increasing the risk of structural failure. Therefore, analyzing thermal effects is crucial in fire engineering to ensure the safety and stability of steel constructions (Moura Correia et al., 2014).

2.5 STRUCTURAL ANALYSIS USING SOFT COMPUTING APPROACHES FOR MECHANICAL LOAD

Utilizing laminates increases design flexibility and provides greater control to modify the material to satisfy regional design specifications. However, compared to isotropic materials, the laminate design presents a far greater challenge in terms of sizing, optimization, and rules for spatial variation (Dinh Nguyen et al., 2020). Mathematical optimization is an obvious method for the design of laminated composite structures because the possibility of achieving an effective design that satisfies the overall criteria and the challenge of choosing values from a vast set of limited design variables (Awad et al., 2012).

2.5.1 Genetic Algorithms

At the University of Michigan in the 1970s, John Holland is credited with coming up with the concept of a genetic algorithm. Holland was more interested in developing artificial systems based on the laws of natural selection than systems that are based on a particular thought process. These artificial systems could be built with the use of computer software and used in several areas that place a strong emphasis on design, optimization, and machine learning. Neural networks and genetic algorithms are entirely separate ideas with quite different applications. To identify ideal or nearly ideal solutions to search and optimization issues, genetic algorithms are search-based optimization algorithms. On the other hand, neural networks are mathematical models that represent the mapping between intricate inputs and outputs. Genetic algorithms are search techniques that use a population of designs and mimic biological evolution. Figure 2.8 shows some basic differences between Genetic Algorithms and Neural Networks.

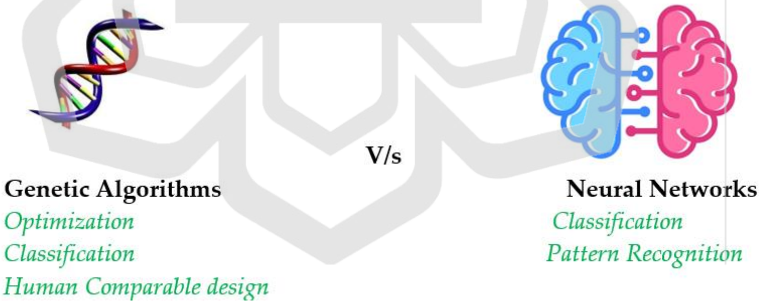

Figure 2.7. Genetic algorithm and neural networks

Genetic algorithms are ideally adapted to solve the combinatorial challenge of designing composite laminates. However, even for a single laminate, thousands of tests may be needed for genetic optimization. As a result, it's crucial to adapt common genetic algorithms to the unique issues related to composite laminates. Stacking sequence optimization issues are ideally suited for genetic algorithms. They cope with combinatorial issues with ease and provide many potential solutions with ease. Their primary drawback is that dozens or even millions of analyses are typically needed. The vast number of necessary analyses is not a concern because the computational costs of a single study are typically relatively inexpensive for many laminate design problems. Figure 2.9 shows the pictorial representation of a genetic algorithm.

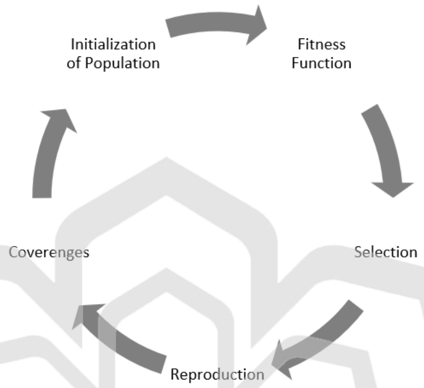

Figure 2.8. Process of genetic algorithm

Almeida and Awruch, (2009) presents a method for designing composite laminated structures that uses a GA and the FEM. The GA is used to search for the optimal design, while the FEM is used to analyze the structural performance of the designs. In the study by Bagheri et al., (2011), a GA is employed to optimize the design of ring-stiffened cylindrical shells. The primary goal is to simultaneously maximize the shell's fundamental frequency and minimize its structural weight. This optimization process considers six design variables: shell thickness, the number, size, and height of stiffeners, eccentricity distribution order of the stiffeners, and spacing distribution order of the stiffeners. Moreover, four constraints related to structural weight, axial buckling force, and radial buckling load are adhered to. Previous research has demonstrated the effectiveness of combining the extended finite element formulation (XFEM) with genetic algorithms (GAs) for identifying structural defects efficiently. This method converges to the real defect by modelling the forward problem using the XFEM and using a GA as the optimization strategy. The study Chatzi et al., (2011) suggests various improvements to the XFEM-GA method, most notably a unique genetic algorithm that quickens the scheme's convergence and reduces entrapment in local optima.

Abueidda et al., (2019) introduces a convolutional neural network (CNN) model to predict mechanical properties of checkerboard composites. It demonstrates that the CNN model, integrated with a genetic algorithm, effectively predicts stiffness, strength, and toughness of composites. Finite element analysis is used for training data, focusing on two phases of materials: soft/ductile and stiff/brittle. The study illustrates machine learning's potential in materials science, particularly for optimizing composite materials' microstructural designs, enhancing their mechanical properties in aerospace and engineering applications. Liu et al., (2023) presents a novel approach for optimizing the weight of laminated composite structures using ANNs and GAs. It introduces a methodology where ANNs are trained to predict buckling loads from finite element analysis data, reducing computational costs significantly. By integrating these models with GAs, the study efficiently optimizes stacking sequences and structural dimensions of laminates. The method's effectiveness is demonstrated through optimization of various composite structures, showcasing its potential in advanced material design and engineering applications. Stephen et al., (2022) study integrates FEA and ANNs to predict the impact performance of fiber-reinforced polymer composites. It evaluates the impact resistance of hybrid and non-hybrid fabric reinforced composites using high-velocity simulations. Key findings indicate a strong correlation between FEA results and ANN predictions, with maximum variation of about 6.6%. The study demonstrates the effectiveness of using computational methods in predicting the impact behavior of composites, suggesting their practical utility in material design and analysis.

Composite laminates can be crafted using straight-fiber layers or a matrix with curved fibers, known respectively as constant stiffness and variable stiffness designs. Ghiasi et al., (2010) research concentrates on the latter, exploring variable stiffness composite laminates. In another study, Badalló et al., (2013) evaluates three prominent genetic algorithms: Neighborhood Cultivation Genetic Algorithm, Archive-based Micro Genetic Algorithm, and Non-dominate Sorting Genetic Algorithm II. They analyze the impact of three different initial population strategies on their performance in terms of solution quality, computation time, and generational efficiency. Meanwhile, (Yong et al., 2008) employs a GA to optimize the response of composite laminates under impact conditions. The two impact scenarios that are discussed are the high-velocity impact of a spherical impactor on a rectangular plate and the low-velocity impact of a thin laminated strip. By adjusting the ply angles in both situations, the GA sought to minimize the peak deflection and penetration, respectively.

Karakaya and Soykasap, (2009), a composite panel made of alternating layers of metal sheets and fiber-reinforced polymer is subjected to biaxial in-plane compressive stresses. The genetic algorithm and generalized pattern search algorithms are used to determine the best stacking order for the panel. By combining an objective on genetic algorithm and a resilient design technique, a new methodology may be used to enhance the mechanical properties and responsiveness of HCSs for off-design scenarios (D. S. Lee et al., 2013). The approach of optimum design for laminated composite structures utilizing the GA and FEM for single-material and hybrid laminates is covered in the (Deka et al., 2005). For 3-D finite element analysis, eight-nodded layered elements have been used. To determine the best combination of laminate sequences for hybrid composite structures, an optimization approach using a distributed/parallel objective on genetic algorithm is connected with an analysis tool for composite structures based on finite element analysis (D. S. Lee et al., 2013).

The objective of the study conducted by Gillet et al., (2010) is to assess the impact of various parameters in the context of composite structure optimization. A study was done on all potential orientations and the makeup of the component materials. A genetic algorithm was used to solve issues with optimizing simple plates and structures that were modelled using finite elements. Because of their computational cost, nonelites approach, and requirement to provide a sharing parameter, objectives evolutionary algorithms (EAs) that use nondominated sorting and sharing have drawn significant criticism. Deb et al., (2002) introduced the nondominated sorting genetic algorithm II, a objectives evolutionary algorithm designed to address several issues. In a study by Cai and Aref, (2015), a genetic algorithm-based optimization approach was applied to determine the optimal distribution of materials like glass fiber-reinforced polymer and concrete in hybrid deck systems, as well as carbon fiber-reinforced polymer and steel in hybrid cable systems. Shrivastava et al., (2018) employed a traditional genetic algorithm combined with a computer-aided engineering solver to reduce the weight of multi-laminate aerospace structures. This endeavor tackles structural weight minimization, an objective on problem optimization that necessitates compliance with design constraints for strength and stiffness.

Sliseris and Rocens, (2013) it is suggested to use a new optimization method for composite plates with discretely variable stiffness. There are three main steps to it. The first phase involves analyzing the best continuous variable bending and shear stiffness of the plate while reducing structural compliance and stress field variations. The second phase involves using a GA to solve a minimization problem to optimize the size of discrete domains. Park et al., (2008) the authors propose novel strategies to decrease the number of fitness function assessments in GAs used for the transdisciplinary optimization of composite laminates.

2.5.2 ML Algorithms

In composite structure design, structural analysis is commonly employed. Typically, to evaluate the mechanical properties of different designs, numerical FEA is used. However, this approach often requires expensive multi-physics computational calculations. The goal is to produce lighter laminates with increased strength while reducing costs and efficiently collecting data for composite optimization. Nevertheless, a major drawback of numerical simulation is the high computational cost associated with setting up model properties and solving complex differential equations. To expedite the FEA process, one approach is to leverage ML and optimization techniques, which have demonstrated great success in various industries, including manufacturing and materials design. ML can work directly on predefined input parameters and automatically predict simulation results, eliminating the need for manual design of composite structures and FEA setups.

ML enables researchers to assess the importance of different features and quickly modify design parameters due to its rapid and accurate prediction of FEA outcomes. This technique can potentially be applied to simulate composite laminate structures as well. Many studies have focused on utilizing ML and surrogate modeling techniques to predict the mechanical properties of composite laminates, such as strength and modulus. These methods provide result-oriented predictions that specify design characteristics. However, they may present challenges when attempting to predict process-oriented outcomes, such as the displacement field of an entire structure. ML plays a crucial role in anticipating failure modes, such as delamination, in the fracture process of composite materials. These ML applications can be combined with popular optimization techniques like genetic algorithms. Figure 2.10 illustrates the various types of machine learning employed in this context.

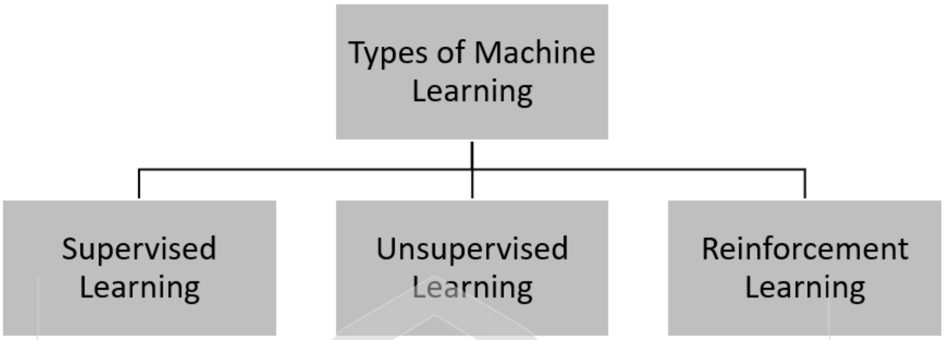

Figure 2.9. Types of machine learning

The groundbreaking study of Furtado et al., (2021) marks the first instance of utilizing machine learning approaches to predict the statistical design allowable for composite laminates. In this study, four machine algorithms are utilized to forecast the notched strength and strength distribution of composite laminates. The approach is statistical, accounting for uncertainties tied to material properties and geometry. In another research endeavor by Jung and Chang, (2021), they devised a structural health monitoring system for intelligent composite structures. This system integrates signal processing, deep learning algorithms, and optimization theory for enhanced performance. The system uses smart composite fabrics embedded with piezoelectric ribbon sensors to enable self-monitoring capabilities. Saberi et al., (2021) employ a deep learning approach using artificial neural networks to determine the free vibration parameters of rectangular bistable composite plates. This marks the first instance of applying deep learning to analyze the behavior of such plates. To streamline the design of composite laminates efficiently, Sorrentino et al., (2022) introduces a theory-guided ML model that merges the Hashin failure theory with classical lamination theory. Table

2 provides an overview of the types of machine learning algorithms employed in recent studies.

Table 2.1 Machine learning algorithm

Reference	**Machine learning mechanism**
(Furtado et al., 2021b)	XG Boost, Gaussian Processes, Artificial Neural Networks and so on.
(Jung and Chang, 2021)	Signal processing, deep learning algorithms
(Sorrentino et al., 2022)	Integrated HFT and CLT
(Machado et al., 2022)	ML based on convolutional NN architecture.
(Zhang et al., 2022)	FEA and ML

Machado et al., (2022) propose a machine-learning strategy based on convolutional neural networks to automate void content analysis in optical microscope images. This method eliminates the necessity for parameter adjustments, ensuring both efficiency and precision in void analysis. On the other hand, Zhang et al., (2022) introduce a technique merging FE analysis with machine learning to evaluate multiple mechanical characteristics of composite laminates. This innovative approach has been effectively applied to scenarios like identifying failure factors and critical buckling eigenvalues in open-hole laminates, delivering valuable insights into composite material behavior.

Furtado et al., (2021a) presents an innovative methodology for predicting the notched strength of composite laminates using machine learning. It explores four algorithms (XGBoost, Random Forests, Gaussian Processes, and Artificial Neural Networks) to predict statistical design allowables. The study not only focuses on Legacy Quad Laminates but also introduces the concept of double-double laminates. The findings show accurate predictions with generalization errors around ±10%, demonstrating the potential of machine learning in enhancing the design and certification process of composite materials in aerospace applications.

Reiner et al., (2021) introduce a novel technique to precisely depict the macroscopic strain-softening behavior in laminated composites when subjected to compressive loads. Their approach involves computer simulations of compact compression tests on quasi-isotropic IM7/8552 carbon fiber-reinforced polymers, resulting in an extensive virtual dataset. They employ two distinct ML methods to train models for predicting the strain-softening response. One approach employs a theory-guided neural network architecture, while the other utilizes recurrent neural networks featuring Long Short-Term Memory architecture. Table 3 summarizes different optimization techniques used in recent studies, along with their respective objectives.

Table 2.2 Optimization techniques

Reference	**Algorithm**	**Objective**
(Bagheri et al., 2011)	Genetic Algorithm	To look for the shell's largest fundamental frequency and lowest structural weight
(Ghiasi et al., 2010)	Genetic Algorithm	Variable stiffness design of composite laminates
(Yong et al., 2008)	Genetic Algorithm	Optimize the reaction of a composite laminate subject to impact
(D. S. Lee et al., 2013)	Genetic Algorithm	To determine the best combination of laminate sequences for hybrid composite structures
(Karakaya and Soykasap, 2009)	Genetic Algorithm	To determine the best stacking order
(Furtado et al., 2021b)	Machine learning	The statistical design allowable for composite laminates are being predicted
(Jung and Chang, 2021)	Machine learning	To develop a system for monitoring the structural integrity of intelligent composite structures.
(Saberi et al., 2021)	Machine learning	The characteristics of free vibrations in rectangular bistable composite plates are identified.

(Machado et al., 2022)	Machine learning	To offer a reliable tool capable of automatically analyzing the void content in optical microscope images without requiring manual parameter adjustments.
(Reiner et al., 2021)	Machine learning	To accurately characterize the overall strain-softening behavior of laminated composites under compressive loads

2.6 STRUCTURAL ANALYSIS USING SOFT COMPUTING APPROACH FOR THERMAL LOADS

Composite laminates are widely used in various industries due to their exceptional mechanical properties and lightweight nature. However, thermal buckling is a critical concern that can affect the structural integrity of composite laminates under temperature variations. Traditional analytical and numerical methods have limitations in accurately predicting thermal buckling behavior due to the complex nature of composite materials Mehar and Panda, (2019). In recent years, soft computing techniques have emerged as valuable tools to address these challenges and enhance the analysis of thermal buckling in composite laminates. This essay explores the application of soft computing techniques in the field of thermal buckling analysis, focusing specifically on composite laminates. Soft computing approaches can be useful for analyzing thermal buckling in composites and columns. However, it's worth noting that the selection of the appropriate soft computing technique depends on the specific requirements of the problem, available data, and the desired level of accuracy. Additionally, combining multiple soft computing approaches or integrating them with traditional numerical methods can provide more robust and accurate predictions for thermal buckling analysis (Men et al., 2022). Figure 2.11 shows the soft computing approaches for thermal buckling. Sarhadi et al., (2022) explores the use of machine learning for detecting thermal imaging damage in glass-epoxy composite materials. It focuses on training a machine learning model with artificially generated thermal images derived from 3D finite element models. The study aims to accurately characterize fatigue damage hotspots in composites, a challenging task due to factors like size, shape, and internal temperature of hotspots. Results show high prediction accuracies (85%-99%), demonstrating machine learning's potential in enhancing damage detection methods for composite materials.

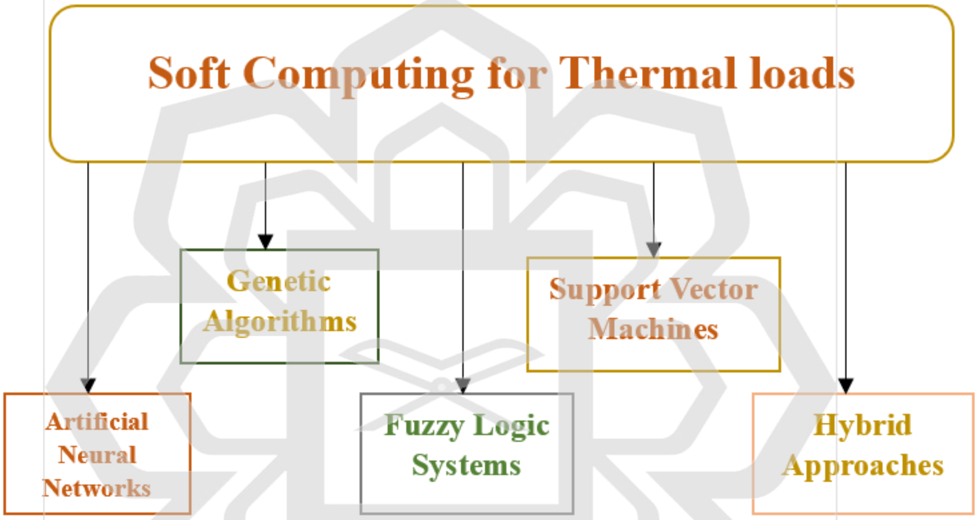

Figure 2.10. Soft computing approaches thermal buckling.

2.6.1 Artificial Neural Networks

Artificial Neural Networks (ANNs) have gained popularity in predicting the thermal buckling behavior of composite laminates. ANNs can learn complex relationships between input parameters (such as material properties, temperature, and geometry) and the buckling response. By training the network on a dataset that includes various input-output pairs, ANNs can effectively model the nonlinear behavior of composite laminates under thermal loading. Once trained, ANNs can accurately predict the buckling behavior for new input conditions, enabling engineers to optimize the design and mitigate thermal buckling risks. Artificial neural networks (ANNs) have been built in Ngamkhanong and Kaewunruen, (2022) to determine the relationship between safe temperature and buckling temperature, two outputs, and various ballasted track circumstances. Similarly, a thin-walled structure for civil constructions' finite element stability was examined in (Susac et al., 2017). A neural network model was improved and utilized to find the thermal bending behavior of the analyzed structure.

2.6.2 Genetic Algorithms

Genetic Algorithms (GAs) are a powerful optimization tool for enhancing the thermal buckling resistance of composite laminates. GAs simulates natural selection and evolution to search for the optimal combination of design variables. In thermal buckling analysis, GAs can optimize parameters like fiber orientation, stacking sequence, and laminate thickness to improve buckling resistance under varying temperatures. By defining appropriate fitness functions that assess buckling behavior, GAs efficiently explores the design space, identifying optimal solutions that minimize the risk of thermal buckling.

In the study by Mahdavi et al., (2020), the FE method is used to find the thermal buckling load of hybrid composite plates with quasi-square cutouts. Employing the Genetic Algorithm, the study identifies the best design variables affecting the thermal buckling load for different stacking sequences and boundary conditions to achieve the maximum thermal buckling load value. It has been examining the streamlining of composite plates that have been overlaid to address thermal buckling under stress and apply contiguity requirements. Utilizing two different methodologies, namely the regression model and the genetic algorithm to numerically simulate design arrangements, evolutionary strategy was used to address the forced discrete advancement issue.

2.6.3 Fuzzy Logic Systems

Fuzzy Logic Systems (FLS) provide a framework to handle uncertainties and imprecisions inherent in thermal buckling analysis. Composite laminates exhibit material property variations, manufacturing defects, and environmental uncertainties that affect their buckling behavior. FLS can capture this uncertainty and fuzziness by defining fuzzy sets and fuzzy rules based on expert knowledge or experimental data. FLS can then model the relationship between input parameters and buckling response, enabling engineers to make informed decisions and assess the risk of thermal buckling in composite laminates.

Research has been conducted in this field due to the diverse applications of the proposed approach. Štemberk and Khmurovska, (2021) introduced a fuzzy logic-based model that considers temperature, relative humidity, and the height of a structure to evaluate the thermal performance of insulated concrete walls in terms of the U-value. The study gathered results and drew meaningful conclusions from the findings.

2.6.4 Support Vector Machines

Support Vector Machines (SVMs) have shown promise in predicting the thermal buckling behavior of composite laminates. SVMs are machine learning algorithms that can be formulated as regression or classification tasks. By training on a dataset that includes input parameters and corresponding buckling responses, SVMs can learn a decision boundary or a mapping function to predict the buckling behavior for new instances (Salcedo et al., 2014). SVMs offer good generalization capabilities and can handle high-dimensional input spaces, making them suitable for thermal buckling analysis of complex composite laminates. For data classification and interpolation, a support vector machine (SVM)-based machine learning technique is employed in (Panels, 2021). A formulation is used to manage the combination of mass minimization and buckling evaluation under combined load. The convergence to an ideal design is sped up by selecting a deterministic algorithm for the optimization cycle.

2.6.5 Integration and Hybrid Approaches

To further enhance the accuracy and robustness of thermal buckling analysis in composite laminates, integration and hybrid approaches combining multiple soft computing techniques or integrating them with traditional numerical methods can be employed. For instance, combining ANNs and GAs can enable the optimization of laminate designs considering the thermal buckling behavior accurately predicted by ANNs (Malekzadeh et al., 2014). Additionally, integrating soft computing techniques with finite element analysis can leverage the strengths of both methods, enabling a comprehensive analysis of thermal buckling in composite laminates.

2.7 RESEARCH GAP

The design of composite thin-walled structures needs careful consideration of structural and mechanical parameters because each parameter for a given structure will result in a distinct set of buckling loads. As composites is not a specialized industry and offers virtually limitless possibilities to combine and build the item, the design of composites adds another level of complexity. Because they are either designed for any kind of structures. As a result, present work either has an approach that is too general or too component specific. Therefore, proposing and using more efficient design for c-section thin-walled composite channel.

The extensive literature survey conducted in this study clearly indicates that the optimization of laminated composites under various loading conditions remains an active and ongoing area of research. It is evident that new techniques for optimizing laminated composites reveal a promising opportunity for enhancing the analysis, especially when considering different components of a composite structure to achieve the most optimal design. Most of the existing optimization efforts have centered around genetic algorithms, while the utilization of modern machine learning approaches for optimization remains scarce in the literature. This highlights a significant gap that can be explored and leveraged to further improve the optimization process for laminated composites. Furthermore, the literature review reveals a limited amount of research focused on the thermal buckling of laminated thin-walled structures with holes. Additionally, the optimization of such structures has been largely unexplored and lacking in the existing body of literature. These findings underscore the importance of investigating and optimizing these specific types of structures to advance our understanding and design capabilities in this field. Table 2.3 illustrated some of the work which has been done in last few years that focusing on critical buckling

Table 2.3 Limitation and technique used in the previous studies

Type of structure	**Technique adopted**	**Focused parameters**	**Limitations**	**Reference**
Laminated plates with holes	FEM and DOE	The signal-to-noise ratio was employed to explore how fiber orientation angles and cutout shapes	Fiber orientation angles and cutout shapes of the plates	EVRAN, (2020)

		influence the critical buckling temperature of the plates.		
Composite plate	FEM	Thermal buckling and dynamic properties of pressured composite plates.	Limited to pressure load which be modified to other factors such as composite materials and structures	Yang, (2022)
Reinforced plates with Hole	FEM and MATLAB simulation	Finite-element buckling analysis of functionally graded GPL-reinforced composite plates featuring a circular aperture.	Functionally graded graphene platelets-reinforced composite rectangular plates were used to simulate with FE model	Geng et al., (2021)
Variable stiffness of composite laminate	FEM	Uncertainty quantification in the buckling strength of variable stiffness laminated composite plates subjected to thermal loading.	The contribution of individual properties is performed for various boundary conditions	Sharma et al., (2021)
Laminate composite plates	FEM	An Investigation of Parametric Variations in the	The composite laminate experienced	Chhorn & Jung, (2020)

		Influence of Elliptical Holes on Thermal Buckling Behavior in Laminate Composite Plates/	thermal loading, and all its edges were clamped for support.	
Functionally graded material plates	ML-ANN	Evaluating the critical buckling load of functionally graded plates through artificial neural network modeling.	This approach is applicable for constructing artificial ANN models to address various intricate structural issues.	Duong et al., (2021)
C-section composite structure	FEM and DOE	Buckling analysis of a structure under mechanical load.	The proposed method can be done under thermal load.	Bin Kamarudin, (2022)

2.8 CHAPTER SUMMARY

Composite materials are composed of multiple materials that collaborate to achieve properties that would be unattainable for the individual components alone. Currently, both major and secondary constructions extensively utilize composite laminates. Composite laminates offer numerous advantages, including design flexibility, cost-effectiveness, enhanced productivity, chemical resistance, consolidated functionality, corrosion resistance, durability, and more. This review emphasizes the significance of composite materials and explores their diverse applications. Furthermore, it delves into optimization methods such as Genetic Algorithms and Machine Learning algorithms, providing a comprehensive explanation of their relevance. Moreover, the review serves as a guide for scientists seeking to implement composite laminates in engineering structures. It offers detailed descriptions and analyses of the literature concerning composite material applications.

Additionally, it presents an overview of research areas within the field of composite materials. By identifying research gaps, researchers can gain insights and identify opportunities for new ideas, especially during the early stages of this research domain. In conclusion, these research gaps provide valuable perspectives and indices to facilitate advancements in various research areas related to composite materials. They serve as a catalyst for researchers to develop innovative ideas, particularly in the nascent phases of this research field.

CHAPTER THREE

RESEARCH METHODOLOGY

3.1 OVERVIEW

Previous studies in the structure and various forms of structural parameters in beams and columns and other types of composite structures are overviewed and summarized. Some key factors were chosen to summarize the existing work such as the problem defined, the methodology adopted and the applications. A data optimization technique to define the composite parameters for structural analysis was explored and criticized. Furthermore, the other common types of optimization methods for different structures have been summarized. Finally, based on the existing work and methodology and a research gap was proposed for the current work.

3.2 FINITE ELEMENT METHOD

The finite element (FE) method is a numerical technique employed to solve partial differential equations (PDEs) governing the behavior of physical systems. It is a powerful tool for analyzing and simulating the behavior of structures and systems under various conditions. In the FEM, a complex problem is divided into smaller, simpler regions or elements. These elements are interconnected at specific points called nodes. By applying appropriate mathematical equations and principles, the behavior of each element and its interaction with neighboring elements can be modeled and analyzed. The basic steps involved in the FE method can be seen in Table 3.1.

Table 3.1 Describe the basic steps involved in the FEM for analyzing structures.

Steps	Action	Description
Pre-processing	Modelling	• Create a geometric model of the structure using CAD software or the FE software's tools. • Define material properties (density, Young's modulus, Poisson's ratio, etc.) for each part.
	Discretization (meshing)	• Divide the model into smaller elements (e.g., beams, shells, solids). • Choose appropriate element types based on geometry and loading conditions. • Aim for a balanced mesh that ensures both accuracy and computational efficiency
	Boundary Conditions	• Apply constraints that restrict movement or deformation (e.g., fixed supports). • Assign loads to represent forces or pressures acting on the structure
Processing (Solving)	Assembly	• Combine individual element equations into a global system of equations representing the entire structure
	Solution	• Solve the system of equations using numerical methods (e.g., matrix algebra, iterative techniques) to determine displacements, stresses, strains, and other results of interest at each node of the mesh
Post-Processing	Visualization	• Display the results graphically to visualize deformations, stress distributions, and other behaviors. • Use contour plots, deformed shapes, animations, and other visual aids
	Interpretation	• Analyse the results to evaluate structural performance, identify critical areas, and assess safety margins.

		• Compare results with design criteria or experimental data.
		• Refine the model or design as needed.
		    o Element Selection: use of SHELL181 elements, which are suitable for analyzing thin-to-moderately thick shell structures.
		    o Validation: f validating the FE model by comparing its results with existing benchmark data or analytical solutions.
		    o Buckling Analysis: it included applying boundary conditions, solving for buckling load factors, and visualizing mode shapes.

3.2.1 Geometry and Modeling

First, the FE model of the thin-walled structure is created using a 3D ANSYS workbench software, and the model is then discretized into smaller elements using meshing options. The mesh size and quality are critical parameters that can significantly affect the accuracy of the results. Figure 3.2 shows the model is a C-section channel made of glass fiber-reinforced polymer. It has a height of 80 mm, a width of 40 mm, and a length of 250 mm. The flanges and web of the channel are composed of eight layers of 0.125 mm laminated sheets, with a total thickness of 1 mm. The details of the model are given below.

- Thickness (flange and web) per layer= 0.125 mm
- Total thickness= 1 mm
- No. of layers= 8
- Orientation = 4 types
- Quasi-isotropic: - (0/90/45/-45) s

- Angle-ply: -(45/-45/45/-45) s
- Cross-ply: -(0/90/0/90/0/90/0/90)
- Balanced: - (-45/30/60/30/-30/45/-60/-30)

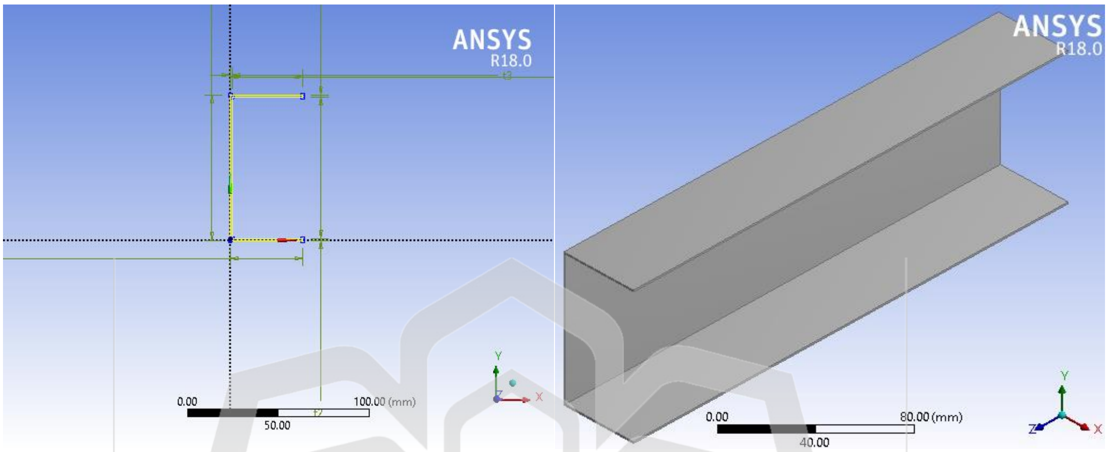

Figure 3.1 Model description (geometry and solid) with its dimension

The FE model was used to investigate the effects of parameters and analysis on the laminated composite shell structure under mechanical and thermal loads. For this, ANSYS software was used to simulate the results. To validate the current FE model existing benchmark results were simulated and compared the results with current ANSYS results. The FE modeling for this research will be conducted using the SHELL181 element. The SHELL181 element is a four-node shell element designed for analyzing shell structures ranging from thin to moderately thick. Each node of this element possesses six degrees of freedom, encompassing translation along the x, y, and z axes, as well as rotation around the x, y, and z-axes. In cases where the membrane option is selected, the element retains only translational degrees of freedom. The SHELL181 element is particularly suitable for applications involving linearity, significant rotations, and large strain nonlinearity.

The SHELL181 element, a four-node shell component, accommodates variations in shell thickness during nonlinear analyses. It offers support for both full and reduced integration schemes within the element domain, considering the effects of distributed pressures, including follower (load stiffness). This element finds relevance in layered applications like composite shells and sandwich structures. The accuracy of modeling composite shells adheres to the first-order shear deformation theory, notably the Mindlin-Reissner shell theory. The formulation of this element relies on logarithmic strain and true stress metrics, permitting finite membrane strains (stretching) while assuming minor curvature changes within each time increment.

To ensure the proper behavior of the developed model, a validation process must precede all intended actions. This model will undergo validation against the one utilized by Doan and Thai, (2020). This scrutiny verifies the suitability of the design model for all simulations. If the error discrepancy is no more than 10% compared to the reference model, the designed model proceeds to the subsequent phase. The validation procedure will be reiterated until an error below 10% is achieved.

3.2.2 Cut-out Shape and Size

Three parameters were investigated in this study: the spacing ratio, the shape of the opening, and the ratio of the opening. Each parameter was examined with three different configurations.

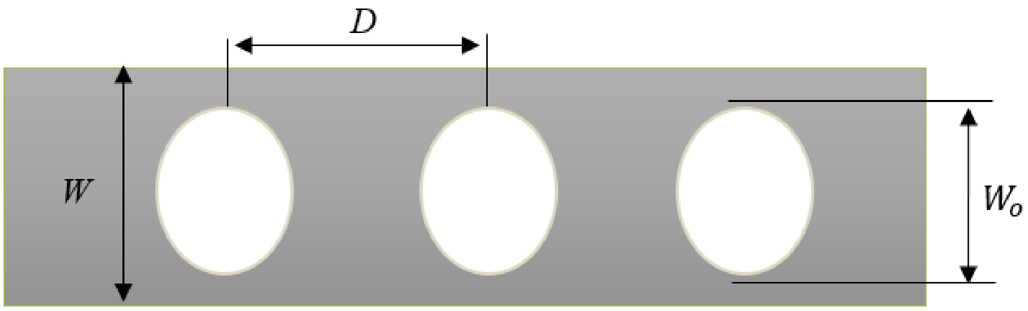

(a)

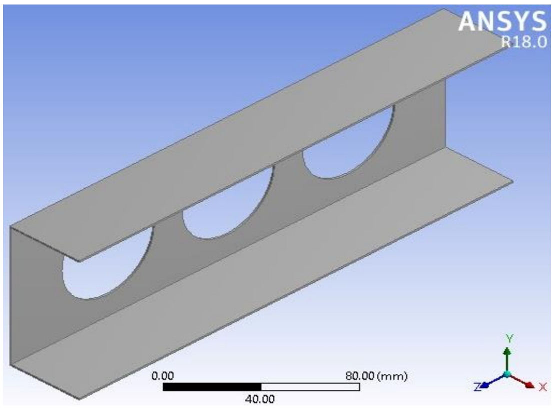

(b)

Figure 3.2 Cut-out size and shape (a) description of opening and spacing ratio (b) current FE model with holes

Figure 3.2 (a) illustrated the circular hole and like this circular hole two other shapes of holes have been considered such as square and hexagonal. The spacing ratio and opening ratio are selected as.

$$1.08 < \frac{D}{W_o} < 1.5 \tag{3.1}$$

$$1.25 < \frac{W}{W_o} < 1.75 \tag{3.2}$$

Figure 3.2 (b) illustrates the FE model employed in this study with holes. The sample of FE model only shows the circular hole and further these holes have been redesigned based on the dimension which has been shown in Figure 3.2 (a).

3.2.3 Material Properties

The mechanical properties of the material are defined in the FE analysis software. Mechanical properties such as Young's modulus, Poisson's ratio, and shear modulus are used to define the constitutive equations that relate the stresses and strains in the material. Next, the material properties of the thin-walled structure are defined including the coefficient of thermal expansion. These properties are used to define the mechanical and thermal behavior of the material when subjected to mechanical and thermal loading.

The type of laminate considered quasi-isotropic and were analyzed using the same thickness of each layer. This laminate type quasi-isotropic [+45/+45/+45/+45] s was introduced into ANSYS benchwork software with their respective properties. The GFRP material used in the analysis had a mass density of 2200 kg/m^3. To perform an analysis of composites a sample rectangular plate has been modelled using two different types of materials which are illustrated in Table 3.2.

3.2.4 Boundary Conditions and Meshing

To mesh the model, we have simply chosen a mesh model on the area and applied fine mesh with a minimum number of nodes and elements. Then refined the nodes to increase the fine mesh and mesh size. To mesh the model a total of 81 elements (100 nodes) have been created for an element type 1 which is chosen for the current model is SHELL181 which has 4 node 181 and storage of layer data change to all layers to increase the mesh.

Table 3.2 Materials properties of the composite structure

Parameter	**Composite material**
Density	2200 kg/m^3
Poisson's Ratio υ_{12}	0.29
Poisson's Ratio υ_{13}	0.29
Poisson's Ratio υ_{23}	0.29
Young's Modulus (E_1)	58 GPa
Young's Modulus (E_2)	10 GPa
Young's Modulus (E_3)	10 GPa
Shear Modulus (G_{12})	8 GPa
Shear Modulus (G_{13})	5 GPa
Shear Modulus (G_{23})	5 GPa
Material type	Sample material

A mesh with a size of 2 mm was selected based on the results of the mesh sensitivity analysis. The bottom end of the column was fixed in all directions, and the load was applied to the upper part of the column at a specific reference point shown in Figure 4. The reference point at the bottom was identified as RP-1, while RP-2 was assigned to the top section.

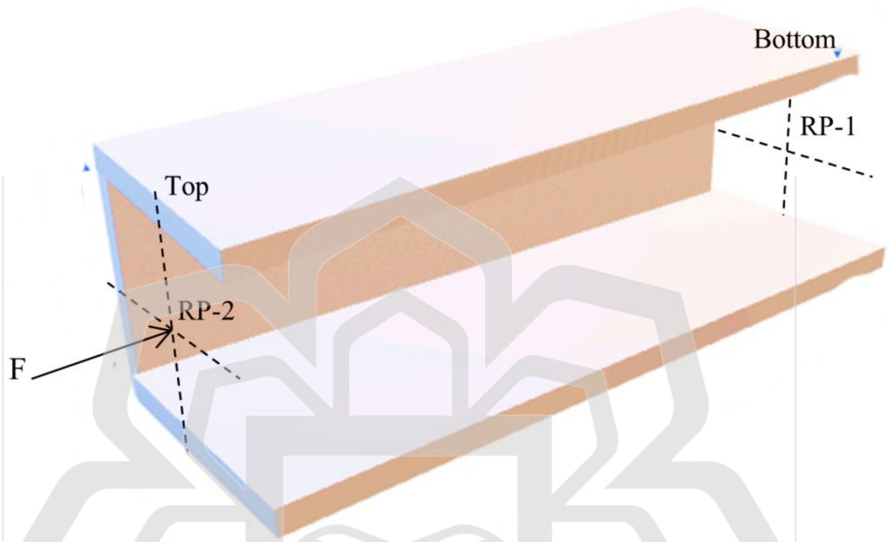

Figure 3.3 Loading conditions on the model

The buckling analysis was performed using the linear perturbation procedure in the ANSYS Workbench postprocessor. The models used multi-layered QUAD4 and SHELL181 elements (Doan and Thai, 2020). In the examination, the x, y, and z rotation angles at the upper end were constrained, while the vertical z-axis remained free. Conversely, at the bottom end, all degrees of freedom were immobilized at the reference point. A uniform load was applied to the upper nodes of the strut using rigid body-pin constraints to emulate the strut's contact with the top plate. The FE model encountered a nominal compressive load of 1.0 N. The critical buckling load was determined by addressing a linear eigenvalue buckling problem, specifically focusing on the first buckling mode, often termed the critical buckling load, to generate the mode shapes relevant to this study.

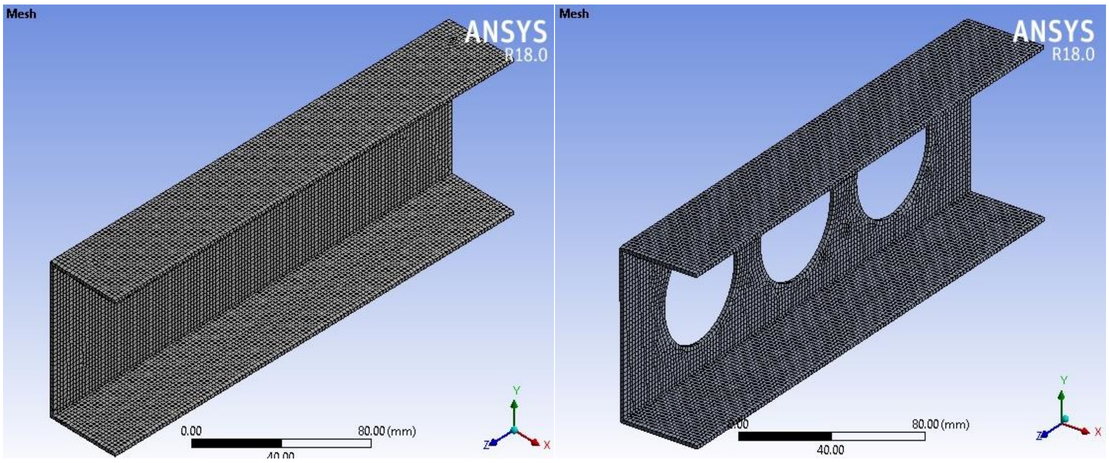

Figure 3.4 FE mesh model without and with holes

Lastly, The FE equations are solved using numerical methods, such as the direct or iterative method, to obtain the temperature and displacement fields. The solution obtained will be the buckling load factor and mode shapes. The results are then post-processed to obtain the critical buckling load factor and mode shapes. The mode shapes are used to identify the type of buckling that occurred in the structure under thermal load. The buckling load factor is used to determine the safety factor and whether the structure is in danger of buckling or not.

The critical buckling load is determined in the analysis through eigenvalue buckling analysis using finite element modeling. This involves solving an eigenvalue problem to obtain buckling load multipliers, which are dimensionless values indicating the relative load at which buckling occurs. For each specific load case (mechanical or thermal), the critical buckling load is calculated by multiplying the corresponding buckling load multiplier with the applied load.

The significance of the critical buckling load lies in its role as a crucial measure for understanding the column's stability under specific loading conditions. It indicates the maximum load the structure can withstand before experiencing buckling failure. This knowledge is vital for ensuring structural integrity and safety under applied loads and allows engineers to optimize composite structure designs for different loading scenarios.

3.2.5 Governing Equation for Critical Buckling Load

The governing equation for the critical buckling load of a C-section column can be derived from the Euler buckling theory. Euler's buckling equation provides a simplified approach for calculating the critical buckling load of columns under compression. For a C-section column, the critical buckling load is given by:

$$P_{cr,mech} = \frac{\pi^2.E.I}{(K.L)^2} \tag{3.3}$$

where:

- Pcr, mech is the critical buckling load due to the mechanical load.
- E is the elastic modulus of the material.
- I is the moment of inertia of the C-section column about its neutral axis.
- K is the effective length factor, which depends on the end conditions of the column.
- L is the effective length of the column.

K is the effective length factor (also known as the column effective length factor), which depends on the end conditions and boundary conditions of the column. For columns with both ends fixed, $K = 0.5$. For columns with one end fixed and the other end free, $K = 2.0$. For columns with both ends pinned, $K = 1.0$. There are other intermediate values for different end conditions.

This equation is used in linear buckling analysis to estimate the critical buckling load of a slender column, assuming small deflections and linear behavior. The equation to solve for thermal buckling is:

$$P_{cr,thermal} = \alpha . E . A . \Delta T \tag{3.4}$$

- $P_{cr,thermal}$ is the critical buckling load due to the thermal load.
- α is the coefficient of thermal expansion of the material.
- E is the elastic modulus of the material.
- A is the cross-sectional area of the C-section column.
- ΔT is the temperature difference applied to the column.

Eigenvalue Buckling Analysis for C-section Column under Mechanical Load: In structural engineering, Eigenvalue Buckling analysis is a linear analysis method used to determine the critical buckling loads and corresponding modes of buckling for various structural systems. This analysis is typically applied to slender columns, beams, and other structural members under compressive loads to understand their buckling behavior.

The governing equation for Eigenvalue Buckling analysis is based on the linear buckling theory and can be expressed as follows:

$$K . u_{mech} = \lambda_{mech} . K_e . u_{mech} \tag{3.5}$$

where:

- K is the global stiffness matrix of the structure, considering both mechanical and thermal loads.
- u is the displacement vector representing the buckled shape (mode shape) of the structure.
- λ is the eigenvalue, representing the buckling load multiplier (a dimensionless quantity).
- K_e is the element stiffness matrix.

Here's a high-level explanation of the steps:

- In Create the global stiffness matrix K for the C-section column, considering both mechanical loads and the effects of thermal expansion.
- Apply the thermal load as an initial displacement to the model, considering the temperature difference and the coefficient of thermal expansion.
- Use Eigenvalue Buckling analysis to solve the eigenvalue problem $\cdot u = uK \cdot u = \lambda \cdot Ke \ \cdot u$ to find the critical buckling load factors (λ) and the corresponding mode shapes (uu).
- The critical buckling load for the C-section column under the combined mechanical and thermal loads can be calculated as $Pcr \ = \lambda \cdot Papplied$, where $Papplied$ is the applied mechanical load on the column.

The eigenvalue buckling analysis provides valuable information about the buckling behavior of a structure and ensures that the structure can safely carry loads without experiencing buckling failure. Eigenvalue Buckling analysis is also a linear analysis technique, but it considers the overall stiffness properties of the entire structure, rather than just the individual column. It is more suitable for complex structures with multiple elements and degrees of freedom. Eigenvalue buckling analysis is based on linear assumptions and is suitable for structures that undergo small deflections and deformations. For large deflections and post-buckling behavior, nonlinear buckling analysis methods are more appropriate.

Eigenvalue Buckling Analysis for C-section Column under Thermal Load: The equation to solve for thermal buckling is:

$$K.u_{thermal} = \lambda_{thermal}.K_e.u_{thermal} \tag{3.6}$$

where:

- K is the global stiffness matrix of the structure considering thermal expansion.
- $u_{thermal}$ is the displacement vector representing the buckled shape (mode shape) of the structure due to thermal expansion.
- $\lambda_{thermal}$ is the eigenvalue, representing the buckling load multiplier (a dimensionless quantity) for thermal expansion.
- K_e is the element stiffness matrix.

By solving the above eigenvalue problem, you can find the critical buckling load factors ($\lambda_{thermal}$) and the corresponding mode shapes ($u_{thermal}$) considering only the thermal load. It's important to note that in Eigenvalue Buckling analysis, the critical buckling load is typically a dimensionless multiplier (λ) that needs to be multiplied by the applied load (P-applied) to obtain the critical buckling load ($Pcr\ = \lambda \cdot Papplied$) for each specific load case.

3.3 MACHINE LEARNING APPROACH

Designing composite laminate materials for specific applications involves complex optimization processes. ML-techniques have emerged as powerful tools for optimizing laminated composite materials, providing insights, efficiency, and accuracy in the design process. Traditional optimization methods involve manually designing and testing different combinations of fiber orientations, layer thicknesses, and stacking sequences. This process is time-consuming, expensive, and limited in exploring the vast design space. Moreover, human intuition alone may not be sufficient to uncover complex relationships between design parameters and material performance. Machine learning techniques offer a data-driven approach to optimize laminated composite materials. ML algorithms can process large datasets to optimize process.

In this research, the FE model is validated through existing work and used to characterize the behavior of composite by various geometric and material parameters and laminated interface. A formulated machine learning model was then developed for the composites. Design examples are provided to illustrate the effectiveness of the proposed machine learning model in describing the response to the release of the composite structures. A vulnerability analysis was then performed to examine the contribution of the selected predictors to the behavior of the composite. Machine learning predictive models and reporting by composite provide powerful tools for solving laminated structural problems in a variety of existing conventional composite structures.

In general, it is important to note with machine learning algorithms that it is random because of the arbitrary weight generated in the hidden layer. This can produce different accuracy depending on the random weights. Simple sequential heuristic search techniques are used to achieve the best accuracy. It is important to note that in LM the number of neurons in the hidden layer is randomly selected. In other words, there are no clear mathematics rules for deducing the right numbers of neurons to train. Huang et al., (2006) have shown that with the differentiable activation functions, the number of neurons required in the hidden layer is smaller than the data size. In this application, some neurons select sigmoid as their activation function based on previous studies (Park et al., 2006). The overall used machine learning for the current work has illustrated in the Figure 3.7.

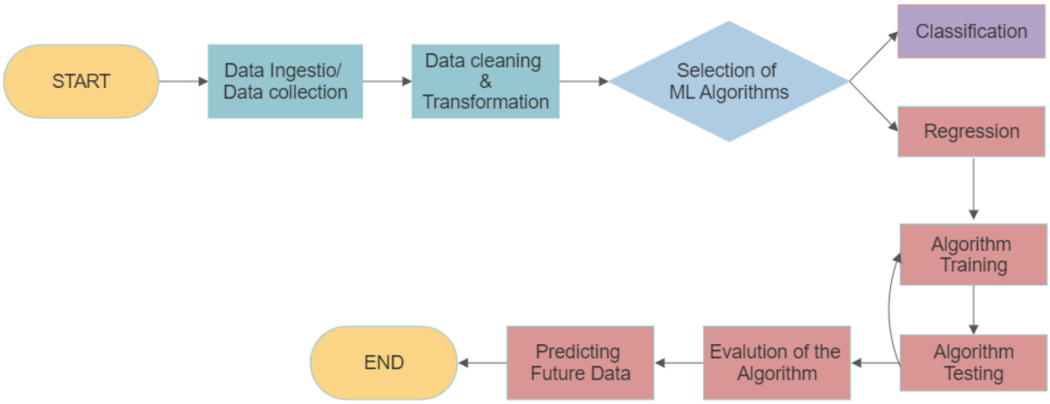

Figure 3.5 Process of machine learning in the current work

3.3.1 Data set and properties

In this study, the effect of load type, cut-outs shape, fiber orientation, opening ratio, spacing ratio on buckling stress was investigated numerically. The data set consists of 5 features and 1 target value. The data set consists of 5 features and 1 target value. Table 3.3 illustrates the feature X1 indicates the load type and X2 indicates the cut-outs shape of the hole in the laminate structure. The features X3 refer to the fiber orientation, composite material. The features X4 and X5 correspond to the opening ratio and spacing ratio of the laminate structure, respectively. Y1 is the target parameter calculated by the machine learning technique and represents the buckling stress. The data set contains 36 data points from numerical studies.

Table 3.3 Data set and their properties

ID	**Property**	**Range**	**Data Type**
X1	Load Type	Mechanical and thermal	Categorized
X2	Cut-outs Shape	Circular, Square and Hexagon	Categorized
X3	Fiber Orientation	Quasi-isentropic, Angle-ply, Cross-ply, and Balance	Categorized
X4	Opening Ratio	1.3, 1.4 and 1.5	Numeric
X5	Spacing Ratio	1.5, 1.6, and 1.7	Numeric

3.3.2 Regression Models

Regression models aim to create a mathematical equation, denoted as

$$Y = f(X, w) \tag{3.7}$$

where Y represents the outcome (continuous or discrete) and X represents the independent variables. The unknown parameters w, also known as regression coefficients or weights, capture the relationship between the outcome and the variables.

Regression analysis enables the quantification of this relationship between the outcome and associated variables. Various statistical prediction techniques have been developed, and for this thesis, four models were examined and compared: Linear Regression (LR), Decision Tree Regression, AdaBoost Decision Tree Regression, and Gradient Boosting Regression.

When assessing the accuracy of predictions made by a model, it is crucial to utilize evaluation metrics that can effectively measure the model's performance in comparison to other models. For evaluating regression performance, the commonly employed evaluation metric includes mean squared error, mean absolute error, explained variance score, and R-squared score.

3.3.2.1 Mean Square Error (MSE)

The Mean Square Error (MSE) quantifies the proximity of predicted values to actual ones. It involves squaring the disparities between predicted and actual values for each input entry and then computing the average of these squared disparities. MSE is a frequently employed gauge for assessing a model's overall effectiveness.

$$MS(y, \bar{y}) = (1/n) * \sum (yi - \bar{y}i)^2 \tag{3.8}$$

3.3.2.2 Root Mean Square Error (RMSE)

The Root Mean Square Error (RMSE) assesses the proximity of predicted values to actual ones. It derives from the Mean Square Error (MSE) by taking its square root. RMSE serves as a prevalent metric for appraising a model's comprehensive performance and is frequently employed alongside MSE for evaluation.

$$RMSE(y, \bar{y}) = \sqrt{((1/n) * \sum (yi - \bar{y}i)^2)} \tag{3.9}$$

The RMSE provides a measure of the typical magnitude of prediction errors. It is often preferred over MSE as it is in the same unit as the original target variable, making it easier to interpret.

3.3.2.3 R² Error

The R² provides an indication of how well the model predicts future samples. The highest achievable score is 1.0, and a negative score implies that the model's performance falls below that of a constant model that consistently predicts the anticipated y-value. The R^2 score is calculated based on the sum of squares of residuals, comparing the predicted values, $\overline{yi}$, with the true values, yi.

$$R^2(y, \bar{y}) = 1 - [(1/n) * \sum (yi - \bar{y}i)^2] / [(1/n) * \sum (yi - \bar{y})^2] \tag{3.10}$$

Where $\bar{y}$ is the mean value of y over all n input rows.

3.3.2.4 Linear Regression

Linear regression constitutes a fundamental technique in regression analysis for capturing the connection between a reliant variable and one or multiple independent variables. The linear regression equation can be articulated in the subsequent manner:

$$y = \beta 0 + \beta 1x1 + \beta 2x2 + \cdots + \beta nxn \tag{3.11}$$

In the equation, y is the output or target variable, $\beta 0$ is the intercept, $\beta 1$, $\beta 2$, ..., βn are the regression coefficients, and $x1$, $x2$, ..., xn are the independent variables.

The direction of the correlation between an independent variable and the dependent variable is revealed by the sign of a regression coefficient. A positive coefficient signifies a positive correlation, while a negative coefficient indicates a negative correlation. The coefficient's magnitude signifies the extent to which the independent variable influences the dependent variable.

To determine the unknown regression coefficients, linear regression employs the method of ordinary least squares (OLS). OLS minimizes the sum of the squared differences between the actual values and the predicted values for the dataset provided. The error or residuals of the linear regression model are calculated using the following formula:

$$E = \sum (yi - f(xi))^2, for\ i = 1\ to\ n \tag{3.12}$$

In the formula, yi is the actual value of the dependent variable, and $f(xi)$ is the predicted value based on the linear regression equation. Once the linear regression model undergoes training and testing, its effectiveness can be evaluated through regression metrics like the R^2 score and mean squared error (MSE). The R^2 score denotes the portion of the variance in the dependent variable anticipated from the independent ones. In contrast, MSE gauges the average squared disparity between actual and predicted values, delivering an assessment of the model's precision.

Linear regression is a simple and fast method to implement, but it may not generalize well for nonlinear data and can perform poorly when there is multicollinearity among the independent variables. To address these limitations, other regression methods such as polynomial regression and linear regression with regularization have been developed.

3.3.2.5 Lasso Regression

Lasso regression, a variant of linear regression, employs regularization to counteract overfitting. Regularization introduces a cost function penalty, compelling the model to diminish coefficients associated with less significant attributes. Lasso regression employs L1 regularization, wherein the penalty is determined by the total absolute values of the coefficients. Consequently, this encourages the model to nullify coefficients linked to less vital attributes, potentially diminishing the number of features, and enhancing performance. The lasso regression equation can be represented as follows:

$$y = \beta 0 + \beta 1 x 1 + \beta 2 x 2 + \cdots + \beta n x n + \lambda \sum |\beta i| \qquad (3.13)$$

In the equation, y is the output or target variable, $\beta 0$ is the intercept, $\beta 1$, $\beta 2$, ..., βn are the regression coefficients, $x 1$, $x 2$, ..., $x n$ are the independent variables, and λ is the regularization parameter. The additional term in the equation, $\lambda \sum |\beta i|$, represents the L1 regularization penalty. The summation ($\sum$) is taken over the absolute values ($|\beta i|$) of the regression coefficients. The regularization parameter λ controls the strength of the penalty. A larger λ value results in more shrinkage of the coefficients towards zero, effectively performing feature selection by eliminating less important features. The objective of lasso regression is to minimize the sum of squared differences between the predicted values and the actual values, as well as the regularization penalty. The cost function for lasso regression can be written as:

$$Cost(y, \hat{y}) = (1/n) * \sum (yi - \hat{y}i)^2 + \lambda \sum |\beta i| \qquad (3.14)$$

In the equation, $\hat{y}$ represents the predicted values based on the lasso regression model, yi is the actual value, $\hat{y}i$ is the predicted value, n is the number of data points, and the second term $\sum |\beta i|$ is the L1 regularization penalty.

The regularization term in lasso regression encourages sparsity in the model by driving some coefficients to exactly zero. As a result, lasso regression not only provides prediction but also performs feature selection, automatically identifying and excluding irrelevant or redundant features. The choice of the regularization parameter λ is crucial. A larger λ value leads to more aggressive regularization and stronger feature selection, while a smaller λ value allows more coefficients to remain non-zero. The optimal value of λ is typically determined through techniques like cross-validation or grid search to find the balance between model complexity and performance.

Lasso regression is widely used in various fields, including statistics, machine learning, and data analysis, as it provides a simple yet effective method for feature selection and regularization in linear regression models. For regression tree construction, where the target variable is continuous, measures like Gini impurity and information gain are not suitable. Instead, the sum-of-squared error is commonly used to evaluate splitting features or splitting points. The split point is chosen to minimize the sum of squared errors. CART trees are known for their good performance, interpretability, and the ability to handle both categorical and numerical features without requiring scaling or standardization. They are often used in ensemble methods, such as ensembles of decision tree models.

Lasso regression, a form of linear regression with regularization, enhances model interpretability and prevents overfitting. Regularization adds a penalty term to the cost function, moderating model complexity for better generalization. The parameter λ controls regularization strength, with higher values leading to sparser models and feature selection. λ strikes a balance between bias and variance, minimizing prediction errors. As λ increases, feature coefficients shrink, some even reaching zero for model simplification. Lasso's impact includes improved interpretability, generalization, and model performance. Visualization of metrics across λ values aids in selecting the optimal regularization strength. Thus, λ is pivotal in Lasso regression for effective model tuning and performance.

3.3.2.6 Decision Tree Regression

Decision tree regression stands as a nonparametric regression method employing a tree-shaped model for prediction. Differing from linear regression, it has the capacity to grasp intricate nonlinear associations between independent variables and the target variable. The decision tree model repetitively divides the input space according to independent variable values and forecasts the target variable by averaging its values within each division. The decision tree regression equation can be represented as follows:

$$y = f(x) \tag{3.15}$$

In the equation, y represents the predicted value of the target variable, and $f(x)$ represents the decision tree model's prediction function based on the input variables x.

The decision tree algorithm follows a top-down approach to construct the tree. It starts with a root node that represents the entire dataset. At each step, the algorithm selects the best split based on a splitting criterion. For regression tasks, the splitting criterion often involves minimizing the sum of squared errors or maximizing the reduction in variance. The splitting process continues until a stopping condition is met. This condition can be the maximum depth of the tree, a minimum number of samples required to split a node, or other pre-defined criteria. Each node in the tree represents a split based on a specific feature and a threshold value. The decision tree branches out based on different combinations of feature values, resulting in a hierarchical structure of nodes and leaves. To predict the target variable for a new input, the decision tree regression algorithm traverses down the tree from the root node to a leaf node. At each node, it checks the corresponding feature value of the input and follows the appropriate branch until it reaches a leaf node. The value associated with the leaf node is then used as the predicted value for the input.

The decision tree regression model is known for its interpretability and its capability to grasp intricate variable interactions. Nevertheless, it is susceptible to overfitting and can be highly responsive to slight alterations in training data. Strategies like pruning, imposing tree depth restrictions, or incorporating ensemble methods like random forests can alleviate these concerns and enhance the model's ability to generalize. Decision tree regression finds extensive use across diverse fields, such as finance, healthcare, and marketing, thanks to its capacity to manage both numerical and categorical variables while remaining interpretable. It provides a flexible and intuitive approach to regression modeling, allowing for the identification of important variables and the exploration of nonlinear relationships.

In Decision Tree Regression, the construction of the tree involves recursive partitioning of the feature space to minimize target variable variance within regions. The process begins at the root node with all training samples. Nodes are split based on selected features and splitting criteria, aiming to segregate data into homogenous subsets regarding the target variable. Splitting points are determined differently for numerical and categorical features: numerical features are assessed for optimal splitting points by examining all possibilities, while categorical features evaluate combinations of categories. Recursive splitting occurs until stopping criteria, like maximum depth or minimum samples per leaf, are met. Leaf nodes hold final predictions, typically the mean or median of the target variable within the leaf. The resulting tree structure represents a sequence of feature splits that partition data into increasingly homogenous subsets concerning the target variable, making it essential for predicting critical buckling loads in thin-walled structures.

3.3.2.7 Random Forest Regression

Random forest regression is an ensemble learning technique that combines multiple decision tree models to make predictions. It is highly effective and widely utilized for regression tasks as it can handle complex relationships and mitigate overfitting issues. By aggregating the predictions from multiple decision trees, random forest regression offers more accurate and robust predictions. The random forest regression equation can be represented as follows:

$$y = f_1(x) + f_2(x) + \cdots + f_n(x) \tag{3.15}$$

In the equation, y represents the predicted value of the target variable, x represents the input variables, and $f_1(x)$, $f_2(x)$, $\cdots$, $f_n(x)$ represent the individual predictions of the decision trees in the random forest.

Random forest regression employs an ensemble of decision trees through a technique known as bagging, or bootstrap aggregating. This process involves generating multiple bootstrap samples from the training data and training a decision tree on each sample. Each decision tree is trained on a different subset of the data, and they are relatively uncorrelated. During the training process, each decision tree in the random forest is constructed using a random subset of features. This random feature subset selection adds an extra level of randomness and helps to de-correlate the trees further. The number of features considered at each split is typically smaller than the total number of features available.

A random forest regression model makes predictions by averaging the predictions of all the individual decision trees in the forest. This helps to reduce the variance of the predictions and improve the overall accuracy of the model. The final prediction is usually the average (or mean) of the predicted values from all the decision trees. This averaging process helps to reduce the impact of outliers and noise in the data, resulting in a more stable and accurate prediction. Random forest regression offers several advantages, including robustness to over fitting, the ability to handle high-dimensional data, and the capability to capture nonlinear relationships and interactions among variables. It also provides an estimate of the feature importance based on the average decrease in impurity or mean decrease in error across all the decision trees. The random forest algorithm is widely used in various domains, including finance, healthcare, and marketing, for tasks such as predicting house prices, estimating stock market trends, and analyzing customer behavior. Its versatility, accuracy, and interpretability make it a popular choice for regression modeling in both academic and practical applications.

3.3.2.8 Gradient Boosting Regression

Gradient boosting regression is a machine learning technique that combines multiple weak prediction models, typically decision trees, into a strong predictive model. It is a powerful algorithm that can handle complex relationships and provide highly accurate predictions. Gradient boosting builds the model iteratively, adding new models that correct the mistakes made by the previous models. This process helps to improve the accuracy of the model over time. The gradient boosting regression equation can be represented as follows:

$$y = f_1(x) + f_2(x) + \cdots + f_n(x) \tag{3.16}$$

In the equation, y represents the predicted value of the target variable, x represents the input variables, and $f_1(x)$, $f_2(x)$, $\cdots$, $f_n(x)$ represent the individual predictions of the weak models in the gradient boosting ensemble. The gradient boosting algorithm starts by fitting an initial model, often a decision tree, to the training data. This model generates predictions, but the initial predictions may not be highly accurate. Successive models are devised to rectify the inaccuracies of their predecessors. Every fresh model undergoes training to forecast the residuals, which represent the disparities between the real target values and the forecasts generated by the previous models.

The novel model undergoes training via a gradient descent technique to determine the optimal parameters that minimize the loss function. This loss function quantifies the dissimilarity between forecasted and factual target values. In gradient boosting regression, the prevalent choice for the loss function is typically the mean squared error (MSE). The new model is trained to minimize the MSE of the residuals. During the training process, the new model is added to the ensemble by determining its weight or contribution to the final prediction. This weight is calculated using a learning rate, which controls the contribution of each model. The learning rate determines the shrinkage applied to each model's predictions to avoid overfitting and improve generalization.

To make predictions, the gradient boosting regression model combines the predictions of all the individual models. The final prediction is typically the sum of the predictions from all the models in the ensemble. The ensemble of models works together to improve the overall prediction accuracy and capture complex relationships in the data. Gradient boosting regression offers several advantages, including its ability to handle complex nonlinear relationships, its flexibility in incorporating different loss functions, and its robustness to overfitting. It is widely used in various domains, including finance, healthcare, and recommendation systems, for tasks such as predicting stock prices, estimating customer churn, and personalized recommendations. The gradient boosting algorithm, with its strong predictive performance, interpretability, and versatility, has become a popular choice for regression modeling in both research and practical applications.

3.3.3 Design and Implementation

3.3.3.1 Data Preparation

The dataset used in this analysis is obtained from ANSYS Workbench, where a C-section composite column is selected for the study. The purpose is to analyze the critical buckling load caused by both structural and thermal loads. The dataset includes various dependent parameters such as 'Opening ratio', 'Spacing ratio', 'Orientation', and 'Shape'. The buckling load is considered as the independent variable. Data is collected for different combinations of these parameters.

To begin the data preparation process, the dataset is loaded from a CSV file using the `pd.read_csv()` function. The merged data is then divided into a 70% training set and a 30% validation set. To get an overview of the dataset, the first few rows are displayed using the `df.head()` method. Next, the categorical features 'Orientation' and 'Shape' are converted into numerical codes. This conversion is achieved by using the `astype('category')` method followed by the `cat.codes` method. Finally, the features ('Opening ratio', 'Spacing ratio', 'Orientation', 'Shape') and the corresponding labels ('Critical Buckling load') are separated into two sets of variables, X and y, respectively. These sets will be used for further analysis and modeling.

3.3.3.2 Data cleaning

Data cleaning is a crucial step in data analysis to ensure the reliability and accuracy of the results. Missing, incomplete, or corrupted data can introduce errors and bias into calculations and statistical functions. By identifying and addressing these issues, we can obtain more reliable insights from the data.

In the given dataset, columns that do not significantly contribute to the analysis are removed. These columns may contain irrelevant or redundant information that does not provide meaningful insights for the specific analysis at hand. In this case, the column containing serial numbers is identified as not playing a substantial role in the analysis and is thus removed from the dataset. Additionally, it is important to note that in this dataset, no missing data was encountered. This means that there were no instances where data points were absent or incomplete, ensuring the dataset's completeness for analysis.

By performing data cleaning and removing irrelevant columns, we can streamline the dataset and focus on the relevant variables that influence the analysis. This process helps to enhance the accuracy and efficiency of subsequent data analysis tasks.

3.3.3.3 Data scaling

Data scaling is a crucial step in data preprocessing that aims to normalize the features in a dataset which is shown in APPENDIX C, ensuring that they have a consistent scale and range. This process helps in improving the performance and stability of machine learning models.

To perform data scaling, the StandardScaler class from the sklearn. Preprocessing module is utilized. First, an instance of the StandardScaler is created. Then, the scaler is fitted on the training data (X_train), which calculates the mean and standard deviation of each feature. Once the scaler is fitted, it can be used to transform both the training and test data (X_train and X_test) by applying the computed mean and standard deviation. This transformation ensures that the features have a mean of 0 and a standard deviation of 1, resulting in a standardized scale across all features. By scaling the data, the model can effectively compare and interpret the features, as they are now on the same scale. This normalization step helps prevent certain features from dominating others due to their larger magnitudes, and it can contribute to more accurate and reliable model training and predictions. Data scaling using the StandardScaler enables the standardization of features by fitting the scaler on the training data and transforming both the training and test data using the computed mean and standard deviation. This process facilitates fair comparisons between features and promotes better performance of machine learning models.

3.4 CHAPTER SUMMARY

This chapter provides a comprehensive explanation of the FE model and ML algorithms utilized in the proposed technique. The extraction process of these models and algorithms is described in a step-by-step manner. Furthermore, the chapter delves into the data collection procedure from the FE model, specifically focusing on C-section channels with and without cut-outs, which is crucial for implementing the ML algorithms. Parametric studies of c-section channel have been done and show the variation of critical buckling load under thermal and mechanical loading conditions. Later, methodology-based work shows the soft computing approaches effective in reducing human efforts particularly genetic algorithms shown in most of the cases in critical buckling loss of thin-walled structures. A detailed overview of the methodology is provided within this chapter.

CHAPTER FOUR

RESULTS AND ANALYSIS

4.1 INTRODUCTION

This chapter provides a comprehensive explanation of the results obtained through the finite element (FE) analysis of C-section thin-walled channels, both with and without holes. The chapter elaborates on all the parameters considered and analyzed during the FE analysis. Moreover, the data obtained from the simulation results is utilized in machine learning algorithms to optimize the current structural model, aiming for improved design in practical applications within the field of structural engineering. The chapter showcases how this optimization process enhances the structural model, offering valuable insights for practical implementation.

4.2 FINITE ELEMENT ANALYSIS AND RESULTS

The finite element equations are solved using numerical methods, such as direct or iterative methods, to calculate the temperature and displacement fields. The outcome of this process provides the buckling load factor and mode shapes. Post-processing of the results is carried out to extract the critical buckling load factor and mode shapes. The mode shapes are then utilized to identify the type of buckling that has occurred in the structure under thermal load. The buckling load factor is used to assess the safety factor and determine whether the structure is at risk of buckling or not.

4.2.1 Mesh Independence Test

A mesh convergence study is conducted to assess the accuracy of the mesh in a current model. The study focuses on a basic model without any cut-outs in the c-section channel. To explore the impact of different mesh sizes, five element sizes ranging from 1.8 mm to 3 mm are tested. The element size that produces the most similar results is selected for further analysis. The mesh refinement is then examined in relation to a specific case in the current work, which is similar to a previous study (Doan and Thai, 2020). The analysis determines that an element size of 2 mm closely aligns with the reference value and exhibits the lowest error, resulting in convergence of the results. This mesh size is subsequently employed for all models, with slight modifications near the holes of the structure to ensure smoother boundaries. According to Table 4, the 2 mm element size yields the lowest error, while the computational time remains reasonable with this mesh setup. These findings support the conclusion that further refinement is unnecessary and that errors are minimized.

Table 4.1 Mesh convergence study for c-section without cut-outs

Sl. No	Element size	No. of elements	No. of nodes	Critical buckling value
1	1.8	24777	25891	9001.5
2	2	20486	21389	9032.7
3	2.4	14199	16002	9082.8
4	3	9281	10281	9164.3

4.2.2 Validation of simulation model

To validate the proposed FE model, this study relied on the buckling outcomes reported by Doan and Thai, (2020). The length and cross-sectional dimensions of the specimen were replicated to match those used in their study, ensuring accuracy in the current work. The buckling behaviour of both the quasi-isotropic laminate and angle-ply laminate FE models was compared to their respective numerical analysis results to assess the reliability of the proposed model. The stacking sequences used were [0/+45/+45/+45/+45]s for the quasi-isotropic laminate. Initially, the beam model without any holes was compared for both laminates to ensure higher reliability. Table 4.2 presents the comparison of the critical buckling load's numerical results with the findings from the previous study.

Table 4.2 Comparison of c-section model under mechanical load

Laminate Types	Structural type	Critical Buckling Load (N)			Percentage error (%)
		Experimental (Doan and Thai, 2020)	ABAQUS (Kamarudin et al., 2022)	Present work ANSYS	
Quasi-isotropic	Without hole	10500 N	11201.2 N	10237.8 N	±2.56 and ±8.6
Quasi-isotropic	With hole	-	8551 N	8625.8 N	±0.86

Another validation of current model under thermal load has been compared with theoretical and numerical results (Rao et al., 2015). The authors compared the FE results for the first mode with the theoretical solution available at the University of Connecticut for isotropic materials. The development of the FE model is based on previous research that examined an FRP composite thin rectangular plate. The plate has in-plane dimensions of 2 m length and 1 m width. The plate's thickness is determined based on the length-to-thickness ratio (s = a/t) and is varied for a specific case. Symmetric quasi-isotropic stacking sequences (90/45/-45/0/0/-45/45/90) were used. The comparison between the FE results and the theoretical solution is provided in Table 4.3.

Table 4.3 Comparison of c-section model under thermal load

Configuration of model (thickness ratio t/b)	Critical Buckling Temperature (^{o}C)		Percentage error (%)
	Theoretical (Rao et al., 2015)	Present work numerical	
Quasi-isotropic	28.2 ^{o}C	25.8 ^{o}C	9.47

4.2.3 Total Deformation

The ANSYS simulation results show that the presence of apertures significantly reduces the load-carrying capacity of a beam before it fails. Figures 4.1 to 4.7 present eigenvalue data, demonstrating the critical buckling load and thermal critical buckling load for different models with and without apertures. Figure 4.1 exhibits the eigenvalues for a C-section channel without any apertures, indicating that these values are expected to be higher compared to the C-section channel with apertures. This suggests that the C-section channel without apertures can withstand a higher load before buckling occurs.

To enhance the beam's strength while reducing its weight, the channel incorporates apertures and is subjected to testing with various shapes and sizes, as depicted in Figures 4.1 to 4.7. These tests help to determine the effects of different aperture configurations on the structural integrity and load-bearing capacity of the beam. Overall, the findings from the ANSYS simulation underscore the importance of carefully designing aperture placements and shapes to maintain the structural integrity of beams and prevent premature failure under axial loads. The research aims to guide the development of more robust and efficient beam designs for various engineering applications.

The significance of the contour results lies in their ability to reveal the distinct behavior of the beam under mechanical and thermal loads, allowing for a comprehensive understanding of its structural response. By extracting contours independently for both conditions, engineers can observe significant variations in eigenvalues, which are critical in determining the buckling load capacity. Despite the similarity in deformation patterns between the mechanical and thermal load cases, the presence of apertures in the C-sectional channel results in a noticeable decrease in buckling load capacity.

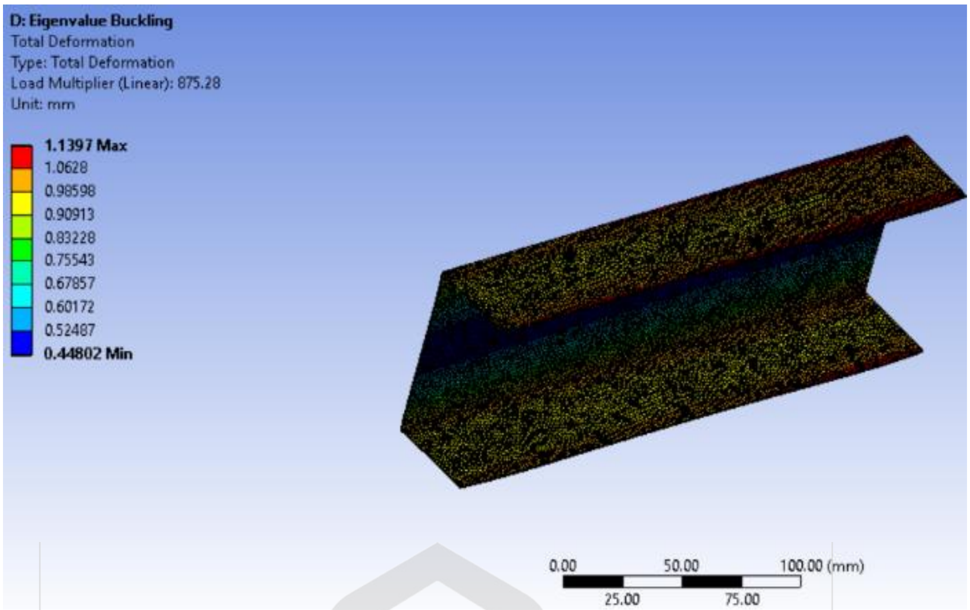

(a) Mechanical

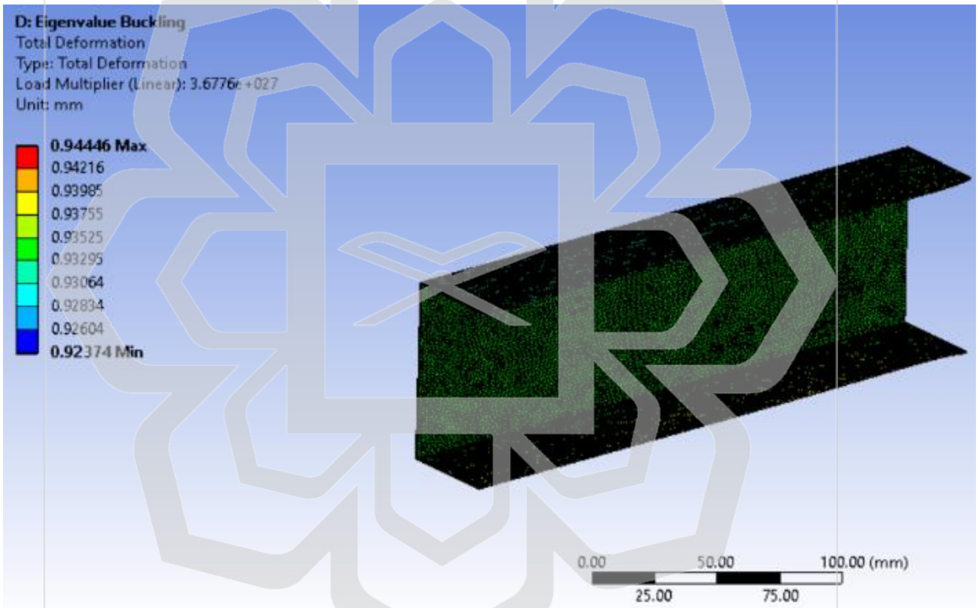

(b) Thermal

Figure 4.1 Total deformation (Eigenvalue buckling) without cut-outs.

This reduction is clear in the plotted data, indicating that apertures have a substantial impact on the beam's ability to withstand external forces before buckling occurs. Understanding these contour results is crucial for design optimization, as engineers can make informed decisions about aperture configurations to enhance structural integrity and load-carrying capacity. It helps identify regions of stress concentration and potential failure points, guiding the development of safer and more efficient beam designs.

Additionally, this knowledge aids in choosing suitable materials and reinforcement strategies to counteract the negative effects of apertures, ensuring the overall reliability and longevity of the beam in practical applications.

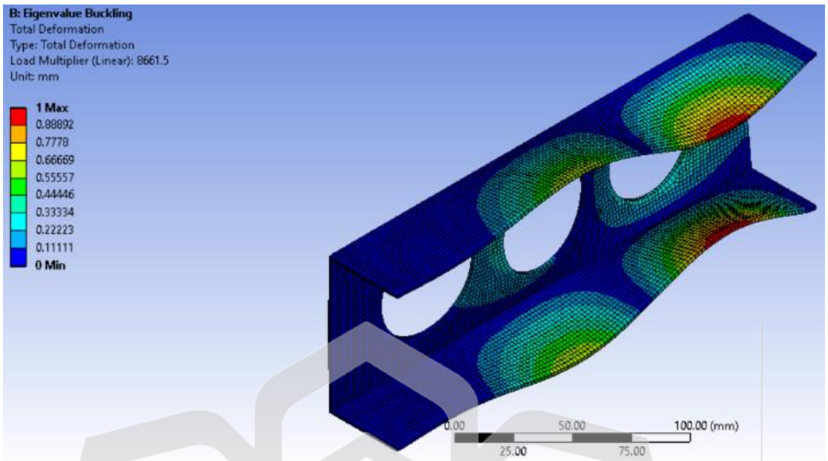

(a)

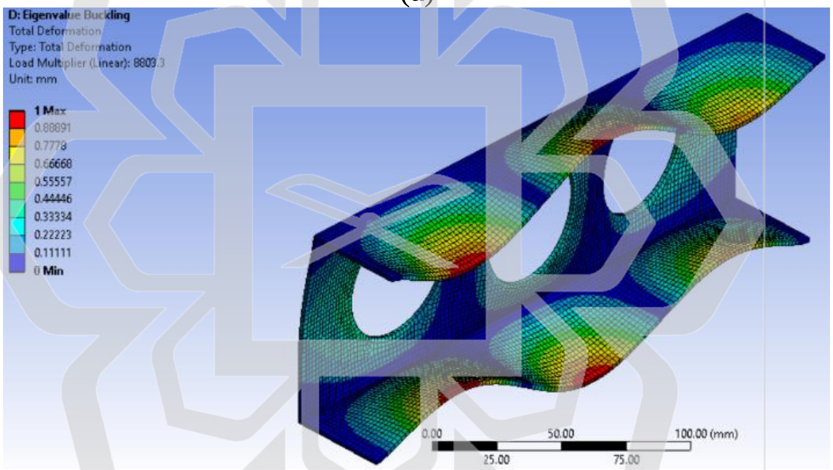

(b)

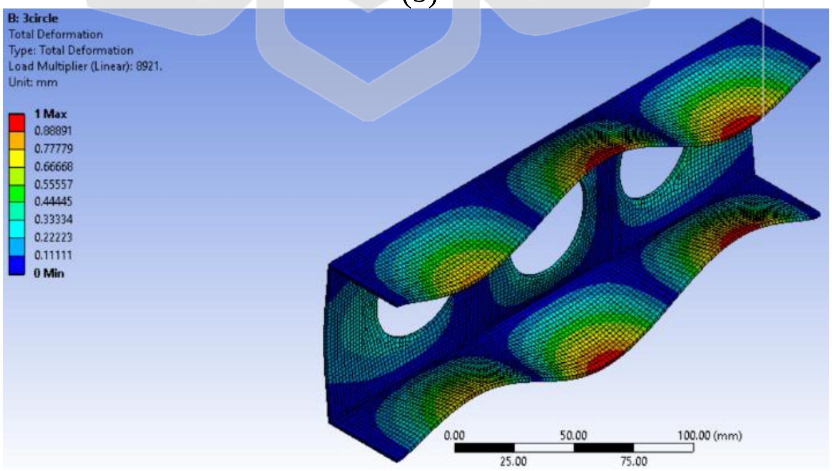

(c)

Figure 4.2 Total deformation (Eigenvalue buckling) under mechanical load for circular cut-outs (a) W/Wo= 1.5, (b) W/Wo= 1.6, (c) W/Wo= 1.7

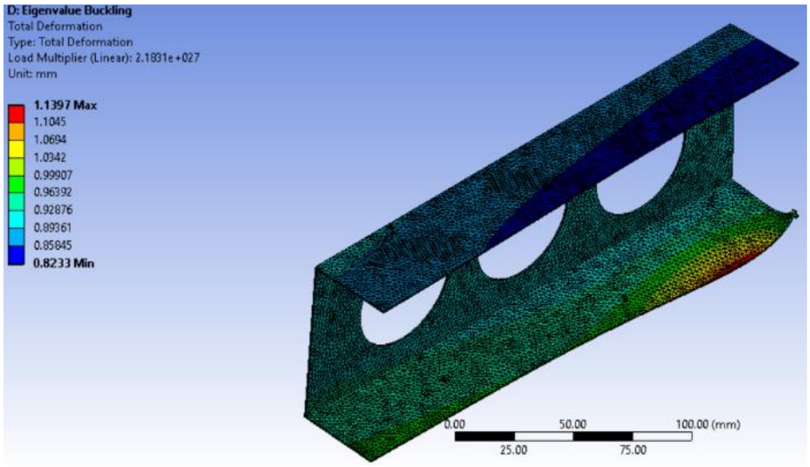

(a)

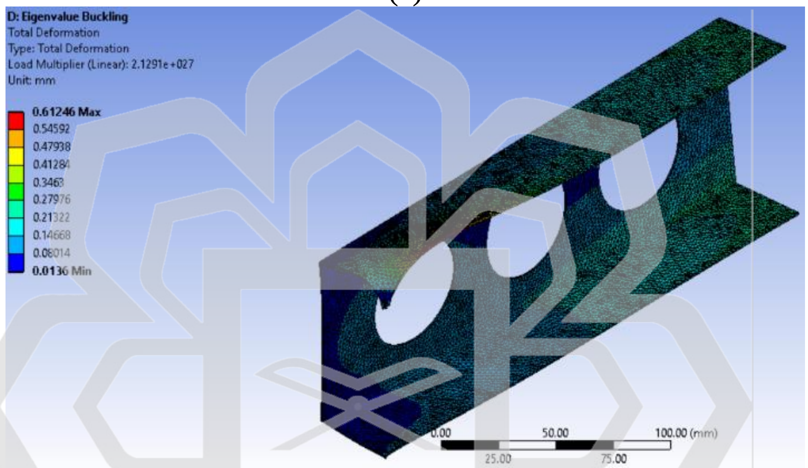

(b)

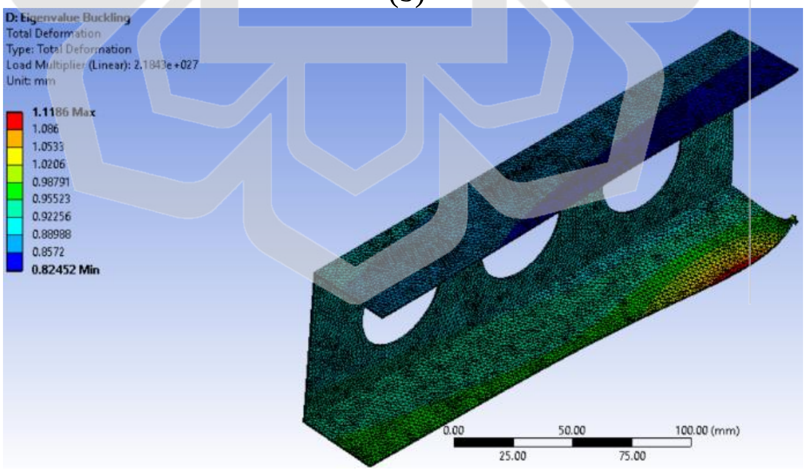

(c)

Figure 4.3 Total deformation (Eigenvalue buckling) under thermal load for circular cut-outs (a) W/Wo= 1.5, (b) W/Wo= 1.6, (c) W/Wo= 1.7

This study investigated three different cases with W/Wo ratios of 1.5, 1.6, and 1.7 to understand the effects of cut-out configurations on the buckling behavior of C-sectional channels. Among these cases, the ratio of 1.3 stood out due to its larger cut-out diameter, which resulted in a lower buckling load and reduced structural stability. However, it's essential to consider that this scenario also had a lower channel weight, indicating a trade-off between weight and buckling load capacity. Conversely, cases with smaller cut-out diameters exhibited increased buckling loads, implying that channels with higher weights can sustain greater loads without buckling when cut-outs are absent. Furthermore, the study compared three different cut-out shapes, with the circular cut-out demonstrating superior strength compared to the other two shapes. The circular cut-out's advantage arises from its lack of sharp edges, enabling a more even distribution of stress and enhancing overall structural integrity. In contrast, the square cut-out, characterized by 90-degree angles, is more susceptible to immediate structural failure due to stress concentration at these sharp corners.

These findings are vital for structural design optimization, as they highlight the impact of cut-out diameter and shape on buckling behavior and channel weight. Engineers can use this knowledge to select appropriate configurations based on specific application requirements. By considering the trade-offs between weight, buckling load, and structural stability, they can make informed decisions to create safer and more efficient C-sectional channel designs. Moreover, understanding the influence of cut-out shape helps prevent the presence of stress concentration points that could compromise the structural integrity of the beam, ensuring long-term reliability and safety in real-world engineering applications.

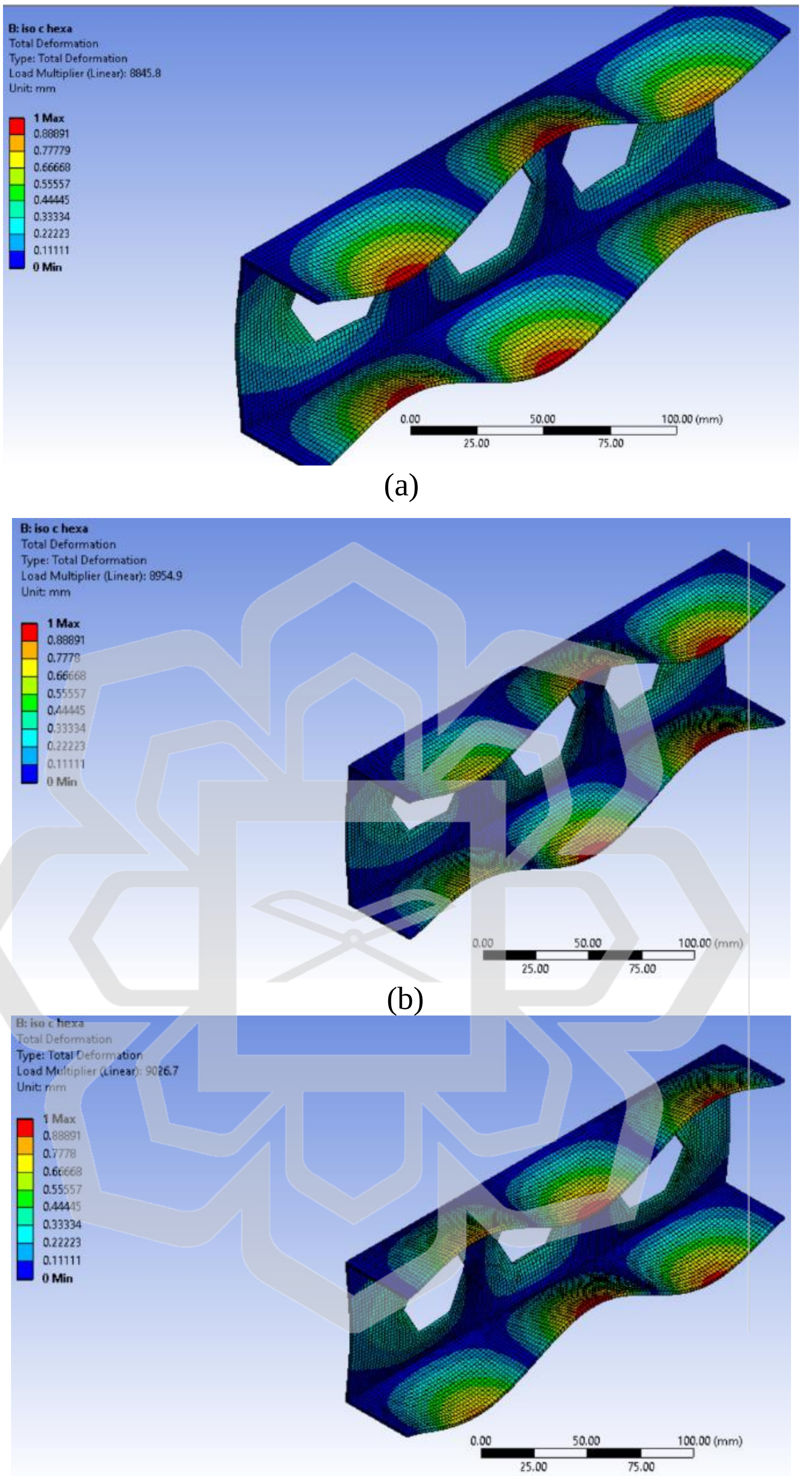

(a)

(b)

(c)

Figure 4.4 Total deformation (Eigenvalue buckling) under mechanical load for hexagon cut-outs (a) W/Wo= 1.5, (b) W/Wo= 1.6, (c) W/Wo= 1.7

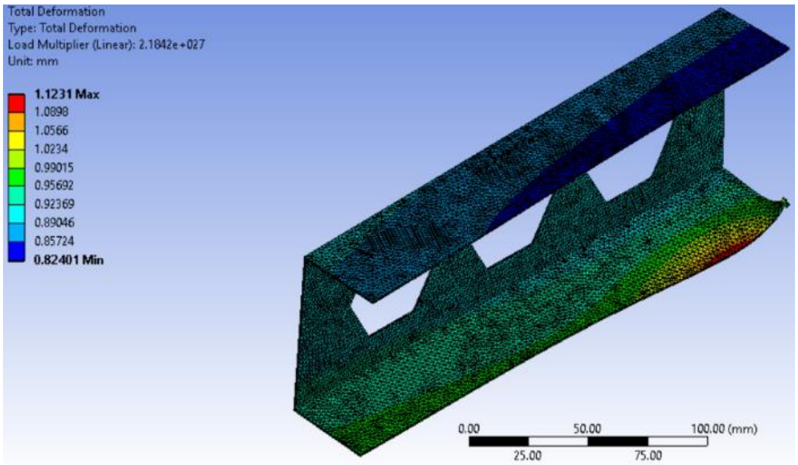

(a)

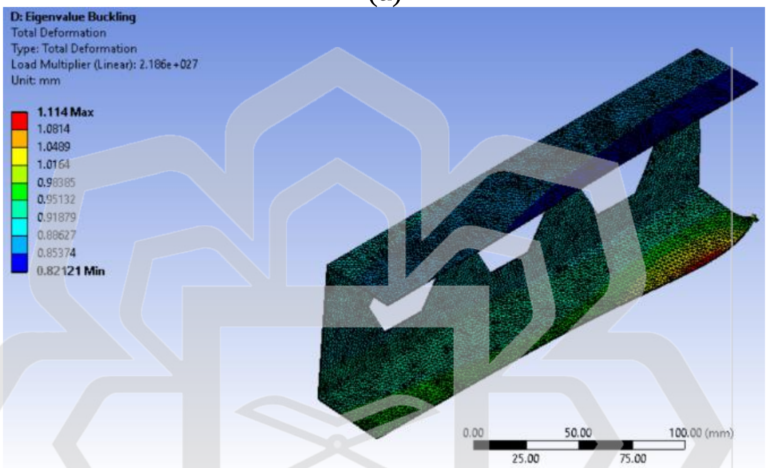

(b)

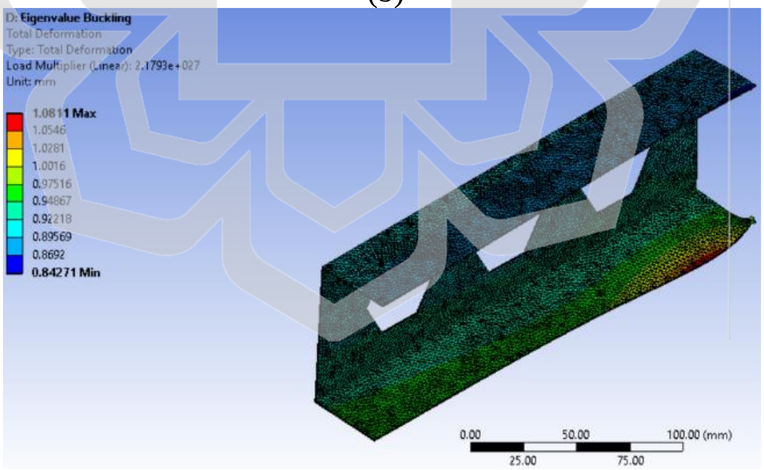

(c)

Figure 4.5 Total deformation (Eigenvalue buckling) under thermal load for hexagon cut-outs (a) W/Wo= 1.5, (b) W/Wo= 1.6, (c) W/Wo= 1.7

The obtained results from the study reveal interesting findings regarding the buckling behavior of thin-wall structures with and without perforations. In all the models analyzed, the flanges displayed a half-wave deformation along the longitudinal axes, attributed to the compressive stresses experienced during the loading process. This phenomenon was consistent across the reference model (without any holes) and the perforated models. The reference model, lacking any perforations, exhibited clear local buckling along the web. On the other hand, in the perforated models, buckling was not only observed along the web but also near the edges of the holes. This suggests that the presence of perforations influences the buckling behavior, leading to localized buckling phenomena near the hole boundaries.

Interestingly, despite the introduction of perforations and variations in their shapes for quasi-isotropic materials, a consistent pattern of half-wave deformation was observed in all models. This implies that the laminate configuration plays a significant role in determining the critical buckling load and the buckling shape of the thin-wall structure. Different laminate configurations can result in diverse buckling behaviors, influencing the structural stability of the thin-wall structure. Furthermore, it was noted that the first mode of buckling observed in all models was Euler buckling, affecting both the web and flanges of the thin-wall structure. Euler buckling refers to the sudden buckling failure of slender columns under axial compression, and its presence in all models highlights its dominance in the structural response of the thin-wall beams.

The study demonstrates that the buckling behavior of thin-wall structures is influenced by the presence of perforations and the laminate configuration. The half-wave deformation pattern along the flanges and the occurrence of localized buckling near hole edges in perforated models suggest that aperture placement can significantly affect structural stability. Moreover, the consistent occurrence of Euler buckling across all models underscores its importance in predicting buckling failures in thin-wall structures. These findings have implications for design optimization and provide valuable insights for engineering applications where thin-wall structures with apertures are commonly used.

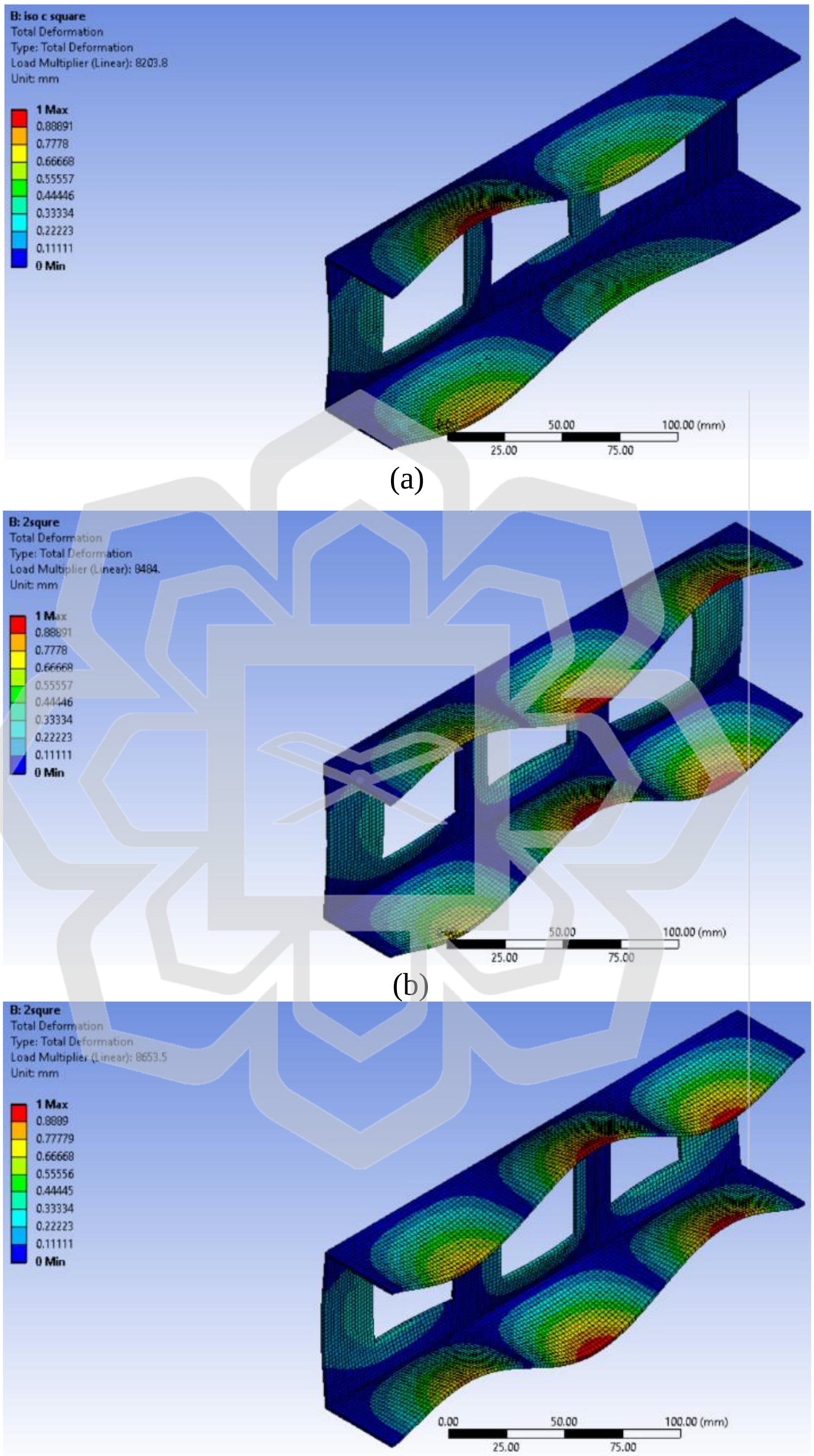

(c)

Figure 4.6 Total deformation (Eigenvalue buckling) under mechanical load for square cut-outs (a) W/Wo= 1.5, (b) W/Wo= 1.6, (c) W/Wo= 1.7

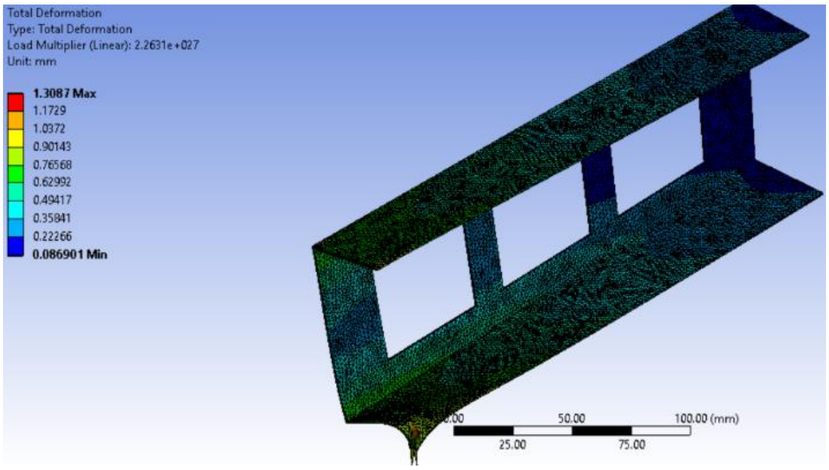

(a)

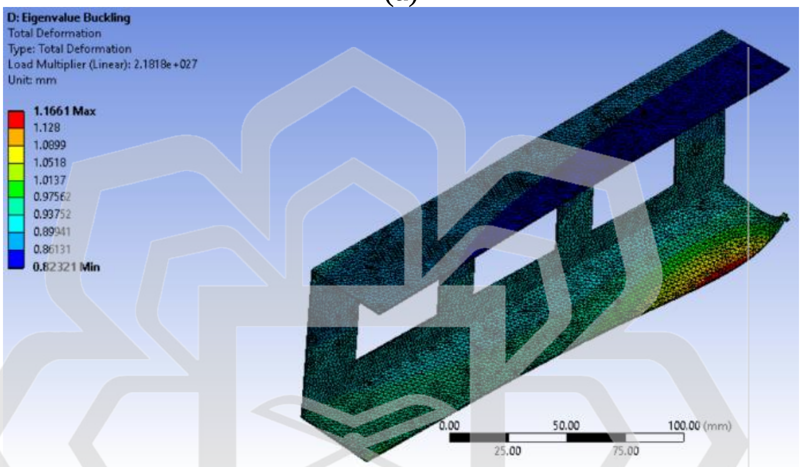

(b)

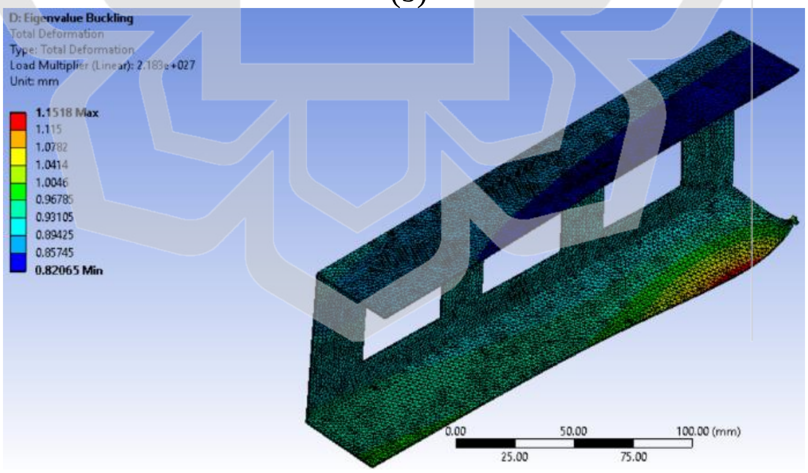

(c)

Figure 4.7 Total deformation (Eigenvalue buckling) under thermal load for square cut-outs (a) W/Wo= 1.5, (b) W/Wo= 1.6, (c) W/Wo= 1.7

4.2.4 Parametric Study on Critical Buckling Load

4.2.4.1 Quasi-isentropic

Figure 4.8 shows the impact of different cut-out shapes with various laminates is shown, while maintaining a constant spacing and opening ratio. The introduction of cut-outs leads to a decrease in the buckling load. Among the cut-out shapes, the circular cut-out exhibits the highest critical buckling load, while the square cut-out has the lowest buckling load capacity. The reduction in load is particularly noticeable with the introduction of holes, which can be attributed to a greater removal of area on the web of the thin wall. The circular shape results in the least amount of area removed, contributing to its higher critical buckling load capacity. Conversely, the square cut-out shape demonstrates the lowest buckling load under mechanical or thermal loads.

Figure 4.9 shows the relationship between the ratio of the opening and the buckling load. As the ratio of the opening decreases, it implies that the size of the holes in the thin-wall GFRP composite member increases. This trend aligns with the observation made in the previous paragraph, which stated that the introduction of greater perforation onto the web of the structure led to a decrease in the buckling load.

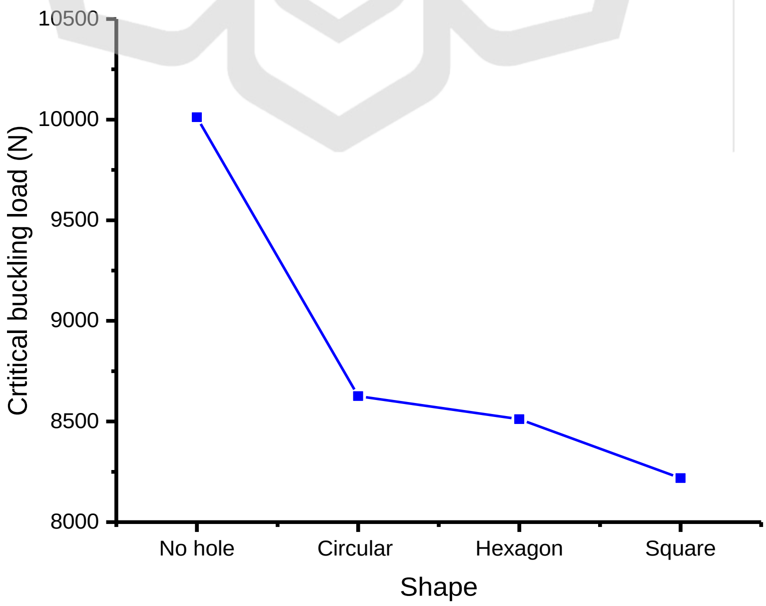

(a) Mechanical

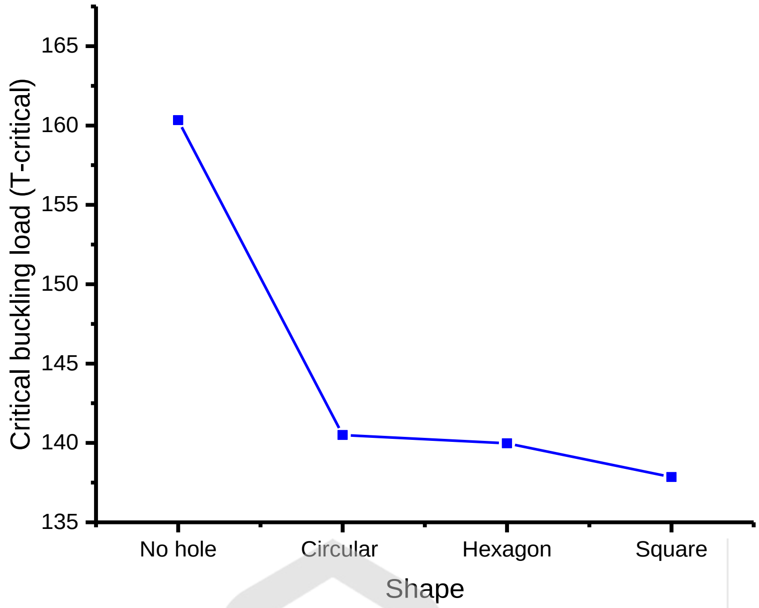

(b) Thermal

Figure 4.8. Influence of different hole shapes on the critical buckling load of quasi-isotropic laminates

In simpler terms, when the ratio of the opening decreases and the holes become larger, it has a negative effect on the buckling load capacity of the thin-wall GFRP composite member. The reduction in the buckling load occurs because larger holes remove more material from the web, weakening the overall structure's ability to withstand mechanical or thermal loads. Therefore, the finding in Figure 4.9 highlights the importance of considering the size of the openings and their impact on the structural behavior of thin-wall composite members.

In all cases studied, the mechanical load resulted in the highest buckling load values, while the thermal load exhibited the lowest range of buckling load. However, Figure 4.9(a) reveals that the critical buckling load remains relatively constant. Under thermal load conditions which is shown in Figure 4.9 (b), the spacing ratio of 1.5 demonstrates higher buckling values. This occurs when the diameter is in a low range, while the body of the structure contains a high proportion of solid regions.

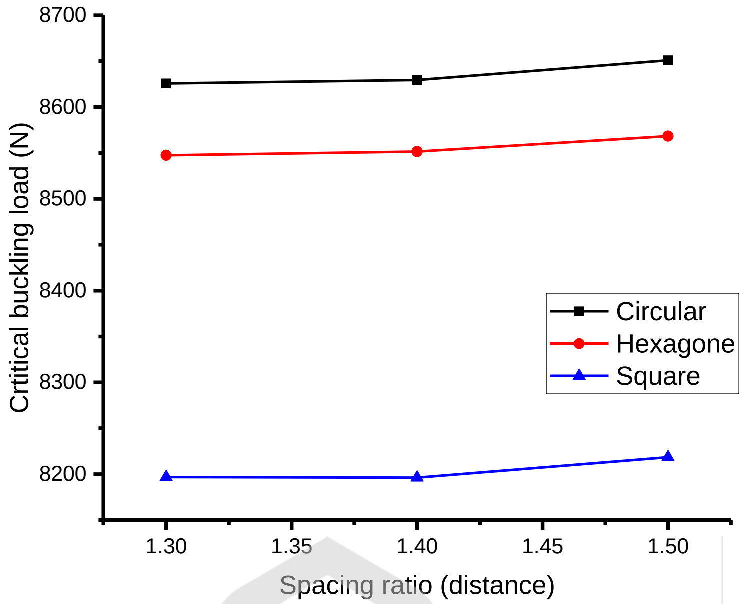

(a) Mechanical

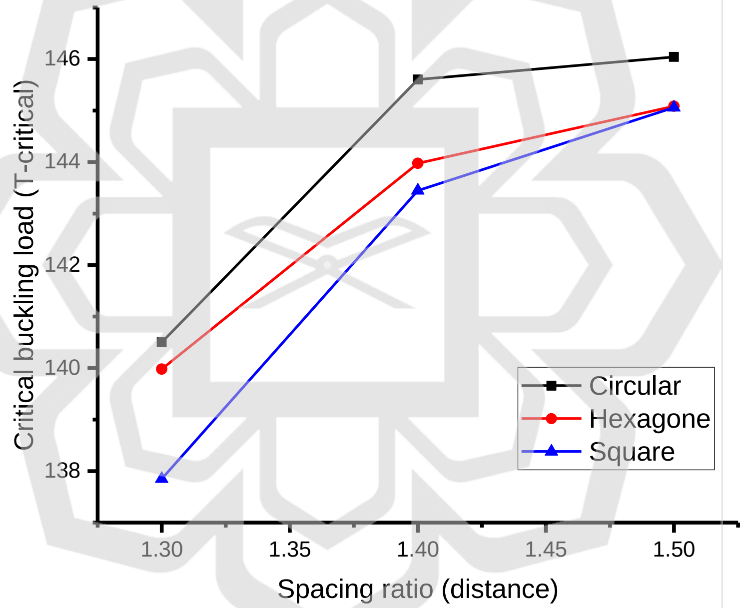

(b) Thermal

Figure 4.9 Influence of different spacing ratio on the critical buckling load of quasi-isotropic laminates

Finally, Figure 4.10 displays graphs that indicate a relatively insignificant decrease in trend as the opening ratio decreases. When the opening ratio remains constant, it can be inferred that the distance between the centers of two holes decreases as the ratio decreases. Considering all the figures mentioned in this section, it can be concluded that, across all laminates, the combination of a circular shape, an opening ratio of 1.7, and a spacing ratio of 1.5 exhibits the highest critical buckling load. This phenomenon holds true for both mechanical and thermal loads. When the distance within the structure is large, the buckling load is found to be higher. Conversely, when the distance is reduced, the buckling load decreases. However, the combined effect of these parameters will be further discussed in subsequent sections.

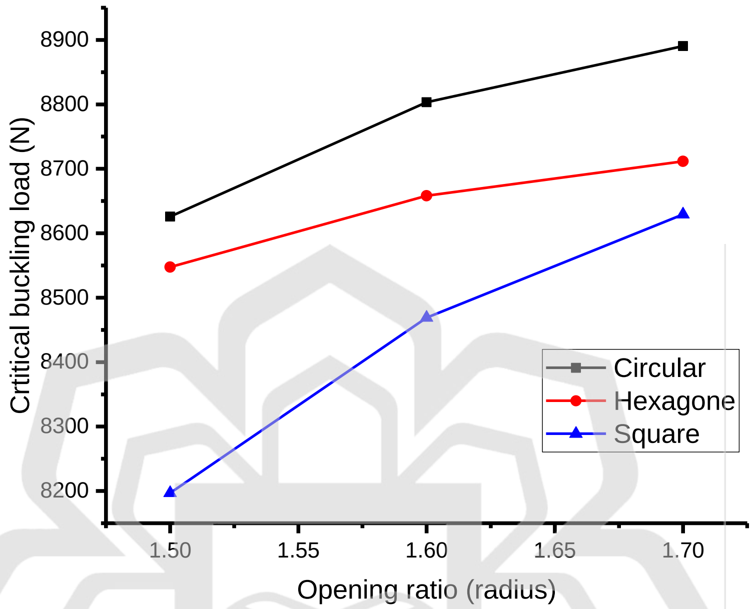

(a) Mechanical

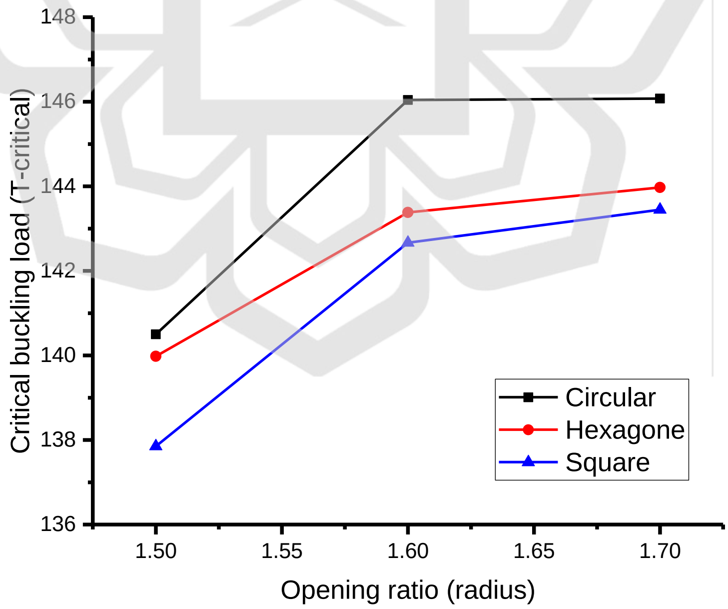

(b) Thermal

Figure 4.10 Influence of different opening ratio on the critical buckling load of quasi-isotropic laminates

4.2.4.2 Angle-ply

Figure 4.11 presents the impact of different cut-out shapes combined with various laminates, which is comparable to Figure 4.8. With the introduction of cut-outs, there is a noticeable decrease in the buckling load. Among the various cut-out shapes examined, the circular cut-out exhibits the highest critical buckling load, while the square cut-out displays the lowest load capacity in terms of buckling. The reduction in load capacity is particularly evident when holes are introduced. This is attributed to a greater removal of area from the web of the thin wall, with the circular shape resulting in the least amount of area being removed. Additionally, when subjected to mechanical or thermal loads, the square cut-out shape demonstrates the lowest buckling load.

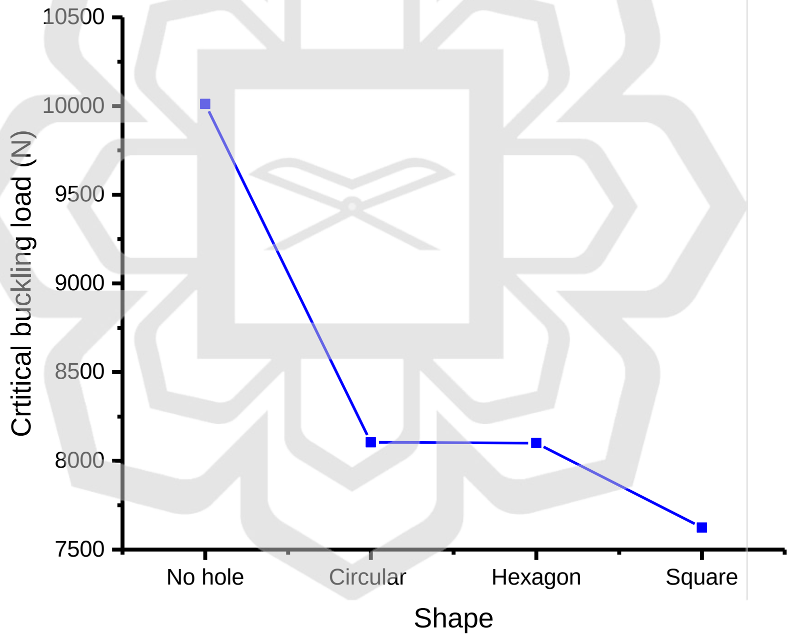

(a) Mechanical

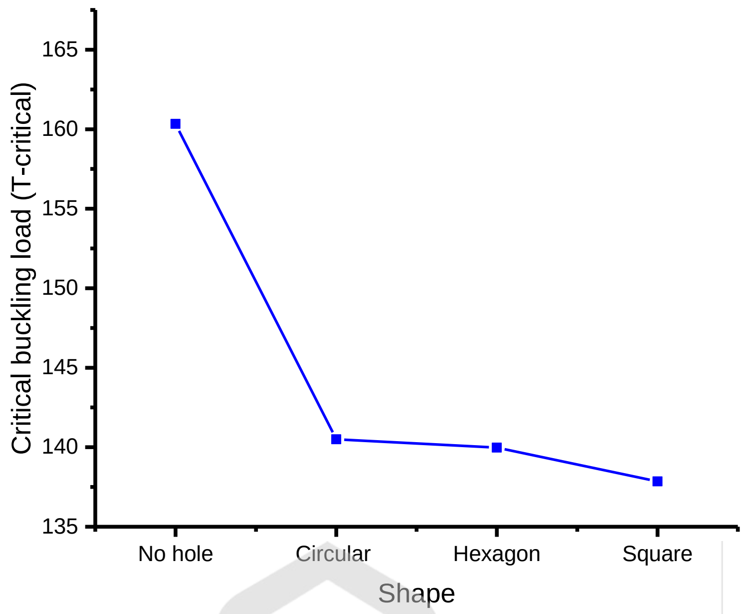

(b) Thermal

Figure 4.11 Influence of different hole shapes on the critical buckling load of angle-ply laminates

Figure 4.12 demonstrates a similar trend in the angle ply model as observed in the quasi-isotropic model results. Specifically, a declining trend is observed as the ratio of the opening decreases, indicating that larger holes are associated with smaller ratios. This finding aligns with the earlier observation that greater perforation on the web of the thin wall GFRP composite member leads to a decrease in the buckling load.

In all the cases examined, the mechanical load consistently resulted in the highest buckling load values, while the thermal load exhibited the lowest range of buckling load. However, Figure 4.12(a) indicates that the critical buckling load remains relatively constant across different ratios. Under thermal load conditions, as depicted in Figure 4.12(b), the spacing ratio of 1.5 demonstrates higher buckling values. This occurs when the diameter is in a low range, while the body of the structure contains a high proportion of solid regions.

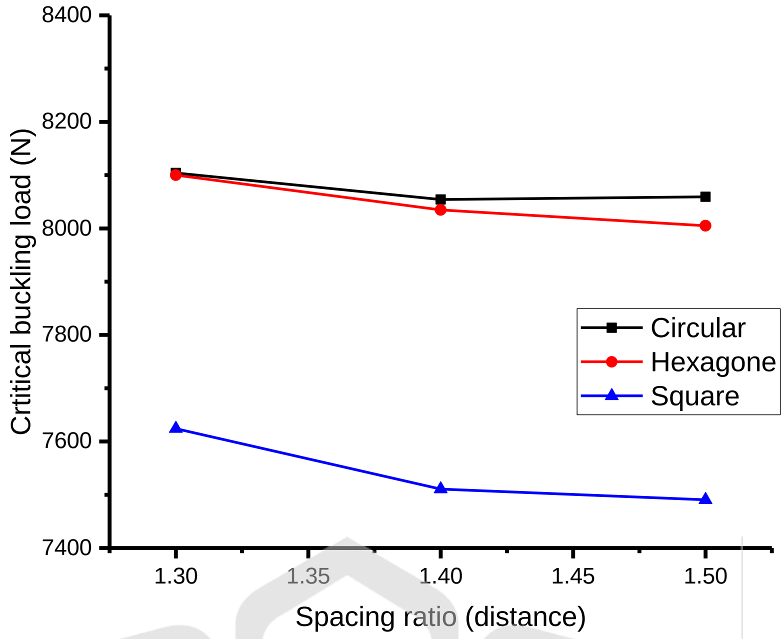

(a) Mechanical

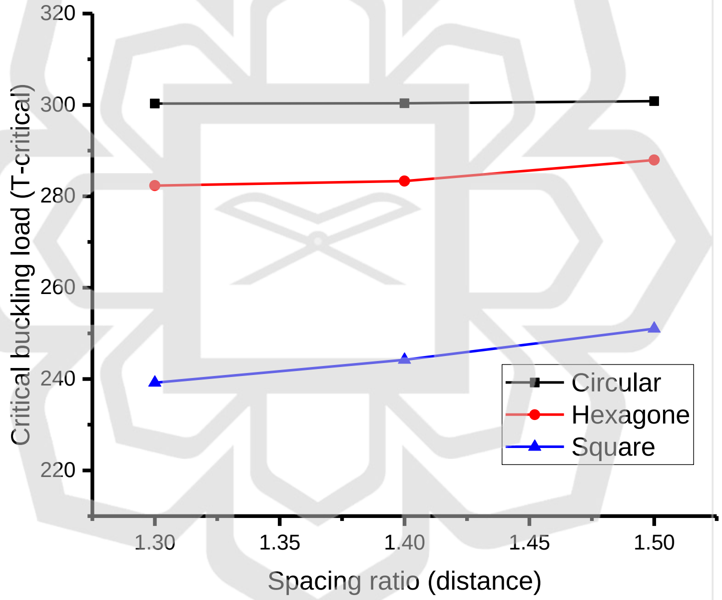

(b) Thermal

Figure 4.12 Influence of different spacing ratio on the critical buckling load of angle-ply laminates

Figure 4.13 presents graphs showing a relatively minor decline as the opening ratio decreases. This suggests that as the ratio decreases, the distance between the centers of two holes also decreases. Based on the analysis of all the figures discussed in this section, it can be concluded that, regardless of the laminate used, the configuration with a circular shape, an opening ratio of 1.7, and a spacing ratio of 1.5 exhibits the highest critical buckling load. This observation holds true for both mechanical and thermal loads. Furthermore, it is noted that a larger distance within the structure corresponds to a higher buckling load, while reducing the distance leads to a decrease in buckling load. However, the combined effect of these parameters will be further explored in subsequent sections.

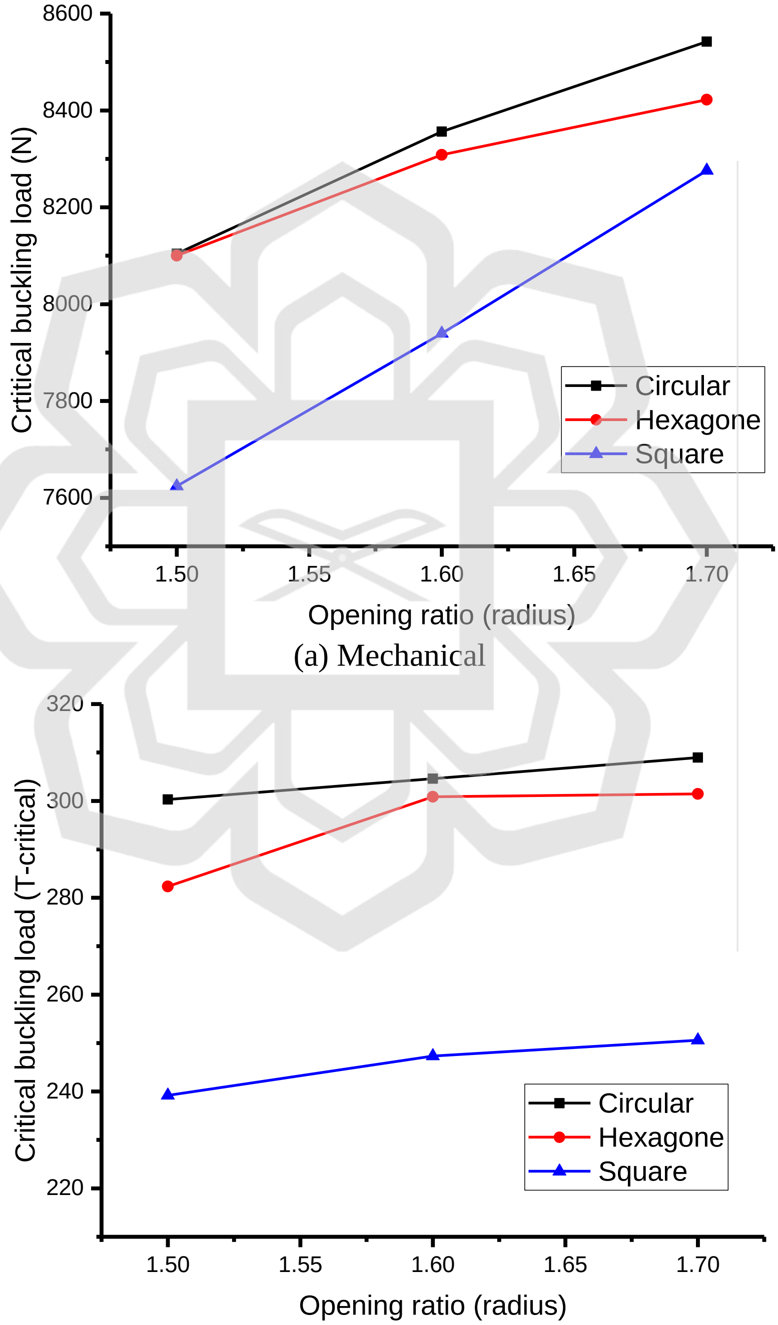

Figure 4.13 Influence of different opening ratio on the critical buckling load of angle-ply laminates

4.2.4.3 Cross-ply

The results presented in Figure 4.14 depict the behavior of a cross-ply fiber orientation in terms of shape. Overall, the trends observed in this model are like the previously discussed models, with variations in the numerical values of the critical buckling load. The maximum critical buckling load reaches approximately 10,000 N when there is no hole in the channel, while the structures have a circular hole the values suddenly decrease to 4200 which shows a good variation compared to the previous two models. On the other hand, the lowest point is found to be around 3,900 N, as shown in Figure 4.14(a). Similarly, the results for thermal buckling load in this model resemble the findings from the previous models, as indicated in Figure 4.14(b).

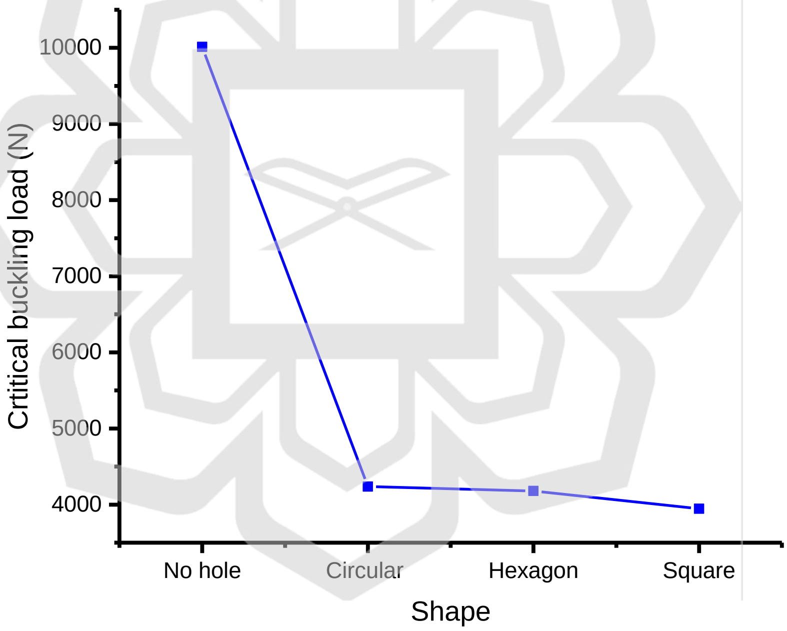

(a) Mechanical

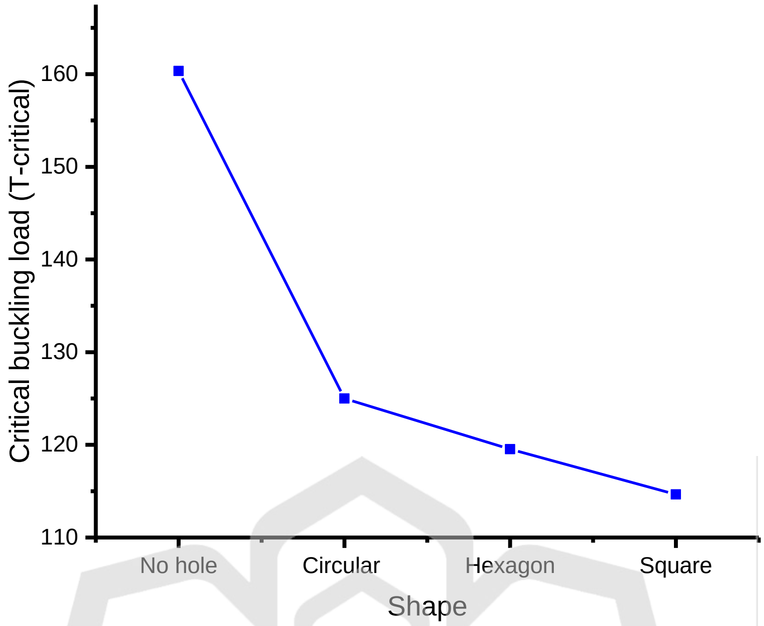

(b) Thermal

Figure 4.14 Influence of different hole shape on the critical buckling load of cross-ply laminates

The impact of the spacing ratio in the cross-model reveals similarities among all the models examined in this study. When considering the square shape, the minimum critical buckling load value of approximately 3,950 N is observed with a spacing ratio of 1.3. However, with a spacing ratio of 1.5, the critical buckling load increases to around 4,050 N. This indicates that an increase in the spacing ratio leads to an increment in the critical buckling load under both mechanical and thermal loads which is illustrated in Figure 4.15.

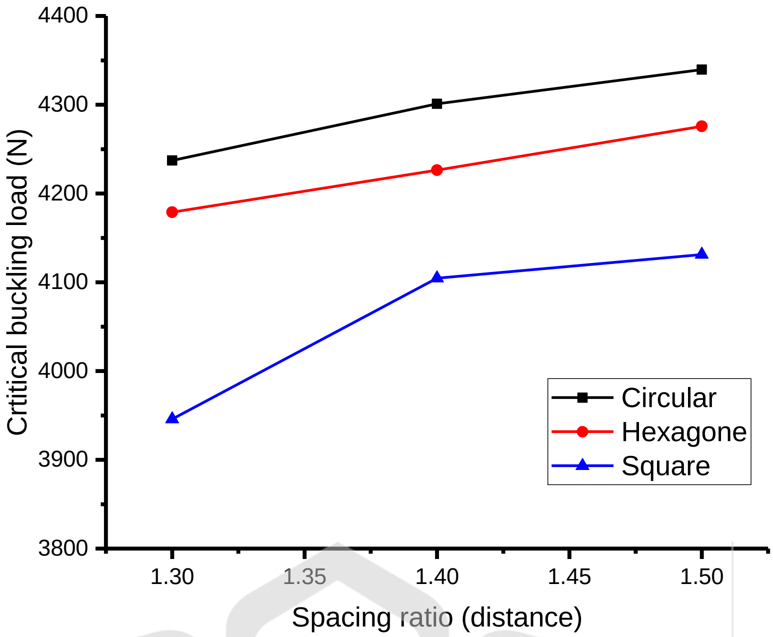

(a) Mechanical

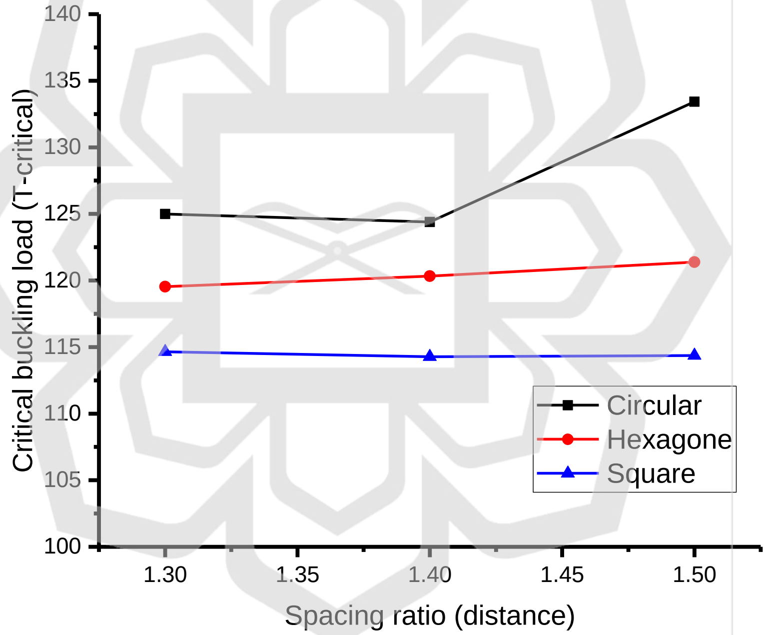

(b) Thermal

Figure 4.15 Influence of different spacing ratio on the critical buckling load of cross-ply laminates

The results shown in Figure 4.16 are similar approximately like the results of Figure 4.10 and 4.13.

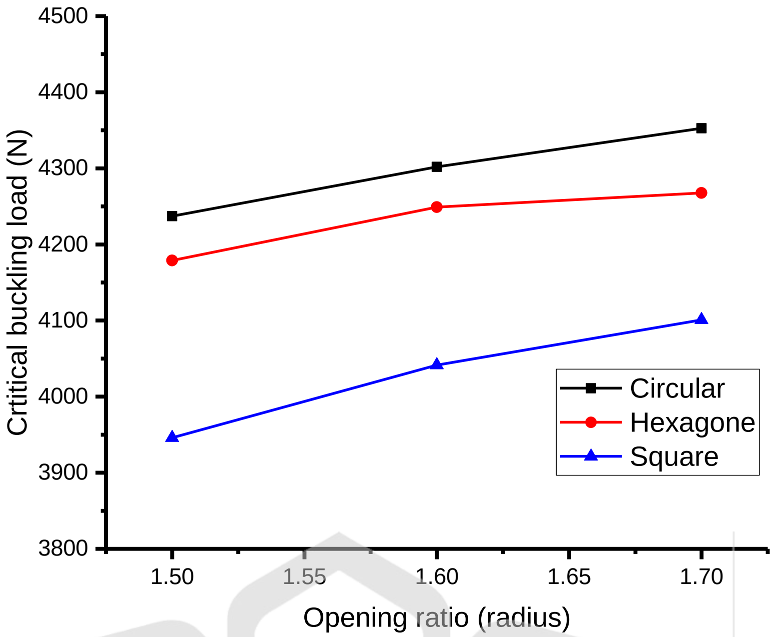

(a) Mechanical

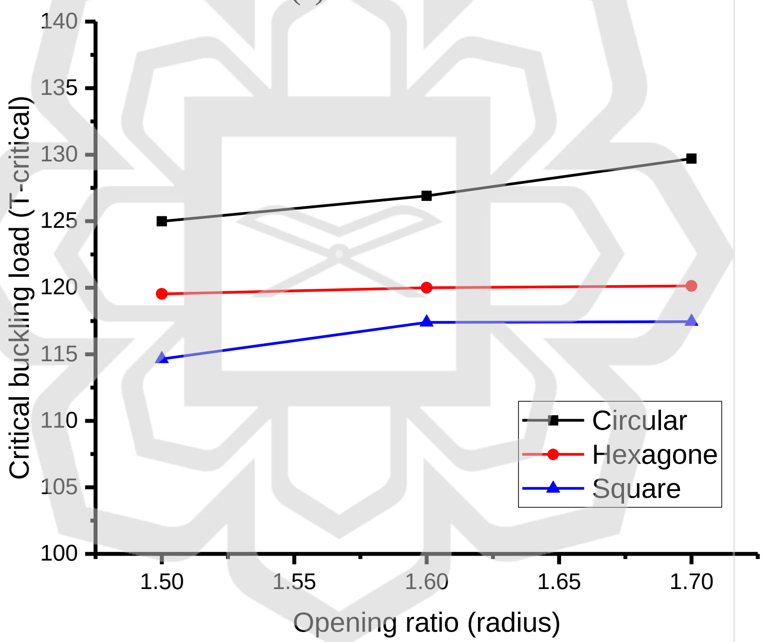

(b) Thermal

Figure 4.16 Influence of different opening ratio on the critical buckling load of cross-ply laminates

4.2.4.4 Balanced

The results of the balanced model in this study exhibit similarities with the outcomes of other models such as the quasi-isentropic, angle-ply, and cross-ply models. The effects of different parameters, including shape, spacing ratio, and opening ratio, were investigated in Figures 4.17, 4.18, and 4.19, respectively, and the behavior of the balanced model was consistent with the trends observed in previous models. In terms of the effect of shape, the critical buckling load under both mechanical and thermal loads was found to be like previous studies. This indicates that the shape of the apertures has a limited impact on the buckling behavior, and the overall trends observed in the balanced model align with previous models.

For the effect of spacing ratio, the critical buckling load in the balanced model was notably higher than in the previous case, exceeding 8000 N. This indicates that the load-carrying capacity of the balanced model is significantly stronger, making it capable of efficiently supporting thin-walled structures. Under thermal load conditions, the T-critical values were in the range of 160 to 175, which is similar to the observations for the spacing ratio. Finally, the results of the opening ratio in the balanced model also demonstrated higher critical buckling loads under both mechanical and thermal loads. This further supports the idea that the balanced model, along with its specific orientations, exhibits superior strength-to-weight ratios, making it a valuable option for designing structures in engineering applications.

Overall, the balanced model shows promising characteristics, offering high strength with low weight. Its critical buckling loads are comparable to or even exceed those of other established models. This suggests that the balanced model can serve as a reliable and efficient option for designing thin-walled structures, especially when considering the performance under both mechanical and thermal loading conditions. Engineers and designers can leverage these findings to optimize thin-walled structures with apertures, enhancing their load-carrying capacity and structural integrity for various engineering applications.

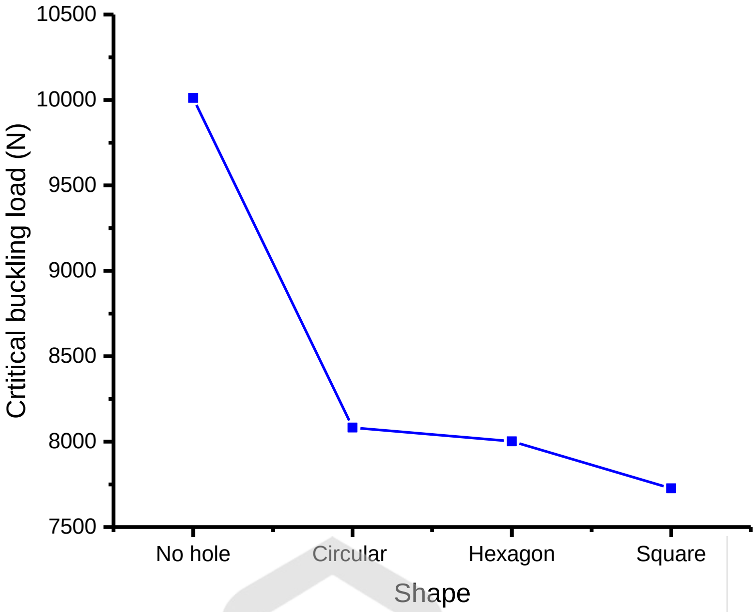

(a) Mechanical

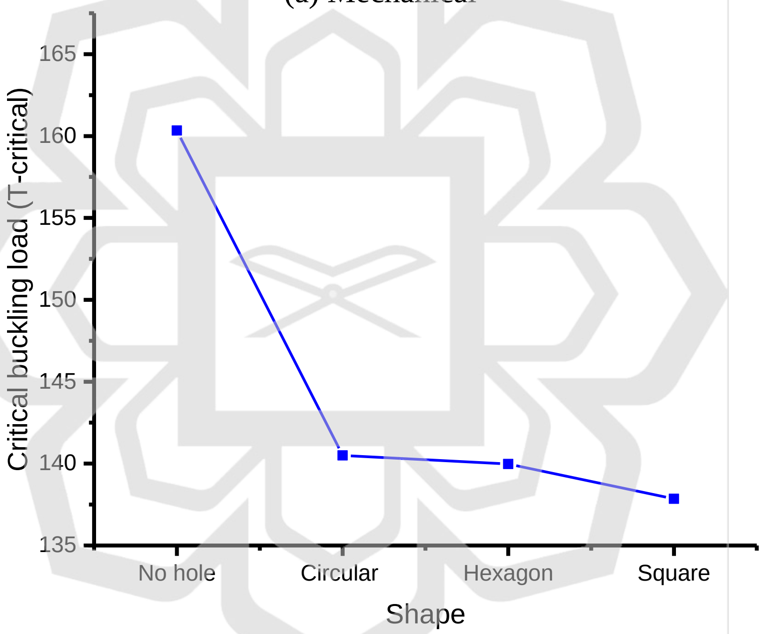

(b) Thermal

Figure 4.17 Influence of different hole shape on the critical buckling load of balanced laminates

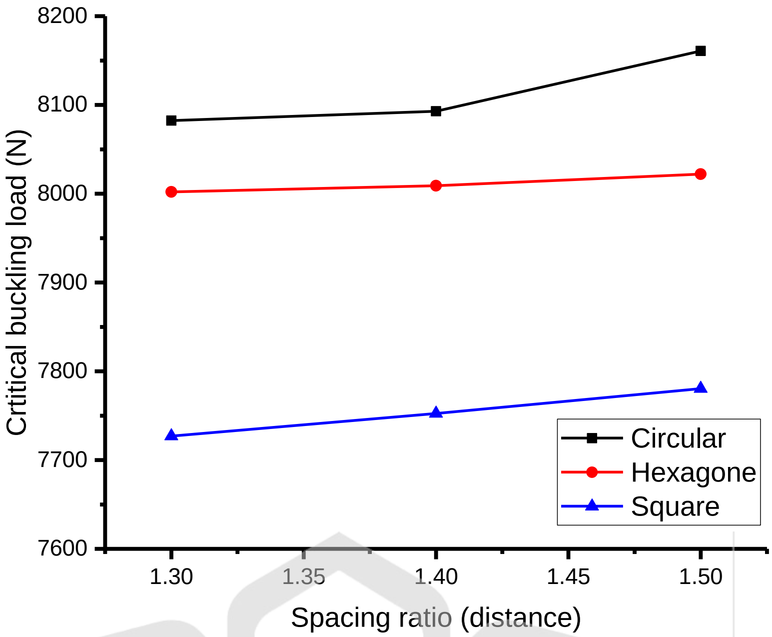

(b) Mechanical

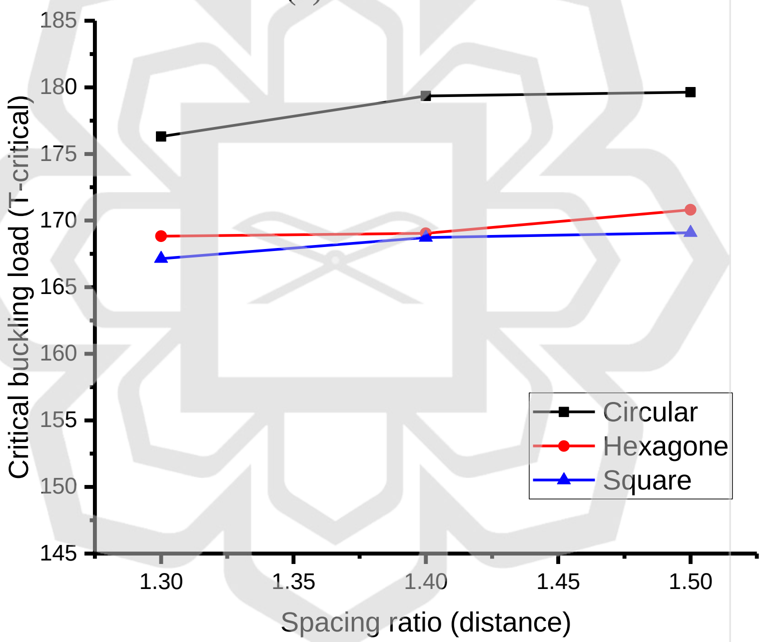

(b) Thermal

Figure 4.18 Influence of different spacing ratio on the critical buckling load of balanced laminates

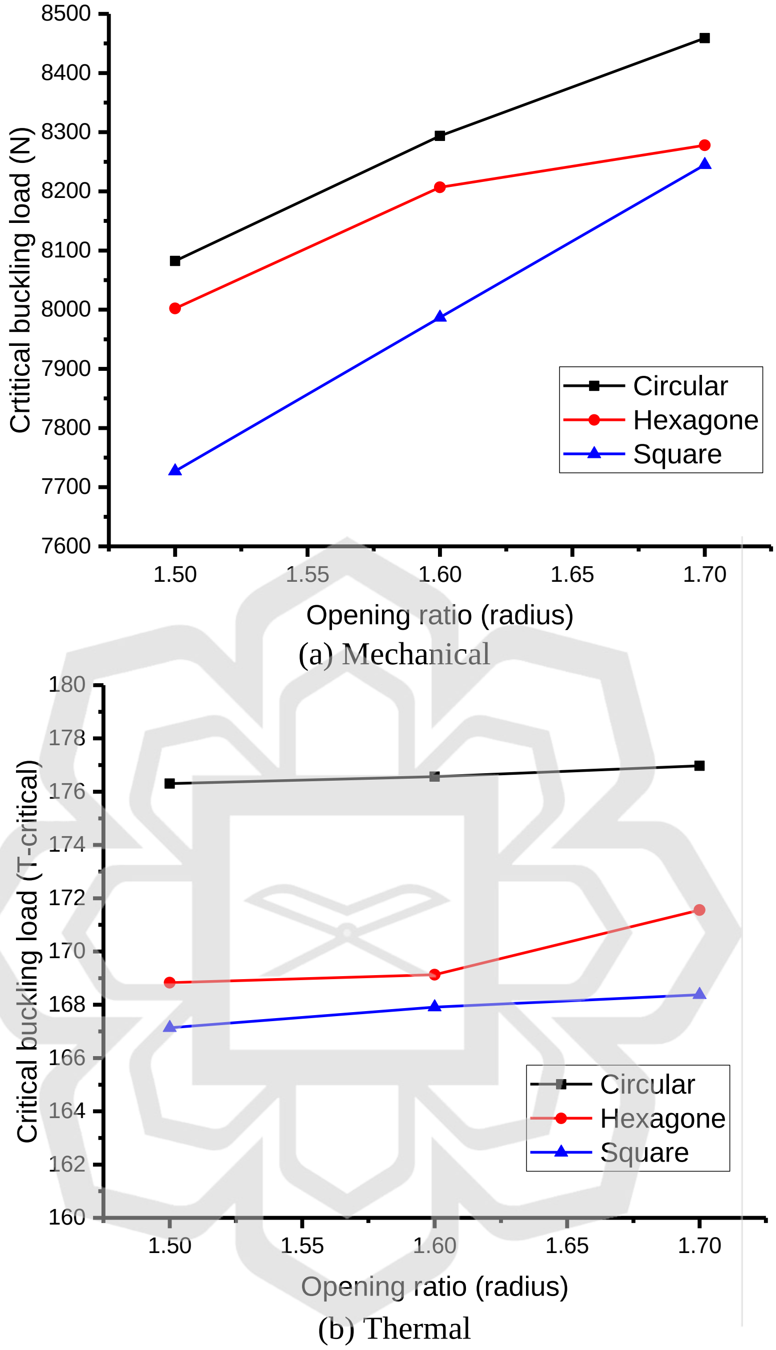

Figure 4.19 Influence of different opening ratio on the critical buckling load of balanced laminates

4.3 MACHINE LEARNING MODELS EVALUATION AND RESULTS

4.3.1 Linear Regression Model Evaluation

In the model training and evaluation stage, a linear regression model is employed to analyze the dataset (Figure 4.20 (a) and 4.20(b)). The following steps are taken: Firstly, the Linear Regression class from the sklearn.linear_model module is utilized to fit a Linear Regression model on the training set. This involves training the model using the scaled training features (X_train_scaled) and corresponding labels (y_train). Next, predictions are generated on the test set by applying the trained model to the scaled test features (X_test_scaled). The `predict()` method is employed to obtain these predicted labels.

The evaluation of the Linear Regression model's performance involves calculating several metrics to assess its accuracy. These metrics include the mean squared error (MSE), root mean squared error (RMSE), and R-squared (R^2) values, which are essential for gauging the model's predictive capabilities. The calculations are performed using functions from the sklearn.metrics module, ensuring accuracy and consistency in the evaluation process.

To calculate MSE, the mean_squared_error() function from the sklearn.metrics module is employed. This metric evaluates the average squared variance between predicted values and actual labels. A lower MSE signifies a more precise model, indicating closer predictions of true values. Additionally, the goodness of fit of the model is evaluated using the R-squared value, which is derived from the R^2_score() function. R^2 quantifies the proportion of predictable variance in the dependent variable stemming from the independent variables. A value closer to 1 signifies a stronger model-data fit.

After computing the MSE, RMSE, and R^2 values, they are printed for easy interpretation and comparison. These metrics provide a quantitative assessment of the model's performance and allow researchers and practitioners to determine its accuracy and reliability in predicting critical buckling loads. Moreover, a scatter plot is created using the matplotlib.pyplot module, visually displaying the predicted labels against the actual labels. This plot enables a direct comparison between the model's predictions and the true values. A well-fitted model will exhibit data points closely clustered around a diagonal line, representing a strong correlation between predicted and actual values. By following these evaluation steps, the Linear Regression model's effectiveness in predicting critical buckling loads can be thoroughly analyzed.

The combination of quantitative metrics and visual representation provides a comprehensive understanding of the model's performance. Engineers and researchers can use this analysis to make informed decisions about the model's reliability and suitability for predicting critical buckling loads in different scenarios based on the given dataset. It also allows for fine-tuning the model and exploring ways to improve its predictive capabilities, contributing to more accurate and efficient engineering analyses.

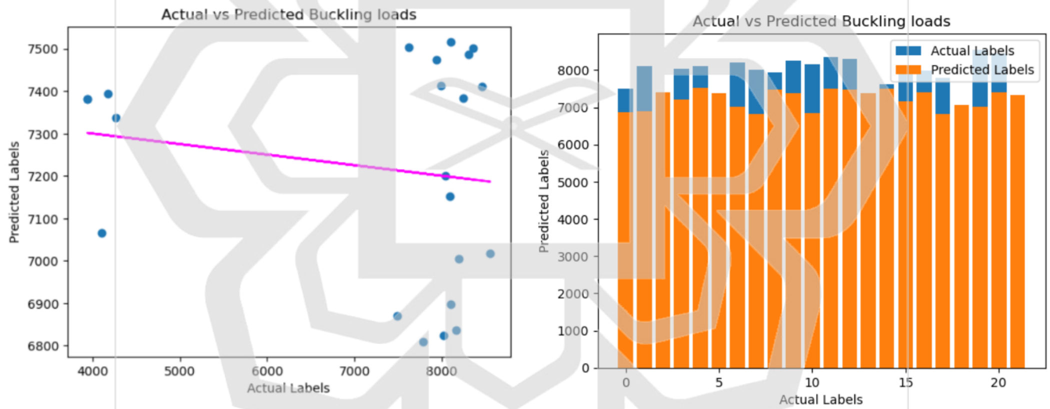

(a) Mechanical Load

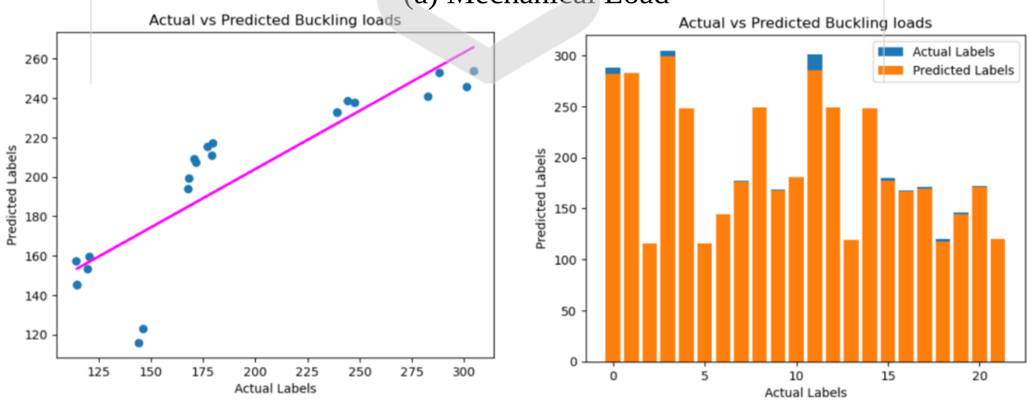

(b) Thermal Load

Figure 4.20 Analysis of linear regression model

4.3.2 Lasso Regression Model Evaluation

In the next stage of model training and evaluation, a lasso regression model is employed (Figure 4.21(a) and (b)). The process involves the following steps: Firstly, the Lasso class from the sklearn.linear_model module is used to fit the Lasso Regression model on the training set. The training features (X_train) and corresponding labels (y_train) are used for model training. Next, predictions are generated on the test set by applying the trained Lasso Regression model to the test features (X_test). The `predict()` method is utilized to obtain these predicted labels.

The assessment of the Lasso Regression model encompasses the computation and analysis of various metrics to gauge its effectiveness in predicting the critical buckling load. Essential metrics including MSE, RMSE, and R^2 values are employed to offer insights into the model's performance. MSE measures the average squared difference between predicted and actual values, with a lower value signifying greater accuracy. RMSE, the square root of MSE, quantifies error in the same units as the target variable. R^2 is a pivotal metric that elucidates the proportion of dependent variable variance accounted for by independent variables, depicting the model's fit to the data, ranging from 0 to 1. Higher R^2 values denote a superior model fit and a greater capacity to explain critical buckling load variability.

After calculating the MSE, RMSE, and R^2 values, they are printed to allow for a quantitative assessment of the Lasso Regression model's performance. These metrics help researchers and practitioners understand how well the model performs in predicting the critical buckling load based on the given dataset. Furthermore, a scatter plot is created to visually compare the predicted labels against the actual labels. This graphical representation provides a clear visualization of the relationship between the predicted and actual values. A well-performing model will exhibit data points closely clustered around a diagonal line, indicating a strong correlation between the predicted and actual values. By following these evaluation steps, a comprehensive analysis of the Lasso Regression model's accuracy in predicting the critical buckling load can be conducted. Engineers and researchers can use this information to assess the model's reliability and suitability for predicting critical buckling loads in different scenarios based on the given dataset. This evaluation process also facilitates model optimization and allows for improvements to enhance its predictive capabilities, contributing to more accurate and efficient engineering analyses.

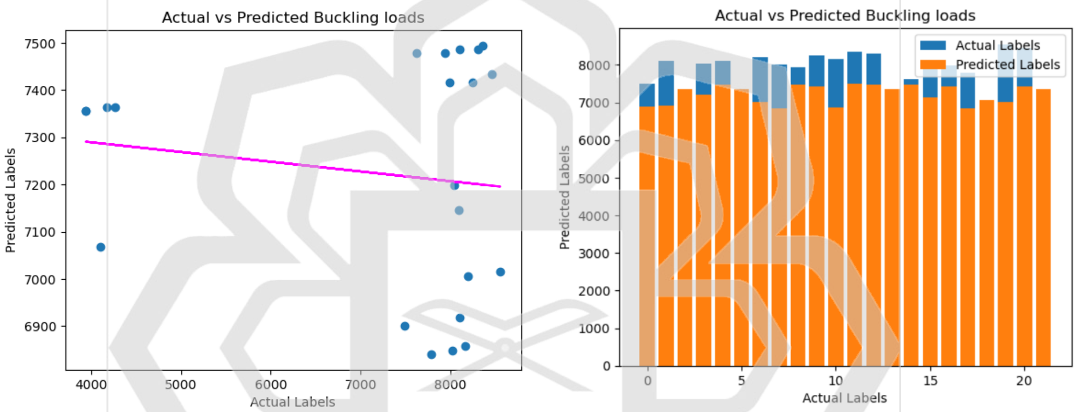

(a) Mechanical Load

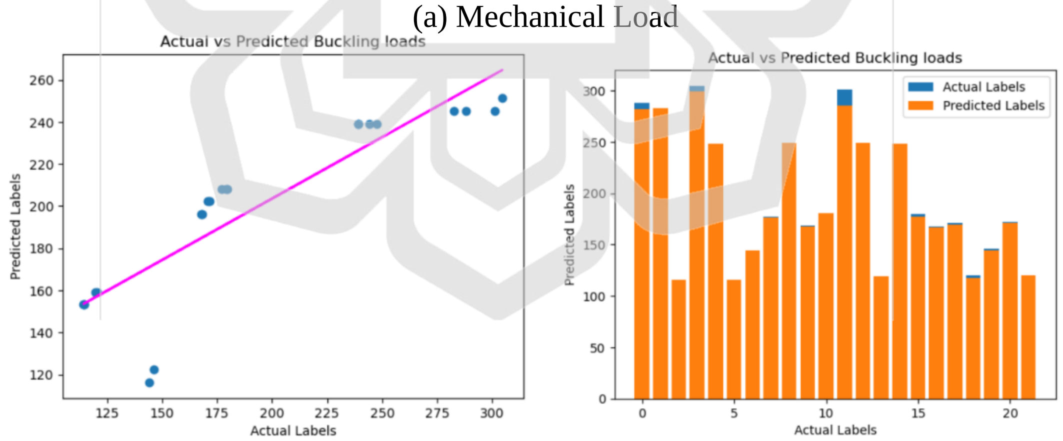

(a) Thermal Load

Figure 4.21 Analysis of lasso regression model

4.3.3 Decision Tree Regression Model Evaluation

In the model training and evaluation process, a decision tree regression model is utilized (Figure 4.22.a & 4.22.b). Here are the steps involved: Firstly, the decision tree regressor class from the sklearn.tree module is employed to fit the Decision Tree Regression model on the training set. The training features (X_train) and corresponding labels (y_train) are used to train the model. Next, predictions are generated on the test set by applying the trained Decision Tree Regression model to the test features (X_test). The `predict()` method is used to obtain these predicted labels.

To evaluate the performance of the Decision Tree Regression model, several metrics are computed to gauge its accuracy in predicting the critical buckling load. Key metrics, such as MSE, RMSE, and R^2 values, are employed to provide valuable insights into the model's fit. MSE quantifies the average squared disparity between predicted values and actual labels, with lower values indicating heightened accuracy. RMSE, derived as the square root of MSE, offers error measurement in the same units as the target variable, enhancing interpretability. R^2, a pivotal metric, evaluates the proportion of critical buckling load variance elucidated by independent variables, with values nearer to 1 signifying superior model-data fit, indicating a greater capacity to clarify critical buckling load variability.

Once the MSE, RMSE, and R^2 values are calculated, they are printed to enable a quantitative assessment of the Decision Tree Regression model's performance. These metrics provide researchers and practitioners with valuable information on how well the model performs in predicting the critical buckling load based on the given dataset. In addition to quantitative evaluation, a scatter plot is created to visually compare the predicted labels against the actual labels. This graphical representation allows for a clear visualization of the relationship between the predicted and actual values. A well-performing Decision Tree Regression model will exhibit data points closely clustered around a diagonal line, indicating a strong correlation between the predicted and actual values.

By following these evaluation steps, a comprehensive analysis of the Decision Tree Regression model's accuracy in predicting the critical buckling load can be conducted. Engineers and researchers can use this information to assess the model's reliability and suitability for predicting critical buckling loads in different scenarios based on the given dataset. The combination of quantitative metrics and visual examination provides a robust understanding of the model's effectiveness, facilitating model optimization and improvements to enhance its predictive capabilities. Ultimately, this evaluation process contributes to more accurate and efficient engineering analyses involving the prediction of critical buckling loads.

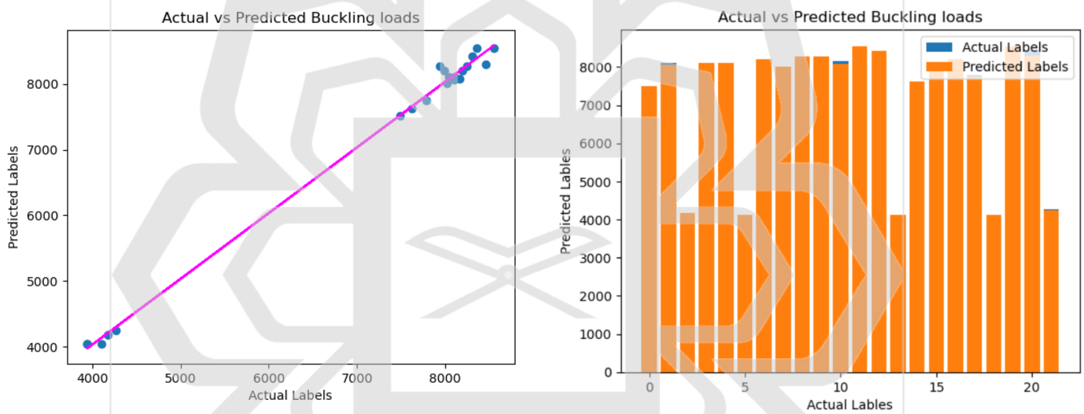

(a) Mechanical Load

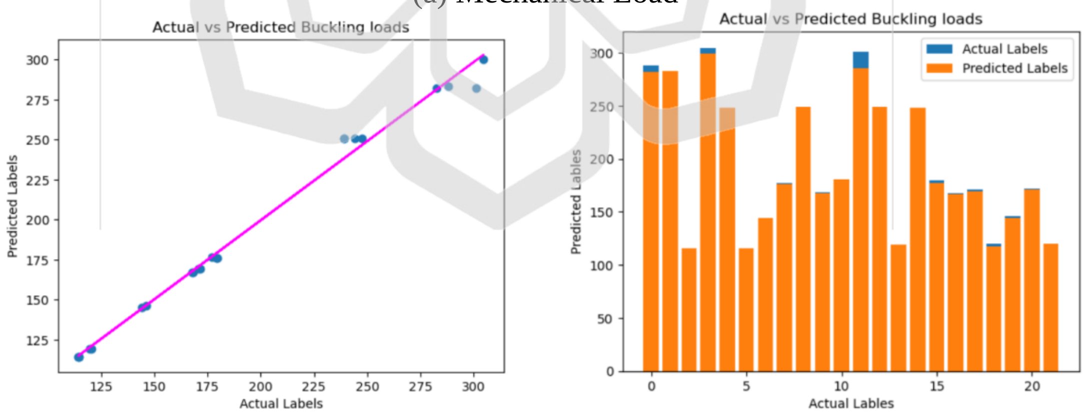

(b) Thermal Load

Figure 4.22 Analysis of decision tree regression model

4.3.4 Random Forest Regression Model

In the model training and evaluation process, a random forest regression model is utilized (Figure 4.23 (a) and (b)). The following steps are taken: Firstly, the Random Forest Regressor class from the sklearn.ensemble module is used to fit the Random Forest Regression model on the training set. The training features (X_train) and corresponding labels (y_train) are used for training the model. Next, predictions are made on the test set by applying the trained Random Forest Regression model to the test features (X_test). The `predict()` method is employed to obtain these predicted labels.

The evaluation of the Random Forest Regression model's effectiveness involves the computation of diverse metrics aimed at assessing its accuracy in predicting the critical buckling load. Key metrics, including MSE, RMSE, and R^2 values, provide valuable insights into the model's fit. MSE calculates the average squared deviation between predicted and actual labels, with lower values indicating greater precision. RMSE, obtained as the square root of MSE, delivers an error metric in the same units as the target variable, enhancing interpretability. R^2, a pivotal metric, evaluates the proportion of critical buckling load variance elucidated by independent variables, with values nearing 1 denoting a superior model-data alignment, signifying a heightened capacity to expound critical buckling load variability. This comprehensive assessment framework facilitates a thorough understanding of the Random Forest Regression model's performance in the context of predicting critical buckling load.

Once the MSE, RMSE, and R^2 values are calculated, they are printed to enable a quantitative assessment of the Random Forest Regression model's performance. These metrics provide researchers and practitioners with valuable information on how well the model performs in predicting the critical buckling load based on the given dataset. In addition to quantitative evaluation, a scatter plot is created to visually compare the predicted labels against the actual labels. This graphical representation allows for a clear visualization of the relationship between the predicted and actual values. A well-performing Random Forest Regression model will exhibit data points closely clustered around a diagonal line, indicating a strong correlation between the predicted and actual values.

By following these evaluation steps, a comprehensive analysis of the Random Forest Regression model's accuracy in predicting the critical buckling load can be conducted. Engineers and researchers can use this information to assess the model's reliability and suitability for predicting critical buckling loads in different scenarios based on the given dataset. The combination of quantitative metrics and visual examination provides a robust understanding of the model's effectiveness, facilitating model optimization and improvements to enhance its predictive capabilities. Ultimately, this evaluation process contributes to more accurate and efficient engineering analyses involving the prediction of critical buckling loads.

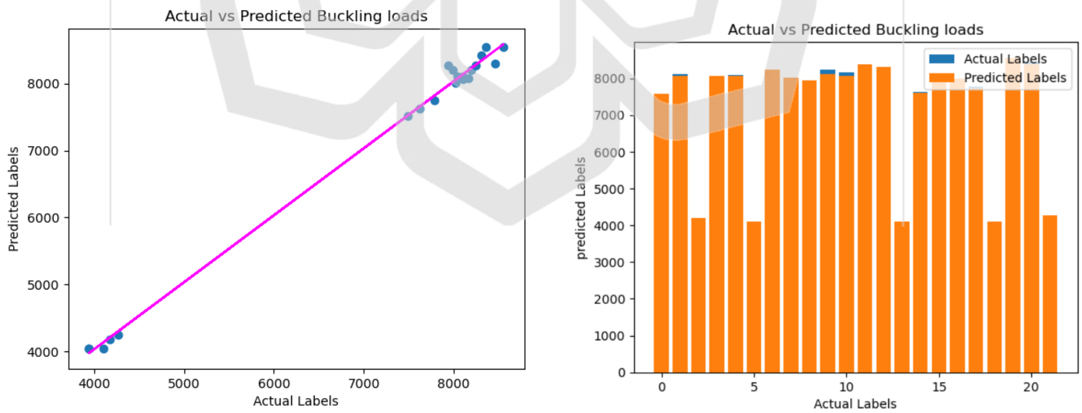

(a) Mechanical Load

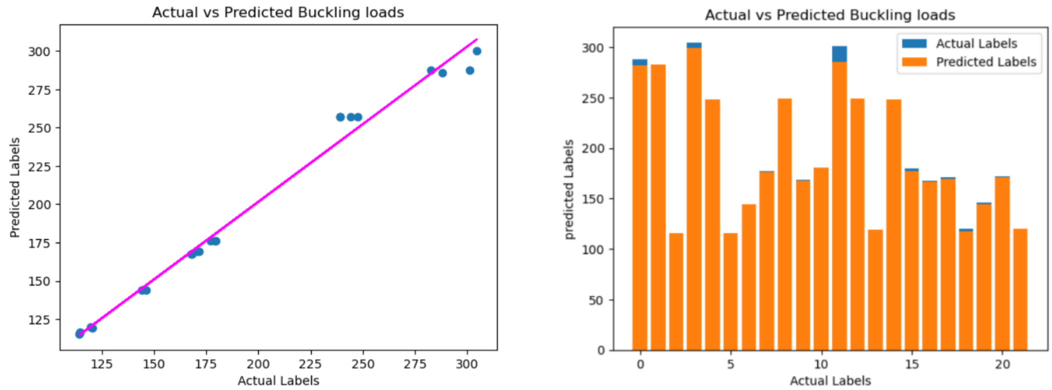

(b) Thermal Load

Figure 4.23 Analysis of random forest regression model

4.3.5 Gradient Boosting Regression Model

In the model training and evaluation process, a Gradient Boosting Regression model is employed (Figure 4.24(a) and (b)). The following steps are involved: Firstly, the Gradient Boosting Regressor class from the sklearn.ensemble module is utilized to fit the Gradient Boosting Regression model on the training set. The training features (X_train) and corresponding labels (y_train) are used for training the model. Next, predictions are made on the test set by applying the trained Gradient Boosting Regression model to the test features (X_test). The `predict()` method is utilized to obtain these predicted labels.

The evaluation of the Gradient Boosting Regression model's performance entails the computation of diverse metrics to gauge its accuracy in predicting the critical buckling load. These pivotal metrics encompass MSE, RMSE, and R^2 values, collectively offering valuable insights into the model's goodness of fit. MSE, the cornerstone of assessment, quantifies the average squared deviation between predicted and actual labels. Lower MSE values are indicative of a more precise model, signifying that its predictions closely align with actual values. RMSE, derived from the square root of MSE, presents an error metric in the same units as the target variable, enhancing interpretability. Furthermore, R^2 serves as a critical metric, evaluating the proportion of variance in the dependent variable (critical buckling load) that can be elucidated by the independent variables within the model. An R^2 value approaching 1 signifies a superior model-data fit, implying an enhanced capacity to elucidate the variability observed in the critical buckling load. This comprehensive assessment framework enables a thorough comprehension of the Gradient Boosting Regression model's performance regarding critical buckling load prediction.

Once the MSE, RMSE, and R^2 values are calculated, they are printed to enable a quantitative assessment of the Gradient Boosting Regression model's performance. These metrics provide researchers and practitioners with valuable information on how well the model performs in predicting the critical buckling load based on the given dataset. In addition to quantitative evaluation, a scatter plot is created to visually compare the predicted labels against the actual labels. This graphical representation allows for a clear visualization of the relationship between the predicted and actual values. A well-performing Gradient Boosting Regression model will exhibit data points closely clustered around a diagonal line, indicating a strong correlation between the predicted and actual values.

By following these evaluation steps, a comprehensive analysis of the Gradient Boosting Regression model's accuracy in predicting the critical buckling load can be conducted. Engineers and researchers can use this information to assess the model's reliability and suitability for predicting critical buckling loads in different scenarios based on the given dataset. The combination of quantitative metrics and visual examination provides a robust understanding of the model's effectiveness, facilitating model optimization and improvements to enhance its predictive capabilities. Ultimately, this evaluation process contributes to more accurate and efficient engineering analyses involving the prediction of critical buckling loads.

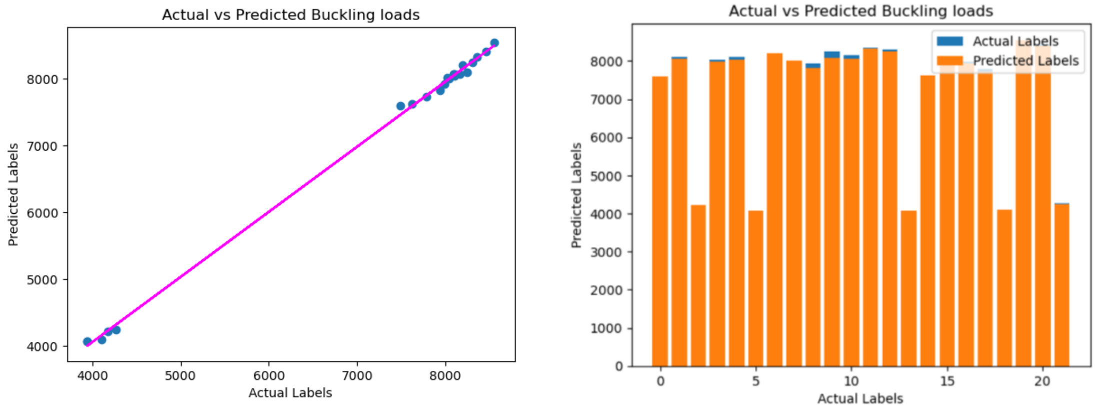

(a) Mechanical Load

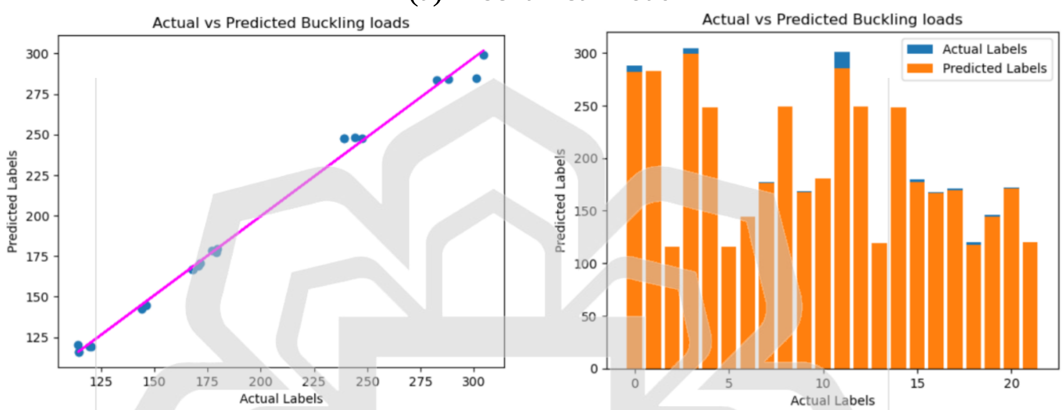

(b) Thermal Load

Figure 4.24 Analysis of gradient boosting regression model

Through the assessment of various ML algorithms, encompassing Linear Regression, Lasso Regression, Decision Tree Regression, and Random Forest Regression, their respective performances in predicting the critical buckling load of thin-walled structures were evaluated. This evaluation relied on essential metrics, including MSE, RMSE, and R^2 values. Additionally, visual comparisons were facilitated through scatter plots. In comparison to finite element analysis, it was discerned that all ML algorithms yielded reasonably precise predictions of the critical buckling load. The models consistently exhibited low MSE and RMSE values, underscoring the proximity of predictions to the actual critical buckling loads. Additionally, high R^2 values were obtained, suggesting that a significant proportion of the variance in the critical buckling loads could be explained by the models. These results are promising as they align well with the outcomes of the finite element analysis, indicating that the chosen ML algorithms can effectively capture the complex behavior of thin-walled structures under different loading conditions.

The advantage of using ML algorithms, such as Random Forest Regression and Gradient Boosting Regression, lies in their ability to handle non-linear relationships and capture intricate interactions among variables. As thin-walled structures often exhibit complex behavior due to geometric configurations and material properties, these algorithms can offer more accurate predictions than traditional linear regression approaches.

The application of ML algorithms to predict critical buckling loads in thin-walled structures can significantly benefit engineering applications. Firstly, these algorithms can save computational time and resources compared to finite element analysis, as they provide rapid predictions once trained. Finite element analysis involves solving complex differential equations, which can be time-consuming and computationally expensive for large-scale models. ML algorithms, once trained on suitable datasets, can quickly predict critical buckling loads for various design configurations, allowing engineers to explore a wide range of possibilities efficiently. Moreover, ML algorithms can help in the optimization of thin-walled structures. Engineers can use these algorithms to identify the key design parameters and their effects on the critical buckling load. By conducting sensitivity analyses, they can determine the most influential factors and optimize the structural design to enhance the load-carrying capacity while minimizing weight. Furthermore, ML algorithms can assist in the early-stage design process, where only limited data or preliminary designs are available. Engineers can use existing data and ML models to make informed decisions and guide the initial design iterations. As more data becomes available from physical testing or simulations, the ML models can be continuously refined and improved.

The successful application of various ML algorithms in predicting the critical buckling load of thin-walled structures demonstrates their effectiveness and potential in engineering applications. By providing accurate and efficient predictions, ML algorithms can significantly aid in the design optimization and decision-making process, leading to safer, more reliable, and cost-effective thin-walled structures in various engineering fields.

4.3.6 Hyperparameter Tuning (Grid Search)

In the hyperparameter tuning stage, a grid search is performed on the Gradient Boosting Regression model using the GridSearchCV class. Here is a breakdown of the steps involved: Firstly, a parameter grid is defined, specifying different combinations of hyperparameters. In this case, the hyperparameters being tuned are the learning rate and the number of estimators. Next, an instance of the GridSearchCV class is created from the sklearn.model_selection module. The Gradient Boosting Regression model and the parameter grid are passed as arguments to the GridSearchCV constructor.

Grid search is then executed by calling the `fit()` method on the GridSearchCV object, providing the training data (X_train and y_train). This step performs an exhaustive search over the hyperparameter grid, evaluating each combination and selecting the best one based on the specified scoring metric. The best combination of hyperparameters is obtained using the `best_params_` attribute of the GridSearchCV object. This provides the optimal values for the learning rate and the number of estimators. Next, the model is retrained using the best hyperparameters obtained from the grid search. This ensures that the model is trained with the optimal settings.

Predictions are made on the test set (X_test) using the `predict()` method of the retrained model.

These above all evaluated metrics provide insights into the accuracy and goodness of fit of the tuned model. Additionally, a scatter plot is created to visually compare the predicted labels against the actual labels, allowing for a graphical assessment of the model's performance. By following these steps, the GridSearchCV enables the systematic exploration of different hyperparameter combinations for the Gradient Boosting Regression model. The best hyperparameters are identified, and the model is retrained and evaluated, resulting in improved predictions for the critical buckling load based on the given dataset.

4.4 MACHINE LEARNING RESULTS MATRIX

The results obtained from each step of the methodology may vary depending on the dataset and specific hyperparameters used. Detailed results for each model can be provided based on the specific dataset and implementation. Where, MSE, RMSE, and R^2 are commonly used performance metrics in regression tasks. Here's an explanation of each metric:

1. Mean Squared Error (MSE) is measuring the average squared difference between the predicted and actual values. It calculates the average of the squared residuals, where the residual is the difference between the predicted and actual values. The MSE gives higher weight to larger errors.

$$MSE = (1/n) * \Sigma(y\_pred - y\_actual)^2 \qquad (4.1)$$

A lower MSE value indicates better model performance, with a value of 0 indicating a perfect fit (where predicted values perfectly match actual values).

2. The Root Mean Squared Error (RMSE) serves as the square root of the MSE and is commonly utilized to gauge the error in units akin to the target variable. It offers an assessment of the typical magnitude of the residuals, rendering it more straightforward to interpret than the MSE.

$$RMSE = sqrt(MSE) \tag{4.2}$$

Like MSE, a lower RMSE value signifies better model performance, with a value of 0 indicating a perfect fit.

3. R^2, also referred to as the coefficient of determination, reflects the fraction of the target variable's variance that can be foreseen from the model's independent variables. It serves as an indicator of the model's goodness of fit and its capacity to elucidate the variations in the target variable.

$$R^2 = 1 - (MSE\_actual \;/\; MSE\_baseline) \tag{4.3}$$

R^2 ranges from 0 to 1, where 0 indicates that the model does not explain any variation in the target variable, and 1 indicates a perfect fit. A higher R^2 value suggests better model performance, but it should be interpreted in the context of the specific problem and data. While MSE and RMSE measure the magnitude of the prediction errors, R^2 provides an indication of the proportion of variance explained by the model. These metrics should be considered together to assess the overall performance and fit of the regression model.

Table 4.4 presents the evaluation results of different ML algorithms for predicting the critical buckling load of thin-walled structures under mechanical load. The following metrics were calculated for each model: MSE, RMSE, and R^2 value. Both Linear Regression and Lasso Regression models have relatively high MSE and RMSE values and negative R^2 values. This suggests that these models do not perform well in predicting the critical buckling load, as the predicted values are far from the actual values. The negative R^2 values indicate that these models do not explain much of the variance in the critical buckling load. The Decision Tree Regression model shows significantly lower MSE and RMSE values compared to the linear-based models, indicating better accuracy in predicting the critical buckling load. The high R^2 value of 0.996 suggests that this model explains a substantial portion of the variance in the critical buckling load. The Random Forest Regression model performs slightly worse than the Decision Tree model, with slightly higher MSE and RMSE values. Nevertheless, it still demonstrates good accuracy with an R^2 value of 0.9951. The Gradient Boosting Regression model outperforms all other models in terms of accuracy. It exhibits the lowest MSE and RMSE values and the highest R^2 value of 0.9978, indicating an excellent fit to the data and accurate predictions of the critical buckling load.

In summary, the Gradient Boosting Regression model is the most accurate among the evaluated models, providing the most reliable predictions for the critical buckling load of thin-walled structures. This model's performance is significantly better than the linear-based models (Linear Regression and Lasso Regression) and comparable to the Decision Tree and Random Forest models, but with even higher accuracy and goodness of fit. The Gradient Boosting Regression model is, therefore, the preferred choice for predicting the critical buckling load in engineering applications, as it offers high accuracy and efficiency in handling complex relationships between variables.

Table 4.4 Evaluation matrix for mechanical load

Sl. No.	Model	MSE	RMSE	R^2
01	Linear Regression	3330969.06	1825.09	-0.16
02	Lasso Regression	3295965.72	1815.48	-0.15
03	Decision Tree	11093.85	105.33	0.996
04	Random Forest	13016.04	114.09	0.9951
05	Gradient Boosting	6115.63	78.20	0.9978

Table 4.5 presents the evaluation results of different ML algorithms for predicting the critical buckling load of thin-walled structures under thermal load. The following metrics were calculated for each model: MSE, RMSE, and R^2 value. Both Linear Regression and Lasso Regression models have moderate MSE and RMSE values, indicating a reasonable level of accuracy in predicting the critical buckling load under thermal load. The R^2 values of 0.7163 and 0.7226 suggest that these models explain a significant proportion of the variance in the critical buckling load under thermal conditions. The Decision Tree Regression model outperforms the linear-based models, with significantly lower MSE and RMSE values. The high R^2 value of 0.9911 indicates that this model explains most of the variance in the critical buckling load under thermal load, making it an excellent fit to the data. The Random Forest Regression model performs slightly worse than the Decision Tree model but still exhibits good accuracy. The MSE and RMSE values are higher than those of the Decision Tree model, but the R^2 value of 0.9854 shows that this model still explains a substantial portion of the variance in the critical buckling load under thermal conditions. The Gradient Boosting Regression model is the most accurate among all the evaluated models. It shows the lowest MSE and RMSE values and the highest R^2 value of 0.9940, indicating a superior fit to the data and highly accurate predictions of the critical buckling load under thermal load.

In summary, the Gradient Boosting Regression model is the most accurate and reliable among the evaluated models for predicting the critical buckling load under thermal load conditions. It outperforms the linear-based models (Linear Regression and Lasso Regression) and offers slightly better accuracy than the Decision Tree and Random Forest models. The Gradient Boosting Regression model is, therefore, the preferred choice for predicting the critical buckling load in engineering applications under thermal load, as it provides highly accurate and efficient predictions in handling the complexities of thermal loading conditions.

Table 4.5 Evaluation matrix for thermal load

Sl. No.	Model	MSE	RMSE	R^2
01	Linear Regression	1127.64	33.5804	0.7163
02	Lasso Regression	1104.25	33.2303	0.7226
03	Decision Tree	35.0631	5.9214	0.9911
04	Random Forest	57.7908	7.6020	0.9854
05	Gradient Boosting	23.7657	4.8750	0.9940

4.5 CHAPTER SUMMARY

In this chapter, we present a detailed overview of the results obtained from our current work. Our investigation involved conducting finite element (FE) analyses to explore the impacts of different parameters on thin-walled composite structures. These parameters included the shape of cutouts, spacing ratio, opening ratio, and fiber orientation. The FE model provided valuable data that we then utilized for machine learning purposes.

The objective of applying machine learning was to predict the optimal model for enhancing the design of thin-walled composite structures. By leveraging the data from the FE model, we employed various machine learning algorithms to develop predictive models. These models aimed to optimize critical design factors and improve the structural performance of thin-walled composite structures. Through the combination of finite element analysis and machine learning, our study sought to provide valuable insights into the behavior of these structures under different conditions. The comprehensive results obtained from both analyses offered crucial information for engineers and designers to make informed decisions in the design and optimization of thin-walled composite structures. This holistic approach is expected to enhance the efficiency, reliability, and cost-effectiveness of engineering applications involving thin-walled composite structures in various industries.

CHAPTER FIVE

CONCLUSION AND RECOMMENDATIONS

5.1 CONCLUSION

In this research, conducted a comparative analysis of the buckling behaviour of a thin-walled C-section channel subjected to mechanical and thermal loads, considering cases both with and without holes. The investigation involved utilizing the FEM to model the structure and simulate the results. Successfully examined the critical buckling load factor and mode shapes for each case.

The findings of this study revealed that the presence of holes has a significant impact on the buckling behaviour of the structure. Notably, the mode shapes of the structure varied between the cases, indicating different buckling behaviours under mechanical and thermal loads. Moreover, the critical buckling load factor was found to be remarkably lower for the C-section channel with holes compared to the one without holes, indicating a higher susceptibility to buckling in the former case. These results emphasize the crucial importance of considering the presence of holes when designing and optimizing C-section channels. The presence of holes alters the structural behaviour and reduces the buckling load capacity, leading to potential buckling risks. Therefore, engineers and designers should carefully account for the influence of holes in their design choices and structural optimization strategies for thin-walled C-section channels.

Also, conducted parametric studies to comprehensively investigate the impact of various factors on the buckling behaviour of the thin-walled C-section channel. These factors included hole shapes, sizes, positions, and materials composition. By systematically varying these parameters, we gained valuable insights into how different configurations of holes influence the mode shapes and critical buckling load factors of the structure.

The stacking sequence, ply orientation angle, spacing ratio, opening ratio, and shape of the hole collectively influence buckling strength and deformation stresses in composite laminates by affecting the distribution of internal stresses and strains, leading to variations in structural stability and response to mechanical and thermal loading. Through the parametric studies, we were able to understand the specific effects of each factor on the structural behaviour under both mechanical and thermal loads. This knowledge provided essential guidance for engineering decisions, enabling designers to make informed choices when designing thin-walled C-section channels. Moreover, the results of the parametric studies played a vital role in optimizing the design of thin-walled C-section channels for enhanced performance and safety in real-world applications. By understanding the influence of different hole configurations, engineers can tailor the design to improve the structural integrity and buckling resistance of the channels, ensuring they can withstand mechanical and thermal loads without compromising safety. The parametric studies conducted in this research offer valuable information that enriches our understanding of the behaviour of thin-walled C-section channels with holes. This knowledge empowers engineers to design more robust and efficient structures, facilitating their application in various engineering fields where safety and performance are paramount concerns.

The data obtained from the ANSYS is used as an input dataset for the ML model. The dataset contains features related to the geometry and orientation of the C-section column, along with the corresponding critical buckling load values due to mechanical load. Additionally, the models were also tested on critical buckling load values due to thermal load separately. The implemented machine learning models include Linear

Regression, Lasso Regression, Decision Tree Regression, Random Forest Regression, and Gradient Boosting Regression. All models were used for the future prediction of the critical buckling load of the C-section column based on the given features.

Based on the model and the results the following conclusions can be made:

- ML Model Performance: The ML models (Linear Regression, Lasso, Decision Tree, RandomForest, and Gradient Boosting) demonstrated strong predictive capabilities for estimating the critical buckling load of the C-section column. All models achieved high accuracy, with R2 scores ranging from 0.994 to 0.998, indicating an excellent fit to the data.
- Feature Importance: Among the input features, the "Orientation" feature showed the highest importance in predicting the critical buckling load. The "Spacing ratio" and "Shape" features also had significant contributions to the predictions.
- Model Comparison: The Decision Tree and RandomForest models exhibited slightly better performance compared to other models, achieving R2 scores close to 1. These models are well-suited for the given dataset and can accurately predict the critical buckling load of the C-section column.
- Optimal Solution: The ML algorithm, particularly the Gradient Boosting model with the best hyperparameter combination (learning_rate: 0.1, n_estimators: 50), can be used to find the optimal solution for the C-section column under mechanical and thermal loads. The ML model can efficiently estimate the critical buckling load, considering different loading conditions and input parameters.
- Practical Application: The ML model provides a valuable tool for structural engineers and designers to quickly assess the stability of C-section columns under mechanical and thermal loads. By inputting the relevant parameters, the model can

estimate the critical buckling load, enabling the evaluation and optimization of the column's design for real-world applications.

ML algorithm, specifically the Decision Tree, RandomForest, and GradientBoosting models, offers an accurate and efficient method to predict the critical buckling load of C-section columns under different loading conditions. The feature importance analysis helps identify the most influential parameters, aiding engineers in making informed decisions during the design process. This ML approach can be utilized to find optimal solutions and ensure the structural integrity of C-section columns in practical engineering applications.

In summary, the main conclusions drawn from this research are as follows:

- The c-section thin-walled laminated composite structure was successfully designed using the finite element method, with validation through comparison to existing work based on critical buckling load results.
- Parametric studies were conducted, revealing the substantial impact of spacing ratio, opening ratio, laminate sequence, fibre orientation, and hole shape on the critical buckling load.
- The application of machine learning algorithms proved effective in optimizing simulation data and identifying the optimal parameter combination essential for the design of the thin-walled structure.
- Based on the results obtained FE and ML approach it has been found that the best optimum critical value is found for the parameter combination:
    - Mechanical load: Quasi-isotropic having circular hole with opening ratio 1.4 and spacing ratio 1.6 and the critical buckling load 8804 N

- Thermal Load: Angle-ply having circular hole with opening ratio 1.4 and spacing ratio 1.7 and the critical buckling load 308.2 (T-critical)

In summary, the study contributes to the understanding of the buckling behaviour of thin-walled structures under mechanical and thermal loading and highlights the importance of considering the presence of holes in the design of C-section channels. The findings of this study can be used to improve the design and optimization of C-section channels and other thin-walled structures subjected to thermal loading. Further research can be done to explore other types of holes and their impact on the buckling behaviour of thin-walled structures.

5.2 RECOMMENDATION

Composite laminated thin-walled structures are composed of multiple materials that collaborate to achieve properties that would be unattainable for the individual components alone. Currently, both major and secondary constructions extensively utilize composite laminates. Composite laminates offer numerous advantages, including design flexibility, cost-effectiveness, corrosion resistance, durability, and more. This work emphasizes the significance of composite materials for thin-walled structures and explores their diverse applications. Furthermore, it delves into optimization methods such as design of experiments, and machine learning algorithms, providing a comprehensive explanation of their relevance. Moreover, the work serves as a guide for scientists seeking to implement composite laminates and thin-walled structures in engineering applications. It offers detailed descriptions and analyses of the literature concerning composite material applications. Additionally, it presents an overview of research areas within the field of composite materials. By identifying research gaps, researchers can gain insights and identify opportunities for new ideas, especially during the early stages of this research domain. In summary, these research gaps provide valuable perspectives and indices to facilitate advancements in various research areas related to composite thin-walled structures. They serve as a catalyst for researchers to develop innovative ideas, particularly in the nascent phases of this research field.

REFERENCES

Abueidda, D. W., Almasri, M., Ammourah, R., Ravaioli, U., Jasiuk, I. M., & Sobh, N. A. (2019). Prediction and optimization of mechanical properties of composites using convolutional neural networks. *Composite Structures*, *227*, 1–33.

Almeida, F. S., & Awruch, A. M. (2009). Design optimization of composite laminated structures using genetic algorithms and finite element analysis. *Composite Structures*, *88*(3), 443–454.

Awad, Z. K., Aravinthan, T., Zhuge, Y., & Gonzalez, F. (2012). A review of optimization techniques used in the design of fibre composite structures for civil engineering applications. *Materials and Design*, *33*(1), 534–544.

Badalló, P., Trias, D., Marín, L., & Mayugo, J. A. (2013). A comparative study of genetic algorithms for the multi-objective optimization of composite stringers under compression loads. *Composites Part B: Engineering*, *47*, 130–136.

Bagheri, M., Jafari, A. A., & Sadeghifar, M. (2011). Multi-objective optimization of ring stiffened cylindrical shells using a genetic algorithm. *Journal of Sound and Vibration*, *330*(3), 374–384.

Barut, A., & Madenci, E. (2010). A complex potential-variational formulation for thermo-mechanical buckling analysis of flat laminates with an elliptic cutout. *Composite Structures*, *92*(12), 2871–2884.

Biagi, V. De, Chiaia, B., Marano, G. C., Fiore, A., Greco, R., Sardone, L., Cucuzza, R., Cascella, G. L., Spinelli, M., & Lagaros, N. D. (2020). Series solution of beams with variable cross-section. *Procedia Manufacturing*, *44*, 489–496.

Birman, V. (2022). Thermal buckling and postbuckling of columns accounting for temperature effect on material properties. *Https://Doi.Org/10.1080/01495739.2022.2118198*, *45*(12), 1043–1056.

Bogetti, T. A., & Gillespie, J. W. (2016). Process-Induced Stress and Deformation in

Thick-Section Thermoset Composite Laminates. *Http://Dx.Doi.Org/10.1177/002199839202600502*, *26*(5), 626–660.

Cai, H., & Aref, A. J. (2015). A genetic algorithm-based multi-objective optimization for hybrid fiber reinforced polymeric deck and cable system of cable-stayed bridges. *Structural and Multidisciplinary Optimization*, *52*(3), 583–594.

Chatzi, E. N., Hiriyur, B., Waisman, H., & Smyth, A. W. (2011). Experimental application and enhancement of the XFEM – GA algorithm for the detection of flaws in structures. *Computers and Structures*, *89*(7–8), 556–570.

Chen, W. J., Lin, P. D., & Chen, L. W. (1991). Thermal buckling behavior of thick composite laminated plates under nonuniform temperature distribution. *Computers and Structures*, *41*(4), 637–645.

Cheng, S., Yan, Q. W., Li, L. Y., & Kim, B. (2015). Thermal Buckling Analysis of Axially Loaded Columns of Thin-Walled Open Section with Nonuniform Sectional Properties. *International Journal of Structural Stability and Dynamics*, *15*(6), 1–17.

Dai, J., Xi, S., & Li, D. (2019). Numerical Analysis of Curing Residual Stress and Deformation in Thermosetting Composite Laminates with Comparison between Different Constitutive Models. *Materials 2019, Vol. 12, Page 572*, *12*(4), 572.

Deb, K., Pratap, A., Agarwal, S., & Meyarivan, T. (2002). A fast and elitist multiobjective genetic algorithm: NSGA-II. *IEEE Transactions on Evolutionary Computation*, *6*(2), 182–197.

Deka, D. J., Sandeep, G., Chakraborty, D., & Dutta, A. (2005). Multiobjective optimization of laminated composites using finite element method and genetic algorithm. *Journal of Reinforced Plastics and Composites*, *24*(3), 273–285.

Dinh Nguyen, P., Vu, Q.-V., Papazafeiropoulos, G., Thi Thiem, H., Vuong, P. M., & Duc, N. D. (2020). Optimization of Laminated Composite Plates for Maximum Biaxial Buckling Load. *VNU Journal of Science: Mathematics - Physics*, *36*(2), 1–12.

Doan, Q. H., & Thai, D. (2020). A Numerical Study of the Effect of Component Dimensions on the Critical Buckling Load of a GFRP Composite Strut under Uniaxial Compression. *Materials*, *13*, 931.

Emam, S. A., & Nayfeh, A. H. (2009). Postbuckling and free vibrations of composite beams. *Composite Structures*, *88*(4), 636–642.

Erkliğ, A., & Yeter, E. (2012). The effects of cutouts on buckling behavior of composite plates. *Science and Engineering of Composite Materials*, *19*(3), 323–330.

Eskandari, S., Andrade Pires, F. M., Camanho, P. P., Cui, H., Petrinic, N., & Marques, A. T. (2019). Analyzing the failure and damage of FRP composite laminates under high strain rates considering visco-plasticity. *Engineering Failure Analysis*, *101*, 257–273.

Furtado, C., Pereira, L. F., Tavares, R. P., Salgado, M., Otero, F., Catalanotti, G., Arteiro, A., Bessa, M. A., & Camanho, P. P. (2021a). A methodology to generate design allowables of composite laminates using machine learning. *International Journal of Solids and Structures*, *233*(May), 111095.

Furtado, C., Pereira, L. F., Tavares, R. P., Salgado, M., Otero, F., Catalanotti, G., Arteiro, A., Bessa, M. A., & Camanho, P. P. (2021b). A methodology to generate design allowables of composite laminates using machine learning. *International Journal of Solids and Structures*, *233*, 111095.

Ghiasi, H., Fayazbakhsh, K., Pasini, D., & Lessard, L. (2010). Optimum stacking sequence design of composite materials Part II: Variable stiffness design. *Composite Structures*, *93*(1), 1–13.

Gillet, A., Francescato, P., & Saffre, P. (2010). Single- and multi-objective optimization of composite structures: The influence of design variables. *Journal of Composite Materials*, *44*(4), 457–480.

Gossard, M. L., Seide, P., & Roberts, W. M. (1952). *Thermal buckling of plates*.

Guo, Y. (2020). *IOP Conference Series: Earth and Environmental Science Overall Buckling Performance of Cold-Formed Steel Axial Compression Lipped Channel*

Members with Circle Holes Overall Buckling Performance of Cold-Formed Steel Axial Compression Lipped Channel Members.

Gupta, R. K., Gunda, J. B., Ranga Janardhan, G., & Venkateswara Rao, G. (2010). Thermal post-buckling analysis of slender columns using the concept of coupled displacement field. *International Journal of Mechanical Sciences*, *52*(4), 590–594.

Gupta, R. K., Jagadish Babu, G., Ranga Janardhan, G., & Venkateswara Rao, G. (2009). Comparative study of thermal post-buckling analysis of uniform slender & shear flexible columns using rigorous finite element and intuitive formulations. *International Journal of Mechanical Sciences*, *51*(3), 204–212.

Hoffmann, J., Cui, H., & Petrinic, N. (2018). Determination of the strain-energy release rate of a composite laminate under high-rate tensile deformation in fibre direction. *Composites Science and Technology*, *164*, 110–119.

Huang, G. Bin, Zhu, Q. Y., & Siew, C. K. (2006). Extreme learning machine: Theory and applications. *Neurocomputing*, *70*(1–3), 489–501.

Hwong, P. Y. (2019). Formulating Structural Design and Analysis Practices Using First Order Analysis. *Journal of Physics: Conference Series*, *1174*(1).

Jung, K. C., & Chang, S. H. (2021). Advanced deep learning model-based impact characterization method for composite laminates. *Composites Science and Technology*, *207*, 108713.

Kamarudin, M. N. Bin, Ali, J. S. M., Aabid, A., & Ibrahim, Y. E. (2022). Buckling Analysis of a Thin-Walled Structure Using Finite Element Method and Design of Experiments. *Aerospace*, *9*(10), 541.

Karakaya, Ş., & Soykasap, Ö. (2009). Buckling optimization of laminated composite plates using genetic algorithm and generalized pattern search algorithm. *Structural and Multidisciplinary Optimization*, *39*(5), 477–486.

Kharghani, N., & Guedes Soares, C. (2018). Experimental, numerical and analytical study of bending of rectangular composite laminates. *European Journal of Mechanics - A/Solids*, *72*, 155–174.

Khazaal, D. S., AL-Khafaji, H. M., & Abdulsahib, I. A. (2021). Parametric Study on Buckling Behavior of Aluminum Alloy Thin-Walled Lipped Channel Beam with Perforations Subjected to Combined Loading. *Engineering and Technology Journal*, *39*(1A).

Kosanke, R. M. (2019). *Structural Analysis of Laminated Composites using Function-Behavior-Structure Model and Virtual Material Method* (Issue May).

Lakshmi Narayana, A., Vijaya Kumar, R., & Krishnamohana Rao, G. (2018). Thermal Buckling Analysis of Laminated Composite Plate with Square/Rectangular, Elliptical/Circular Cutout. *Materials Today: Proceedings*, *5*(2), 5354–5363.

Lee, D. S., Morillo, C., Oller, S., Bugeda, G., & Oñate, E. (2013). Robust design optimisation of advance hybrid (fiber-metal) composite structures. *Composite Structures*, *99*, 181–192.

Lee, J., Nguyen, H. T., & Kim, S.-E. (2009). Buckling and post buckling of thin-walled composite columns with intermediate-stiffened open cross-section under axial compression. *International Journal of Steel Structures*, *9*(3), 175–184.

Li, D., Li, X., & Dai, J. (2017). Process Modelling of Curing Process-Induced Internal Stress and Deformation of Composite Laminate Structure with Elastic and Viscoelastic Models. *Applied Composite Materials 2017 25:3*, *25*(3), 527–544.

Li, Z., Xu, W., Wang, C., Liu, X., & Sun, Y. (2023). Investigation on Vibration Characteristics of Thin-Walled Steel Structures under Shock Waves. *Materials*, *16*(13), 1–17.

Liu, P. F., & Zheng, J. Y. (2008). Progressive failure analysis of carbon fiber/epoxy composite laminates using continuum damage mechanics. *Materials Science and Engineering: A*, *485*(1–2), 711–717.

Liu, P. F., & Zheng, J. Y. (2010). Recent developments on damage modeling and finite element analysis for composite laminates: A review. *Materials & Design*, *31*(8), 3825–3834.

Liu, X., Qin, J., Zhao, K., Featherston, C. A., Kennedy, D., Jing, Y., & Yang, G. (2023).

Design optimization of laminated composite structures using artificial neural network and genetic algorithm. *Composite Structures*, *305*.

Lvov, G., Pupazescu, A., Beschetnikov, D., & Zaharia, M. (2015). Buckling analysis of a thin-walled cylindrical shell strengthened by fiber - Reinforced polymers. *Materiale Plastice*, *52*(1), 28–31.

Machado, J. M., Tavares, J. M. R. S., Camanho, P. P., & Correia, N. (2022). Automatic void content assessment of composite laminates using a machine-learning approach. *Composite Structures*, *288*, 115383.

Mahdavi, S., Shaterzadeh, A., & Jafari, M. (2020). Determination of optimum effective parameters on thermal buckling of hybrid composite plates with quasi-square cut-out using a genetic algorithm. *Engineering Optimization*, *52*(1), 106–121.

Malekzadeh, P., Vosoughi, A. R., Sadeghpour, M., & Vosoughi, H. R. (2014). Thermal Buckling Optimization of Temperature-Dependent Laminated Composite Skew Plates. *Journal of Aerospace Engineering*, *27*(1), 64–75.

Mehar, K., & Panda, S. K. (2019). Multiscale modeling approach for thermal buckling analysis of nanocomposite curved structure. *Advances in Nano Research*, *7*(3), 181.

Men, X., Pan, Y., Jiang, Z., Zhang, T., Zhao, H., & Fu, X. (2022). Study on Linear and Nonlinear Thermal Buckling Mode and Instability Characteristics for Engine Rotating Thin-Walled Blade. *Applied Sciences (Switzerland)*, *12*(5).

Mondal, S., Patra, A. K., Chakraborty, S., & Mitra, N. (2015). Dynamic performance of sandwich composite plates with circular hole/cut-out: A mixed experimental-numerical study. *Composite Structures*, *131*(November), 479–489.

Moura Correia, A. J. P., Rodrigues, J. P. C., & Real, P. V. (2014). Thermal bowing on steel columns embedded on walls under fire conditions. *Fire Safety Journal*, *67*, 53–69.

Nemeth, M. P. (1995). Buckling and postbuckling behaviour of laminated composite plates with a cut-out. *Buckling and Postbuckling of Composite Plates*, 260–298.

Ngamkhanong, C., & Kaewunruen, S. (2022). Prediction of Thermal-Induced Buckling Failures of Ballasted Railway Tracks Using Artificial Neural Network (ANN). International Journal of Structural Stability and Dynamics, 22(5).

Ouyang, T., Sun, W., Bao, R., & Tan, R. (2021). Effects of matrix cracks on delamination of composite laminates subjected to low-velocity impact. *Composite Structures*, *262*, 113354.

Özaslan, E., Güler, M. A., Yetgin, A., & Acar, B. (2019). Stress analysis and strength prediction of composite laminates with two interacting holes. *Composite Structures*, *221*, 110869.

Panels, C. W. (2021). *Composite Wing Panels*. 1–26.

Park, C. H., Lee, W. Il, Han, W. S., & Vautrin, A. (2008). Improved genetic algorithm for multidisciplinary optimization of composite laminates. *Computers and Structures*, *86*(19–20), 1894–1903.

Park, S., Ahmad, S., Yun, C. B., & Roh, Y. (2006). Multiple crack detection of concrete structures using impedance-based structural health monitoring techniques. *Experimental Mechanics, 46*(5), 609–618.

Paul, A. (2014). *Buckling of Columns - Euler Theory for Elastic Buckling*.

Rao, B. S., Rao, G. S., & Kumar, J. S. (2015). Buckling Analysis of thin FRP laminate under Thermal Loading. *Materials Today: Proceedings*, *2*(4–5), 3093–3099.

Reiner, J., Vaziri, R., & Zobeiry, N. (2021). Machine learning assisted characterisation and simulation of compressive damage in composite laminates. *Composite Structures*, *273*, 114290.

Rio Prabowo, A., Tuswan, T., Adiputra, R., Do, Q. T., Sohn, J. M., Surojo, E., & Imaduddin, F. (2021). Mechanical behavior of thin-walled steel under hard contact with rigid seabed rock: Theoretical contact approach and nonlinear FE calculation. *Journal of the Mechanical Behavior of Materials*, *30*(1), 156–170.

Różyło, P. (2017). Experimental-numerical test of open section composite columns stability subjected to axial compression. *Archives of Materials Science and Engineering*, *84*(2), 58–64.

Rozylo, P., & Debski, H. (2020). Stability and load-carrying capacity of short composite Z-profiles under eccentric compression. *Thin-Walled Structures*, *157*.

Rozylo, P., & Falkowicz, K. (2021). Stability and failure analysis of compressed thin-walled composite structures with central cut-out, using three advanced independent damage models. *Composite Structures*, *273*(June), 114298.

Różyło, P., & Wrzesińska, K. (2016). Numerical Analysis of the Behavior of Compressed Thin-Walled Elements With Holes. *Advances in Science and Technology Research Journal*, *10*(31), 199–206.

Saberi, S., Ghayour, M., Mirdamadi, H. R., & Ghamami, M. (2021). Free vibration analysis and mode management of bistable composite laminates using deep learning. *Archive of Applied Mechanics*, *91*(6), 2795–2816.

Salcedo-Sanz, S., Rojo-Álvarez, J. L., Martínez-Ramón, M., & Camps-Valls, G. (2014). Support vector machines in engineering: an overview. *Wiley Interdisciplinary Reviews: Data Mining and Knowledge Discovery*, *4*(3), 234–267.

Sanghi, D., Singh, D., & Gautam, V. (2016). Structural Analysis of Composite Laminates using Analytical and Numerical Techniques. *MATEC Web of Conferences*, *78*, 4–10.

Sarhadi, A., Albuquerque, R. Q., Demleitner, M., Ruckdäschel, H., & Eder, M. A. (2022). Machine learning based thermal imaging damage detection in glass-epoxy composite materials. *Composite Structures*, *295*(April), 115786.

Shaterzadeh, A. R., Abolghasemi, S., & Rezaei, R. (2014). Finite element analysis of thermal buckling of rectangular laminated composite plates with circular cut-out. *Journal of Thermal Stresses*, *37*(5), 604–623.

Shiau, L. C., Kuo, S. Y., & Chen, C. Y. (2010). Thermal buckling behavior of composite laminated plates. *Composite Structures*, *92*(2), 508–514.

Shrivastava, S., Mohite, P. M., Yadav, T., & Malagaudanavar, A. (2018). Multi-objective multi-laminate design and optimization of a Carbon Fibre Composite wing torsion box using evolutionary algorithm. *Composite Structures*, *185*(May 2017), 132–147.

Sliseris, J., & Rocens, K. (2013). Optimal design of composite plates with discrete variable stiffness. *Composite Structures*, *98*, 15–23.

Sorrentino, L., Liao, Z., Qiu, C., Yang, J., Yang, J., & Yang, L. (2022). Accelerating the Layup Sequences Design of Composite Laminates via Theory-Guided Machine Learning Models. *Polymers 2022, Vol. 14, Page 3229*, *14*(15), 3229.

Štemberk, P., & Khmurovska, Y. (2021). Fuzzy logic assessment of thermal performance of concrete wall. *AIP Conference Proceedings*, *2322*(February).

Stephen, C., Thekkuden, D. T., Mourad, A. H. I., Shivamurthy, B., Selvam, R., & Behara, S. R. (2022). Prediction of impact performance of fiber reinforced polymer composites using finite element analysis and artificial neural network. *Journal of the Brazilian Society of Mechanical Sciences and Engineering*, *44*(9), 1–11.

Sudhirsastry, Y. B., Budarapu, P. R., Madhavi, N., & Krishna, Y. (2015). Buckling analysis of thin wall stiffened composite panels. *Computational Materials Science*, *96*(PB), 459–471.

Susac, F., Beznea, E. F., & Baroiu, N. (2017). Artificial Neural Network Applied to Prediction of Buckling Behavior of the Thin Walled Box. *Advanced Engineering Forum*, *21*, 141–150.

Tsukrov, I., Drach, B., Bayraktar, H., & Goering, J. (2014). Modeling of cure-induced residual stresses in 3D woven composites of different reinforcement architectures. *Key Engineering Materials*, *577–578*, 253–256.

Ye, J., Meza, F. J., Hajirasouliha, I., Becque, J., Shepherd, P., & Pilakoutas, K. (2019). Experimental investigation of the local and distortional buckling interaction and deflection of CFS back-to-back channel sections. *Journal of Structural Engineering*, *145*(7).

Yong, M. Ã., Falzon, B. G., & Iannucci, L. (2008). *On the application of genetic algorithms for optimising composites against impact loading*. *35*, 1293–1302.

Zhang, C., Li, Y., Jiang, B., Wang, R., Liu, Y., & Jia, L. (2022). Mechanical properties prediction of composite laminate with FEA and machine learning coupled method. *Composite Structures*, *299*, 116086.

Zhao, G., Wang, B., Wang, T., Hao, W., & Luo, Y. (2019). Detection and monitoring of delamination in composite laminates using ultrasonic guided wave. *Composite Structures*, *225*, 111161.

PUBLICATIONS AND CONFERENCES

Published and Under Review Journals

- **Omar Shabbir Ahmed,** Abdul Aabid, Jaffar Syed Mohamed Ali*, Meftah Hrairi, Norfazrina Mohd Yatim, "Application of composite laminates and thin-walled structures for engineering design: A systematic review," ACS Omega. (ISI Q2 IF: 4.132) (Published)

- **Omar Shabbir Ahmed**, Abdul Aabid, Jaffar Syed Mohamed Ali*, Meftah Hrairi, and Norfazrina Mohd Yatim, "Buckling Analysis of a Thin-Walled C-Section Channel under Mechanical and Thermal Load," Journal of Advanced Research in Applied Mechanics. (Scopus Indexed) (Published)

- **Omar Shabbir Ahmed,** Abdul Aabid, Jaffar Syed Mohamed Ali*, Meftah Hrairi, and Norfazrina Mohd Yatim, "Parametric Analysis of Critical Buckling in Composite Laminate Structures under Mechanical and Thermal Loads: A Finite Element and Machine Learning Approach," Materials. (ISI Q2 IF: 3.4) (Under Revision)

APPENDIX A: FINITE ELEMENT ANALYSIS

A.1 Methodology procedure

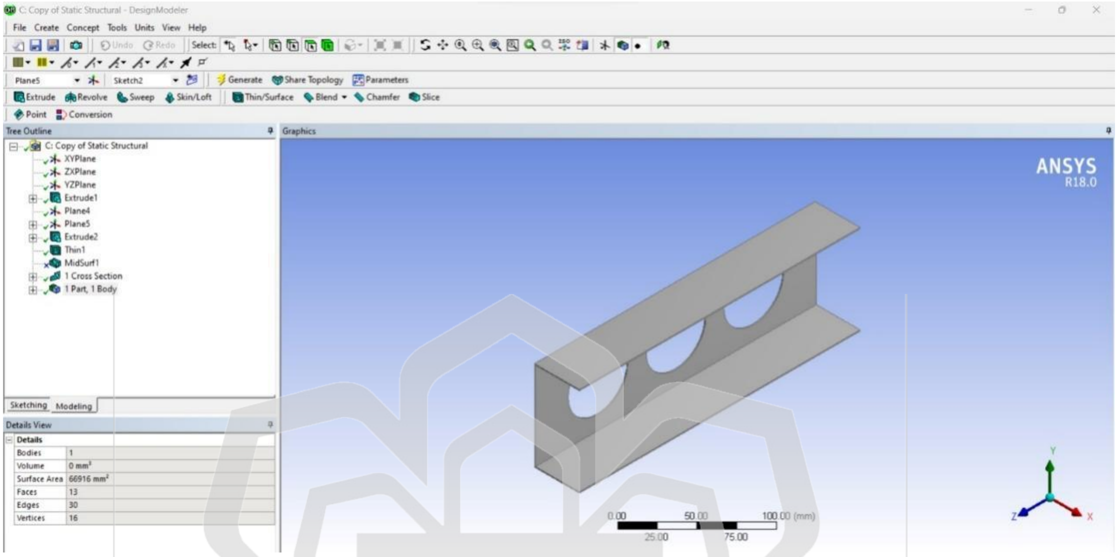

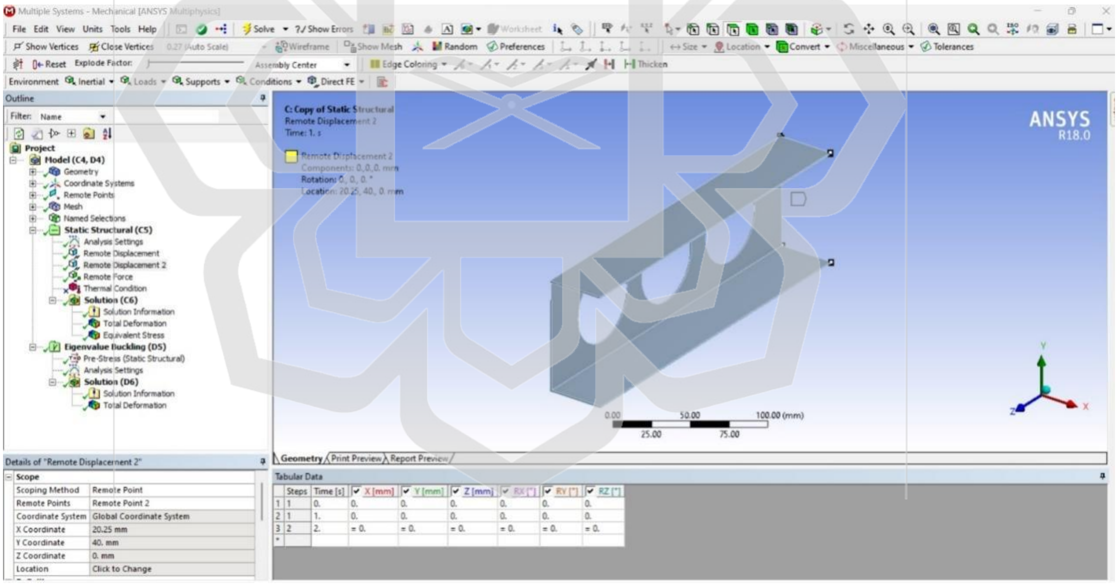

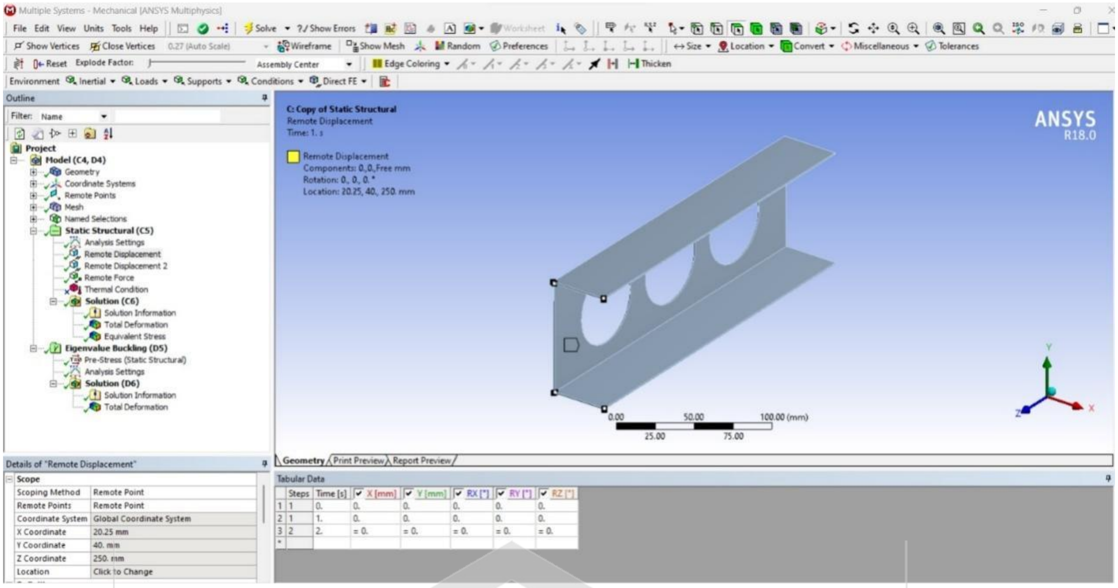

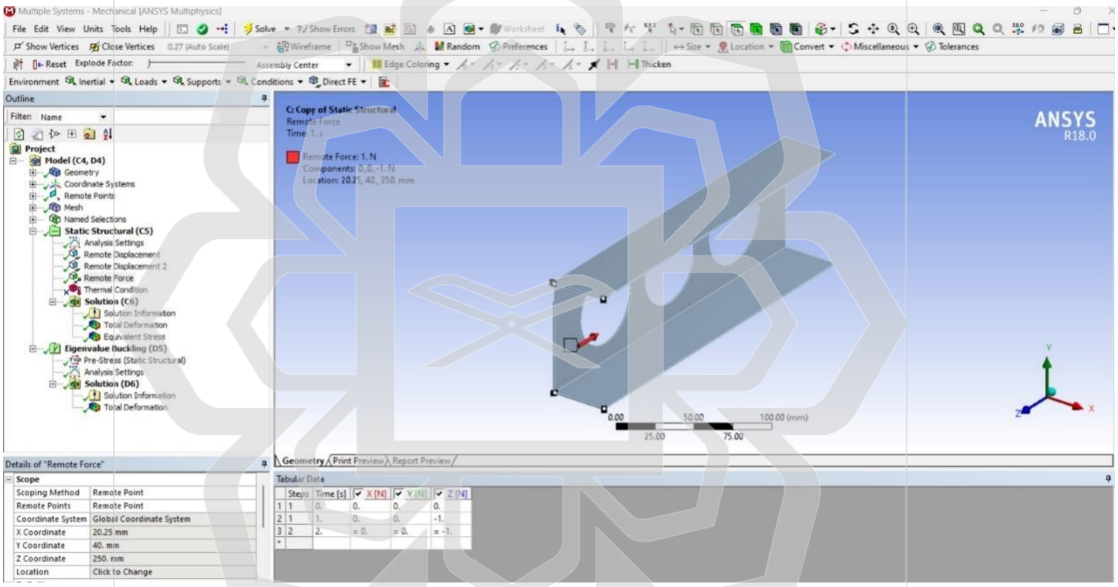

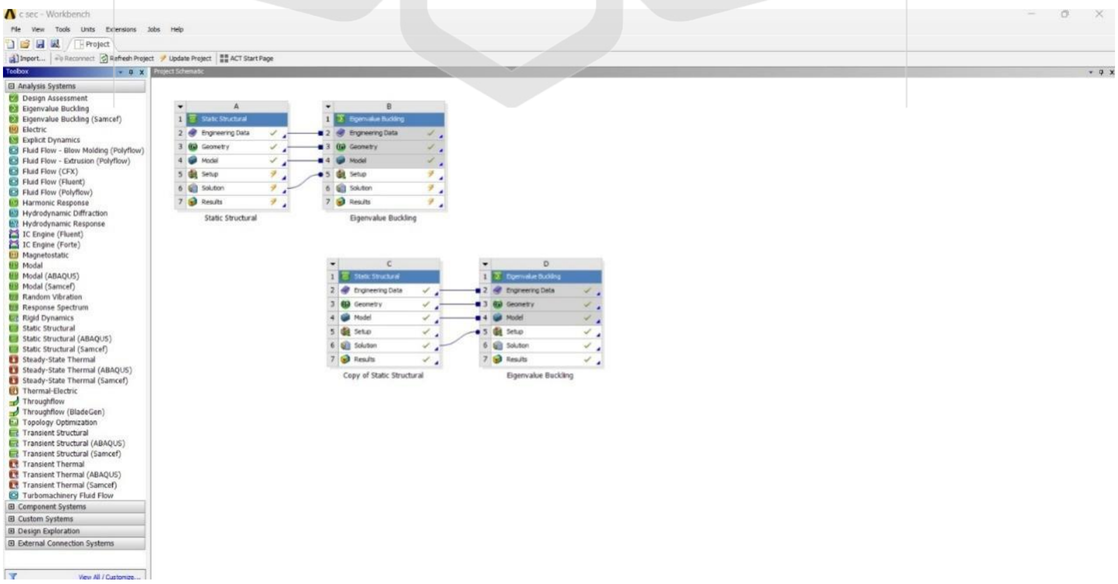

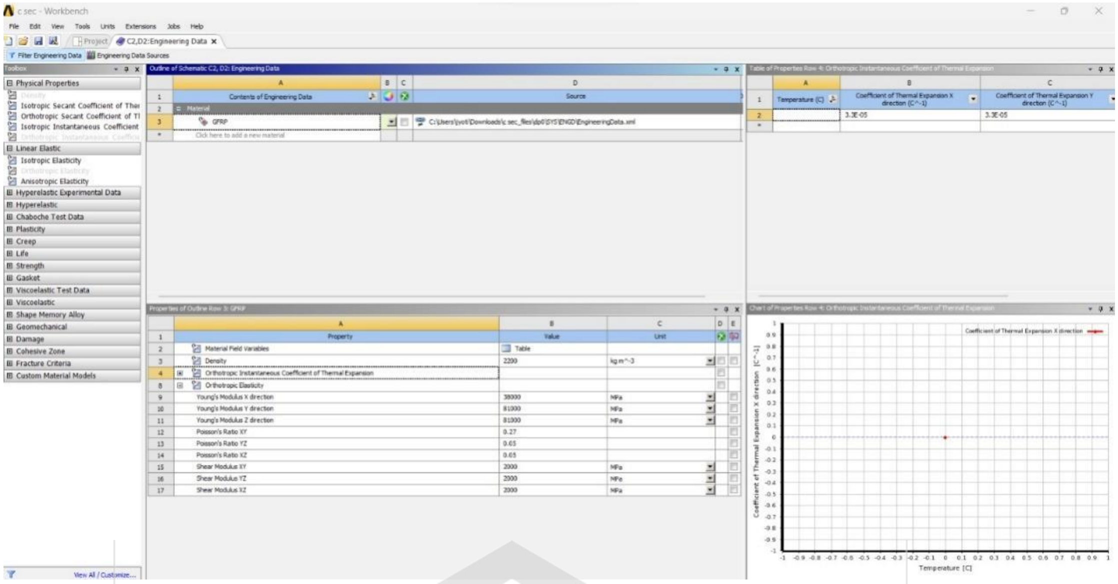
c sec - Workbench
Outline of Schematic C2, D2: Engineering Data
GFRP
Properties of Outline Row 3: GFRP
Density
Orthotropic Instantaneous Coefficient of Thermal Expansion
Orthotropic Elasticity
Young's Modulus X direction
Young's Modulus Y direction
Young's Modulus Z direction
Poisson's Ratio XY
Poisson's Ratio YZ
Poisson's Ratio XZ
Shear Modulus XY
Shear Modulus YZ
Shear Modulus XZ
Temperature [C]

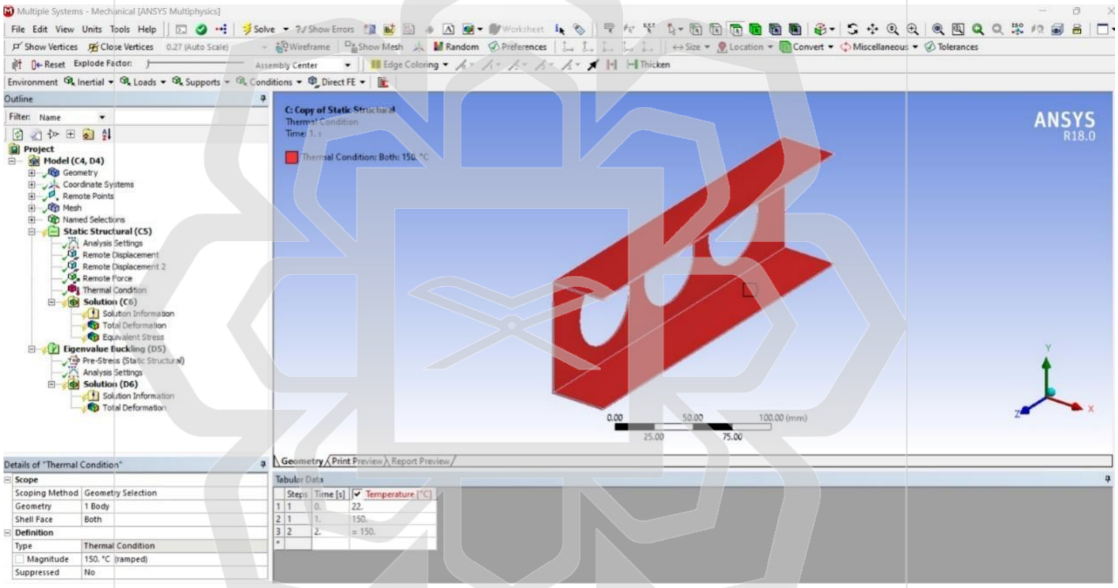
Multiple Systems - Mechanical [ANSYS Multiphysics]
ANSYS
R18.0
Project
Model (C4, D4)
Geometry
Coordinate Systems
Remote Points
Mesh
Named Selections
Static Structural (C5)
Analysis Settings
Remote Displacement
Remote Displacement 2
Remote Force
Thermal Condition
Solution (C6)
Solution Information
Total Deformation
Equivalent Stress
Eigenvalue Buckling (D5)
Pre-Stress (Static Structural)
Analysis Settings
Solution (D6)
Solution Information
Total Deformation
Details of "Thermal Condition"
Scoping Method Geometry Selection
Geometry 1 Body
Shell Face Both
Type Thermal Condition
Magnitude 150. °C (ramped)
Suppressed No
Tabular Data
Steps Time [s] Temperature [°C]
1 0. 22.
1 1. 150.
2 2. = 150.

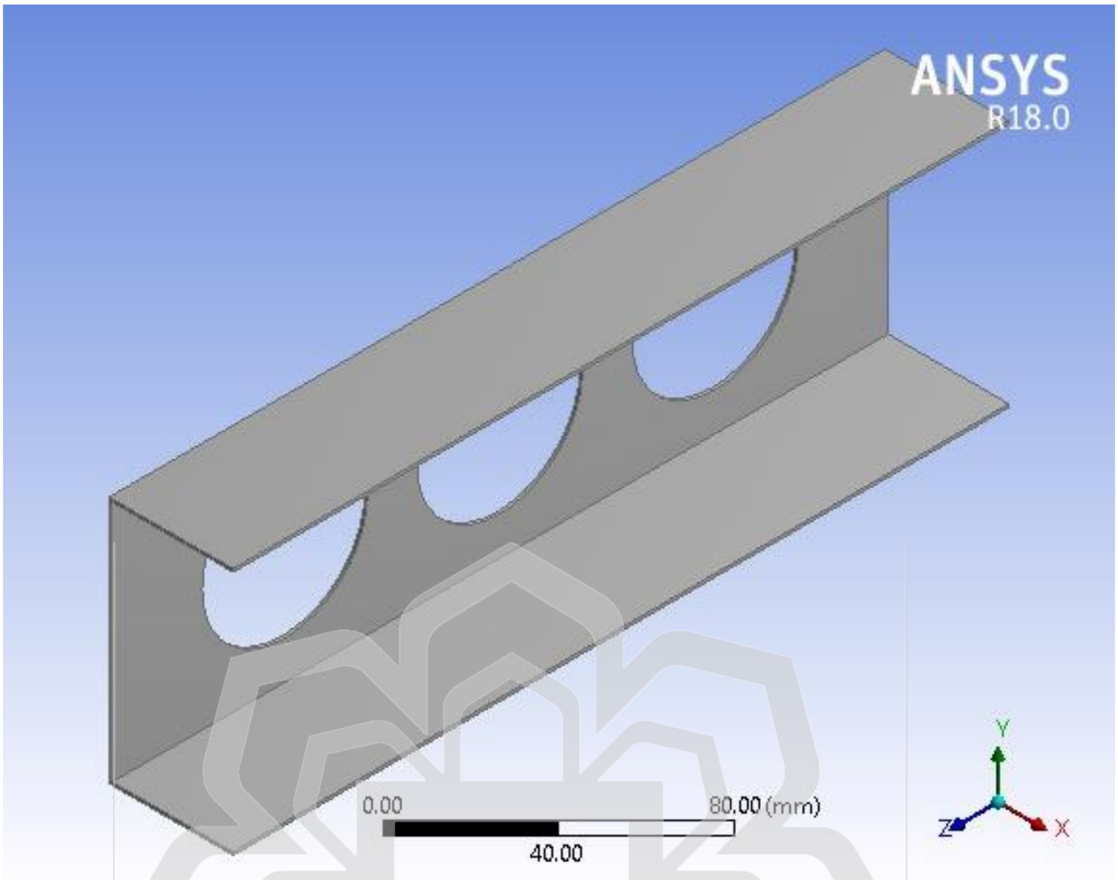
ANSYS
R18.0
0.00
80.00 (mm)
40.00
Y
Z
X

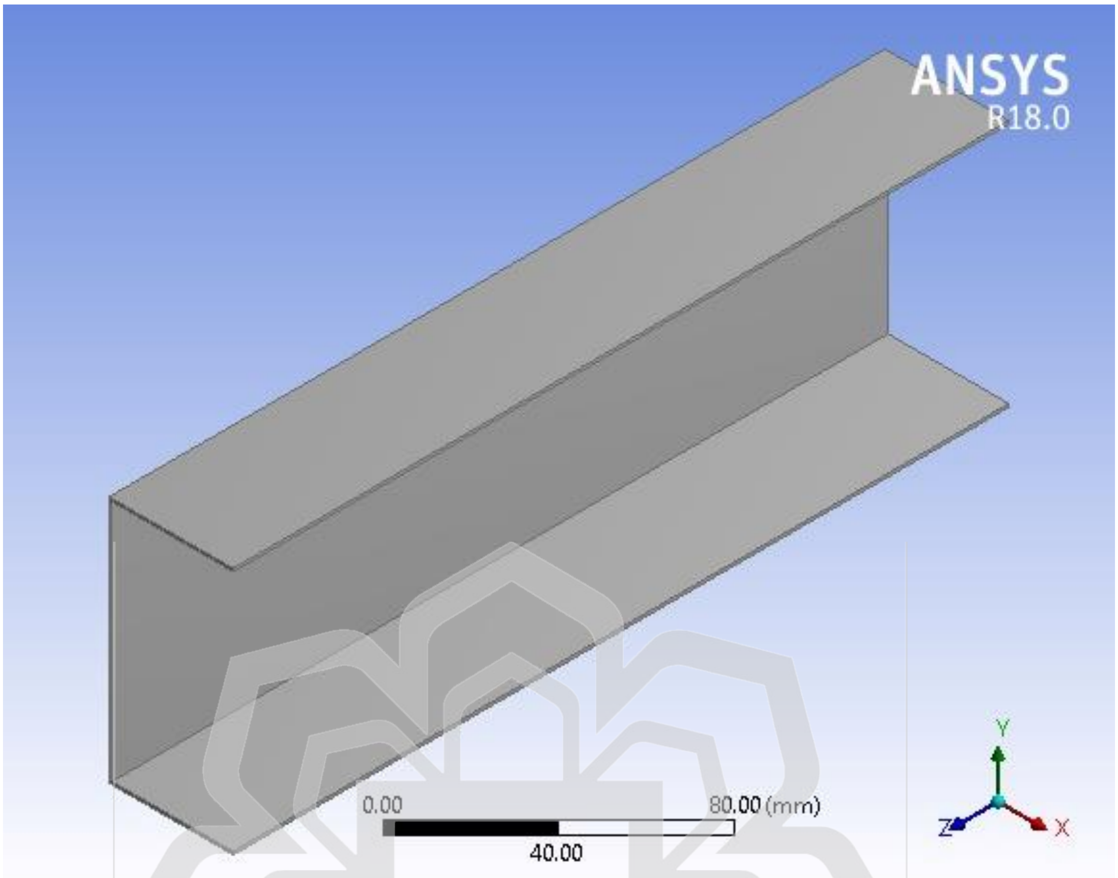
ANSYS
R18.0
0.00
80.00 (mm)
40.00
Y
Z
X

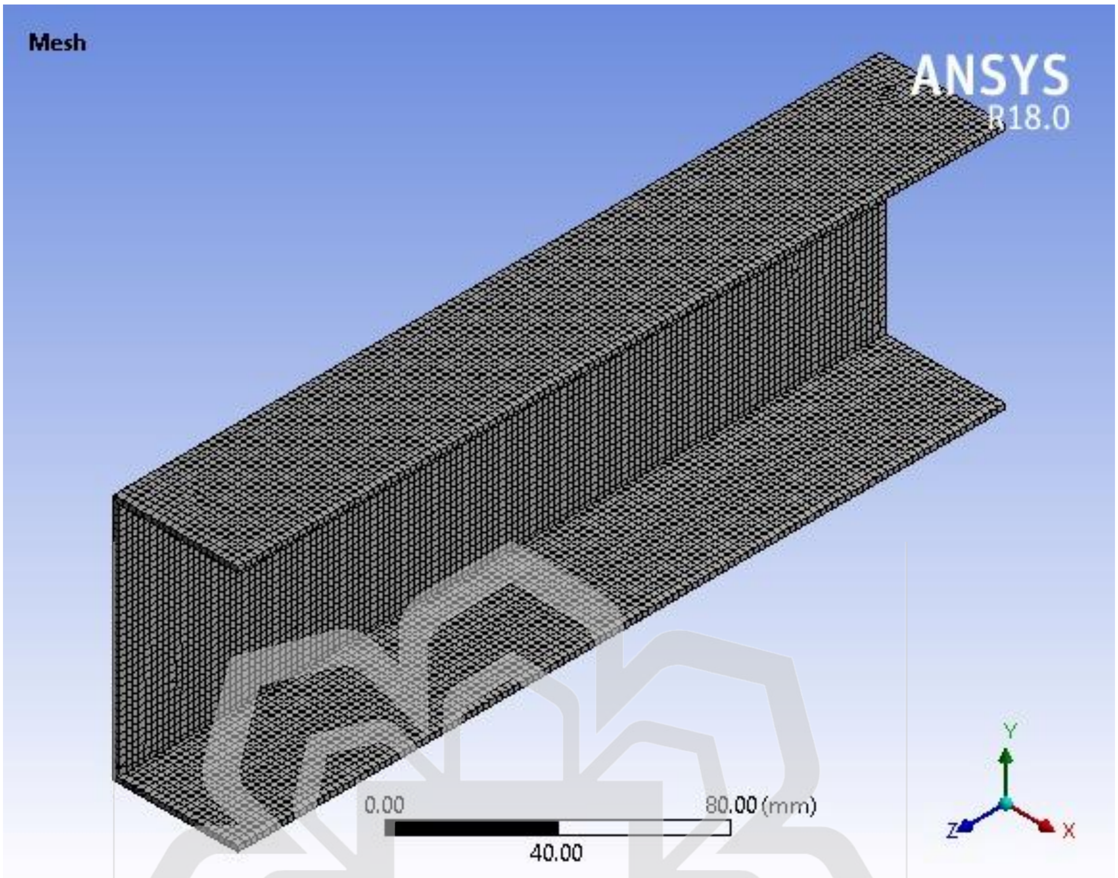
Mesh
ANSYS
R18.0
0.00
80.00 (mm)
40.00
Y
Z
X

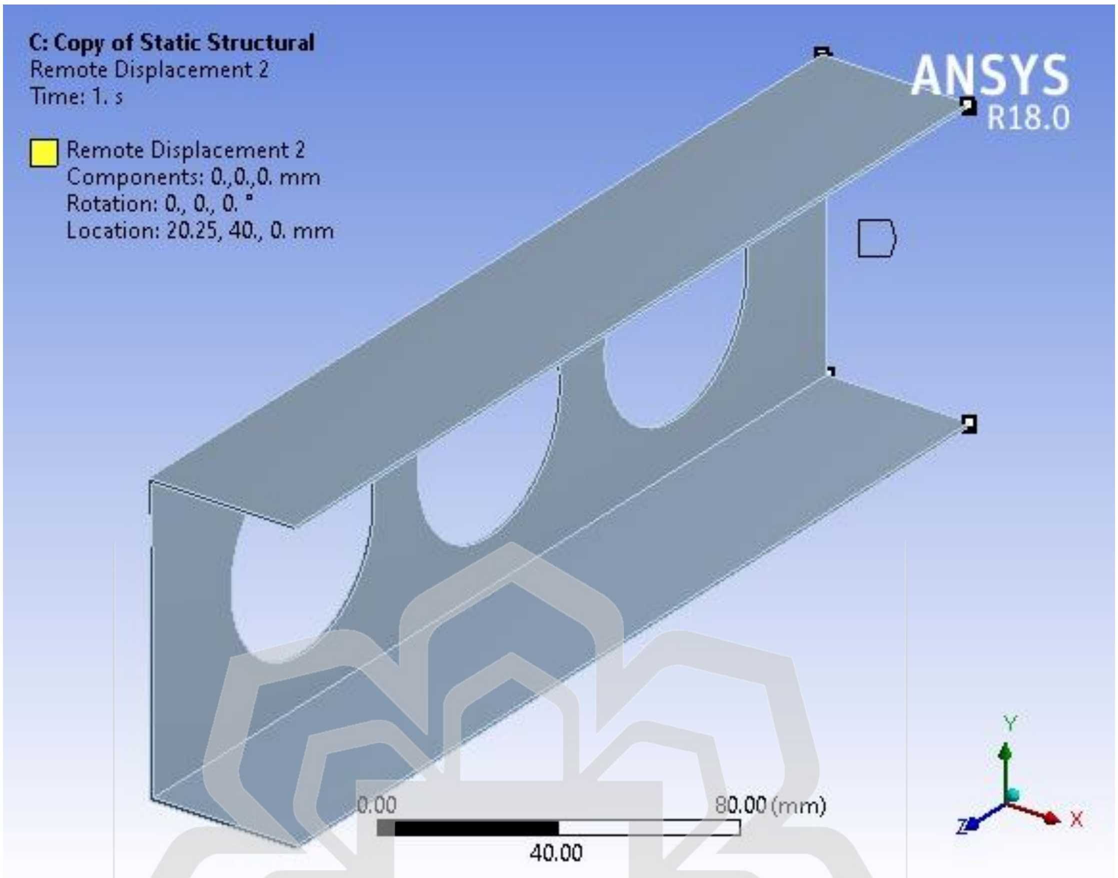
C: Copy of Static Structural
Remote Displacement 2
Time: 1. s
Remote Displacement 2
Components: 0.,0.,0. mm
Rotation: 0., 0., 0. °
Location: 20.25, 40., 0. mm
ANSYS
R18.0
0.00
80.00 (mm)
40.00
Y
X
Z

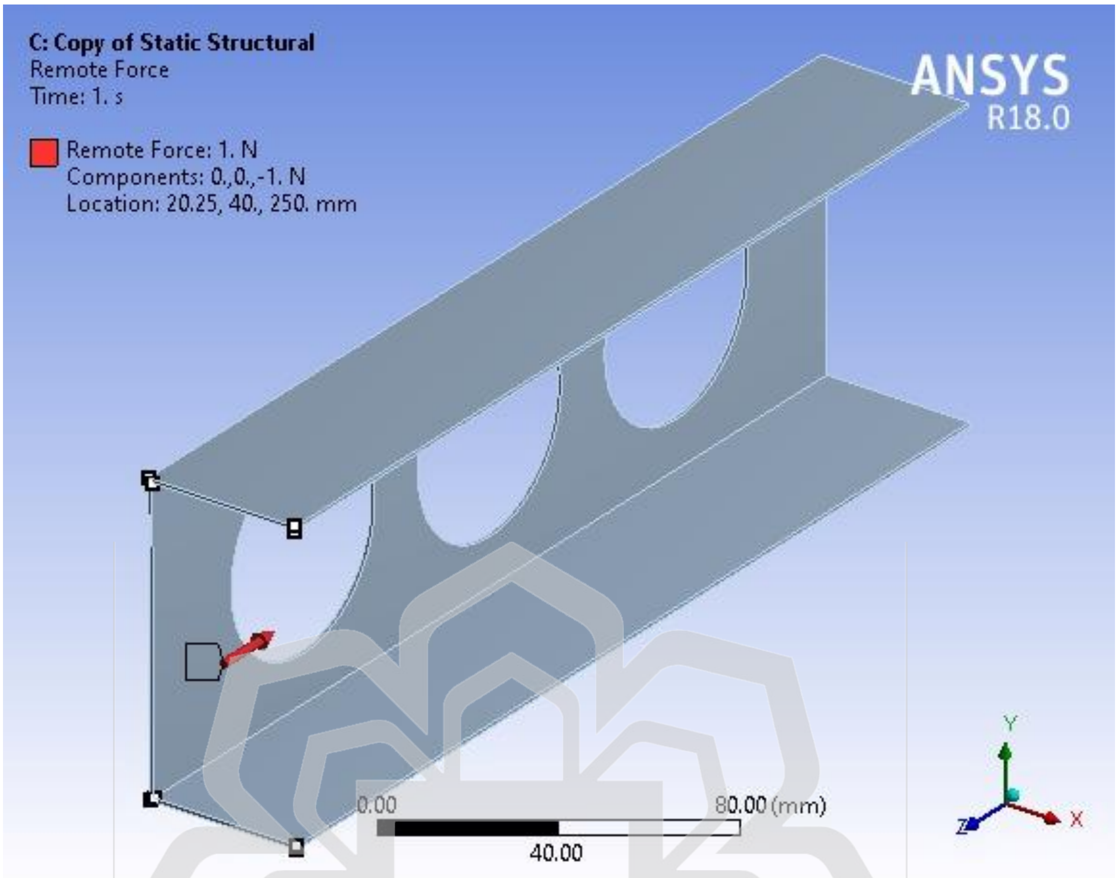
C: Copy of Static Structural
Remote Force
Time: 1. s
Remote Force: 1. N
Components: 0.,0.,-1. N
Location: 20.25, 40., 250. mm
ANSYS
R18.0
0.00
80.00 (mm)
40.00
Y
Z
X

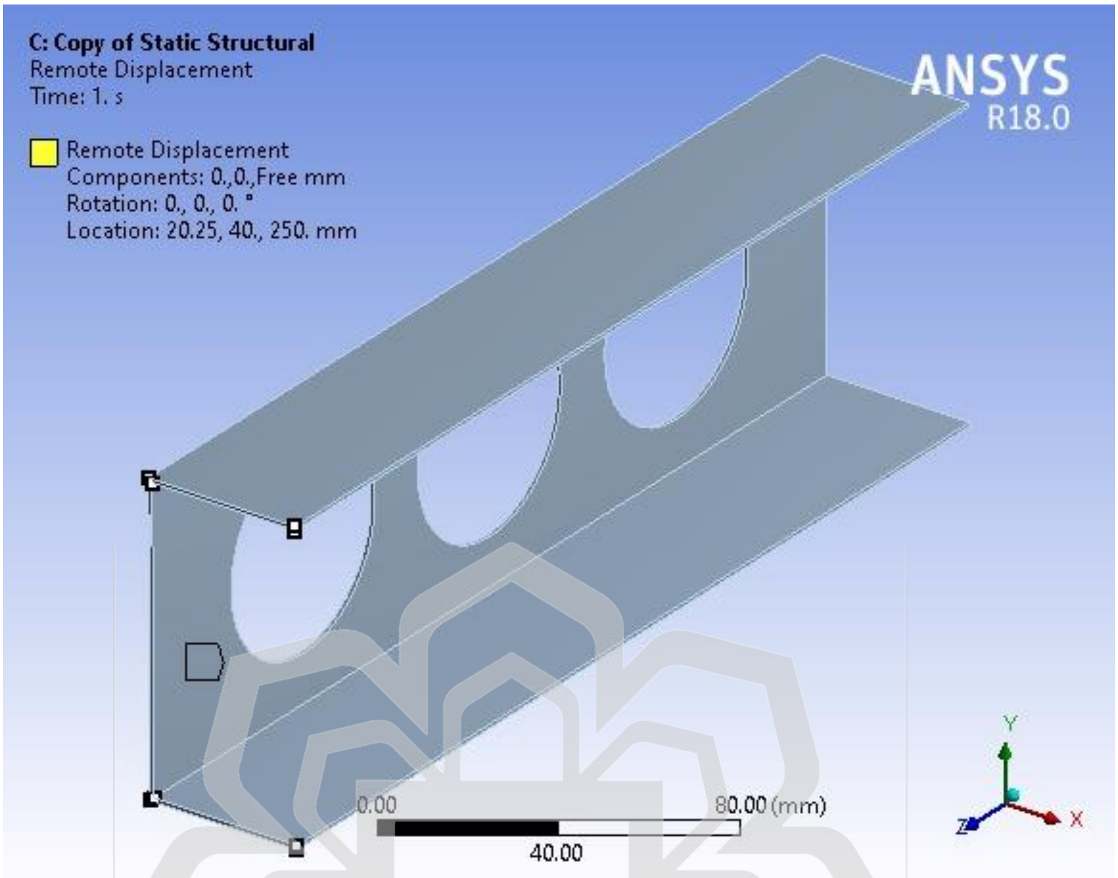
C: Copy of Static Structural
Remote Displacement
Time: 1. s
Remote Displacement
Components: 0.,0.,Free mm
Rotation: 0., 0., 0. °
Location: 20.25, 40., 250. mm
ANSYS
R18.0
0.00
80.00 (mm)
40.00
Y
Z
X

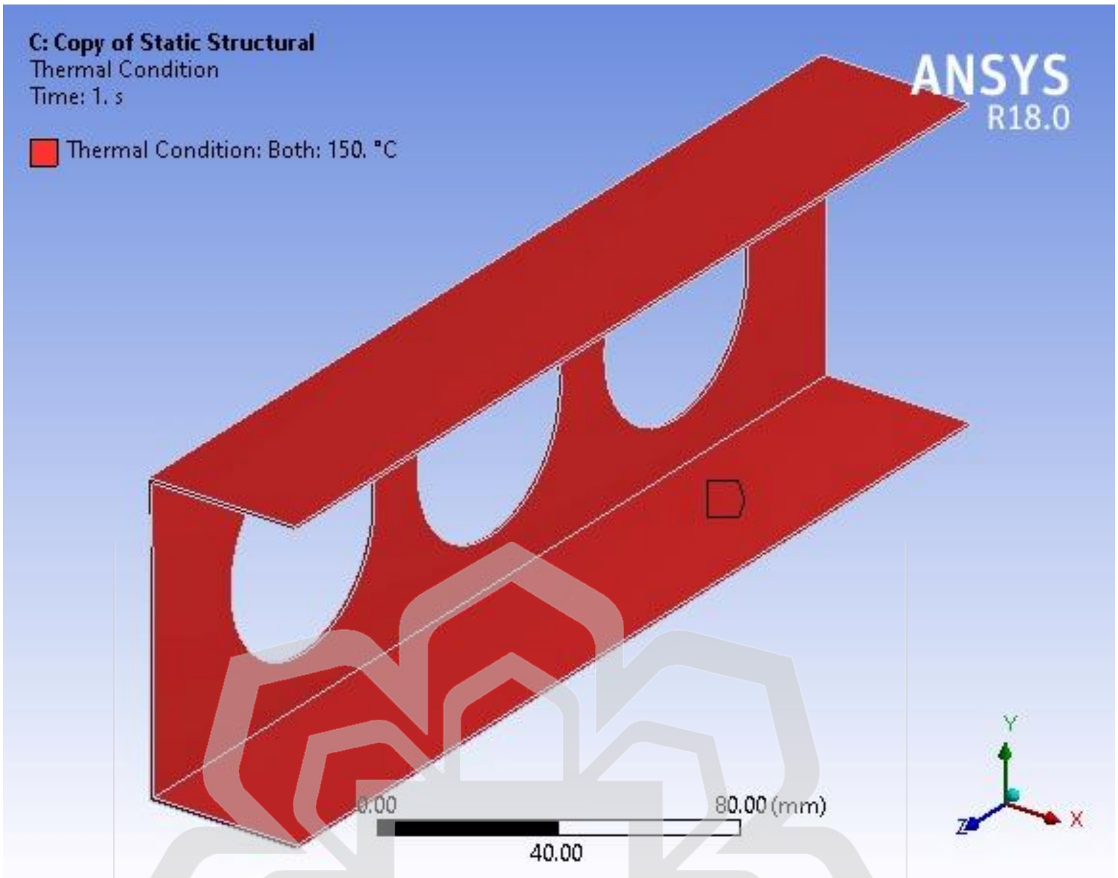
C: Copy of Static Structural
Thermal Condition
Time: 1. s
Thermal Condition: Both: 150. °C
ANSYS
R18.0
0.00
80.00 (mm)
40.00
Y
Z
X

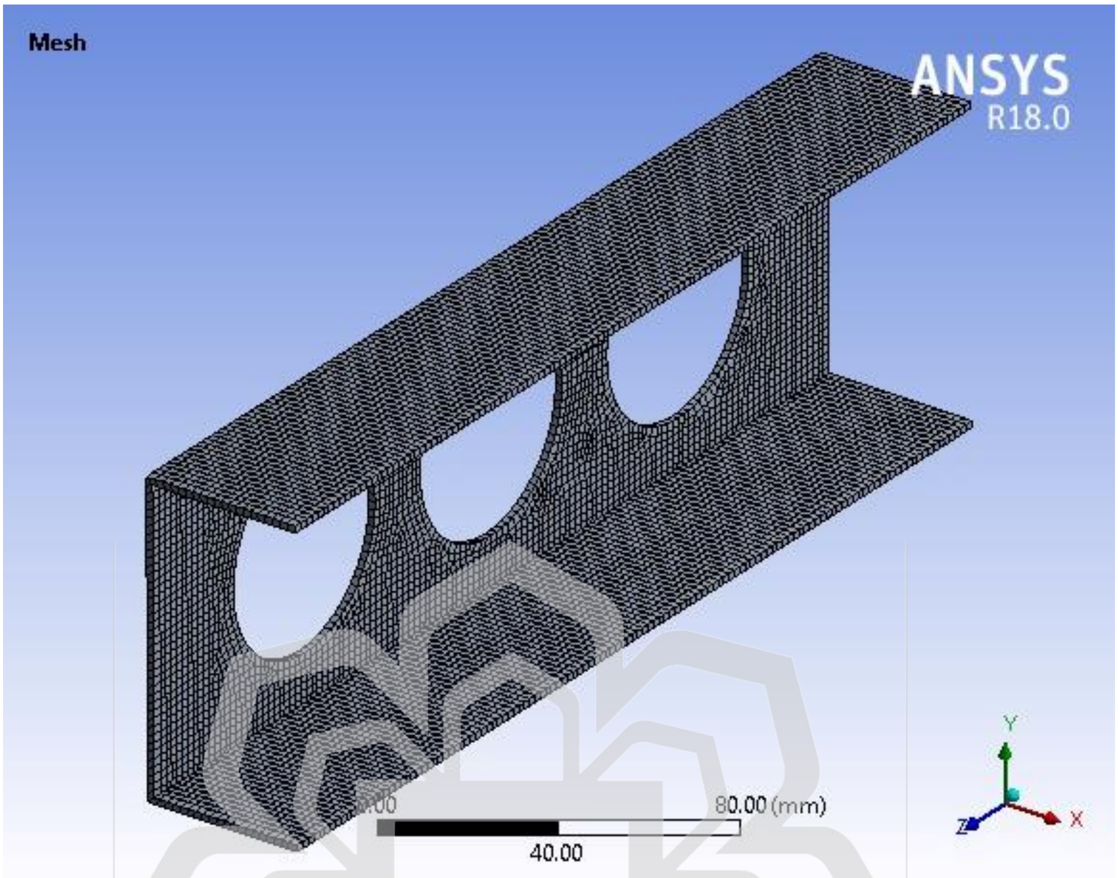
Mesh
ANSYS
R18.0
80.00 (mm)
40.00
Y
Z
X

A.2 Some Other Contours of Simulation Results

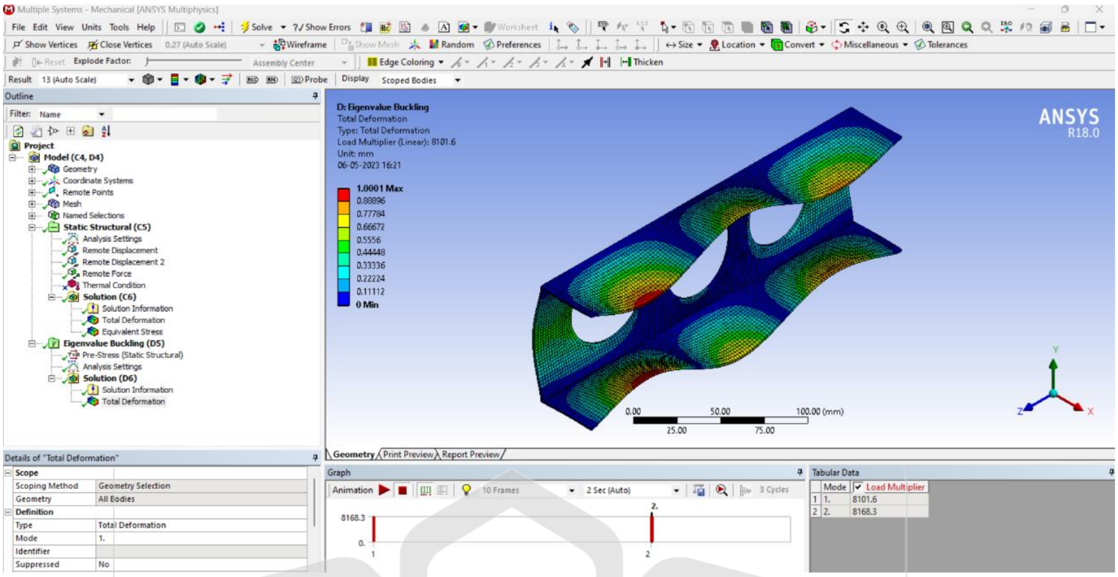

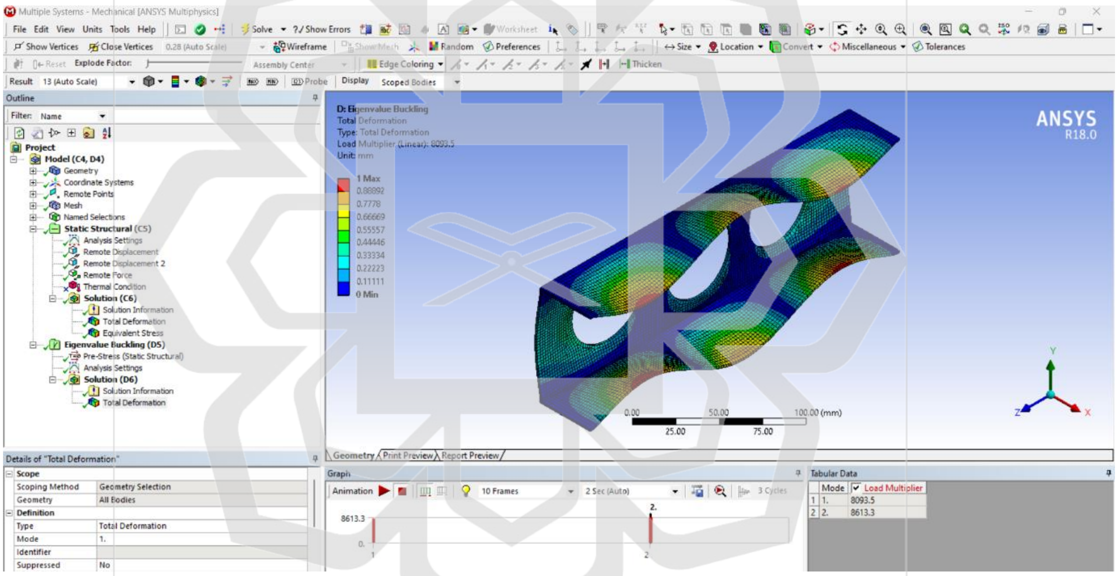

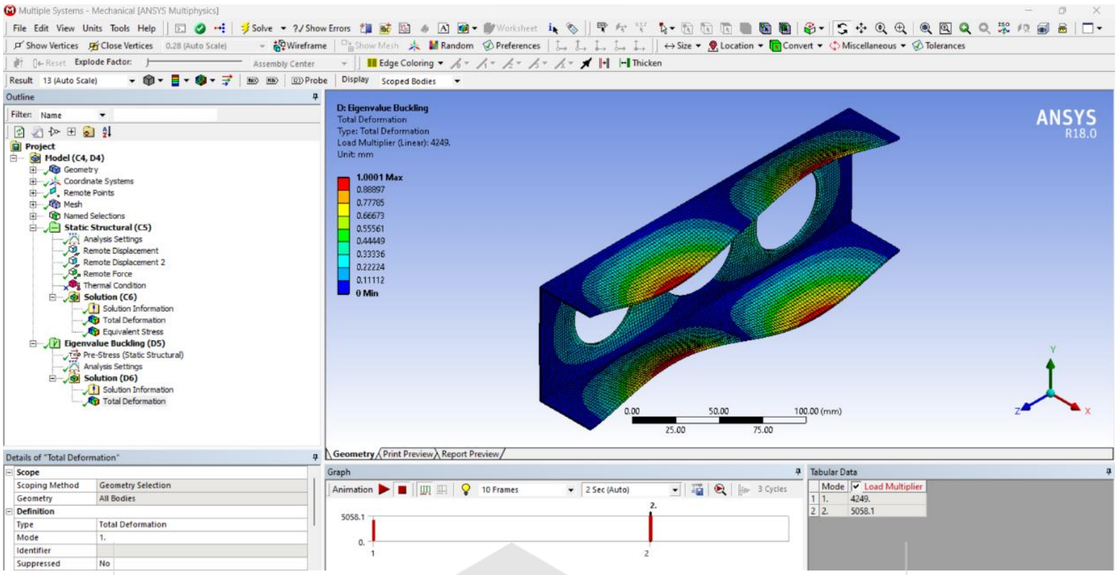
D: Eigenvalue Buckling
Total Deformation
Type: Total Deformation
Load Multiplier (Linear): 4249.
Unit: mm
1.0001 Max
0.88897
0.77785
0.66673
0.55561
0.44449
0.33336
0.22224
0.11112
0 Min
ANSYS
R18.0
Mode
Load Multiplier
1.
4249.
2.
5058.1

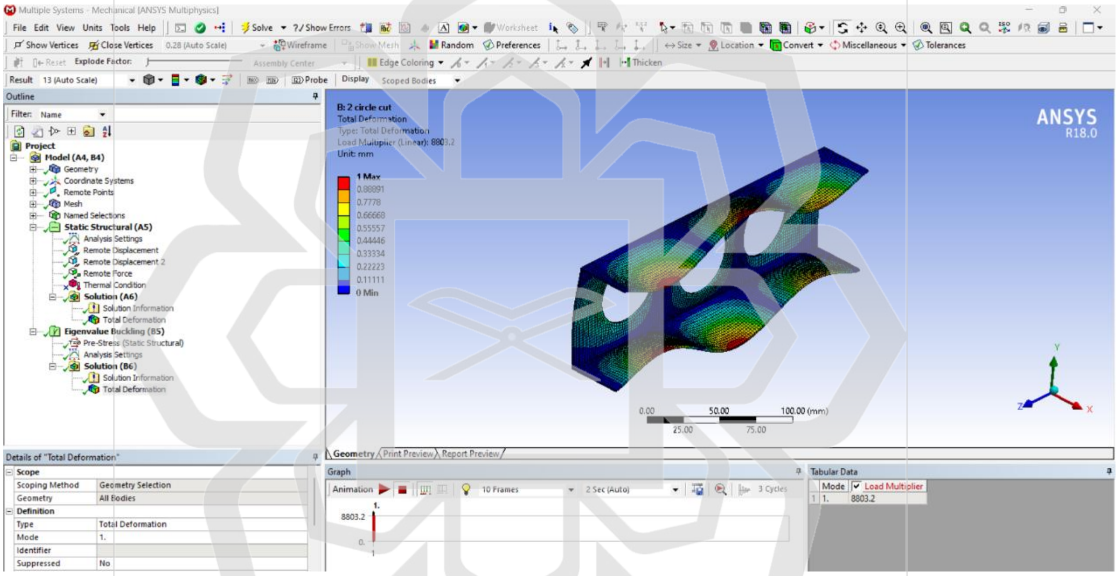
B: 2 circle cut
Total Deformation
Type: Total Deformation
Load Multiplier (Linear): 8803.2
Unit: mm
1 Max
0 Min
ANSYS
R18.0
Mode
Load Multiplier
1.
8803.2

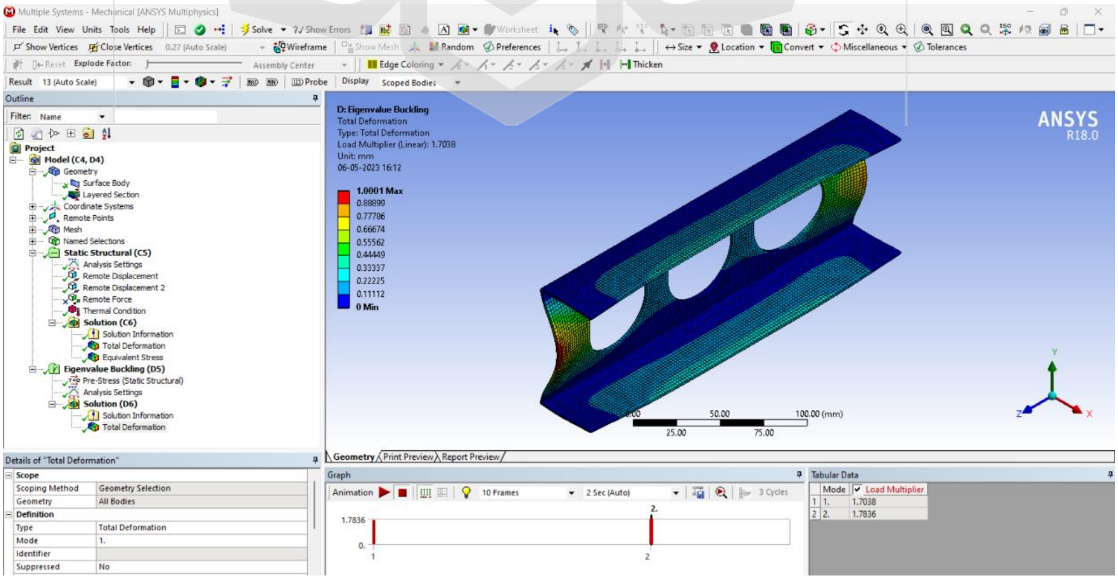
D: Eigenvalue Buckling
Total Deformation
Type: Total Deformation
Load Multiplier (Linear): 1.7038
Unit: mm
06-05-2023 16:12
1.0001 Max
0.88899
0.77786
0.66674
0.55562
0.44449
0.33337
0.22225
0.11112
0 Min
ANSYS
R18.0
Mode
Load Multiplier
1.
1.7038
2.
1.7836

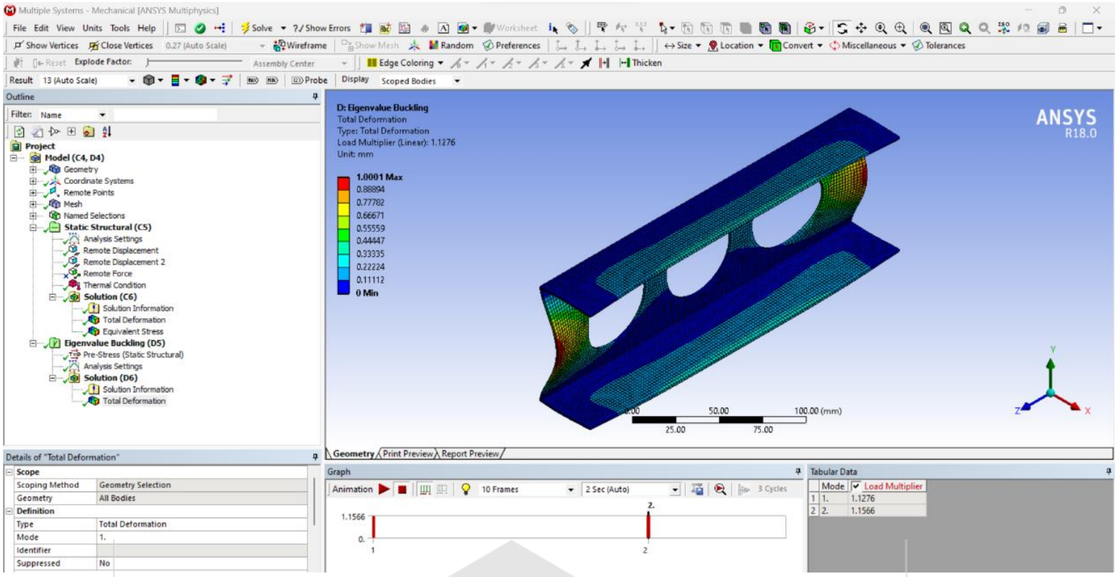
D: Eigenvalue Buckling
Total Deformation
Type: Total Deformation
Load Multiplier (Linear): 1.1276
Unit: mm
1.0001 Max
0.88894
0.77782
0.66671
0.55559
0.44447
0.33335
0.22224
0.11112
0 Min
ANSYS
R18.0
Mode
Load Multiplier
1. 1.1276
2. 1.1566

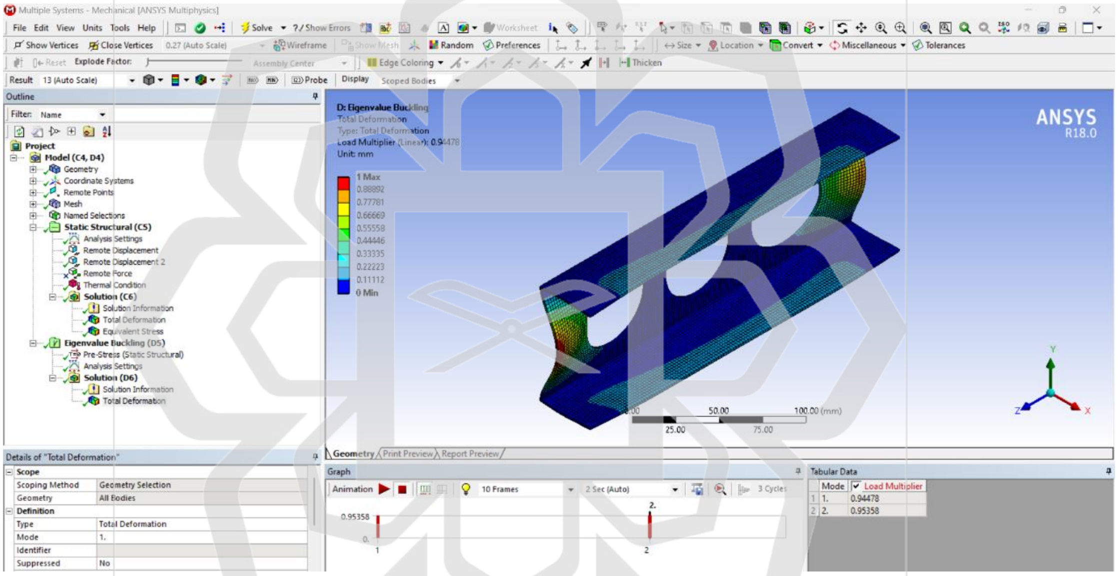
D: Eigenvalue Buckling
Total Deformation
Type: Total Deformation
Load Multiplier (Linear): 0.94478
Unit: mm
1 Max
0.88892
0.77781
0.66669
0.55558
0.44446
0.33335
0.22223
0.11112
0 Min
ANSYS
R18.0
Mode
Load Multiplier
1. 0.94478
2. 0.95358

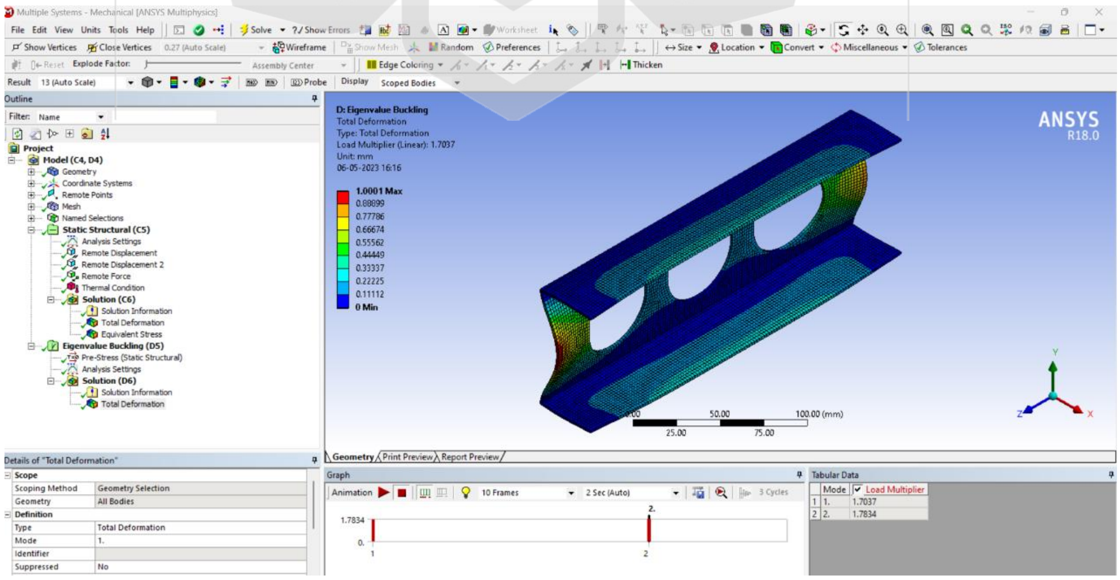
D: Eigenvalue Buckling
Total Deformation
Type: Total Deformation
Load Multiplier (Linear): 1.7037
Unit: mm
06-05-2023 16:16
1.0001 Max
0.88899
0.77786
0.66674
0.55562
0.44449
0.33337
0.22225
0.11112
0 Min
ANSYS
R18.0
Mode
Load Multiplier
1. 1.7037
2. 1.7834

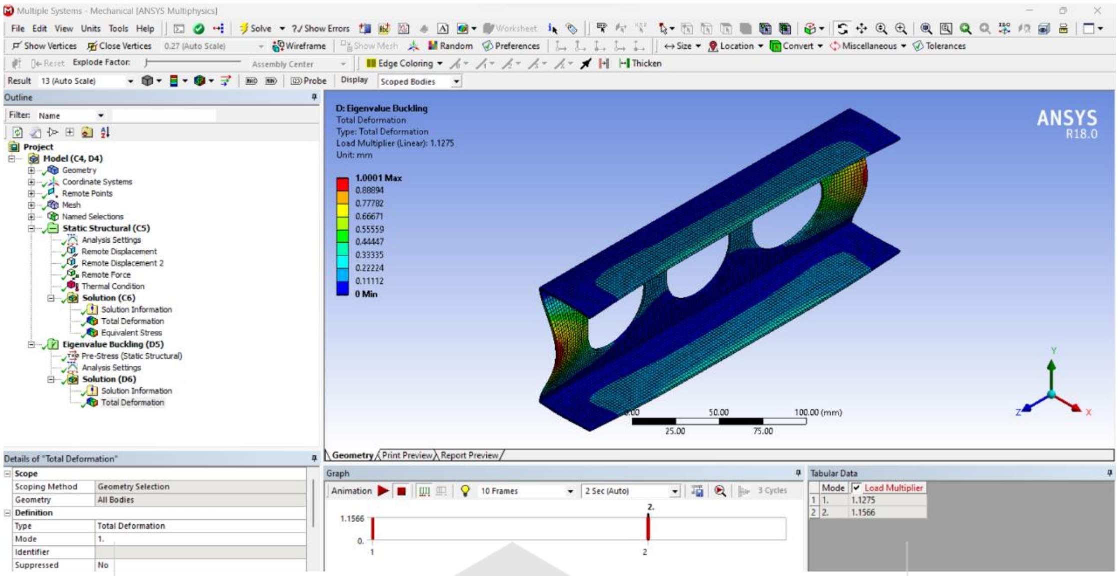
Multiple Systems - Mechanical [ANSYS Multiphysics]
D: Eigenvalue Buckling
Total Deformation
Type: Total Deformation
Load Multiplier (Linear): 1.1275
Unit: mm
1.0001 Max
0.88894
0.77782
0.66671
0.55559
0.44447
0.33335
0.22224
0.11112
0 Min
ANSYS
R18.0
Project
Model (C4, D4)
Geometry
Coordinate Systems
Remote Points
Mesh
Named Selections
Static Structural (C5)
Analysis Settings
Remote Displacement
Remote Displacement 2
Remote Force
Thermal Condition
Solution (C6)
Solution Information
Total Deformation
Equivalent Stress
Eigenvalue Buckling (D5)
Pre-Stress (Static Structural)
Analysis Settings
Solution (D6)
Solution Information
Total Deformation
Details of "Total Deformation"
Scoping Method
Geometry Selection
Geometry
All Bodies
Type
Total Deformation
Mode
1.
Suppressed
No
Tabular Data
Mode
Load Multiplier
1.
1.1275
2.
1.1566

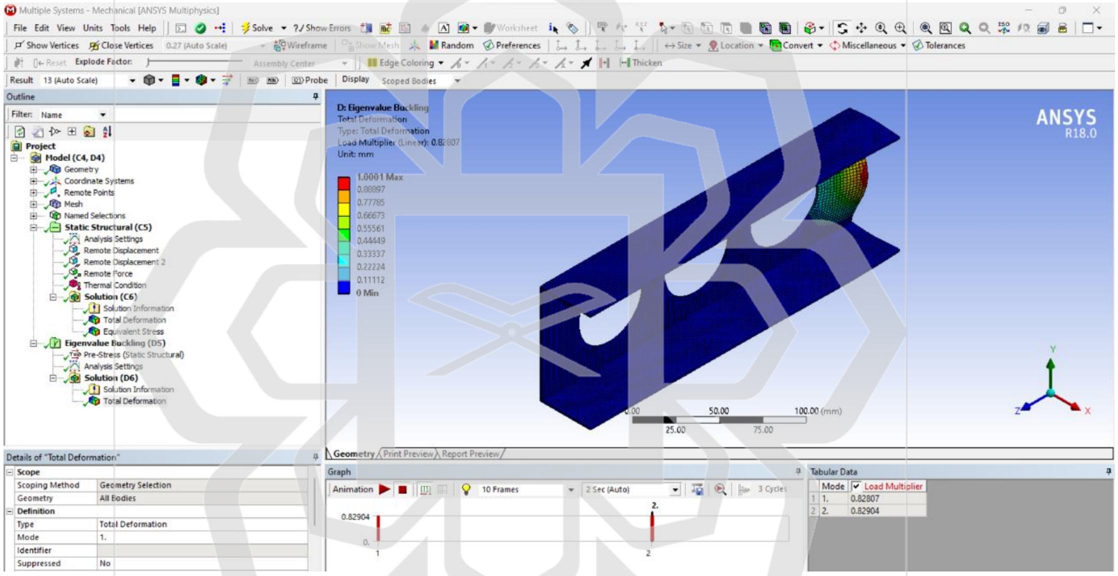
Multiple Systems - Mechanical [ANSYS Multiphysics]
D: Eigenvalue Buckling
Total Deformation
Type: Total Deformation
Unit: mm
1.0001 Max
0 Min
ANSYS
R18.0
Details of "Total Deformation"
Tabular Data
Mode
Load Multiplier
1.
0.82807
2.
0.82904

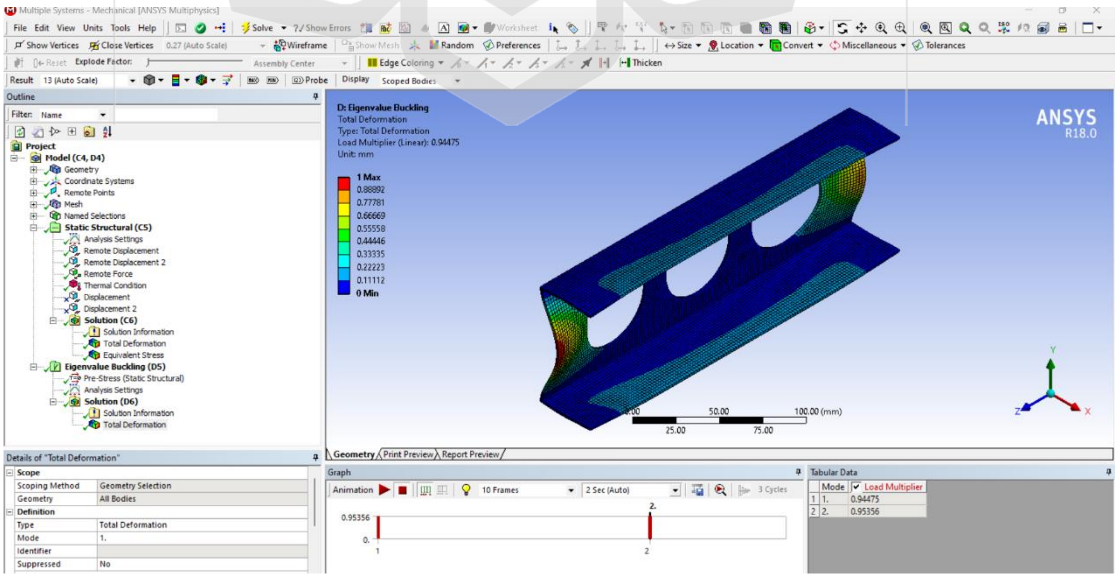
Multiple Systems - Mechanical [ANSYS Multiphysics]
D: Eigenvalue Buckling
Total Deformation
Type: Total Deformation
Load Multiplier (Linear): 0.94475
Unit: mm
1 Max
0.88892
0.77781
0.66669
0.55558
0.44446
0.33335
0.22223
0.11112
0 Min
ANSYS
R18.0
Details of "Total Deformation"
Tabular Data
Mode
Load Multiplier
1.
0.94475
2.
0.95356

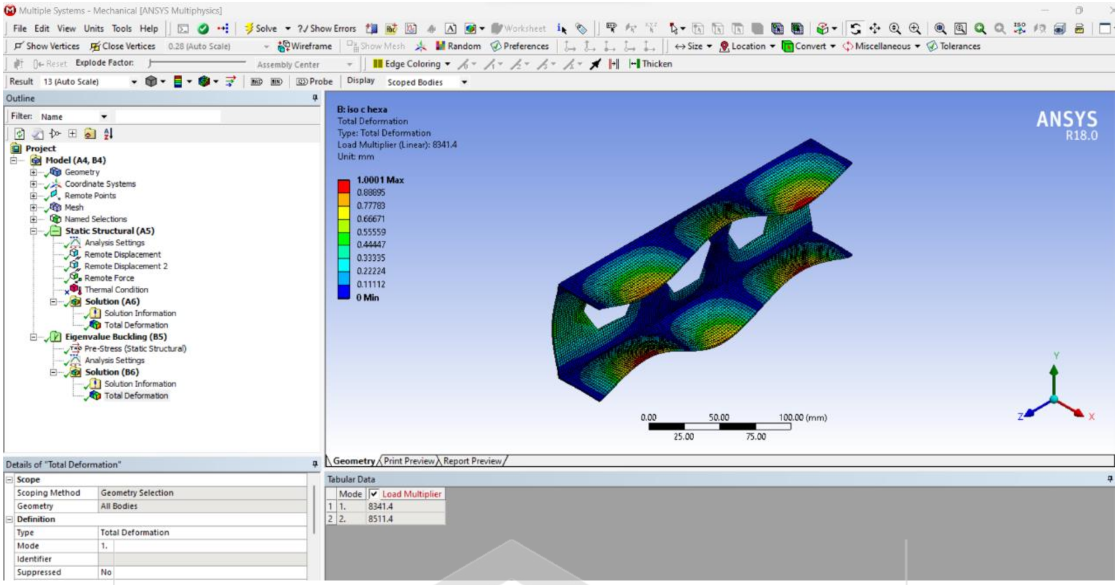

Multiple Systems - Mechanical [ANSYS Multiphysics]
B: iso c hexa
Total Deformation
Type: Total Deformation
Load Multiplier (Linear): 8341.4
Unit: mm
1.0001 Max
0.88895
0.77783
0.66671
0.55559
0.44447
0.33335
0.22224
0.11112
0 Min
ANSYS
R18.0
0.00
50.00
100.00 (mm)
25.00
75.00
Details of "Total Deformation"
Scoping Method Geometry Selection
Geometry All Bodies
Type Total Deformation
Mode 1.
Suppressed No
Tabular Data
Mode Load Multiplier
1. 8341.4
2. 8511.4

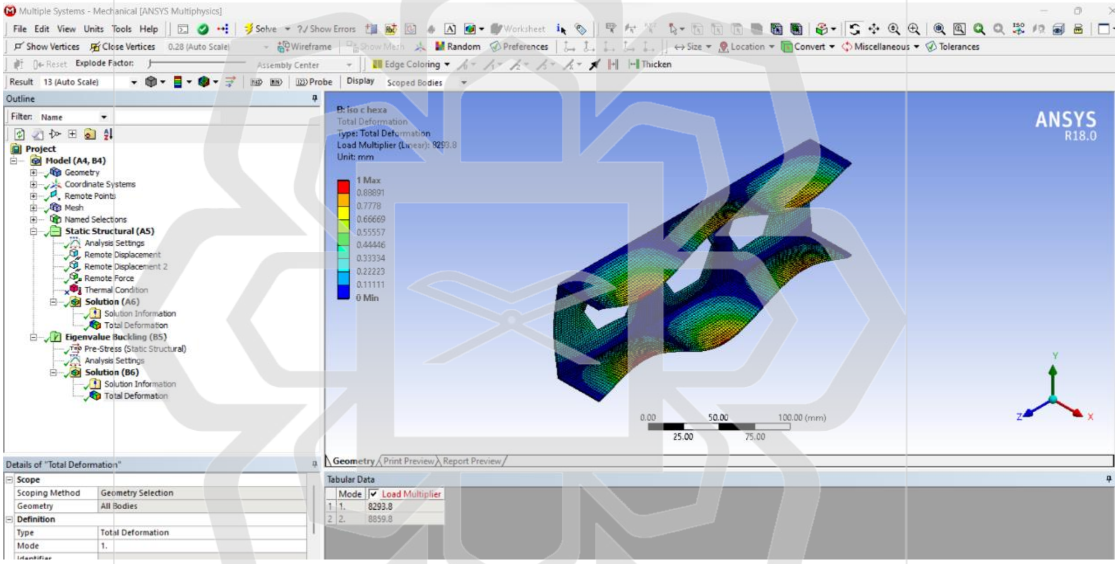

Multiple Systems - Mechanical [ANSYS Multiphysics]
B: iso c hexa
Total Deformation
Type: Total Deformation
Load Multiplier (Linear): 8293.8
Unit: mm
1 Max
0.88891
0.7778
0.66669
0.55557
0.44446
0.33334
0.22223
0.11111
0 Min
ANSYS
R18.0
0.00
50.00
100.00 (mm)
25.00
75.00
Details of "Total Deformation"
Scoping Method Geometry Selection
Geometry All Bodies
Type Total Deformation
Mode 1.
Tabular Data
Mode Load Multiplier
1. 8293.8
2. 8859.8

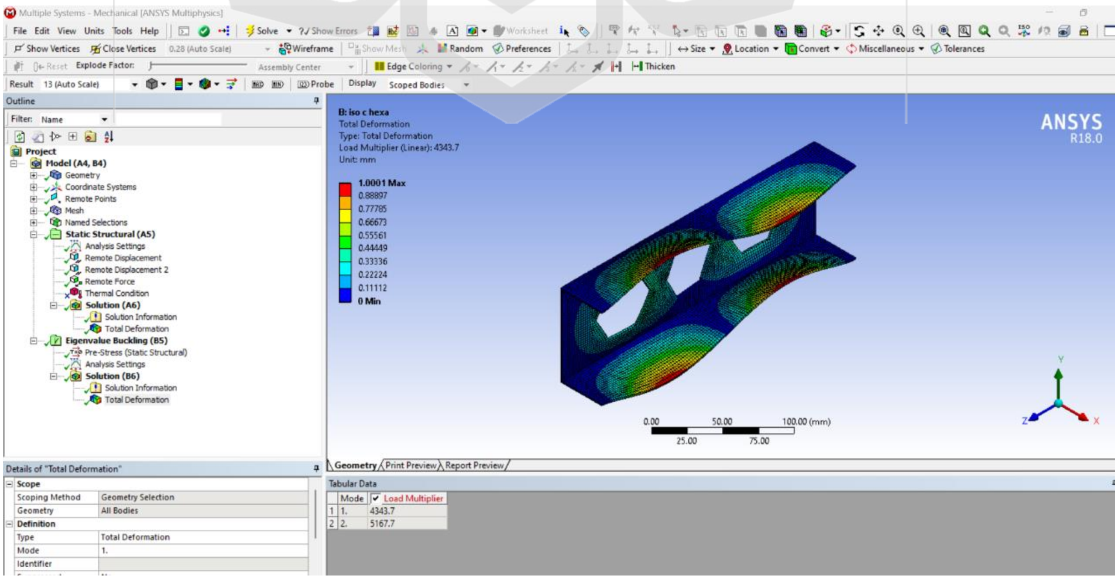

Multiple Systems - Mechanical [ANSYS Multiphysics]
B: iso c hexa
Total Deformation
Type: Total Deformation
Load Multiplier (Linear): 4343.7
Unit: mm
1.0001 Max
0.88897
0.77785
0.66673
0.55561
0.44449
0.33336
0.22224
0.11112
0 Min
ANSYS
R18.0
0.00
50.00
100.00 (mm)
25.00
75.00
Details of "Total Deformation"
Scoping Method Geometry Selection
Geometry All Bodies
Type Total Deformation
Mode 1.
Tabular Data
Mode Load Multiplier
1. 4343.7
2. 5167.7

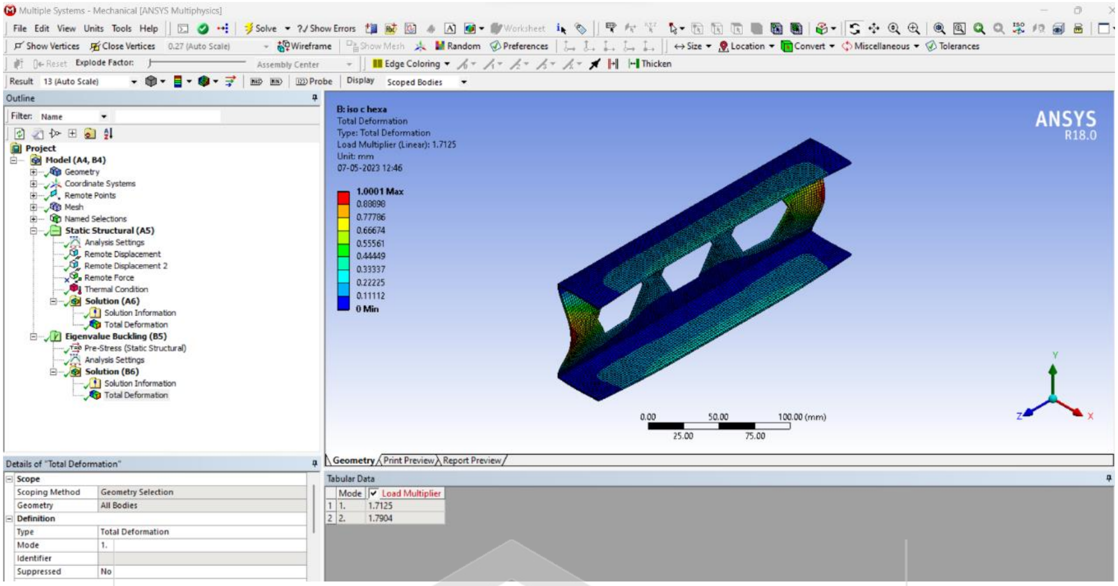
B: iso c hexa
Total Deformation
Type: Total Deformation
Load Multiplier (Linear): 1.7125
Unit: mm
07-05-2023 12:46
1.0001 Max
0 Min
ANSYS
R18.0
Mode | Load Multiplier
1. 1.7125
2. 1.7904

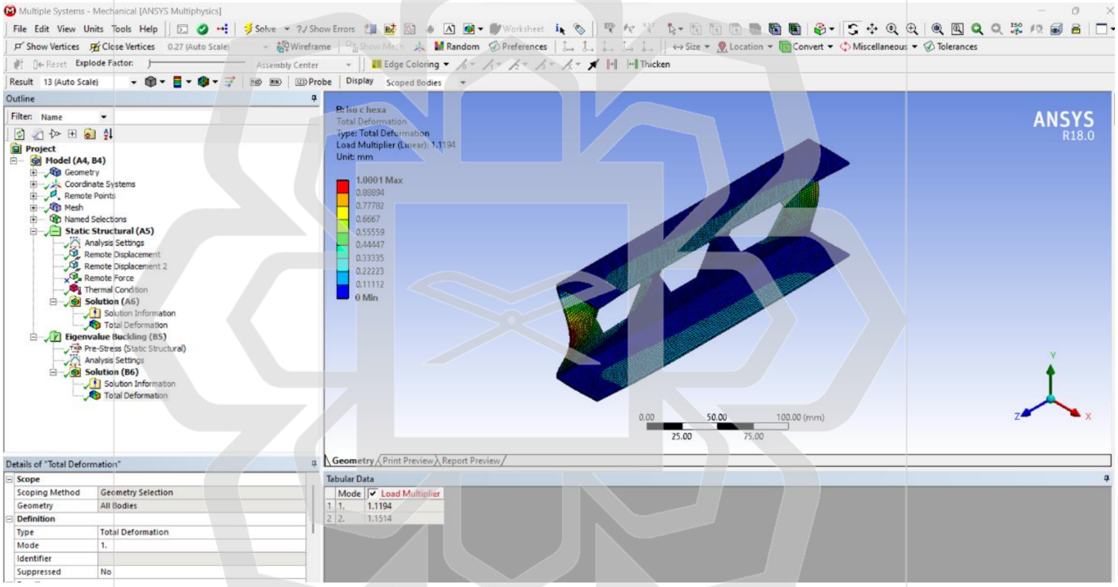
B: iso c hexa
Total Deformation
Type: Total Deformation
Load Multiplier (Linear): 1.1194
Unit: mm
1.0001 Max
0 Min
ANSYS
R18.0
Mode | Load Multiplier
1. 1.1194
2. 1.1514

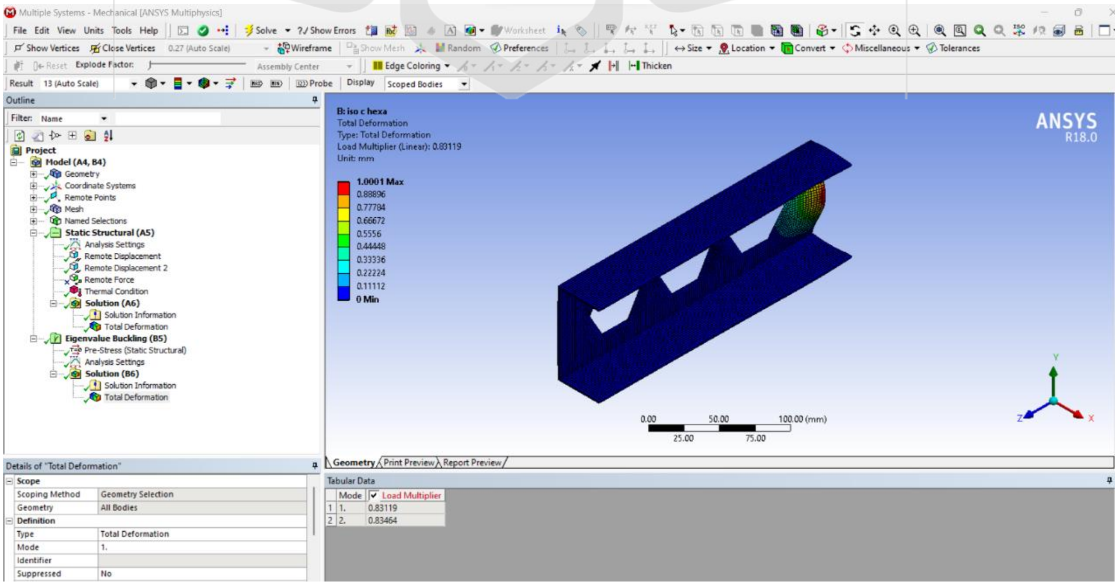
B: iso c hexa
Total Deformation
Type: Total Deformation
Load Multiplier (Linear): 0.83119
Unit: mm
1.0001 Max
0 Min
ANSYS
R18.0
Mode | Load Multiplier
1. 0.83119
2. 0.83464

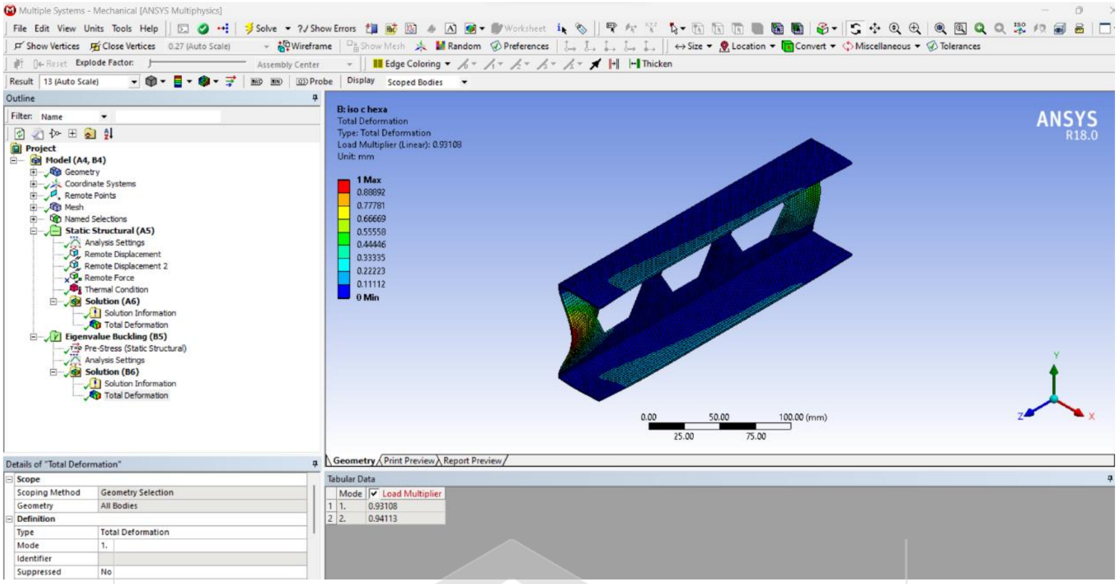

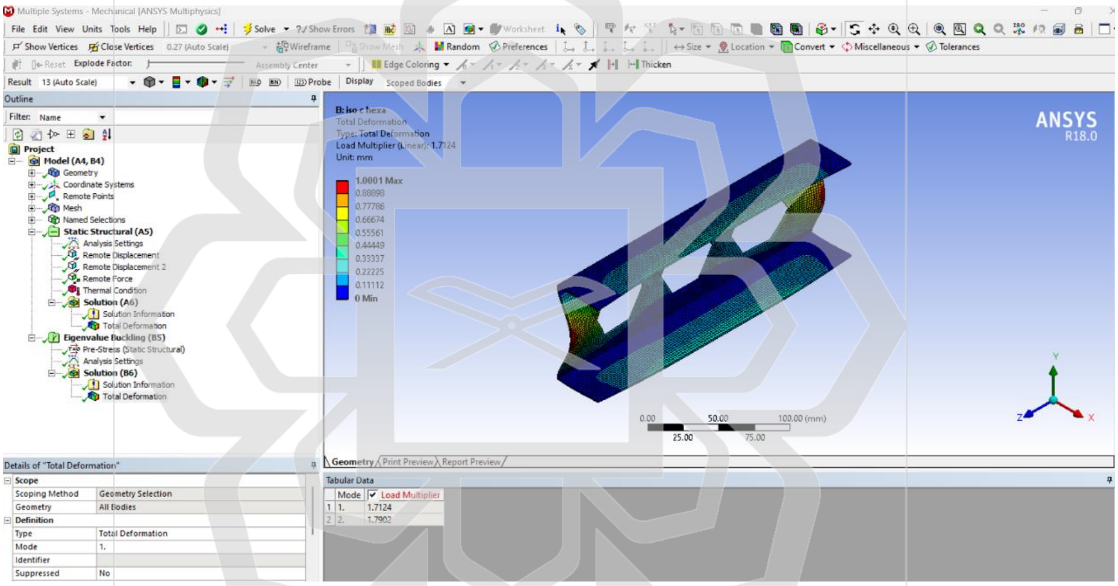

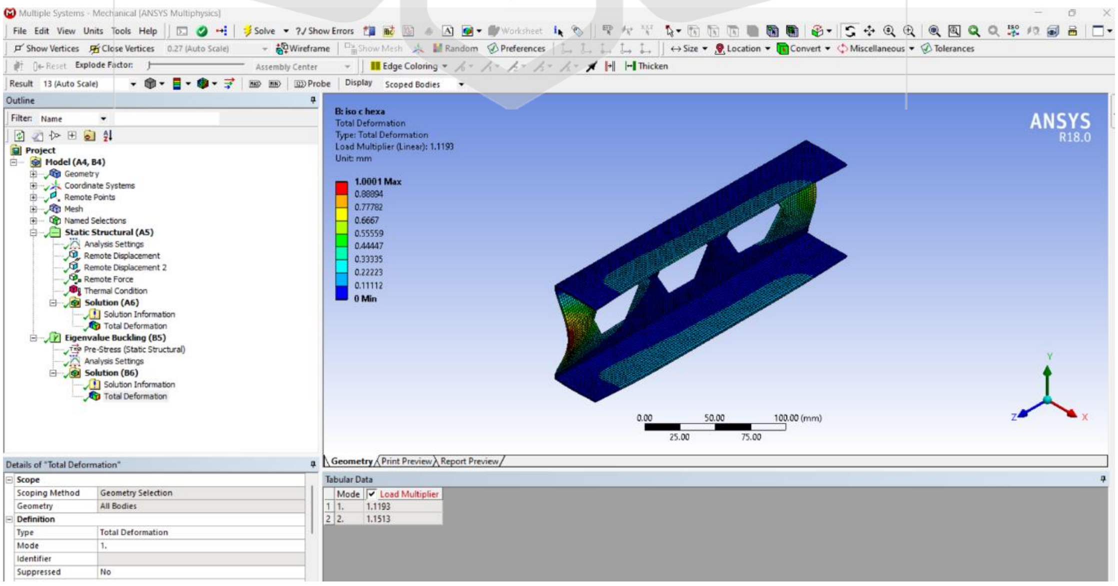

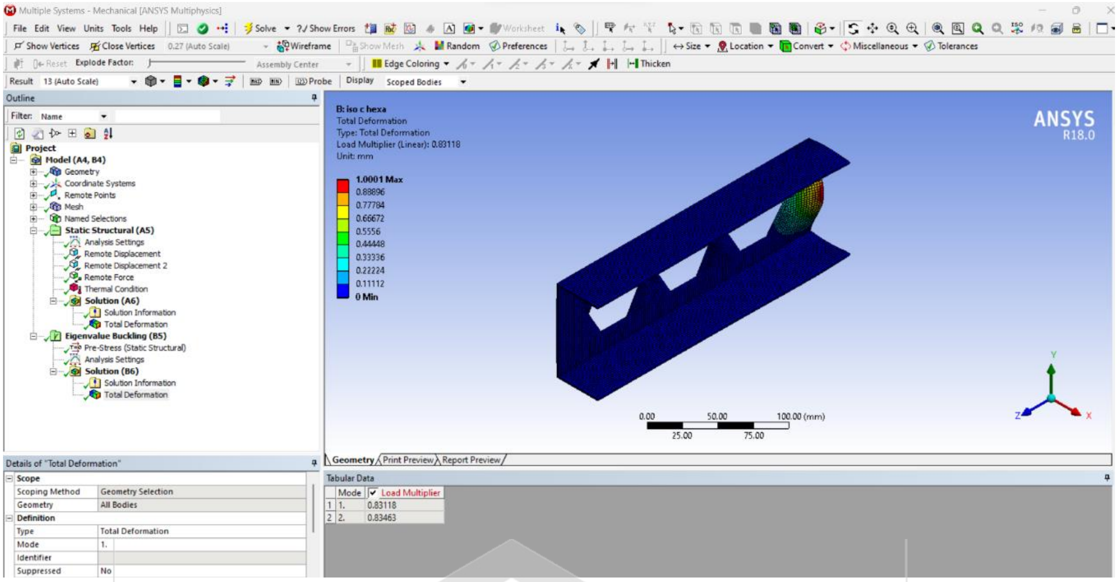
Multiple Systems - Mechanical [ANSYS Multiphysics]
B: iso c hexa
Total Deformation
Type: Total Deformation
Load Multiplier (Linear): 0.83118
Unit: mm
1.0001 Max
0.88896
0.77784
0.66672
0.5556
0.44448
0.33336
0.22224
0.11112
0 Min
ANSYS
R18.0
Tabular Data
Mode | Load Multiplier
1. | 0.83118
2. | 0.83463

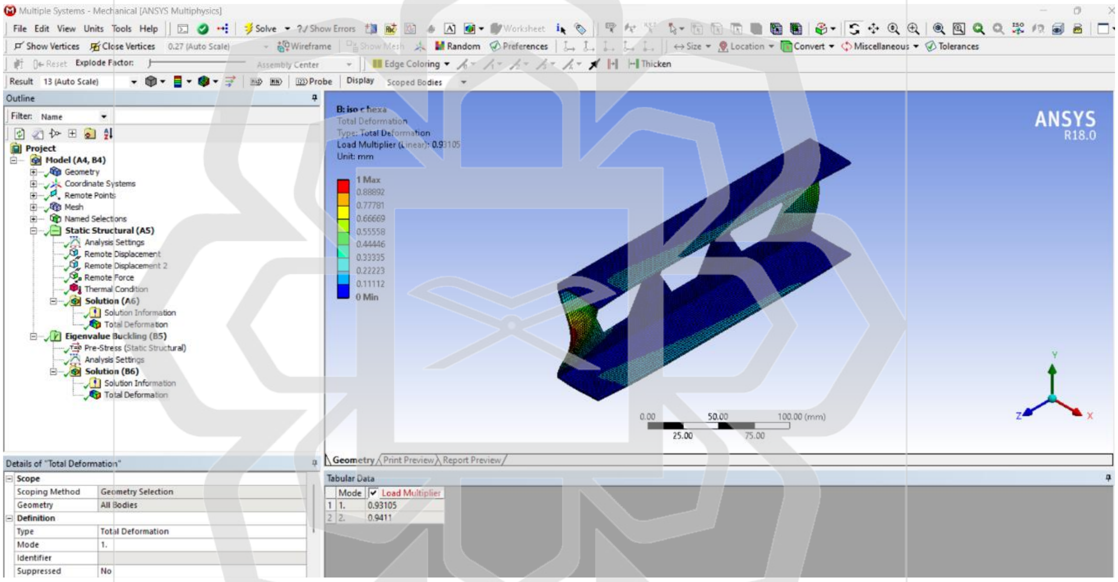
Multiple Systems - Mechanical [ANSYS Multiphysics]
B: iso c hexa
Total Deformation
Type: Total Deformation
Load Multiplier (Linear): 0.93105
Unit: mm
1 Max
0.88892
0.77781
0.66669
0.55558
0.44446
0.33335
0.22223
0.11112
0 Min
ANSYS
R18.0
Tabular Data
Mode | Load Multiplier
1. | 0.93105
2. | 0.9411

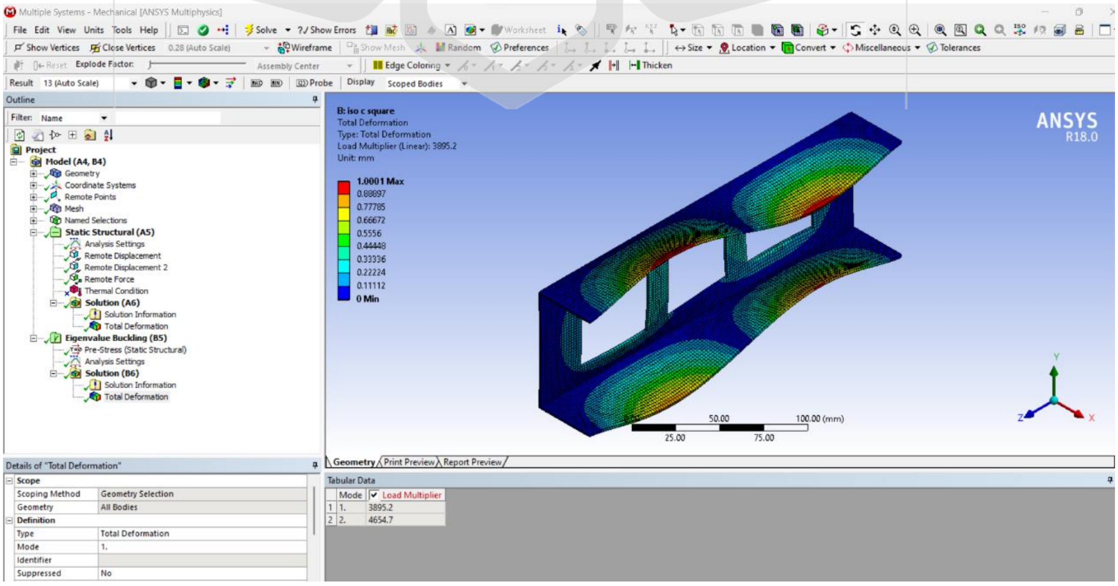
Multiple Systems - Mechanical [ANSYS Multiphysics]
B: iso c square
Total Deformation
Type: Total Deformation
Load Multiplier (Linear): 3895.2
Unit: mm
1.0001 Max
0.88897
0.77785
0.66672
0.5556
0.44448
0.33336
0.22224
0.11112
0 Min
ANSYS
R18.0
Tabular Data
Mode | Load Multiplier
1. | 3895.2
2. | 4654.7

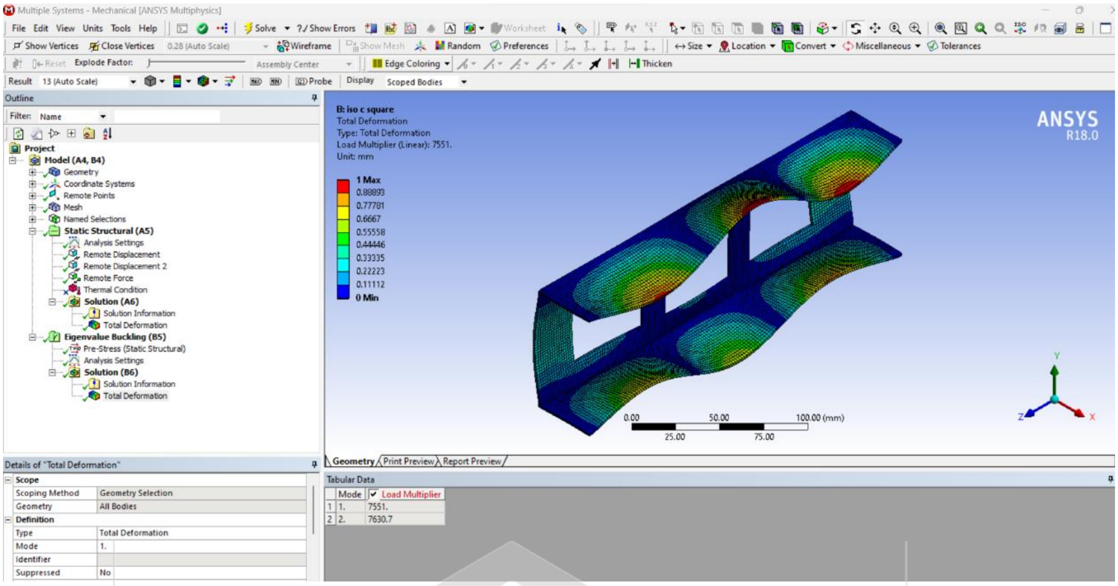
B: iso c square
Total Deformation
Type: Total Deformation
Load Multiplier (Linear): 7551.
Unit: mm
ANSYS
R18.0
Tabular Data
Mode
Load Multiplier
1. 7551.
2. 7630.7

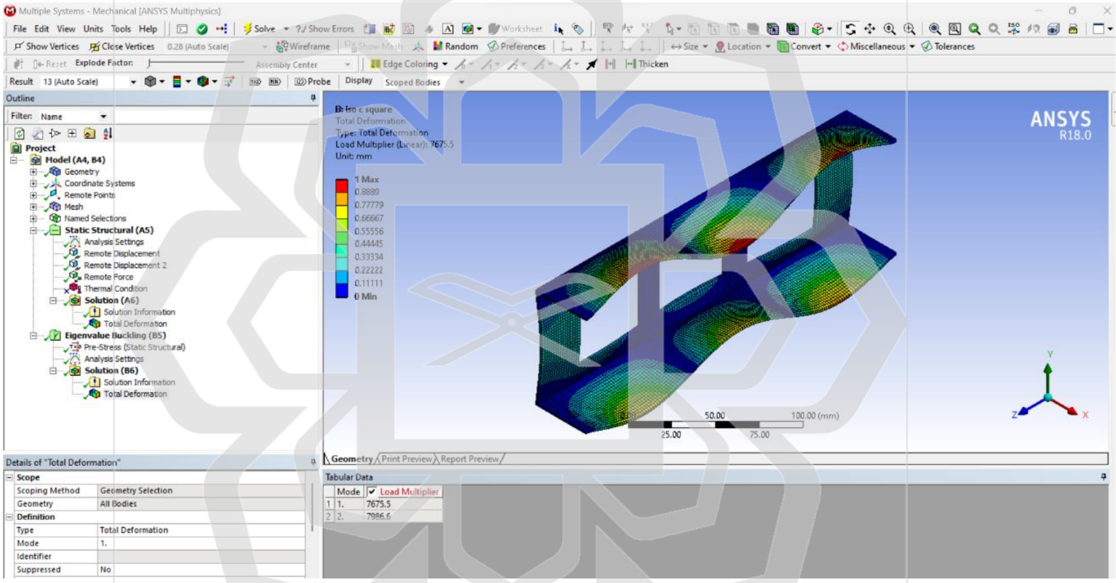
B: iso c square
Total Deformation
Type: Total Deformation
Load Multiplier (Linear): 7675.5
Unit: mm
ANSYS
R18.0
Tabular Data
Mode
Load Multiplier
1. 7675.5
2. 7986.6

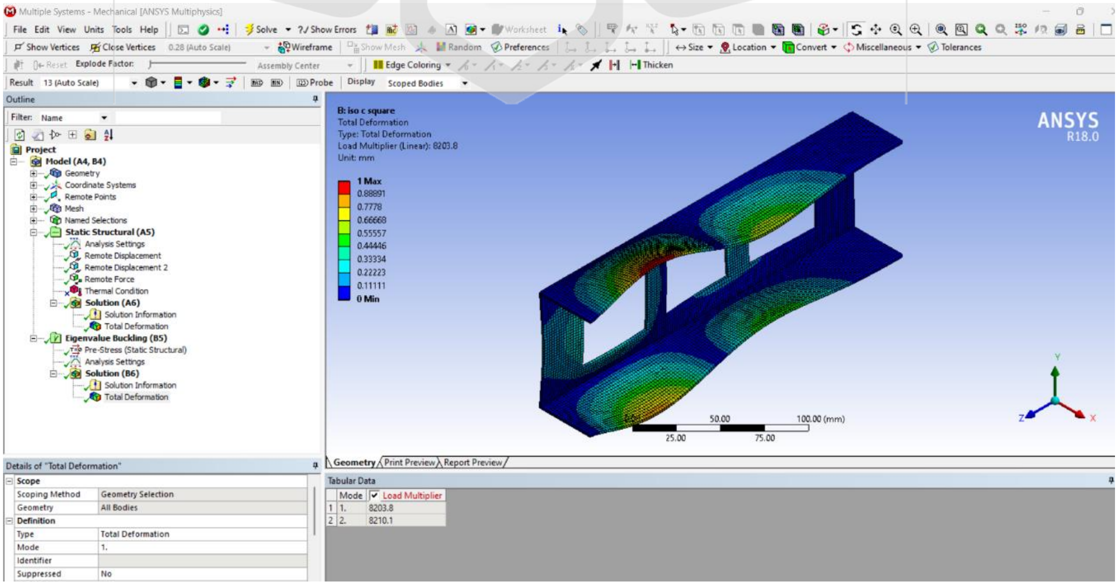
B: iso c square
Total Deformation
Type: Total Deformation
Load Multiplier (Linear): 8203.8
Unit: mm
ANSYS
R18.0
Tabular Data
Mode
Load Multiplier
1. 8203.8
2. 8210.1

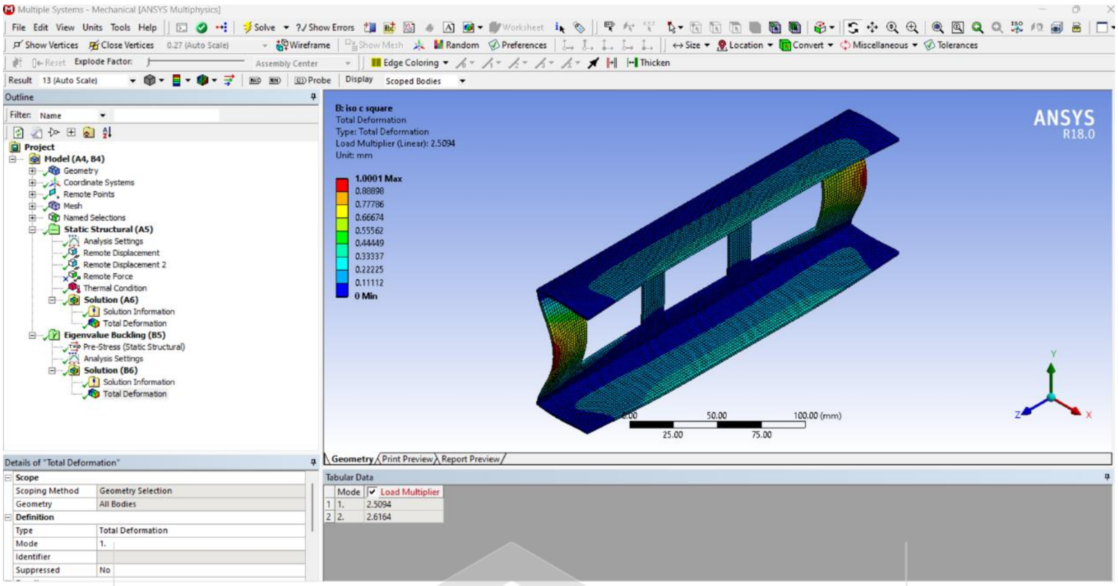
B: iso c square
Total Deformation
Type: Total Deformation
Load Multiplier (Linear): 2.5094
Unit: mm
1.0001 Max
0.88898
0.77786
0.66674
0.55562
0.44449
0.33337
0.22225
0.11112
0 Min
ANSYS
R18.0
Tabular Data
Mode Load Multiplier
1. 2.5094
2. 2.6164

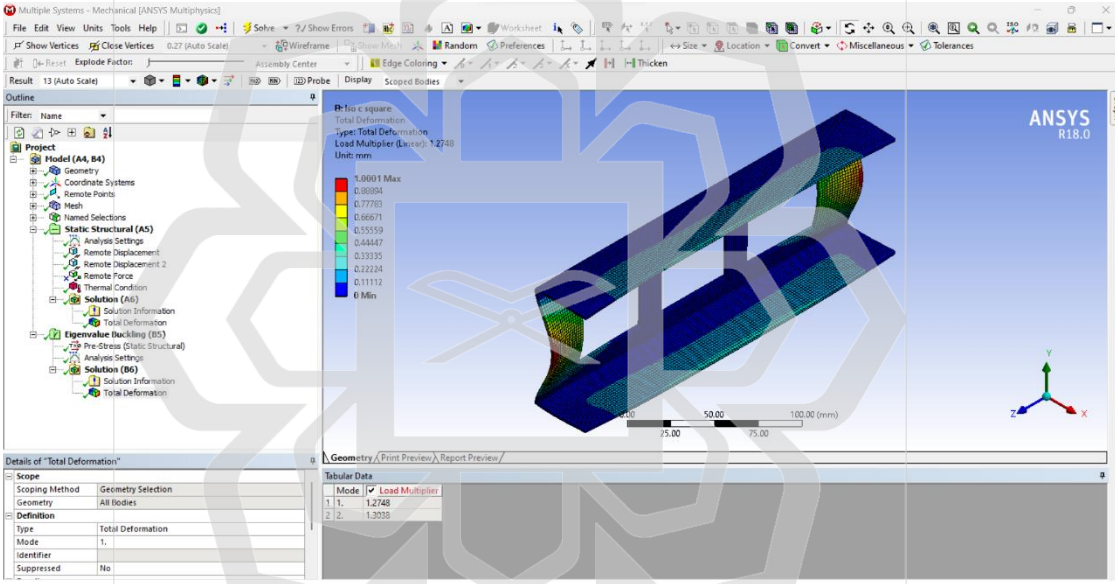
B: iso c square
Total Deformation
Type: Total Deformation
Load Multiplier (Linear): 1.2748
Unit: mm
1.0001 Max
0.88894
0.77783
0.66671
0.55559
0.44447
0.33335
0.22224
0.11112
0 Min
ANSYS
R18.0
Tabular Data
Mode Load Multiplier
1. 1.2748
2. 1.3038

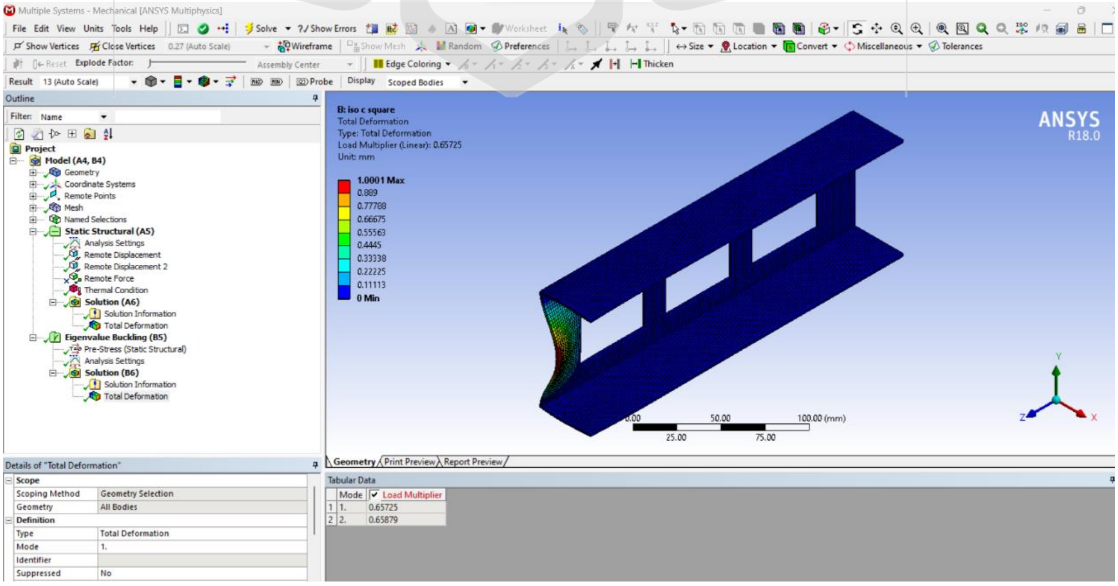
B: iso c square
Total Deformation
Type: Total Deformation
Load Multiplier (Linear): 0.65725
Unit: mm
1.0001 Max
0.889
0.77788
0.66675
0.55563
0.4445
0.33338
0.22225
0.11113
0 Min
ANSYS
R18.0
Tabular Data
Mode Load Multiplier
1. 0.65725
2. 0.65879

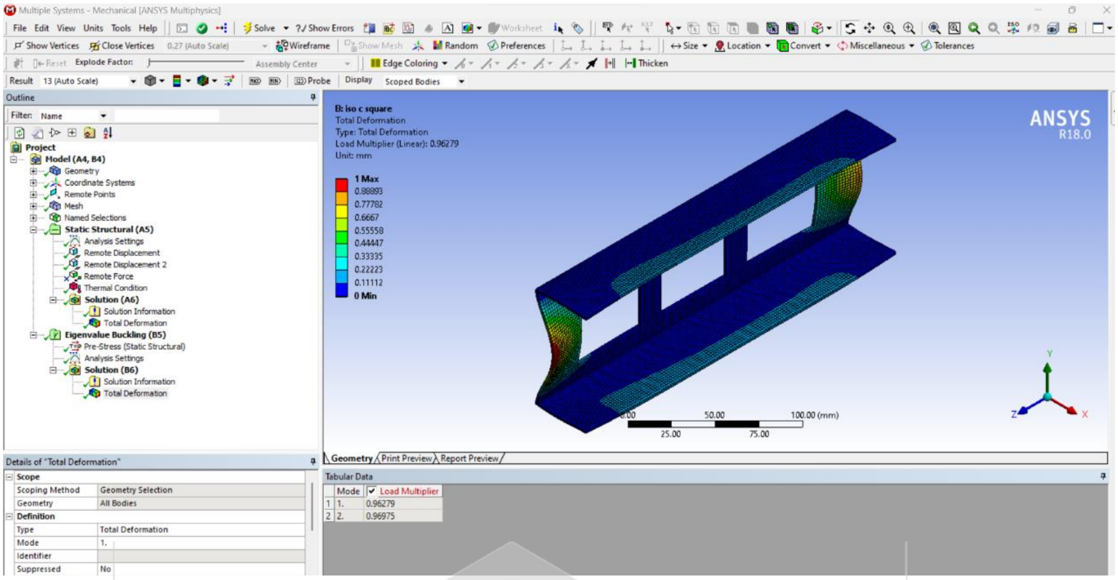
B: iso c square
Total Deformation
Type: Total Deformation
Load Multiplier (Linear): 0.96279
Unit: mm
ANSYS
R18.0

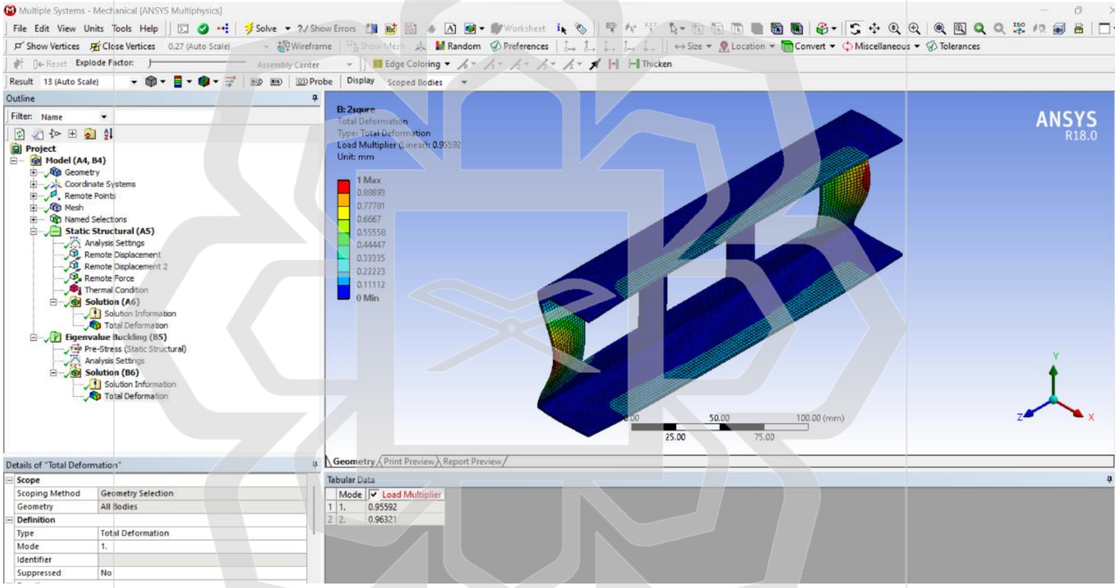
B: 2square
Total Deformation
Type: Total Deformation
Load Multiplier (Linear): 0.95592
Unit: mm
ANSYS
R18.0

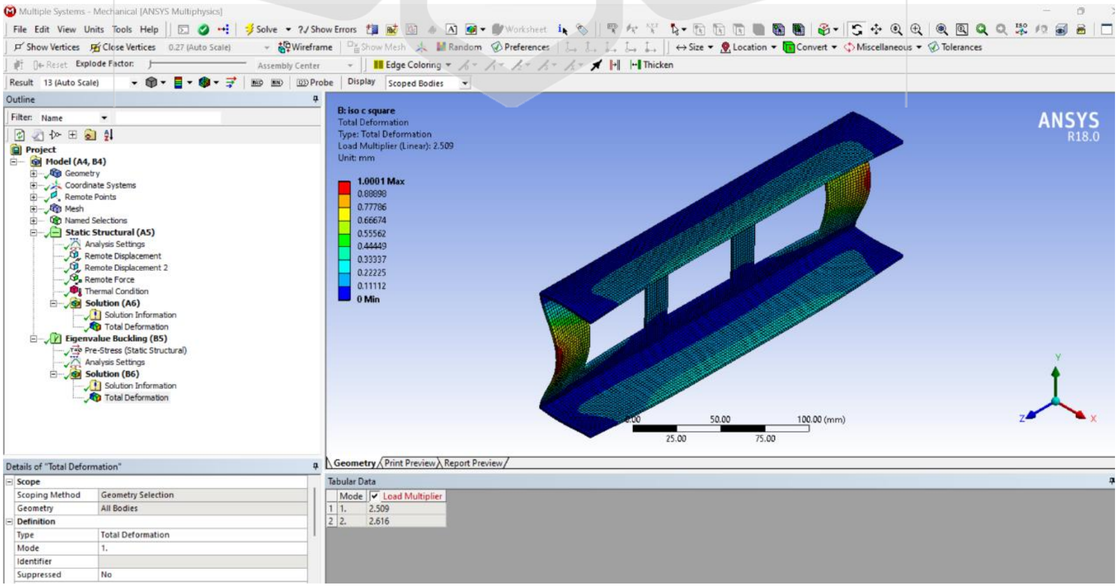
B: iso c square
Total Deformation
Type: Total Deformation
Load Multiplier (Linear): 2.509
Unit: mm
ANSYS
R18.0

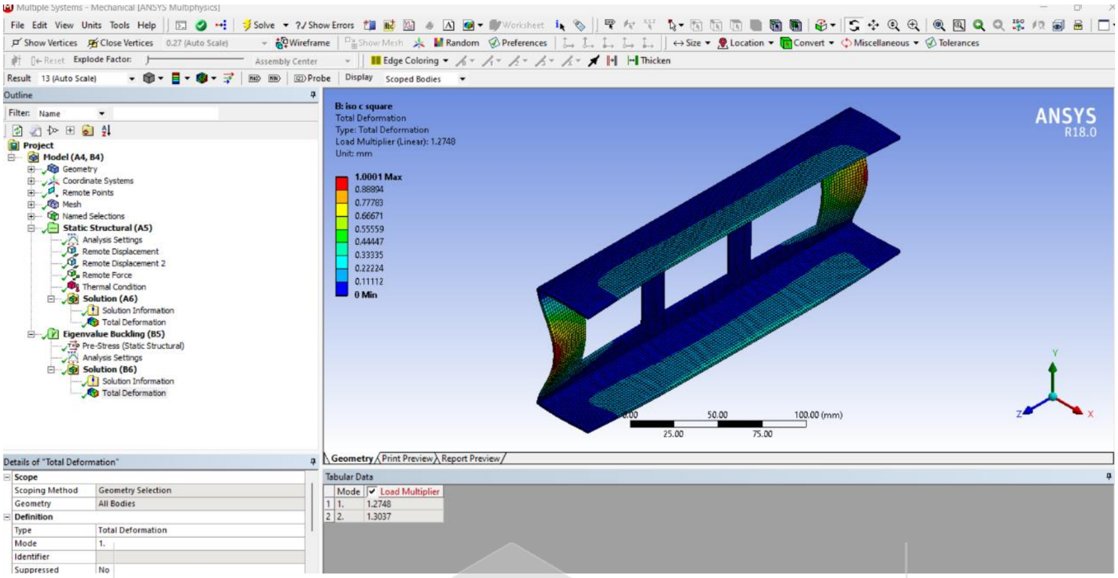
B: iso c square
Total Deformation
Type: Total Deformation
Load Multiplier (Linear): 1.2748
Unit: mm
1.0001 Max
0 Min
ANSYS
R18.0
Tabular Data
Mode | Load Multiplier
1. | 1.2748
2. | 1.3037

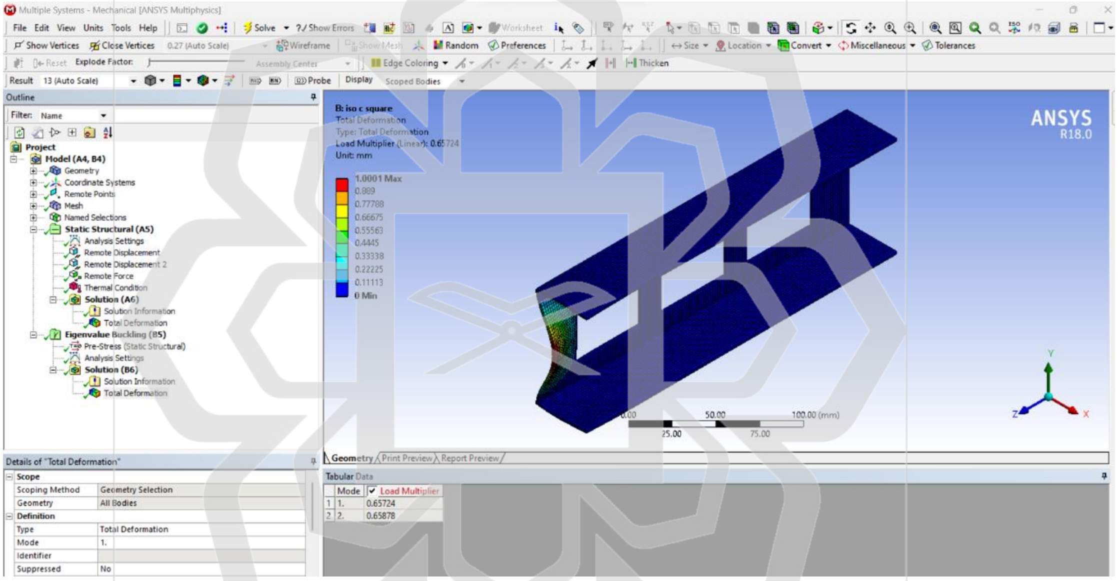
B: iso c square
Total Deformation
Type: Total Deformation
Load Multiplier (Linear): 0.65724
Unit: mm
1.0001 Max
0 Min
ANSYS
R18.0
Tabular Data
Mode | Load Multiplier
1. | 0.65724
2. | 0.65878

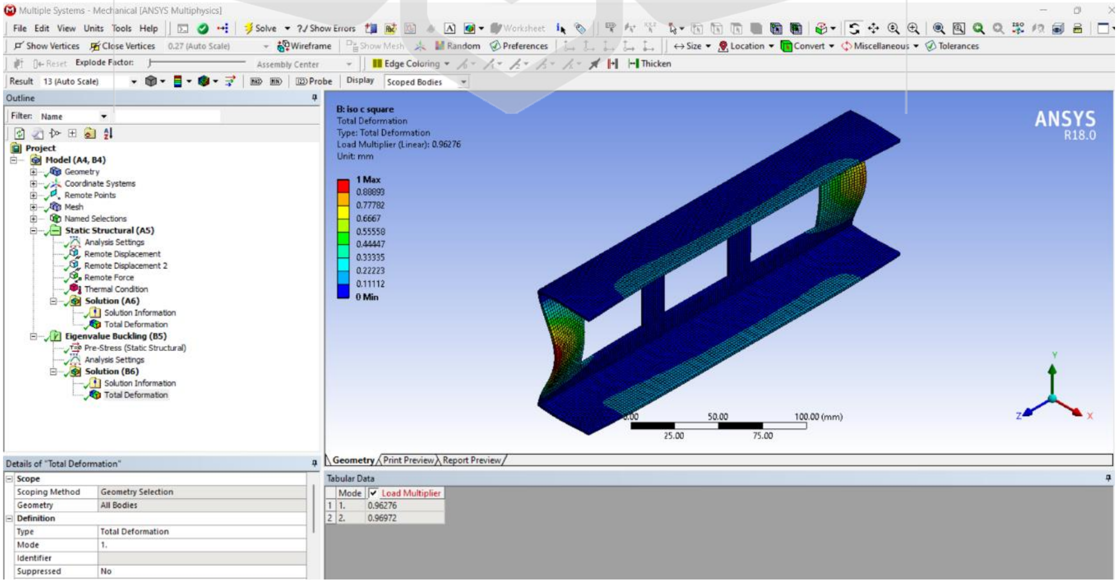
B: iso c square
Total Deformation
Type: Total Deformation
Load Multiplier (Linear): 0.96276
Unit: mm
1 Max
0 Min
ANSYS
R18.0
Tabular Data
Mode | Load Multiplier
1. | 0.96276
2. | 0.96972

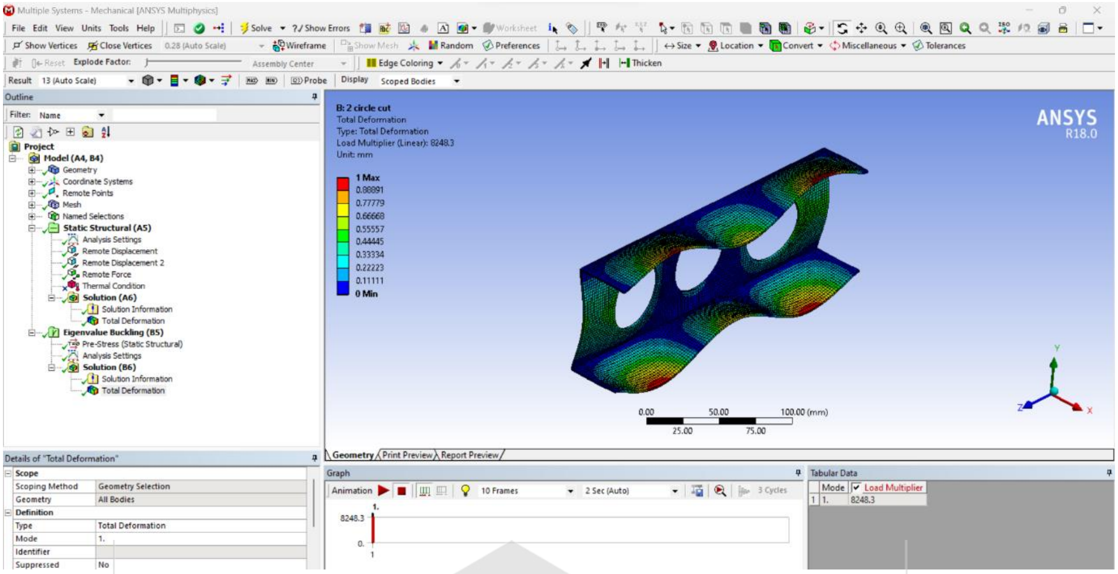
B: 2 circle cut
Total Deformation
Type: Total Deformation
Load Multiplier (Linear): 8248.3
Unit: mm
1 Max
0.88891
0.77779
0.66668
0.55557
0.44445
0.33334
0.22223
0.11111
0 Min
ANSYS
R18.0

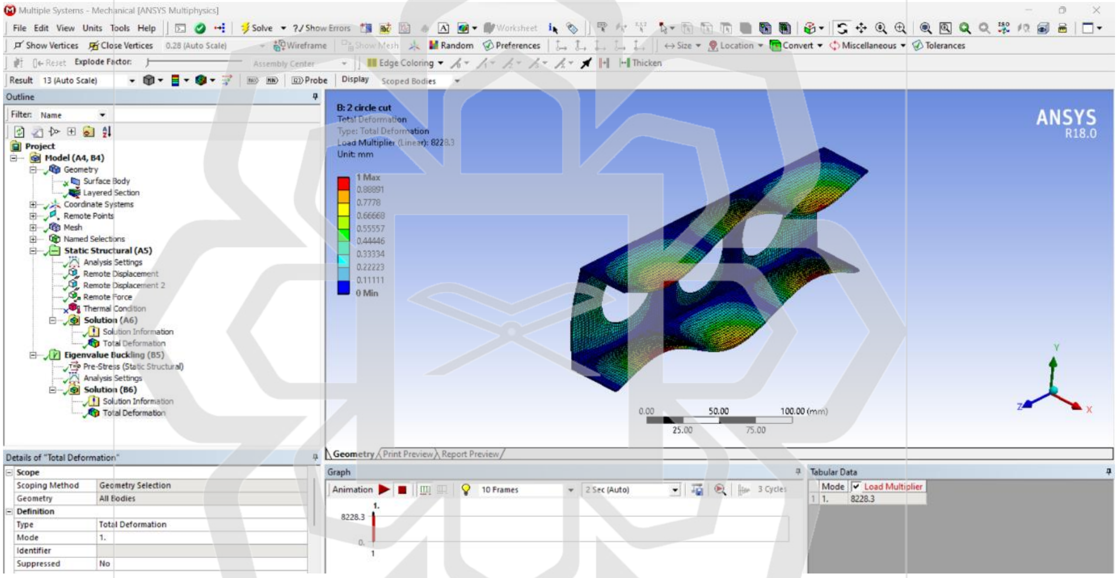
B: 2 circle cut
Total Deformation
Type: Total Deformation
Load Multiplier (Linear): 8228.3
Unit: mm
ANSYS
R18.0

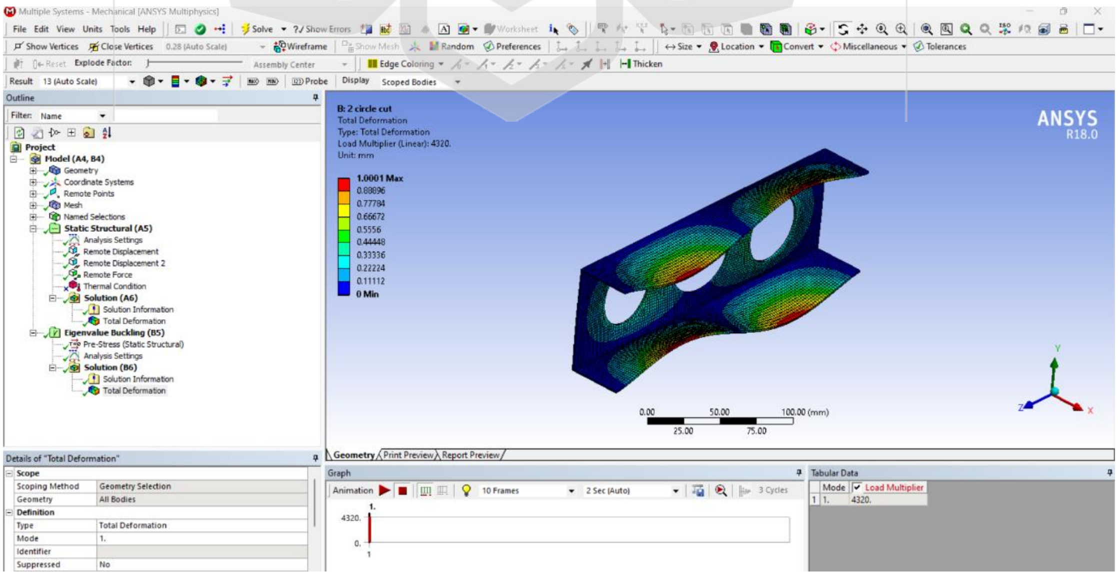
B: 2 circle cut
Total Deformation
Type: Total Deformation
Load Multiplier (Linear): 4320.
Unit: mm
1.0001 Max
0.88896
0.77784
0.66672
0.5556
0.44448
0.33336
0.22224
0.11112
0 Min
ANSYS
R18.0

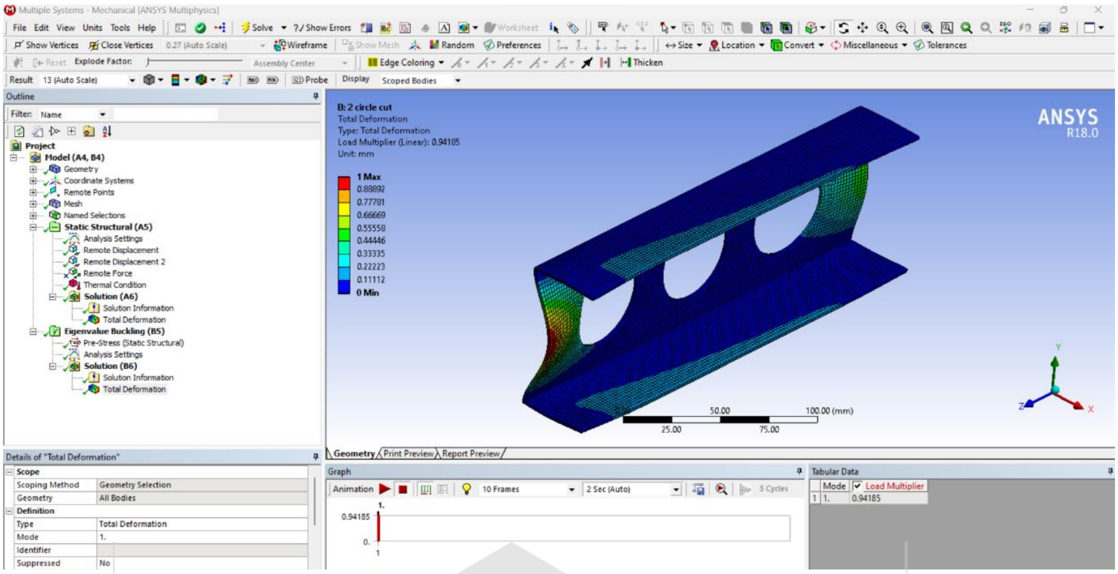
B: 2 circle cut
Total Deformation
Type: Total Deformation
Load Multiplier (Linear): 0.94185
Unit: mm
1 Max
0.88892
0.77781
0.66669
0.55558
0.44446
0.33335
0.22223
0.11112
0 Min
ANSYS
R18.0

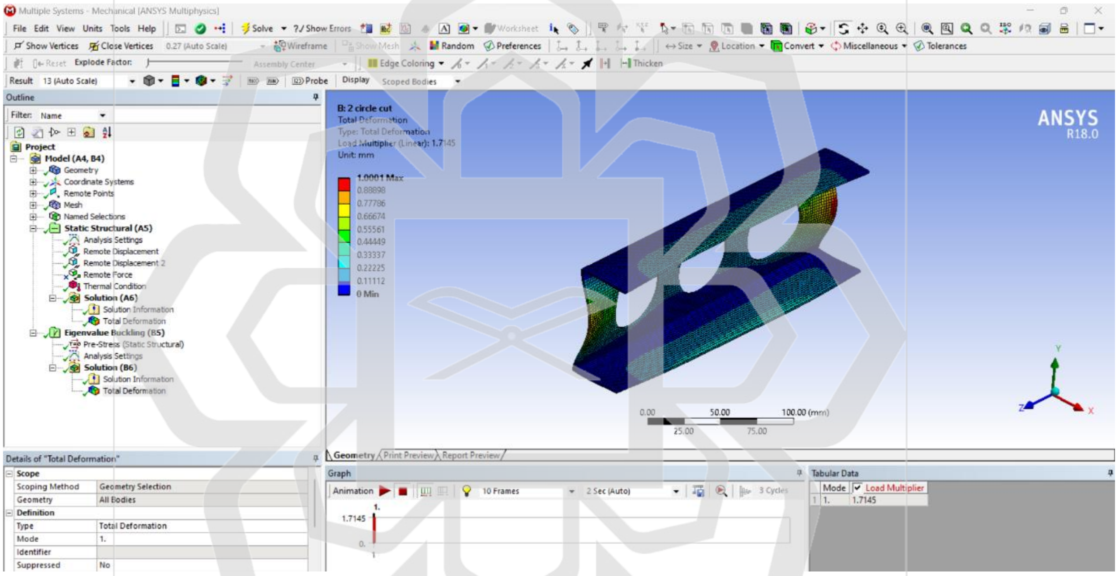
B: 2 circle cut
Total Deformation
Type: Total Deformation
Load Multiplier (Linear): 1.7145
Unit: mm
1.0001 Max
0.88898
0.77786
0.66674
0.55561
0.44449
0.33337
0.22225
0.11112
0 Min
ANSYS
R18.0

APPENDIX B: MACHINE LEARNING ALGORITHMS

In [1]:
```
import numpy as np
import pandas as pd
import seaborn as sns
import matplotlib.pyplot as plt
%matplotlib inline
```

In [2]:
```
df =pd.read_csv("mechnical.csv")
```

In [3]:
```
df.head()
```

Out[3]:

	Opening ratio	Spacing ratio	Orientation	Shape	Critical Buckling load
0	1.3	1.5	Qusi-isentropic	Circular	8625.8
1	1.4	1.5	Qusi-isentropic	Circular	8629.5
2	1.5	1.5	Qusi-isentropic	Circular	8651.0
3	1.3	1.5	Qusi-isentropic	Hexagon	8547.5
4	1.4	1.5	Qusi-isentropic	Hexagon	8551.6

In [4]:
```
# convert to cateogry dtype
df['Orientation'] = df['Orientation'].astype('category')
# convert to category codes
df['Orientation'] = df['Orientation'].cat.codes
```

In [5]:
```
df['Shape'] = df['Shape'].astype('category')
# convert to category codes
df['Shape'] = df['Shape'].cat.codes
```

In [6]:
```
df
```

Out[6]:

	Opening ratio	Spacing ratio	Orientation	Shape	Critical Buckling load
0	1.3	1.5	3	0	8625.8
1	1.4	1.5	3	0	8629.5
2	1.5	1.5	3	0	8651.0
3	1.3	1.5	3	1	8547.5
4	1.4	1.5	3	1	8551.6
...	...	...	...	...	...
67	1.3	1.6	1	1	8207.0
68	1.3	1.7	1	1	8278.0
69	1.3	1.5	1	2	7727.0
70	1.3	1.6	1	2	7986.9
71	1.3	1.7	1	2	8244.9

72 rows × 5 columns

In [7]:
```
# Separate features and labels
X, y = df[['Opening ratio','Spacing ratio', 'Orientation','Shape']].values, df['Critical Buckling load'].values
print('Features:',X[:10], '\nLabels:', y[:10], sep='\n')
```

```
Features:
[[1.3 1.5 3.  0. ]
 [1.4 1.5 3.  0. ]
 [1.5 1.5 3.  0. ]
 [1.3 1.5 3.  1. ]
 [1.4 1.5 3.  1. ]
 [1.5 1.5 3.  1. ]
 [1.3 1.5 3.  2. ]
 [1.4 1.5 3.  2. ]
 [1.5 1.5 3.  2. ]
 [1.5 1.5 3.  0. ]]

Labels:
[8625.8 8629.5 8651.  8547.5 8551.6 8568.3 8196.8 8196.3 8218.4 8625.8]
```

```
In [8]: from sklearn.model_selection import train_test_split

        # Split data 70%-30% into training set and test set
        X_train, X_test, y_train, y_test = train_test_split(X, y, test_size=0.30, random_state=0)

        print ('Training Set: %d rows\nTest Set: %d rows' % (X_train.shape[0], X_test.shape[0]))

        Training Set: 50 rows
        Test Set: 22 rows
```


```
In [8]: from sklearn.model_selection import train_test_split

        # Split data 70%-30% into training set and test set
        X_train, X_test, y_train, y_test = train_test_split(X, y, test_size=0.30, random_state=0)

        print ('Training Set: %d rows\nTest Set: %d rows' % (X_train.shape[0], X_test.shape[0]))

        Training Set: 50 rows
        Test Set: 22 rows
```


```
In [9]: X_train

Out[9]: array([[1.5, 1.5, 3. , 0. ],
               [1.4, 1.5, 2. , 1. ],
               [1.3, 1.7, 3. , 0. ],
               [1.3, 1.5, 3. , 1. ],
               [1.3, 1.5, 1. , 0. ],
               [1.5, 1.5, 2. , 0. ],
               [1.3, 1.6, 3. , 0. ],
               [1.5, 1.5, 2. , 1. ],
               [1.3, 1.6, 2. , 1. ],
               [1.3, 1.7, 2. , 2. ],
               [1.3, 1.5, 1. , 1. ],
               [1.3, 1.7, 0. , 1. ],
               [1.3, 1.7, 3. , 1. ],
               [1.3, 1.5, 1. , 2. ],
               [1.4, 1.5, 0. , 0. ],
               [1.3, 1.7, 0. , 0. ],
               [1.3, 1.6, 2. , 2. ],
               [1.3, 1.7, 0. , 2. ],
               [1.3, 1.5, 0. , 0. ],
```

```
In [10]: from sklearn.preprocessing import StandardScaler

         # Assuming you have already defined and assigned values to X_train and X_test

         # Create an instance of the StandardScaler
         scaler = StandardScaler()

         # Fit the scaler on the training data
         scaler.fit(X_train)

         # Scale the training and test data
         X_train_scaled = scaler.transform(X_train)
         X_test_scaled = scaler.transform(X_test)
         #y_train_scaled = scaler.transform(y_train.reshape(-1, 1))  # Reshape y_train to (n_samples, 1)
         #y_test_scaled = scaler.transform(y_test.reshape(-1, 1))  # Reshape y_test to (n_samples, 1)
```

```
In [11]: X_train_scaled

Out[11]: array([[ 1.71746271, -0.66601018,  1.16275535, -1.11631261],
                [ 0.50798193, -0.66601018,  0.26832816,  0.12403473],
                [-0.70149886,  1.89556742,  1.16275535, -1.11631261],
                [-0.70149886, -0.66601018,  1.16275535,  0.12403473],
                [-0.70149886, -0.66601018, -0.62609903, -1.11631261],
                [ 1.71746271, -0.66601018,  0.26832816, -1.11631261],
                [-0.70149886,  0.61477862,  1.16275535, -1.11631261],
                [ 1.71746271, -0.66601018,  0.26832816,  0.12403473],
                [-0.70149886,  0.61477862,  0.26832816,  0.12403473],
                [-0.70149886,  1.89556742,  0.26832816,  1.36438208],
                [-0.70149886, -0.66601018, -0.62609903,  0.12403473],
                [-0.70149886,  1.89556742, -1.52052622,  0.12403473],
                [-0.70149886,  1.89556742,  1.16275535,  0.12403473],
                [-0.70149886, -0.66601018, -0.62609903,  1.36438208],
                [ 0.50798193, -0.66601018, -1.52052622, -1.11631261],
                [-0.70149886,  1.89556742, -1.52052622, -1.11631261],
                [-0.70149886,  0.61477862,  0.26832816,  1.36438208],
                [-0.70149886,  1.89556742, -1.52052622,  1.36438208],
                [-0.70149886, -0.66601018, -1.52052622, -1.11631261],
```

```
In [12]: # Train the model
         from sklearn.linear_model import LinearRegression

         # Fit a linear regression model on the training set
         model = LinearRegression().fit(X_train, y_train)
         print (model)

         LinearRegression()
```

In [14]:
```
import numpy as np

predictions = model.predict(X_test)
np.set_printoptions(suppress=True)
print('Predicted labels: ', np.round(predictions)[:10])
print('Actual labels   : ' ,y_test[:10])
```

```
Predicted labels:  [6870. 6897. 7395. 7200. 7517. 7381. 7004. 6823. 7474. 7384.]
Actual labels   :  [7490.6 8104.1 4179.  8034.7 8100.  3945.9 8196.3 8022.  7939.5 8244.9]
```

In [16]:
```
import matplotlib.pyplot as plt

%matplotlib inline

plt.scatter(y_test, predictions)
plt.xlabel('Actual Labels')
plt.ylabel('Predicted Labels')
plt.title('Buckling loads')
# overlay the regression line
z = np.polyfit(y_test, predictions, 1)
p = np.poly1d(z)
plt.plot(y_test,p(y_test), color='magenta')
plt.show()
```


In [16]:
```
import numpy as np

predictions = model.predict(X_test)
np.set_printoptions(suppress=True)
print('Predicted labels: ', np.round(predictions)[:10])
print('Actual labels   : ' ,y_test[:10])
```

```
Predicted labels:  [6870. 6897. 7395. 7200. 7517. 7381. 7004. 6823. 7474. 7384.]
Actual labels   :  [7490.6 8104.1 4179.  8034.7 8100.  3945.9 8196.3 8022.  7939.5 8244.9]
```


In [17]:
```
X=df.values[:, range(0,4)]
Y=df.values[:,4]
model=LinearRegression().fit(X,Y)
print(model.coef_)
print(model.intercept_)
```

```
[   7.76860771 1579.04546118 -235.04555556 -177.5017732 ]
5276.117370110921
```

In [18]:
```
newdata=[[1.5, 1.7, 3, 0],
         [1.5, 1.7, 3, 1],
         [1.5, 1.7, 3, 2]]
```

In [19]:
```
print(model.predict(newdata))
```

```
[7267.01089901 7089.5091258  6912.0073526 ]
```

In [20]:
```
from sklearn.metrics import mean_squared_error, r2_score

mse = mean_squared_error(y_test, predictions)
print("MSE:", mse)

rmse = np.sqrt(mse)
print("RMSE:", rmse)

r2 = r2_score(y_test, predictions)
print("R2:", r2)
```

```
MSE: 3073046.011416155
RMSE: 1753.010556561527
R2: -0.07273560101698706
```

In [21]:
```python
from sklearn.linear_model import Lasso

# Fit a lasso model on the training set
model = Lasso().fit(X_train, y_train)
print (model, "\n")

# Evaluate the model using the test data
predictions = model.predict(X_test)
mse = mean_squared_error(y_test, predictions)
print("MSE:", mse)
rmse = np.sqrt(mse)
print("RMSE:", rmse)
r2 = r2_score(y_test, predictions)
print("R2:", r2)

# Plot predicted vs actual
plt.scatter(y_test, predictions)
plt.xlabel('Actual Labels')
plt.ylabel('Predicted Labels')
plt.title('Buckling loads')
# overlay the regression line
z = np.polyfit(y_test, predictions, 1)
p = np.poly1d(z)
plt.plot(y_test,p(y_test), color='magenta')
plt.show()
```

```
Lasso()

MSE: 3042892.0123141953
RMSE: 1744.3887216770795
R2: -0.06220947539780064
```


In [21]:
```python
from sklearn.linear_model import Lasso

# Fit a lasso model on the training set
model = Lasso().fit(X_train, y_train)
print (model, "\n")

# Evaluate the model using the test data
predictions = model.predict(X_test)
mse = mean_squared_error(y_test, predictions)
print("MSE:", mse)
rmse = np.sqrt(mse)
print("RMSE:", rmse)
r2 = r2_score(y_test, predictions)
print("R2:", r2)

# Plot predicted vs actual
plt.scatter(y_test, predictions)
plt.xlabel('Actual Labels')
plt.ylabel('Predicted Labels')
plt.title('Buckling loads')
# overlay the regression line
z = np.polyfit(y_test, predictions, 1)
p = np.poly1d(z)
plt.plot(y_test,p(y_test), color='magenta')
plt.show()
```

```
Lasso()

MSE: 3042892.0123141953
RMSE: 1744.3887216770795
R2: -0.06220947539780064
```


In [23]:
```python
X=df.values[:, range(0,4)]
Y=df.values[:,4]
model = Lasso().fit(X, Y)
print(model.coef_)
print(model.intercept_)
```

```
[   -0.          1403.54761905 -234.24555556 -176.13125    ]
5556.14244047619
```

In [27]:
```python
from sklearn.tree import DecisionTreeRegressor
from sklearn.tree import export_text

# Train the model
model = DecisionTreeRegressor().fit(X_train, y_train)
print (model, "\n")

# Visualize the model tree
tree = export_text(model)
print(tree)
```

```
DecisionTreeRegressor()

|--- feature_2 <= 2.50
|   |--- feature_2 <= 1.50
|   |   |--- feature_1 <= 1.55
|   |   |   |--- feature_3 <= 1.50
|   |   |   |   |--- feature_3 <= 0.50
|   |   |   |   |   |--- feature_0 <= 1.35
|   |   |   |   |   |   |--- feature_2 <= 0.50
|   |   |   |   |   |   |   |--- value: [8104.10]
|   |   |   |   |   |   |--- feature_2 >  0.50
|   |   |   |   |   |   |   |--- value: [8082.30]
|   |   |   |   |   |--- feature_0 >  1.35
|   |   |   |   |   |   |--- feature_2 <= 0.50
|   |   |   |   |   |   |   |--- feature_0 <= 1.45
|   |   |   |   |   |   |   |   |--- value: [8054.30]
|   |   |   |   |   |   |   |--- feature_0 >  1.45
|   |   |   |   |   |   |   |   |--- value: [8059.20]
|   |   |   |   |   |   |--- feature_2 >  0.50
```

In [29]:
```python
# Evaluate the model using the test data
predictions = model.predict(X_test)
mse = mean_squared_error(y_test, predictions)
print("MSE:", mse)
rmse = np.sqrt(mse)
print("RMSE:", rmse)
r2 = r2_score(y_test, predictions)
print("R2:", r2)

# Plot predicted vs actual
plt.scatter(y_test, predictions)
plt.xlabel('Actual Labels')
plt.ylabel('Predicted Labels')
plt.title('Actual vs Predicted Buckling loads')
# overlay the regression line
z = np.polyfit(y_test, predictions, 1)
p = np.poly1d(z)
plt.plot(y_test,p(y_test), color='magenta')
plt.show()
```

```
MSE: 12450.751818181801
RMSE: 111.58293694907748
R2: 0.9956537049282137
```

In [31]:
```python
from sklearn.metrics import mean_squared_error, r2_score

mse = mean_squared_error(y_test, predictions)
print("MSE:", mse)

rmse = np.sqrt(mse)
print("RMSE:", rmse)

r2 = r2_score(y_test, predictions)
print("R2:", r2)
```

In [32]:
```python
X=df.values[:, range(0,4)]
Y=df.values[:,4]
model = DecisionTreeRegressor().fit(X, Y)
#print(model.coef_)
#print(model.intercept_)
print('Feature Importances:', model.feature_importances_)
```

```
Feature Importances: [0.00021781 0.00638424 0.98567688 0.00772108]
```

```
In [36]: from sklearn.ensemble import RandomForestRegressor

# Train the model
model = RandomForestRegressor().fit(X_train, y_train)
print (model, "\n")

# Evaluate the model using the test data
predictions = model.predict(X_test)
mse = mean_squared_error(y_test, predictions)
print("MSE:", mse)
rmse = np.sqrt(mse)
print("RMSE:", rmse)
r2 = r2_score(y_test, predictions)
print("R2:", r2)

# Plot predicted vs actual
plt.scatter(y_test, predictions)
plt.xlabel('Actual Labels')
plt.ylabel('Predicted Labels')
plt.title('Actual vs Predicted Buckling loads')
# overlay the regression line
z = np.polyfit(y_test, predictions, 1)
p = np.poly1d(z)
plt.plot(y_test,p(y_test), color='magenta')
plt.show()
```

```
In [42]: # Train the model
from sklearn.ensemble import GradientBoostingRegressor

# Fit a lasso model on the training set
model = GradientBoostingRegressor().fit(X_train, y_train)
print (model, "\n")

# Evaluate the model using the test data
predictions = model.predict(X_test)
mse = mean_squared_error(y_test, predictions)
print("MSE:", mse)
rmse = np.sqrt(mse)
print("RMSE:", rmse)
r2 = r2_score(y_test, predictions)
print("R2:", r2)

# Plot predicted vs actual
plt.scatter(y_test, predictions)
plt.xlabel('Actual Labels')
plt.ylabel('Predicted Labels')
plt.title('Actual vs Predicted Buckling loads')
# overlay the regression line
z = np.polyfit(y_test, predictions, 1)
p = np.poly1d(z)
plt.plot(y_test,p(y_test), color='magenta')
plt.show()
```

```
In [48]: from sklearn.model_selection import GridSearchCV
         from sklearn.metrics import make_scorer, r2_score

         # Use a Gradient Boosting algorithm
         alg = GradientBoostingRegressor()

         # Try these hyperparameter values
         params = {
          'learning_rate': [0.1, 0.5, 1.0],
          'n_estimators' : [50, 100, 150]
          }

         # Find the best hyperparameter combination to optimize the R2 metric
         score = make_scorer(r2_score)
         gridsearch = GridSearchCV(alg, params, scoring=score, cv=3, return_train_score=True)
         gridsearch.fit(X_train, y_train)
         print("Best parameter combination:", gridsearch.best_params_, "\n")

         # Get the best model
         model=gridsearch.best_estimator_
         print(model, "\n")

         # Evaluate the model using the test data
         predictions = model.predict(X_test)
         mse = mean_squared_error(y_test, predictions)
         print("MSE:", mse)
         rmse = np.sqrt(mse)
         print("RMSE:", rmse)
         r2 = r2_score(y_test, predictions)
         print("R2:", r2)

         # Plot predicted vs actual
         plt.scatter(y_test, predictions)
         plt.xlabel('Actual Labels')
         plt.ylabel('Predicted Labels')
         plt.title('Actual vs Predicted Buckling loads')
         # overlay the regression line
         z = np.polyfit(y_test, predictions, 1)
         p = np.poly1d(z)
         plt.plot(y_test,p(y_test), color='magenta')
         plt.show()
```

APPENDIX C: DATA SET AND SCALING

Data set for machine learning(Mechanical and Thermal)

	Opening ratio	Spacing ratio	Orientation	Shape	Critical Buckling load
0	1.3	1.5	Qusi-isentropic	Circular	8625.8
1	1.4	1.5	Qusi-isentropic	Circular	8629.5
2	1.5	1.5	Qusi-isentropic	Circular	8651.0
3	1.3	1.5	Qusi-isentropic	Hexagon	8547.5
4	1.4	1.5	Qusi-isentropic	Hexagon	8551.6
5	1.5	1.5	Qusi-isentropic	Hexagon	8568.3
6	1.3	1.5	Qusi-isentropic	Square	8196.8
7	1.4	1.5	Qusi-isentropic	Square	8196.3
8	1.5	1.5	Qusi-isentropic	Square	8218.4
9	1.5	1.5	Qusi-isentropic	Circular	8625.8
10	1.3	1.6	Qusi-isentropic	Circular	8803.3
11	1.3	1.7	Qusi-isentropic	Circular	8890.5
12	1.3	1.5	Qusi-isentropic	Hexagon	8547.5
13	1.3	1.6	Qusi-isentropic	Hexagon	8658.2
14	1.3	1.7	Qusi-isentropic	Hexagon	8711.6
15	1.3	1.5	Qusi-isentropic	Square	8196.8
16	1.3	1.6	Qusi-isentropic	Square	8469.0
17	1.3	1.7	Qusi-isentropic	Square	8629.2
18	1.3	1.5	Angle-ply	Circular	8104.1
19	1.4	1.5	Angle-ply	Circular	8054.3
20	1.5	1.5	Angle-ply	Circular	8059.2
21	1.3	1.5	Angle-ply	Hexagon	8100.0
22	1.4	1.5	Angle-ply	Hexagon	8034.7
23	1.5	1.5	Angle-ply	Hexagon	8005.0
24	1.3	1.5	Angle-ply	Square	7624.1
25	1.4	1.5	Angle-ply	Square	7510.7
26	1.5	1.5	Angle-ply	Square	7490.6
27	1.5	1.5	Angle-ply	Circular	8104.1
28	1.3	1.6	Angle-ply	Circular	8356.4
29	1.3	1.7	Angle-ply	Circular	8542.0
30	1.3	1.5	Angle-ply	Hexagon	8100.0
31	1.3	1.6	Angle-ply	Hexagon	8308.4
32	1.3	1.7	Angle-ply	Hexagon	8422.3
33	1.3	1.5	Angle-ply	Square	7624.1
34	1.3	1.6	Angle-ply	Square	7939.5
35	1.3	1.7	Angle-ply	Square	8275.9
36	1.3	1.5	Cross-ply	Circular	4237.2
37	1.4	1.5	Cross-ply	Circular	4301.0
38	1.5	1.5	Cross-ply	Circular	4339.5
39	1.3	1.5	Cross-ply	Hexagon	4179.0

	Spacing ratio	Opening ratio	Orientation	Shape	Critical buckling load
0	1.5	1.3	3	0	140.50000
1	1.5	1.4	3	0	145.60320
2	1.5	1.5	3	0	146.04090
3	1.5	1.3	3	0	140.50000
4	1.6	1.3	3	0	146.04090
5	1.7	1.3	3	0	146.07424
6	1.5	1.3	3	1	139.97880
7	1.5	1.4	3	1	143.97370
8	1.5	1.5	3	1	145.08350
9	1.5	1.3	3	1	139.97880
10	1.6	1.3	3	1	143.38360
11	1.7	1.3	3	1	143.97370
12	1.5	1.3	3	2	137.85020
13	1.5	1.4	3	2	143.44700
14	1.5	1.5	3	2	145.05920
15	1.5	1.3	3	2	137.85020
16	1.6	1.3	3	2	142.66560
17	1.7	1.3	3	2	143.44700
18	1.5	1.3	0	0	300.31040
19	1.5	1.4	0	0	300.36160
20	1.5	1.5	0	0	300.81760
21	1.5	1.3	0	0	300.31040
22	1.6	1.3	0	0	304.58560
23	1.7	1.3	0	0	308.96320
24	1.5	1.3	0	1	282.33920
25	1.5	1.4	0	1	283.33600
26	1.5	1.5	0	1	287.95200
27	1.5	1.3	0	1	282.33920
28	1.6	1.3	0	1	300.86080
29	1.7	1.3	0	1	301.44960
30	1.5	1.3	0	2	239.19040
31	1.5	1.4	0	2	244.21440
32	1.5	1.5	0	2	251.02080
33	1.5	1.3	0	2	239.19040
34	1.6	1.3	0	2	247.30560
35	1.7	1.3	0	2	250.59520
36	1.5	1.3	2	0	124.99648
37	1.5	1.4	2	0	124.38848
38	1.5	1.5	2	0	133.42400
39	1.5	1.3	2	0	124.99648

Data scaling of Mechanical and Thermal loads

	Opening ratio	Spacing ratio	Orientation	Shape	Critical Buckling load
0	1.3	1.5	3	0	8625.8
1	1.4	1.5	3	0	8629.5
2	1.5	1.5	3	0	8651.0
3	1.3	1.5	3	1	8547.5
4	1.4	1.5	3	1	8551.6
5	1.5	1.5	3	1	8568.3
6	1.3	1.5	3	2	8196.8
7	1.4	1.5	3	2	8196.3
8	1.5	1.5	3	2	8218.4
9	1.5	1.5	3	0	8625.8
10	1.3	1.6	3	0	8803.3
11	1.3	1.7	3	0	8890.5
12	1.3	1.5	3	1	8547.5
13	1.3	1.6	3	1	8658.2
14	1.3	1.7	3	1	8711.6
15	1.3	1.5	3	2	8196.8
16	1.3	1.6	3	2	8469.0
17	1.3	1.7	3	2	8629.2
18	1.3	1.5	0	0	8104.1
19	1.4	1.5	0	0	8054.3
20	1.5	1.5	0	0	8059.2
21	1.3	1.5	0	1	8100.0
22	1.4	1.5	0	1	8034.7
23	1.5	1.5	0	1	8005.0
24	1.3	1.5	0	2	7624.1
25	1.4	1.5	0	2	7510.7
26	1.5	1.5	0	2	7490.6
27	1.5	1.5	0	0	8104.1
28	1.3	1.6	0	0	8356.4
29	1.3	1.7	0	0	8542.0
30	1.3	1.5	0	1	8100.0
31	1.3	1.6	0	1	8308.4
32	1.3	1.7	0	1	8422.3
33	1.3	1.5	0	2	7624.1
34	1.3	1.6	0	2	7939.5
35	1.3	1.7	0	2	8275.9
36	1.3	1.5	2	0	4237.2
37	1.4	1.5	2	0	4301.0
38	1.5	1.5	2	0	4339.5
39	1.3	1.5	2	1	4179.0

	Spacing ratio	Opening ratio	Orientation	Shape	Critical buckling load
0	1.5	1.3	3	0	140.50000
1	1.5	1.4	3	0	145.60320
2	1.5	1.5	3	0	146.04090
3	1.5	1.3	3	0	140.50000
4	1.6	1.3	3	0	146.04090
5	1.7	1.3	3	0	146.07424
6	1.5	1.3	3	1	139.97880
7	1.5	1.4	3	1	143.97370
8	1.5	1.5	3	1	145.08350
9	1.5	1.3	3	1	139.97880
10	1.6	1.3	3	1	143.38360
11	1.7	1.3	3	1	143.97370
12	1.5	1.3	3	2	137.85020
13	1.5	1.4	3	2	143.44700
14	1.5	1.5	3	2	145.05920
15	1.5	1.3	3	2	137.85020
16	1.6	1.3	3	2	142.66560
17	1.7	1.3	3	2	143.44700
18	1.5	1.3	0	0	300.31040
19	1.5	1.4	0	0	300.36160
20	1.5	1.5	0	0	300.81760
21	1.5	1.3	0	0	300.31040
22	1.6	1.3	0	0	304.58560
23	1.7	1.3	0	0	308.96320
24	1.5	1.3	0	1	282.33920
25	1.5	1.4	0	1	283.33600
26	1.5	1.5	0	1	287.95200
27	1.5	1.3	0	1	282.33920
28	1.6	1.3	0	1	300.86080
29	1.7	1.3	0	1	301.44960
30	1.5	1.3	0	2	239.19040
31	1.5	1.4	0	2	244.21440
32	1.5	1.5	0	2	251.02080
33	1.5	1.3	0	2	239.19040
34	1.6	1.3	0	2	247.30560
35	1.7	1.3	0	2	250.59520
36	1.5	1.3	2	0	124.99648
37	1.5	1.4	2	0	124.38848
38	1.5	1.5	2	0	133.42400
39	1.5	1.3	2	0	124.99648